IntechOpen

Trends in Modern Cosmology

Edited by Abraao Jesse Capistrano de Souza

TRENDS IN MODERN COSMOLOGY

Edited by **Abraao Jesse Capistrano de Souza**

Trends in Modern Cosmology
http://dx.doi.org/10.5772/66010
Edited by Abraao Jesse Capistrano de Souza

Contributors

Hing-Tong Cho, Chun-Hung Chen, Alan Cornell, Youcai Zhang, Weiguang Cui, Brian Albert Robson, Nicholas Campion, Eri Atahualpa Mena, Marco Fedi, Valeriy Sbitnev, Paraskevi Divari, Koichi Hirano, Salah Nasri, Abdessamad Abada, Ruggero Stanga, Luca Lusanna

Notice

First published in Croatia, 2017 by INTECH d.o.o.
eBook (PDF) Published by IN TECH d.o.o.
Place and year of publication of eBook (PDF): Rijeka, 2019.
IntechOpen is the global imprint of IN TECH d.o.o.
Printed in Croatia

Legal deposit, Croatia: National and University Library in Zagreb

Additional hard and PDF copies can be obtained from orders@intechopen.com

Trends in Modern Cosmology
Edited by Abraao Jesse Capistrano de Souza

p. cm.

Print ISBN 978-953-51-3209-7

Online ISBN 978-953-51-3210-3

eBook (PDF) ISBN 978-953-51-4810-4

Meet the editor

Professor Abraão Jessé Capistrano de Souza is a graduate of Physics awarded by Federal University of Pará, Brazil (2004) and obtained his master's degree in Physics (2006) and doctorate in Theoretical Physics from Universidade de Brasília, Brazil (2009). His research focused on problems in mathematical physics, quantum fields, astrophysics, cosmology, and gravitation. Also, he is performing studies in rocket science and robotics focused on undergraduate engineering projects as well as activities in teaching physics and astronomy to a broader audience through institutional extension projects. He is currently a full professor at Federal University of Latin American Integration and collaborator researcher at Casimiro Montenegro Filho Astronomy Center (Technological Park of Itaipu).

Contents

Preface

The modern cosmology has been turned into an outstanding field of active research through the years. Historically, since its origin as a search of understanding the universe came from a mythological, religious, or philosophical point of view, the cosmology depended from essentially what culture, society, and/or what time we are referring to. It was not considered strictly speaking as a *natural science* rather than a philosophical thinking about the world we are living in. The breakthrough occurred in the sixteenth century with Galileo Galilei and his enhanced version of telescope and the finding of new ways of not only thinking about the natural world but new ways *to see* the world. Accordingly, the scenario radically changed in the beginning of the twentieth century. To get this far, it is important to note that this development has been long in the making. This is a fine example of the scientific *way of thinking* and its *modus faciendi* as a human construction of knowledge. More importantly, any advance comes from a collective work and collaborative spirit since our generation is embedded in the greatest challenging issues of scientific history. For instance, we cite seminal works from Henrietta Leavitt with the observations of variable stars, Albert Einstein's general relativity, Friedman's metric launching the basics of the standard cosmological model of an expanding universe, Vesto Slipher with the measurements of radial velocities of galaxies and the use of spectroscopy for astronomical observations that led to the finding of galactic redshift, Edwin Hubble's expanding universe, and Fritz Zwicky's anomalies in velocities of the clusters of galaxies that were not predicted by Newtonian theory of gravity. Today, such anomaly is called *the dark matter problem*. This was reinforced by Vera Rubin's observations in spiral galaxies in the 1970s also showing a huge discrepancy of Newton's law to observations and further developments in both theoretical and observational methods from generations of scientists.

Particularly, in the last two decades, we have an intense growth of scientific interest in cosmology due to the improvement of observational instruments of astronomical science, which motivated theoretical advances from the necessity to deal with the resulting huge amount of scientific data that should be taken into account, analyzed, and properly justified. Accordingly, cosmology as a discipline turned to be a scientific ground-based branch of physics. Today, we have more scientific data in modern cosmology (and also astronomy and astrophysics) than we could get rid of it, which makes the present days an exciting era for scientific knowledge.

In 1998, we have the discovery that our universe is not only expanding but expanding in an accelerated way. The currently simpler explanation to this effect is that the universe is fulfilled with a negative pressure fluid (regarded as fluctuations of the quantum vacuum energy density) producing some sort of *dark energy* that drives the universe to speed up. Of course, this is just one of the explanations for the accelerated regime of the universe, which has been

confirmed again by the recent Planck mission (European space agency) in their last report in 2015. Accordingly, more effort is currently made to understand the physics of the so-called dark sector. Intriguingly enough, roughly 4% of the universe is barely known, and the rest is not properly explained by the standard particle physics or cosmology, and new fresh modes of perception are needed.

More recently, we had an incredible technological advance from the discovery of gravitational waves in the Laser Interferometer Gravitational-Wave Observatory (LIGO) confirming Einstein's prediction. It has given to scientific community a brand new open arena for physics and several areas, particularly on the understanding of black hole physics, another challenging problem on gravitational physics and astrophysics.

The title of this book could be no other. The chapters presented discuss different aspects of cosmology pointed out by some experts in different areas. This book is divided into three sections with related chapters. The first section is devoted to cultural aspects of cosmology in which, as a human construction, it influenced other human activities such as arts, philosophy, and politics during the human history. The subsequent chapters are intended to discuss technical scientific advances in the field with capital themes today as the problems of the physics of dark sector (dark matter and dark energy problems), black holes, galaxies, large structure formation, and particles. In fact, it shows our endless searching for better understanding of the universe, and it remembers the human odyssey that is a journey of knowledge as a legacy for next generations. It has been a great opportunity to work with InTech's editorial team and such an honor to read all the chapters proposed by professional researchers in the field.

Abraão Jessé Capistrano de Souza,
Federal University of Latin American Integration,
Casimiro Montenegro Filho Astronomy Center
(Technological Park of Itaipu),
Brazil

Section 1

Cosmology and Culture

Chapter 1

The Importance of Cosmology in Culture: Contexts and Consequences

Nicholas Campion

Additional information is available at the end of the chapter

http://dx.doi.org/10.5772/67976

Abstract

Scientific cosmology is the study of the universe through astronomy and physics. However, cosmology also has a significant cultural impact. People construct anthropological cosmologies (notions about the way the world works), drawing in scientific theories in order to construct models for activities in disciplines, such as politics and psychology. In addition, the arts (literature, film and painting, for example) comment on cosmological ideas and use them to develop plot lines and content. This chapter illustrates examples of such work, arguing that scientific cosmology should be understood as a significant cultural influence.

Keywords: cosmology, culture, politics, psychology, literature, film, space travel

1. Introduction

Modern scientific cosmology is valuable in itself for what it reveals about the nature of the cosmos we inhabit [1]. It is a demonstration of the power of modern science to transform our understanding of who we are and where we came from. However, most cosmologists focus on scientific questions and are not fully aware of the impact of cosmological theories on culture, including politics and the arts. This chapter introduces this wider context on the basis that both scientists and the public should be aware of the broader importance of their work and its influence on the way we think. Cosmologists often rely on the fascination the subject brings: as Rowe observed in his textbook way back in 1968, 'In the fields of astronomy and cosmology we live in a period of excitement' [2]. Cosmology therefore both impacts culture and is described and represented by it. This chapter explores some ways in which this happens. As Muriel Rukeyser wrote, 'The universe is made of stories, not of atoms' [3]; see also Impey [4].

If we select four fundamental causes of changes in our perceptions of the world in the last century, then they would be first relativity, second quantum mechanics, third the expanding universe and fourth, the space programme. The first three date from a fairly narrow time band, if we date special relativity from 1905, general relativity from 1915, that the universe is expanding and is much bigger than previous thought from Edwin Hubble's publications from 1924 to around 1930 and quantum mechanics from Niels Bohr and Werner Heisenberg's formulation of the Copenhagen interpretation in 1925–1927 [5]. This epic revision of scientific knowledge of underlying structures of the universe was therefore concentrated into just a quarter of a century. The dramatic period of the human space programme was concentrated into just over 8 years from the first human space flight in 1961 to the Moon landing in 1969.

All have fundamentally altered the way that we think about life here on Earth. Often these changes are taken for granted. For example, mobile phone technology, dependent as it is on satellite networks, is transforming not only the social lives of teenagers in the west, but also the economic muscle of poor farmers across the third world. Meanwhile, super-fast quantum computing makes use of phenomena such as entanglement and is driving the development of artificial intelligence, and hence of robotics. The implications for society over the next few decades are potentially enormous. The most important conclusion to be drawn from this combination of revolutionary changes is the role of the observer: as the basis of differing perspectives of time and space in relativity, an influence on the world (at least, at the sub-atomic level) in quantum mechanics, and the witness for the first time, of the spherical earth, hanging in space, in photographs taken by Apollo astronauts in 1968. Such ideas and experiences have decisively underpinned modern ideas that one person's complete individual experience or perception is as equally valid as anyone else's. Einstein is held particularly responsible for these ideas [6, 7] as a result of popular equations between relativity on the one hand, and cultural relativism (the idea that no one culture is superior or inferior to another) on the other. Moral relativism (the idea that no one culture is morally superior or inferior to another) is controversial and widely rejected, but cultural relativism does have beneficial scholarly consequences. This is especially the case in the new field of cultural anthropology in which academic rigour requires that in order to better understand other cultures, researchers must abandon any idea that one culture is superior or inferior to another.

2. Defining cosmology

The term cosmology can be traced to the 1730s, although its appearance in a scientific sense dates from only after the Second World War [8]. The *logos*, which is the root of 'logy', means 'an account', so that, as a preliminary working definition, cosmology is simply 'an account of the cosmos'. The primary Latin equivalent of the Greek *Kosmos* is *Universus*, from *Unus verto*, or 'changing into one', thereby suggesting unity. We can divide the definitions of cosmology into two: the scientific and the anthropological. The scientific are perhaps the more familiar, but even here there is variation. Scientific definitions range from the narrow, such as 'the study of the universe' [9], to the broad ('the science, theory or study of the universe as an orderly system, and of the laws that govern it; in particular, a branch of astronomy that deals with the

http://dx.doi.org/10.5772/67976

structure and evolution of the universe') [10]. The idea that cosmology is synonymous with astronomy is widespread [2, 11]. Yet the relationship between astronomy and cosmology is not settled, and Hawley and Holcomb [9] argue that cosmology is a separate discipline, which combines features of both astronomy and physics. There are other places where disciplines overlap. For example, astronomy has to include geophysics precisely because the Earth itself is in space [12].

Anthropological cosmologies are based on the proposition that ideas about the cosmos are integral part of human cultural and social systems. For example, the archaeologist Timothy Darvill talks of a cosmology as being, 'The world view and belief system of a community based upon their understanding of order in the universe' [13]. George Gumerman and Miranda Warburton argued that '… to truly comprehend a culture we must have some sense of its cosmology – the group's conception of themselves in relation to the heavens' [14]. And without diminishing the scientific status of modern cosmology, ideas do not come from theory and experiment alone, but can be inspired by wider cultural influences, as Holton [15] illustrates in relation to Einstein's reading and education before he formulated the theory of special relativity. Heisenberg [16] actually argued that science and art are parallel attempts to describe the world, and may both be part of a wider cultural picture. Bell [17] then talks of 'complex subsystems of cosmic exchange' which underpin mundane systems of behaviour, such as socio-economic exchange, but are designed to reinforce individual and social existence within the cosmos.

3. Defining cosmology

The philosopher Terry Eagleton concluded, '"Culture" is said to be one of the two or three most complex words in the English language' [18]. A good working definition, though, is offered by the anthropologist Clifford Geertz, who argued that culture is 'an historically transmitted pattern of meanings embodied in symbols, a system of inherited conceptions expressed in symbolic forms by means of which men communicate, perpetuate and develop their knowledge of and attitudes toward life' [19]. The influence of cosmology on culture then becomes a matter of exploring its impact on political and religious ideas, and its use in the arts, perhaps mainly in literature, painting and film. Michael Rowan-Robinson wrote that 'the intellectual horizon of the human race at any time has always been inextricably bound up with the scale of the universe… there can be little doubt that a people's perceived scale of the universe must play a fundamental role in its culture and consciousness' [20]. He could equally have said that culture and consciousness are bound up with conceptions of the universe as a whole. It was Einstein himself who made the case for the cosmologist intervening in culture. In 1936 he wrote, 'the physicist cannot simply surrender to the philosopher the critical contemplation of the theoretical foundations' of the universe, and 'the critical thinking of the physicist cannot possibly be restricted to examination of his own field. He cannot proceed without considering critically a much more difficult problem, the problem of analysing the nature of everyday thinking' [21]. Mostly the cosmologist does not intervene directly in modern culture. Instead other people interpret and represent cosmological ideas.

4. Politics

Cosmology has had a substantial impact on political theory and continues to do so. We can therefore talk about 'political cosmology' [22]. The earliest recorded societies used the stars or planets to represent their rulers or guide their actions, functions which tended to overlap with religion. The Egyptians and Inca saw their rulers embodied in the Sun, the Chinese in the Pole Star, and in Babylon the chief god, Marduk, was represented by Jupiter. On a practical level, most pre-modern cultures structured their religious sanctuaries, and sometimes their urban communities, according to their conceptions of the cosmos. Hence we may speak of 'cosmopolises' or 'cosmograms'. A 'cosmic state' is one in which the entire state is organized to embody the structure of the cosmos.

The significant step into modelling politics on the cosmos as an organised system was taken by the Greek philosopher Plato (ca. 428/7?–348/7). Plato's cosmos emanated out of a single consciousness which existed in a realm of unchanging eternity. The material world was then an imperfect representation of the world of Ideas (Plato spoke of the physical world being embedded in the world-soul) and was governed by time, the mathematically regulated, harmonious rhythms measurable by the motions of the planets. Plato's mathematical universe provides a rationale for scientific speculation to the present day [23, 24].

Plato advocated an education emphasising such subjects as music, mathematics and geometry, and a political system based on rule by philosophers, all designed to harmonise society with the cosmos, for the common good. This concept of the perfect society underpins the entire history of utopianism down to the present day. There were two main consequences of Plato's system, with consequences down to the present day. First, the perfect ruler was envisioned as the Philosopher King, whose right to rule was justified by his wisdom and understanding of cosmic principles. Second, the system tended to be authoritarian because, being founded on cosmic principle, it could brook no opposition. Plato's ideas were revived in Renaissance Europe and were to become extremely influential. The notion of human history as the progressive unfolding of the world soul towards a final, perfect condition was central to the ideas of Georg Friedrich Hegel (1770–1831). Hegel's influence on Karl Marx (1818–1883) led the twentieth century philosopher of science, Popper [25], to see Plato's thought as the foundation of modern totalitarianism: where Plato influenced Marx, via Hegel, was in the notion that history has an inescapable trajectory, founded in the structure of the cosmos itself. For revolutionary Marxists, such as Lenin, Stalin and Mao Tse-tung, it was then inconceivable that anyone could oppose their rule, for to do so was to oppose the cosmos.

Separate to the platonic strand in European political cosmology, the astronomical discoveries from Copernicus onwards all helped shape western politics. Copernicus' argument that the Sun, not the Earth, is the centre of the universe (or the solar system as we would now say) was attached to the ancient idea that the Sun is associated with kings. It was then used to support claims that, just as the entire universe orbits the Sun, so the whole of society orbits the king [26]. Propaganda in support of absolute monarchy then reached its height in the iconography of the French king Louis XIV. Such authoritarian ideas were directly countered by what I have called Political Newtonianism [22]. This held that, just as Newton had argued that one law

http://dx.doi.org/10.5772/67976

governed the whole universe, so the same principle must apply to terrestrial affairs and one law must govern the whole of human society. In principle, then, all people were equal, and there was no justification for monarchy. Such ideas were influential among both the American revolutionaries of 1776 [27] and the French in 1789.

Newtonianism was taken one step further by Auguste Comte (1798–1857), the founder of sociology. Adding Galileo and Kepler to Newton as sources of authority, Comte [28] argued that if the entire universe was a mathematically regulated mechanism, so human society must also be governed by the same principle. If planets moved in mathematically determined patterns, Comte reasoned, so must people. By collecting and analysing data on human behaviour, Comte concluded, the same laws that controlled the wider universe should be discovered in human affairs. And in turn the state, governed by experts who were the modern equivalent of Plato's philosophers, could be managed for the good of all. This remains the foundation of twenty-first century sociology.

There have been a few attempts, for example, to identify Einsteinian relativity either as a form of political discourse, or to draw political implications from it. As far as the former is concerned, I refer to the French feminist and social theorist Luce Irigaray who has identified the theory of relativity as a political rather than scientific formula [29]. Sokal and Bricmont [28], meanwhile, noted how the notion of relativity in time and space was used by postmodern theorists in order to advocate cultural relativity on the grounds that, if the universe has no single centre, neither does culture.

The anthropologist Falzon [30] has defended multi-sited ethnography against the charge of lack of depth by arguing that it takes into account shifting perceptions of space and time. The anthropologist Marcus [31] refers to 'space-time compression', in which the essential difference between space and time contracts in light of the recognition that both are socially produced as a result of what Falzon calls 'a product of interrelations'; Marcus derived his understanding from special relativity, and so directly from his understanding of Einstein. Elsewhere, Einstein's call for humanity in general to take on the implications of the new cosmology has been used to advocate a collaborative global order in which international problems are solved thought global institutions rather than war [32].

5. Psychology

The consequences of Newtonianism (the belief that the entire universe is mathematically regulated) permeate western thought wherever there has been a search for a universal law based on supposedly hard data. Psychology is a prime example. When the word 'psychology' was coined around 1800, it was thought that, since Newtonian science explained everything that exists and occurs in the material world, there could and should be just one science explaining what exists and occurs in the psychological world. As Gilbert Ryle wrote, '"Psychology" was supposed to be the title of the empirical study of "mental phenomena"', a counterpart to Newtonian celestial mechanics [33]. Concepts such as normality and deviation have dominated some of the major schools of western psychology, their roots in Newtonian cosmology's

devotion to predictable order unrecognised and forgotten. The measurement and mathematical analysis of the human mind then became the basis of much psychiatry and academic psychology. Even the notion developed by Sigmund Freud (1856–1939), that psychic—or psychological—material can be 'repressed', as if by some kind of downward pressure, is derived from Newtonian mechanics through the influential German physicist Hermann von Helmholtz (1821–1894) [34]. The goal of Freudian psychoanalysis is for the patient to become aware of such repressed material through the so-called talking cure, the conversations which take place during sessions with the psychoanalyst, thus releasing in downward pressure.

Freud's student C.G. Jung opened a radically different strand of thought in modern psychology which is highly influential in many schools of psychotherapy and counselling practiced in society as a whole, although usually outside the academic system. Jung revived the Platonic theory that everything in the world is a manifestation of an original pure idea or archetype. Jung's system, known as analytical psychology, adheres to a kind of archetypal philosophy in which all psychological types correspond to an archetype, such as the eternal youth (the puer aeternus), anima (female principle) or senex (wise old man), which exist in the collective unconscious, Jung's update of the Platonic world-soul. The aim of Jung's therapeutic model is for the individual to become truly themselves by recognising the role of the archetypes in their lives and, in effect, understanding their true connections to the cosmos. The idea that one can become one who truly is also relates back to Aristotelian cosmology in which it was thought that the four elements (fire, earth, air and water) all try to find their natural place in the world. This, Aristotle thought, was why flames go up to the sky, where fire belongs, and water falls to the ground, because that is where it finds its natural home. In Aristotelian politics, kings are at the top of society and peasants at the bottom, because that is the natural state of affairs; in Aristotelian psychology every individual then has a natural way of being. Jung, though, was equally concerned with the latest science, and formed a collaboration and friendship with the quantum physicist Wolfgang Pauli (1900–1958) [35]. Together they formulated the concept of synchronicity by which meaningful events are connected because they take place at the same time, without any causal connection [36]. Newtonian psychology—the belief that all mental states can be measured—survives in university departments and psychiatry. But in the wider world, where increasing numbers of people seek counselling and psychotherapy, Einstein is taken as the inspiration for the argument that therapists and analysts must be 'less concerned with the basic nature of time and more with the human experience of it' [37].

6. Literature and film

One of the major genres of writing in western culture goes under the name 'celestial journey literature', derived from ancient texts on the soul's journey. The soul's journey was secularised in Dante's (1265–1321) 'Divine Comedy' [38]. Inspired by Plato's myth of Er, Dante is guided by the poet Virgil and his love, Beatrice, through the spheres of Hell, Purgatory and Paradise (Hell and Purgatory are structured in spheres analogous to the spheres on which the planets and stars orbit). The last great example of the celestial journey of the soul or a dream world was Johannes Kepler's 'Somnium', an account of lunar astronomy written in 1608 but published in 1634,

http://dx.doi.org/10.5772/67976

and sometimes referred to as the first work of science fiction. The genre took a decisive step forward in Francis Godwin's 'Man in the Moon' [39], published in 1638. Like Dante, Godwin used his story to describe the structure of the cosmos, now, after Johannes Kepler and Galileo, rejecting the planetary spheres and challenging the Aristotelian idea that all things have their natural place. Godwin departed from the old idea of a journey of the soul or a dream world. Instead, his hero, Gonzales, flies to the Moon carried by giant geese. From Godwin onwards the celestial journey becomes physical, arriving at the Moon rocket in Jules Verne's 1865 novel, 'From the Earth to the Moon'. Verne's book was one of the inspirations for what may be the first space film, Georges Méliès' 'Le Voyage dans la Lune'—in English 'A Trip to the Moon'—after which astronomy and cosmology have a regular presence in film culture [40]. In Méliès' film, the astronomers encounter the inhabitants of the Moon, known as Selenites, in what is clearly a parable for European colonialism: the film was released midway through the so-called 'Scramble for Africa', the final face of the European take-over of Africa from the 1880s to 1914. From Méliès on, the major celestial journey novels have often been filmed. Perhaps the most famous is Stanley Kubrick's film of Arthur C. Clarke's '2001: A Space Odyssey'. Clarke's metaphysical story is vividly portrayed first through the transition from ape to human, and then, in the final scene, the transformation of the dying astronaut into the star child. Accompanied by the stirring music of Wagner's 'Also sprach Zarathustra', Kubrick created a vivid evocation of both ancient beliefs in the soul's ascent to the stars and modern ideas that human destiny may take us to realms beyond our current imagination.

While celestial journey films can be enjoyed as simple adventures, they often contain deeper meanings. The 1951 movie 'The Day the Earth Stood Still' exploited the current public interest in Flying Saucers. Released at a time when the Cold War was reaching its height with the conflict in Korea, the story featured a wise alien who arrived from space in order to reveal to humanity the error of its ways. The rejection of the alien's words of wisdom presented a gloomy view of humanity as incapable of solving its problems. Cosmology, through film, then becomes a means of commenting on societal change. 'Star Trek', the biggest celestial journey TV franchise of them all, was launched in 1966. 'Star Trek' was altogether more sophisticated than 'Lost in Space' and was entirely more optimistic. It is set in a utopian future in which there is one world government, collaborating with other worlds through United Federation of Planets, and money has been abolished. In the crew's adventures, the European voyages of the fifteenth and sixteenth centuries are replayed in a universe of an infinite number of galaxies, except that now alien cultures are to be respected and preserved rather than conquered and destroyed. The values espoused by the Federation were American: freedom from tyranny, freedom of expression and respect for minorities. Compared to 'Star Trek', the blockbuster film franchise, 'Star Wars', launched in 1976 and still going strong forty years later, projects into space a simpler version of the endless struggle for freedom against an evil empire, very much an update of anti-Nazi war films. In all such cases the cosmos is seen as a blank slate, a tabula rasa, on which human concerns are imposed.

There is a constant strand of literary comment on cosmology in the nineteenth century. Edgar Allan Poe (1809–1849), often known as the author of the first detective novel, wrote a remarkable work which he called 'Eureka' [41], deliberately suggesting an imaginative breakthrough in the understanding of the cosmos. Poe realised that in a Newtonian universe the stars are

likely to collapse in on each other, and that therefore the universe must be evolving [42]. Thomas Hardy (1840–1928) was as fascinated by cosmology as Poe, but unlike him lived to see the publication of Darwin's 'Origin of Species' in 1959 (when he was just 19). For Hardy evolution was a reality. He combined his encyclopaedic knowledge of myth, astronomy and cosmology into a 'moral astrophysics' [43] which provided the background for the individual conflicts and tragedies in novels such as 'Far from the Madding Crowd' (1874) and 'Tess of the d'Urbervilles' (1891/1892). Virginia Woolf (1882–1941) used Edwin Hubble's discovery of the expanding universe in the 1920s as a metaphor for personal and political insecurity in the 1930s. In Woolf's view, as we all live together on the same delicate, vulnerable planet in a vastness of space, it is incumbent upon us to live together rather than fight [44]. The Marxist playwright Bertolt Brecht (1898–1956) looked back to an earlier cosmology but equally wanted to illustrate a modern point in his 1938 play, 'Galileo'. His portrayal of Galileo as the heroic intellectual defending Copernicus, struggling against an obscurantist Inquisition (inaccurate because many in the senior Catholic hierarchy were Copernicans), was an allegory of the revolutionary struggles of the 1930s.

One of the other familiar tropes derived from modern cosmology is time travel, a topic rarely dealt with in 'Star Trek', in spite of the regular use of faster-than-light travel. There is now a considerable literature which draws on Gerald Feinberg's 1967 paper 'Possibility of faster-than-light particles', which proposed the existence of the tachyon [45]. This hypothetical particle, the tachyon, might as Martin Rees [46], says alter the order of events, if a signal from a tachyon arrived before it was sent. The genre's earliest notable example was Wells' novel 'The Time Machine' (1895) [47]. Wells coined the phrase time machine to describe a time-travelling vehicle which moved because the fourth dimension was of time rather than space. Wells was a utopian socialist and his main preoccupation was to explore varieties of human society, considering whether progress inevitably resulted in human improvement: it's clear that he didn't think that this was the case, and that ignorance and superstition could easily flourish in the future. Neither does 'Dr Who', the most successful TV time travel franchise, explain how it is possible to travel to the distant past or future. The time machine, the TARDIS (short for Time and Relative Dimensions in Space), is bigger inside than outside and references Einstein by referencing relativity in its name. The Doctor himself is increasingly represented as a lonely figure, destined to exist in perpetual sadness caused by the death or departure of his companions.

The concept of alienation is developed by Alan Lightman in his 'Einstein's Dreams' [48], a journal set in 1905—the 'annus mirabilis' when Einstein developed the theory of Special Relativity. Lightman's character experiences the alienation of a world in which any particular point in space-time is delicate, temporary and liable to vanish, an 'exile in time' [48]. In a later entry, Lightman's diarist writes 'There is a place where time stands still. Raindrops hang motionless in air. Pendulums of clocks float mid-swing' [49]. At the centre of space-time nothing moves. The concept that all time exists simultaneously actually has a long lineage. It is central to Plato's cosmology, occurs in the Bible (Ecclesiastes 3.15), and was elaborated by St. Augustine (V.9) in the fifth century [50]. He described a universal paradox whereby even if a future event in our individual lives already exists, it depends on an act of our free-will in order to take place. T.S. Elliot, impressed by Einstein, combined the lessons of relativity with

http://dx.doi.org/10.5772/67976

Plato, Ecclesiastes and Augustine. Following Einstein's English visit in 1921, the year he won the Nobel Prize, Elliot wrote, 'Einstein the Great has visited England (and) has taken his place in the newspapers with the comet, the sunspots, the poisonous xxx-jellyfish and octopus at Margate, and other natural phenomena' [51].

In two poems composed in the 1930s, and published in 1941–1942, Elliot considered the conundrum of time for the human condition. In 'Burnt Norton' he wrote that 'All time is unredeemable', for if the past exists in the future and the future exists in the past, all possibilities are eternally present, and in 'East Coker' he wrote the famous line 'In my beginning is my end' [52]. Elliot's speculations on time were shared by Priestly in such metaphysical plays as 'Time and the Conways' (1937) and, perhaps his most famous work, 'An Inspector Calls' (1947), in which a detective from the future extracts confessions of guilt for a poor girl's suicide from a comfortable middle class family. Priestley's immediate inspiration was Dunne's [53] work on time, which drew on Einstein (a cautiously supportive note was included by Arthur Eddington in the appendix to the third edition) in order to explain why the future could be predicted by precognition.

The popular end of such speculation is best represented by the collected works of Philip K. Dick (1928–1982). Like Elliot, Dick was inspired by ancient philosophy and modern science, especially the conclusions of quantum mechanics as expressed in Heisenberg's uncertainty principle and Erwin Schrödinger's famous thought-experiment with the cat (1935), ideas responsible for modern multi-verse theory. If one cannot tell both where a particle is and where it is travelling to, whether it is even a particle at all (or a wave), and how far the act of observing it has altered its state, how can one ever trust what appears to be real. For example, in the 'The Cosmic Puppets' (1957), an ordinary suburban couple return to their hometown after a gap of several years to find that everyone and everything has changed, and nobody recognises them. The novel then shifts into a traditional religious mode, located in the Zoroastrian (Persian) struggle between the good god Ormazd and his evil rival Ahriman. Eventually Ormazd triumphs, the illusory world created by Ahriman is removed, and reality returns. In Dick's award-winning counter-factual history, 'The Man in the High Castle' (1962), the ability of the observer to act on—and change—the material world is described via the lead characters' use of the Chinese oracle, the I Ching, to alter the future.

Dick's intensity is absent from the most whimsical of recent cosmological fiction, that of Italo Calvino (1923–1985). Calvino took cosmological ideas and exaggerated them until they were absurd. His short story, 'The Form of Space' (2002), points out that if one fell in curved space, one would logically fall for ever, while 'the Distance of the Moon' imagines a time in the distant past when the Moon was closer to the Earth, close enough for people to jump up to it and gather such delicacies as Moon-milk.

7. The visual arts

Representations of the sky, stars or cosmos in visual form date back to the Stone Age and are familiar throughout the ancient world. They may be symbolic, as in Egyptian

astronomical-ceilings, or take on human form, as in Roman images of planetary deities. Later they might be decorative, as in Renaissance star maps, or attempt accuracy, as in modern star maps, or be entirely abstract, as in twentieth century surrealism. The Sun and Moon make regular appearances in western painting, as one would expect. The cosmological statements, though, are often simple. Often the Sun and Moon are poetic additions, symbolising time or heaven in medieval and Renaissance art, casting light or embodying the power of nature, and even serve as political satire in the nineteenth century [54]. Cosmological changes encouraged the new spirit: the philosopher Berlin [55] argued that the astronomical revolution's abandonment of the old crystalline planetary spheres in favour of a universe without boundaries encouraged the emergence of the chaos and adventurism of Romantic art. Painting began the shift towards the abstract with the extraordinary work of Joseph Turner, who drew on both esoteric wisdom and the latest science in his portrayal of light [56, 57]. Perhaps the most famous example of nineteenth century astronomical art is van Gogh's 1889 masterpiece 'The Starry Night', a painting partly inspired by the pre-dawn rising of Venus, but easily interpreted as representing the swirling chaos of van Gogh's inner world.

The relationship between modern art movements and science is complicated by many artists' multiple affiliations. For example, many notable early twentieth century painters were followers of Theosophy, a spiritual teaching highly indebted to Plato, Renaissance alchemy and Freudian psychoanalysis, all of which could deal with unseen realities and the interdependence of all things in the cosmos. It is therefore not easy to distinguish scientific influences on twentieth art from mystical or magic ones and it is up to art historians to interpret [58]. However, it is clear that the new physics encouraged the move towards radical, abstract forms of expression. Heisenberg's uncertainty principle appears to have supported the playful, apparently chaotic, practices of Dada, in which nothing is quite as it seems. When Marcel Duchamp (1887–1968) displayed a urinal in 1917 he was making a radical statement that, if art is not what one imagines it is, neither is anything else.

André Breton (1896–1966), the poet and author of the Surrealist Manifesto, singled out Einstein (along with Freud) as significant in 1922. J.W. Dunne's adaptation of Einstein to precognition and psychology was popular with the surrealists, as it as with Priestley. That the observer stands at the centre of time and space, as popular conceptions of relativity and quantum mechanics assume, underpins the playful juxtaposition of images and ideas, sense and nonsense, which runs through the entire history of modern abstract and conceptual art. When Joan Miro paints a picture such as 'Dog barking at the Moon' (1926), he is alluding to ideas that the Moon makes one mad— lunatic—as well as departing significantly from naturalism, but also raising a smile.

A separate strand of painting drew on mathematical conceptions of the universe, as did Duchamp's earlier painting 'Nude Descending a Staircase' (1912), or Man Ray's (1890–1976) geometrical models, such as 'Polyèdres' (1934–1936). The distinctive angular lines of Picasso's painting were also decisively influenced by the idea of multi-dimensional mathematics as explained by Miller [59]. By contrast, the whirling lines in Max Ernst's '…sur le plan de la Physique' (1943) evoke the spinning of atoms. And for Klee [60], writing in 1920, movement in painting was essential because everything in the universe is characterised by motion.

http://dx.doi.org/10.5772/67976

Perhaps the most famous portrayals of the new physics are Salvador Dali's (1904–1989) paintings of bent clocks as representations of distorted space-time, as in 'The Persistence of the Disintegration of Memory' (1952).

8. Space flight

It is well understood that the photographs of the whole Earth taken by the Apollo astronauts encouraged concepts of the global village, a world devoid of racial divisions, religious schism and political boundaries [61, 62]. The first major use of the Apollo photographs was on the cover of the first Whole Earth Catalogue in 1968, placed there by the editor, political activist Stewart Brand. Subsequently, the photographs became an inspiration for the emerging environmental movement.

Since 1968/1969 we have been able to look down on our sky from space. The euphoric consequences of this experience, still enjoyed by a few hundred people, was named the 'Overview Effect' by Frank White in 1987 [63]. Interviewed on BBC Radio 4's iPM programme on 25 May 2013, the astronaut Geoff Hoffman described his own experience of the effect [64]. He recalled the strange sensation of looking down at the Earth, watching the terrestrial sky from above instead of from below, witnessing the flash of lightning storms and streaks of light as meteors plunged into the atmosphere. He saw the world as one, drawing salutary ecological lessons from the visible deforestation of tropical areas. Inspired by the ethereal nature of the Earth's halo, Hoffman hesitated to use the word 'spiritual', put to him by his interviewer in a leading question, but was happy to describe the condition he experienced on his mission as being a 'state of grace', words which he said had been suggested to him by a Jesuit priest. Shamans, Pharaohs and Platonic souls may have seen the Earth in their imaginations, but astronauts experience it physically.

The 'Overview Effect' has been institutionalised in the Overview Institute, whose purpose is to utilise the Effect for the common good. The Institute's apocalyptic and utopian agenda draws a direct connection between the experience of space travel and the need to save the Earth: 'We live at a critical moment in human history. The challenges of climate change, food, water and energy shortages as well as the increasing disparity between the developed and developing nations are testing our will to unite, while differences in religions, cultures, and politics continue to keep us apart. The creation of a 'global village' through satellite TV and the Internet is still struggling to connect the world into one community. At this critical moment, our greatest need is for a global vision of planetary unity and purpose for humanity as a whole' [65]. In this sense, the institute completes the earlier visions of Virginia Woolf and Stewart Brand.

9. Conclusion

Modern scientific cosmology needs to be valued not just for what it tells us about the universe, but for how what it tells us informs the ways that people think and behave in wider culture. A

number of themes emerge, including the vastness of space as a metaphor for loneliness and insecurity, and the new physics as a source of freedom and adventure. Scientific cosmology's wider significance needs to be more widely acknowledged, for modern society still benefits from 'complex subsystems of cosmic exchange' between scientists —cosmologists—and the general public.

Author details

Nicholas Campion

Address all correspondence to: n.campion@tsd.uwtsd.ac.uk

University of Wales Trinity Saint David, Swansea, Wales, UK

References

[1] Campion N. Cosmos and Cosmology. In: Segal R, Stukrad K, editors. *Vocabulary for the Study of Religion*. Leiden: Brill; 2015. pp. 359–364.

[2] Rowe AP. *Astronomy & Cosmology*. London: Thames and Hudson; 1968. pp. 2–9.

[3] Rukeyser M. The Speed of Darkness, IX. In: *The Collected Poems of Muriel Rukeyser*. 1992. Available from: https://www.poetryfoundation.org/poems-and-poets/poems/detail/56287 *[accessed: 06-02-17]*

[4] Impey C. *How it Ends: From You to the Universe*. New York: W.W. Norton and Co; 2010, p. 11.

[5] Heisenberg W. *The Physical Principles of the Quantum Theory*. New York: Dover Publications; 1998 [Chicago: Chicago University Press; 1930].

[6] Isaacson W, Schucking EL. *Einstein: His Life and Universe*. New York: Simon and Schuster; 2007. pp. 278–279.

[7] Johnson P. Modern Times: the World from the Twenties to the Nineties. New York: Harper Collins, 1991. p. 3–5.

[8] Kragh HS. *Conceptions of Cosmos. From Myths to the Accelerating Universe: A History of Cosmology*. Oxford: Oxford University Press; 2007. p. 1.

[9] Hawley JE, Holcomb KA. *Foundations of Modern Cosmology*, 2nd ed. Oxford: Oxford University Press; 2005. pp. 4–5.

[10] Hetherington ND. *The Encyclopaedia of Cosmology: Historical, Philosophical and Scientific Foundations of Modern Cosmology*. Oxford and New York: Routledge; 1993. p. 116.

[11] Freedman RA, Geller RM, Kaufmann III WJ. *Universe*. 10th ed. Basingstoke: W.H. Freeman and Company; 2014. p. 15.

[12] Rowan-Robinson M. *Ripples in the Cosmos: A View Behind the Scenes of the New Cosmology*. Oxford: W.H. Freeman and Company; 1993. p. 25.

[13] Darvill T. Archaeology. In: *Concise Oxford Dictionary of Archaeology*. Oxford: Oxford University Press; 2008.

[14] Gumerman GJ, Warburton M. The Universe in a Cultural Context: An Essay. In: Fountain JW, Sinclair RM, editors. *Current Studies in Archaeoastronomy: Conversations Across Time and Space*. Durham NC: Carolina Academic Press; 2005. pp. 15–24.

[15] Holton G. Einstein and the Cultural Roots of Modern Science. *Daedalus* 127.1. 1998; 1–44.

[16] Heisenberg W. *Physics and Philosophy: The Revolution in Modern Science*. London: Allen and Unwin; 1958. pp. 97–98.

[17] Bell C. *Ritual: Perspectives and Dimensions*. Oxford: Oxford University Press; 1997. p. 122.

[18] Eagleton T. *The Idea of Culture*. Oxford: Blackwell; 2000. p. 1.

[19] Geertz C. *The Interpretation of Cultures*. New York: Basic Books; 1973. p. 89.

[20] Rowan-Robinson M. *The Cosmological Distance Ladder: Distance and Time on the Universe.* New York: W.H. Freeman and Company; 1985. p. 1.

[21] Einstein A. Physics and Reality. *The Journal of the Franklin Institute* 221.3. 1936; 349–382.

[22] Campion N. Astronomy and Political Theory. In: Valls-Gabaud D, Boksenberg A, editors. *The Role of Astronomy in Society and Culture*, International Astronomical Union Symposium 260; 19–23 January 2008; UNESCO, Paris. Cambridge: Cambridge University Press; 2011. pp. 595–602.

[23] Penrose R. *The Emperor's New Mind: Concerning Computers, Minds and the Laws of Physics*. London: Vintage; 1991. p. 554.

[24] Penrose R. *The Road to Reality: A Complete Guide to the Laws of the Universe*. London: Vintage Books; 2005. pp. 11–12.

[25] Popper K. *The Open Society and its Enemies*, 2 vols. London and New York: Routledge; 1957 [1945].

[26] Hutchison K. Towards a Political Iconology of the Copernican Revolution. In: Curry P, editor. *Astrology, Science and Society*. Woodbridge, Suffolk: Boydell Press; 1987. pp. 95–142.

[27] Becker C. *The Declaration of Independence: A Study in the History of Political Ideas*. New York: Vintage; 1958.

[28] Comte A. *System of Positive Polity: Or, Treatise on Sociology, Instituting the Religion of Humanity*, 4 vols. Bridges JH, translator. London: Longmans; 1875 [Paris 1851–1854].

[29] Sokal A, Bricmont J. *Intellectual Impostures*. London: Profile Books; 1998. p. 100.

[30] Falzon MA. *Multi-sited Ethnography: Theory, Praxis and Locality in Contemporary Research*. Abingdon: Ashgate; 2009. p. 7.

[31] Marcus GE. Ethnography In/Of the World System: The Emergence of Multi-Sited Ethnography. *Annual Review of Anthropology* 24. 1995; 95–117.

[32] Holt RR. Can Psychology Meet Einstein's Challenge? *Political Psychology* 5.2. 1984; 199–225.

[33] Ryle, G. *The Concept of Mind*. Harmondsworth, Middlesex: Penguin 1976; p. 301[p8]

[34] Bernfeld S. Freud's Earliest Theories and the School of Herman von Helmholtz. *The Psychoanalytic Quarterly* 13. 1944; 341–362.

[35] Miller AI. *Deciphering the Cosmic Number: The Strange Friendship of Wolfgang Pauli and Carl Jung*. New York: W.W. Norton and Co; 2009.

[36] Jung CG. *Synchronicity: An Acausal Connecting Principle*. London: Routledge and Kegan Paul; 1972 [1950].

[37] Stadter M, Scharff DE, *Dimensions of Psychotherapy; Dimensions of Experience: Time, Space, Number and State of Mind*. London: Routledge; 2005.

[38] Alighieri D. *The Divine Comedy*, 3 vols. Musa M, translator. Harmondsworth, Middlesex: Penguin; 1971.

[39] Weber A. Changes in Celestial Journey Literature, 1400–1650. *Culture and Cosmos* 1.1. 1997; 34–50.

[40] Garcia B, Reynoso E, Pérez Alvarez S, Gabellone R. Inspiration of Astronomy in the movies: A History of a Close Encounter. Campion N, Sinclair R, editors. *The Inspiration of Astronomical Phenomena*, *Culture and Cosmos* 15.1–2. 2012; 357–371.

[41] Poe EA. *Eureka: A Prose Poem*. New York: Geo. P. Putnam; 1848.

[42] Molaro P, Cappi A. Edgar Allan Poe: The First Man to Conceive a Newtonian evolving Universe. Campion N, Sinclair R, editors. *The Inspiration of Astronomical Phenomena, Culture and Cosmos* 15.1–2. 2012; 225–239.

[43] Gossin P. *Thomas Hardy's Novel Universe: Astronomy, Cosmology, and Gender in the Post-Darwinian World*. Aldershot: Ashgate; 2007.

[44] Henry H. *Virginia Woolf and the Discourse of Science: The Aesthetics of Astronomy*. Cambridge: Cambridge University Press; 2003. pp. 137–138.

[45] Feinberg G. Possibility of Faster-Than-Light Particles. *Physical Review* 159.5. 1967; 1089–1105.

[46] Rees M. *Before the Beginning*. London: Simon and Schuster; 1997. p. 230.

[47] Wells HG. *The Time Machine*. London: William Heinemann; 1895.

[48] Lightman A. *Einstein's Dreams*. London: Bloomsbury; 1993. p. 70.

[49] Lightman A. *The Accidental Universe: The World You Thought You Knew*. London: Corsair; 2014.

[50] Augustine. *City of God*. Bettenson H, translator. Harmondsworth, Middlesex: Penguin; 1972.

[51] Elliot TS. London Letter July 1921. *The Dial*. 1921. Available from: http://www.std.com/~raparker/exploring/tseliot/works/london-letters/london-letter-1921-08.html [accessed 2017-02-05].

[52] Elliot TS. The Four Quartets, 'Burnt Norton' and 'East Coker'. In: *The Complete Poems and Plays*. London: Faber and Faber; 2004.

[53] Dunne JW. *An Experiment With Time*. London: A & C Black Ltd; 1929.

[54] Olson RJM, Pasachoff JM. Fire in the Sky: Comets and Meteors, the Decisive Centuries. In: *British Art and Science*. Cambridge: Cambridge University Press; 1998.

[55] Berlin I. *The Crooked Timber of Humanity: Chapters in the History of Ideas*. New York: Random House; 1991 [1959]. p. 43.

[56] Bullen JB, editor. *The Sun is God: Painting, Literature and Mythology in the Nineteenth Century*. Oxford: Oxford University Press; 1989.

[57] Hamilton J. *Turner and the Scientists*. London: Tate Gallery; 1998.

[58] Parkinson G. *Surrealism, Art and Modern Science. Relativity, Quantum Mechanics, Epistemology*. New Haven CT and London: Yale University Press; 2008.

[59] Miller AI. *Einstein, Picasso: Space, Time and the Beauty that Causes Havoc*. New York: Basic Books; 2001.

[60] Klee P. Creative Confession. In: *Creative Confession and other writings*. London: Tate Publishing; 2013. p. 10.

[61] Cosgrove D. *Apollo's Eye: A Cartographic Genealogy of the Earth in the Western Imagination*. Baltimore MD: Johns Hopkins University Press; 2001.

[62] Campion N. Introduction: Discoursing with the Heavens. In: Campion N, editor. *Heavenly Discourses*. Lampeter: Sophia Centre Press; 2016. pp. xiv–xxviii

[63] White F. *The Overview Effect: Space Exploration and Human Evolution*. Boston MA: Houghton-Mifflin; 1987.

[64] Hoffman G. BBC Radio 4, iPM, 25 May 2013. Available at: http://www.bbc.co.uk/programmes/b01sjn9l [accessed 2016-04-07]

[65] Overview Institute: Declaration of Vision and Principles. Available at: http://www.overviewinstitute.org/index.php/about-us/declaration-of-vision-and-principles [accessed 2013-05-25]

Section 2

Dark Matter Phenomenology

Chapter 2

Constraining the Parameters of a Model for Cold Dark Matter

Abdessamad Abada and Salah Nasri

Additional information is available at the end of the chapter

http://dx.doi.org/10.5772/intechopen.69044

Abstract

This chapter aims at reviewing how modeling cold dark matter as weakly interacting massive particles (WIMPs) gets increasingly constrained as models have to face stringent cosmological and phenomenological experimental results as well as internal theoretical requirements like those coming from a renormalization-group analysis. The review is based on the work done on a two-singlet extension of the Standard Model of elementary particles. We conclude that the model stays viable in physically meaningful regions that soon will be probed by direct-detection experiments.

PACS numbers: 95.35.+d; 98.80.−k; 12.15.−y; 11.30.Qc

Keywords: cold dark matter, light WIMP, extension of Standard Model, rare decays, RGE

1. Introduction

Dark matter accounts for about 26.5% of the total mass-energy density of the Universe [1], but we still do not know what it is. It is called dark because it is not accounted by the visible matter, the conventional baryons and leptons, which take about 4.9% of the total mass-energy density [1]. As it clearly interacts through gravity, some argue that it could still be baryonic, in the form of massive astrophysical compact halo objects (MACHOs) which emit dim or no light [2] or some sort of huge gravitational objects like galaxy-sized black holes. Indeed, such high concentrations of matter would bend passing light, the so-called gravitational lensing phenomenon, including microlensing, in ways we can detect. But the amount of dark matter we know of would produce gravitational lensing with a significantly higher number of occurrences than what observation accounts for.

Neutrinos have long been thought of composing the dark matter around us. However, Standard Model neutrinos are light, and so too fast-moving (hot) to compose the (cold) dark matter

structures we see. But sterile neutrinos, non-Standard Model particles, can be heavier, and so could be dark matter candidates. This possibility has been reignited with the recent detection of an X-ray emission line at an energy of 3.55 keV coming from galaxy clusters, the Andromeda galaxy, the Galactic Center and the Draco dwarf spheroidal galaxy. This line is consistent with the decay of a 7.1 keV sterile neutrino [3].

In fact, there is by now quasi-consensus that dark matter ought to be understood outside the realm of conventional matter. One other scenario is that of (pseudo)scalar particles of tiny mass $\sim 10^{-22}$ eV, the so-called ultralight axions that could account for the dark matter content of the Universe. This is supported by high-resolution cosmological simulations [4]. Axions originated in quantum chromodynamics, the theory of quarks and gluons, in relation to the axial anomaly in this theory and the strong Charge Conjugation Parity Symmetry Violation (CP violation) problem. But like anything else related to dark matter, they elude detection. The Axion Dark Matter Experiment (ADMX) may bring in answers in the near future [5].

But maybe the most popular candidate for dark matter is an electrically neutral and colorless weakly interacting massive particle (WIMP). Such a particle originated in supersymmetric (SUSY) extensions of the Standard Model. The most obvious such a candidate is the neutralino, a neutral *R*-odd supersymmetric particle. Indeed, neutralinos are only produced or destroyed in pairs, thus constituting the lightest SUSY particles. However, alas, as rich, attractive and beautiful as SUSY can be, supersymmetric particles continue to elude detection at the Large Hadron Collider (LHC), at least in Run 1 experiments with a center-of-mass energy $\sqrt{s} = 8$ TeV [6]. Run 2 experiments with $\sqrt{s} = 13$ TeV are currently under way, targeting a final luminosity of about 100 fb^{-1}, and so are tested in more involved and less stringent formulations of supersymmetry [7].

It must be stressed that until now, we have not detected dark matter, at least not in a conclusive manner. Indeed, we know dark matter is there only because of its gravitational interactions, and this is why and how we believe it contributes about a quarter of the mass energy of the known Universe. But we still do not know whether dark matter really interacts with ordinary matter. We believe it does, even if very weakly. We believe these interactions can yield signals with enough strength so that we can detect dark matter or produce it in collisions of Standard Model particles [8].

We must also understand that a detection process relies primarily on a theory or a model. A theory like supersymmetry, which originated in the realm of elementary particle physics, is devised as an extension to the Standard Model that is based on a yet-to-be-detected symmetry between fermionic and bosonic states [9]. Its DM connection came only later. In fact, in the rather long period between the Higgs mechanism proposal [10] and the detection of the Higgs particle [11], various extensions of the Standard Model were proposed in order to alleviate some of its shortcomings, the so-called "Beyond the Standard Model" (BSM) Physics [12]. A number of these BSM models bear in them extra fields, meaning extra particles with specific properties. Until today, such particles have never been detected. With time and change in focus, the most stable of these hypothetical particles have then been proposed as candidates for dark matter, many in the form of WIMPs. The advantage of such a paradigm is clear: the calculational techniques that built strength in the realm of particle physics were ready at the

service of dark matter search with little extra effort in development. But the experimental framework was also ready. Such a state of affairs could partly explain the popularity of WIMP physics, compared to other possible scenarios for dark matter.

Accordingly, many experiments have been devised specifically to detect dark matter. Each, of course, must be based on a specific scheme that is based on a specific scenario. There are experiments that try to detect dark matter directly, through missing energy momentum after a WIMP collides directly with an ordinary nucleus. The low-background DAMA (NaI) and then DAMA/LIBRA (NaI[Ti]) experiments at Gran Sasso in Italy [13] add a twist to this by trying to detect dark matter in the galactic halo via its suggested model-independent flux annual modulation [14]. The CoGeNT experiment [15] in Soudan (Minnesota, USA) also tries to detect this annual modulation, but in the region where the WIMP mass is $\lesssim$10 GeV. The CDMS I (Stanford, USA) [16], then CDMS II (Soudan, USA) [17], and now the superCDMS (Soudan, USA, then SNOLAB, Sudbury, Canada) [18] perform direct detection, measuring ionization and phonon signals resulting from a WIMP-nucleus collision, sensitive in the low-mass region. The XENON10 [19], then XENON100 [20], then the coming XENON1t [21], all in Gran Sasso, Italy, use liquid Xenon as a detecting medium for WIMP-nucleon and WIMP-electron collisions. There is also the Large Underground Xenon (LUX) experiment (South Dakota, USA) [22], as a direct-detection experiment, and its more sensitive successor LZ experiment [23]. The CRESST experiment [24], followed by CRESST II [25], both at Gran Sasso, Italy, also try to detect dark matter directly with low mass. We also have the series of EDELWEISS experiments [26] (Modane, France), which target low-mass WIMPs. The list is exhaustive, and could not be accounted here due to space constraints.

The above experiments are terrestrial, with instruments buried underground to reduce noise. But there are other experiments which are space borne that carry out indirect detection in cosmic rays. There is the Fermi Gamma-Ray Space Telescope (Fermi-LAT), which has found excess of gamma rays in the galactic center that cannot be explained by conventional sources and which is compatible with the presence of dark matter [27]. Fermi-LAT uses what we call indirect methods, namely, collecting gamma-ray signals and removing from these those emitted by all possible known sources. Another space-borne experiment is the Alpha Magnetic Spectrometer (AMS) experiment at the international space station [28], collecting and analyzing signals from cosmic rays. In addition, the Payload for Antimatter Matter Exploration and Light-nuclei Astrophysics (PAMELA) experiment [29] is a particle identifier that uses a permanent magnet spectrometer for space cosmic-ray direct measurements.

A third prong in the dark matter search enterprise is to produce it in particle colliders like the LHC [8]. There is an added difficulty here, which is that we do not know in which mass range we should look into. It could well be that the present center-of-mass energy that is available, 13 TeV, may not be sufficient. Nevertheless, the search for dark matter at the LHC is intense. One reason is that, experimentally, this is feasible now: small amounts of missing energy and transverse momentum can be detected now. Note that the present detectors are not built to detect dark matter directly. Rather, the latter would appear as a missing energy or missing momentum. For example, we now look at events in which a Z boson and a missing transverse momentum are produced in a proton-proton collision at $\sqrt{s} = 13$ TeV. The Z boson decays

into two charged leptons, a recognizable signature, and a possible missing transverse momentum, which would indicate the production of dark matter in the process. A similar search, conducted previously by the CMS Collaboration and based on data collected with $\sqrt{s} = 8$ TeV (Run 1), found no evidence of new physics and hence set limits on dark matter production. A recent search performed by the ATLAS Collaboration with $\sqrt{s} = 13$ TeV with an integrated luminosity of 3.2 fb^{-1} also reported no evidence [30].

What should be clear by now is that interpreting signals as dark matter necessitates modeling. On the other hand, any model needs experimental results to restrict the range of its free parameters, to fine-tune these parameters, and, ultimately, in many cases, to be eliminated. The aim of this chapter is to shed light on the main steps a phenomenologist takes when building a model for dark matter, then testing the model against experimental results. It is an attempt to look into the modeling process itself, from the "cradle to the grave," so to speak. The discussion is based on a model proposed in Ref. [31] for cold dark matter, exposed to particle-physics phenomenology in [32], and further restricted by internal consistency in Ref. [33]. We will see how gradually the parameters of the model are constrained, and how the region of viability is reached. To carry out the discussion smoothly, we have chosen a model which is simple enough to avoid confusion created by the often involved details of the calculations and could-be-complexity of the model itself, but at the same time rich enough to be able to accommodate a vast range of experimental results. The material presented in this chapter is drawn from the works just cited.

This chapter is organized as follows. After this Introduction, Section 2 motivates and then presents the model based on WIMP physics, namely, a two-singlet extension of the Standard Model of elementary particles. We will try to avoid lengthy arguments and focus on the essentials. Section 3 shows how the measured amount of dark matter relic-density constrains the value of the dark matter annihilation cross-section, a constraint any model has to satisfy. We then discuss how the two-singlet extension fits into this, and add to it a perturbativity ingredient. Section 4 takes the two-singlet model into the arena of particle phenomenology and sees how it copes with rare meson decays. Section 5 goes back to the fundamentals and runs a renormalization-group analysis to inquire into the sustainability of the model. Section 6 puts all these constraints together and determines the regions of viability of the model. Section 7 is left for concluding remarks.

2. A model for dark matter: motivation and parametrization

As mentioned in the Introduction, the most popular candidate for dark matter is an electrically neutral colorless weakly interacting massive particle (WIMP), and the neutralino, the lightest supersymmetric particle, is a robust fit for this role. However, as explained in Ref. [31] and references therein, it is hard to argue in favor of a neutralino when it comes to light cold dark matter, say, a WIMP mass of up to 10 GeV. In addition, up to now, we have not detected supersymmetric signatures at the LHC [34].

Therefore, with no prior hints as to what the internal structure of the WIMP might be, one adopts a bottom-up approach, in which one extends the Standard Model by adding to it the

simplest of fields, one real spinless scalar, which will be the WIMP. This field must be a Standard Model gauge singlet so that we avoid any "direct contact" with any of the Standard Model particles. It is allowed to interact with visible particles only via the Higgs field. It is made stable against annihilation by enforcing upon it the simplest of symmetries, a discrete $\mathbb{Z}_2$ symmetry that does not break spontaneously. This construction is called the minimal extension to the Standard Model. In view of its cosmological implication, the minimal extension has first been proposed in Ref. [35] and has been extensively studied and explored in Ref. [36]. However, this model is shown in Ref. [37] to be inadequate if we want the WIMP to be light.

In the logic of this bottom-up approach, adding another real scalar seems the natural step forward. This field will also be endowed with a $\mathbb{Z}_2$ symmetry, but this one we will break spontaneously, and the reason is to open new channels for dark matter annihilation, which implies an increase in the corresponding annihilation cross-section, which in turn would allow smaller WIMP masses, something we want to achieve. Needless to say that this auxiliary field must also be a Standard Model gauge singlet.

Therefore, we extend the Standard Model by adding two real, spinless and $\mathbb{Z}_2$-symmetric fields: the dark matter field S_0 for which the $\mathbb{Z}_2$ symmetry is unbroken and an auxiliary field for which it is spontaneously broken. Both fields are Standard Model gauge singlets and hence can interact with "visible" particles only via the Higgs doublet, taken in the unitary gauge. We must also assume all processes calculable in perturbation theory. The details of the spontaneous breaking of the electroweak gauge symmetry and the additional auxiliary $\mathbb{Z}_2$ symmetry are left aside [31].

The potential function that involves the physical scalar Higgs field h, the dark matter field S_0, and the physical auxiliary scalar field S_1 is as follows:

$$\begin{aligned} U = {} & \frac{1}{2}m_0^2 S_0^2 + \frac{1}{2}m_h^2 h^2 + \frac{1}{2}m_1^2 S_1^2 \\ & + \frac{\lambda_0^{(3)}}{2} S_0^2 h + \frac{\eta_{01}^{(3)}}{2} S_0^2 S_1 + \frac{\lambda^{(3)}}{6} h^3 + \frac{\eta_1^{(3)}}{6} S_1^3 + \frac{\lambda_1^{(3)}}{2} h^2 S_1 + \frac{\lambda_2^{(3)}}{2} h S_1^2 \\ & + \frac{\eta_0}{24} S_0^4 + \frac{\lambda^{(4)}}{24} h^4 + \frac{\eta_1^{(4)}}{24} S_1^4 + \frac{\lambda_0^{(4)}}{4} S_0^2 h^2 + \frac{\eta_{01}^{(4)}}{4} S_0^2 S_1^2 + \frac{\lambda_{01}^{(4)}}{2} S_0^2 h S_1 \\ & + \frac{\lambda_1^{(4)}}{6} h^3 S_1 + \frac{\lambda_2^{(4)}}{4} h^2 S_1^2 + \frac{\lambda_3^{(4)}}{6} h S_1^3. \end{aligned} \tag{1}$$

The quantities $m_0, m_h,$ and m_1 are the masses of the corresponding fields S_0, h, and S_1, respectively, and all the other parameters are real coupling constants. Also, the part of the Standard Model Lagrangian that is relevant to Dark matter annihilation is given in terms of the physical fields h and S_1 by the following potential function:

$$\begin{aligned} U_{\mathrm{SM}} = {} & \sum_f \left(\lambda_{hf} h \bar{f} f + \lambda_{1f} S_1 \bar{f} f\right) + \lambda_{hw}^{(3)} h W_\mu^- W^{+\mu} + \lambda_{1w}^{(3)} S_1 W_\mu^- W^{+\mu} \\ & + \lambda_{hz}^{(3)} h \left(Z_\mu\right)^2 + \lambda_{1z}^{(3)} S_1 \left(Z_\mu\right)^2 + \lambda_{hw}^{(4)} h^2 W_\mu^- W^{+\mu} + \lambda_{1w}^{(4)} S_1^2 W_\mu^- W^{+\mu} \\ & + \lambda_{h1w} h S_1 W_\mu^- W^{+\mu} + \lambda_{hz}^{(4)} h^2 \left(Z_\mu\right)^2 + \lambda_{1z}^{(4)} S_1^2 \left(Z_\mu\right)^2 + \lambda_{h1z} h S_1 \left(Z_\mu\right)^2. \end{aligned} \tag{2}$$

The coupling constants in the above expression are given by the following relations, in which the quantities m_f, m_w, and m_z are the masses of the fermion f, the W, and the Z gauge bosons, respectively:

$$\begin{aligned}
&\lambda_{hf} = -\frac{m_f}{v}\cos\theta; \quad \lambda_{1f} = \frac{m_f}{v}\sin\theta;\\
&\lambda_{hw}^{(3)} = 2\frac{m_w^2}{v}\cos\theta; \quad \lambda_{1w}^{(3)} = -2\frac{m_w^2}{v}\sin\theta;\\
&\lambda_{hz}^{(3)} = \frac{m_z^2}{v}\cos\theta; \quad \lambda_{1z}^{(3)} = -\frac{m_z^2}{v}\sin\theta;\\
&\lambda_{hw}^{(4)} = \frac{m_w^2}{v^2}\cos^2\theta; \quad \lambda_{1w}^{(4)} = \frac{m_w^2}{v^2}\sin^2\theta; \quad \lambda_{h1w} = -\frac{m_w^2}{v^2}\sin 2\theta;\\
&\lambda_{hz}^{(4)} = \frac{m_z^2}{2v^2}\cos^2\theta; \quad \lambda_{1z}^{(4)} = \frac{m_z^2}{2v^2}\sin^2\theta; \quad \lambda_{h1z} = -\frac{m_z^2}{2v^2}\sin 2\theta.
\end{aligned} \tag{3}$$

The angle θ is the mixing angle between the fields h and S_1 [31]. The quantities v and v_1, both positive, are the vacuum expectation values of the Higgs and auxiliary fields, respectively.

This model has nine free parameters to start with, three mass parameters and six coupling constants [31]. As already mentioned, perturbativity is assumed, which means all the original coupling constants are small. The dark matter self-coupling constant η_0 in Eq. (1) will not enter the lowest-order calculations we will consider, and so this parameter stays free for the time being and we are left with eight parameters. The spontaneous breaking of the electroweak and $\mathbb{Z}_2$ symmetries for the Higgs and auxiliary fields, respectively, introduces the two vacuum expectation values v and v_1. The value of v is fixed experimentally to be 246 GeV [38] and for the present discussion, we fix the value of v_1 at the order of the electroweak scale, say, 100 GeV. In addition, the Higgs mass is now known [11], $m_h = 125$ GeV. Hence, five free parameters remain. Three of these are chosen to be the two physical masses m_0 (dark matter) and m_1 (S_1 field), plus the mixing angle θ between S_1 and h. The two last parameters we choose are the two physical mutual coupling constants $\lambda_0^{(4)}$ (dark matter—Higgs) and $\eta_{01}^{(4)}$ (dark matter—S_1 particle), see Eq. (1).

3. Constraints from cosmology and perturbativity

Any model of dark matter has to comply with astrophysical observations. Indeed, dark matter is believed to have been produced in the early Universe. A most popular paradigm for this production is the so-called "freeze-out scenario" by which dark matter, thought of as a set of elementary particles, interacts with ordinary matter, weakly but with enough strength to generate common thermal equilibrium at high temperature. However, as the cosmos is cooling down, at some temperature T_f, the rate of expansion of the Universe becomes higher than the rate of dark matter particle annihilation, which forces dark matter to decouple from ordinary matter, and hence a "freeze-out"—T_f is thus called the freeze-out temperature. The DM relic density $\Omega_{\rm DM}$ is essentially the one we measure today [1]:

$$\Omega_{\rm DM}\overline{h}^2 = 0.1199 \pm 0.0022 \approx 0.12, \tag{4}$$

where $\overline{h}$ is Hubble constant in units of 100 km $\times$ s^{-1} $\times$ Mpc^{-1}.

In a model where dark matter is seen as WIMPs that can annihilate into ordinary elementary particles, the relic density $\Omega_{\rm DM}$ can be related to the annihilation DM cross-section $\sigma_{\rm ann}$. Indeed, in the framework of the standard cosmological model, one can derive the following relation [39]:

$$\Omega_{\rm DM}\overline{h}^2 \simeq \frac{1.07 \times 10^9 x_f}{\sqrt{g_*} m_{\rm Pl} \langle \sigma_{\rm ann} v \rangle \ {\rm GeV}}; \quad x_f \simeq \ln \frac{0.0038 m_{\rm Pl} m_0 \langle \sigma_{\rm ann} v \rangle}{\sqrt{g_* x_f}}. \tag{5}$$

The quantity $m_{\rm Pl} = 1.22 \times 10^{19}$GeV is the Planck mass, m_0 is the dark matter mass, $x_f = m_0/T_f$, and g_* is the number of relativistic degrees of freedom with a mass less than T_f. The quantity $\langle \sigma_{\rm ann} v \rangle$ is the thermally averaged annihilation cross-section of a pair of two dark matter particles multiplied by their relative speed in their center-of-mass reference frame. Solving (4) with the current value (5) for $\Omega_{\rm DM}$ with x_f between 19.2 and 21.6 [40], we obtain the following constraint on the annihilation cross-section:

$$\langle \sigma_{\rm ann} v \rangle \simeq 2 \times 10^{-9} {\rm GeV}. \tag{6}$$

This is one major constraint any WIMP model like the one we discuss here has to satisfy. Indeed, the quantity $\langle \sigma_{\rm ann} v \rangle$ is calculable in perturbation theory, and so, the implementation of (6) will induce an admittedly complicated but important relation between the free parameters of the model, hence reducing their space of freedom, reducing their number by one. Also, the constraint induced by (6) can be used to examine aspects of the theory like perturbativity. To implement perturbativity in the present two-singlet model, we use (6) to obtain the mutual coupling constant $\eta_{01}^{(4)}$ (coupling between the DM field S_0 and auxiliary field S_1) in terms of the dark matter mass m_0 for given values of $\lambda_0^{(4)}$ (coupling between S_0 and Higgs) and study its behavior to tell which dark matter mass regions are consistent with perturbativity. It should be mentioned that once the two mutual coupling constants $\lambda_0^{(4)}$ and $\eta_{01}^{(4)}$ are small, all the other physical coupling constants will be small.

The quantity $\langle \sigma_{\rm ann} v \rangle$ is calculated in perturbation theory using all possible annihilation channels the model allows for [31]. As the model has many parameters, the behavior of the mutual coupling constant $\eta_{01}^{(4)}$ is bound to be rich. Sampling is therefore necessary. In this review, we briefly comment on the behavior of $\eta_{01}^{(4)}$ for two sets of the parameters $(\theta, m_1, \lambda_0^{(4)})$. A more substantial discussion can be found in Ref. [31].

The first set of parameters is a small mixing angle $\theta = 10^{\rm o}$, a weak mutual S_0-Higgs coupling constant $\lambda_0^{(4)} = 0.01$, and a S_1-mass $m_1 = 10$ GeV. The corresponding behavior of $\eta_{01}^{(4)}$ versus m_0 is shown in **Figure 1**. The range of m_0 displayed is from 0.1 to 200 GeV. In this regime, the first feature we see is that the relic-density constraint on dark matter annihilation forbids WIMP

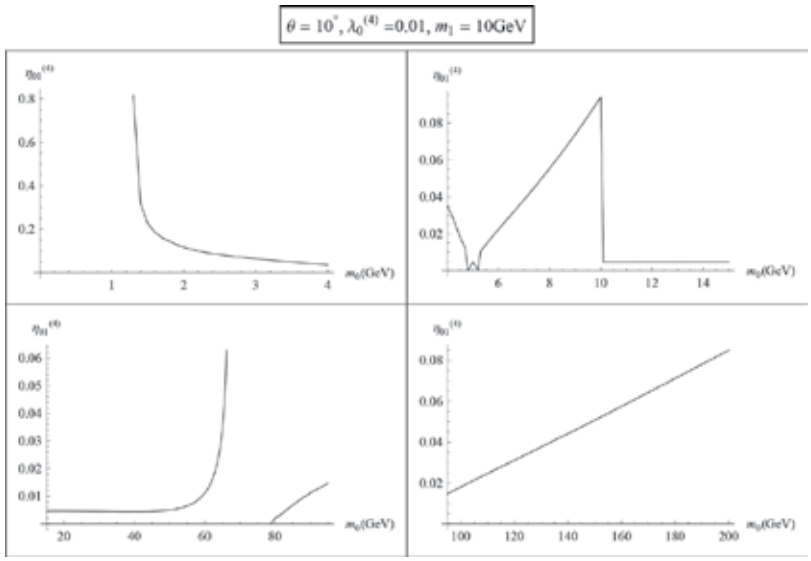

Figure 1. $\eta_{01}^{(4)}$ versus m_1 for very light S_1, small mixing, and very small WIMP-Higgs coupling.

masses $m_0 \lesssim 1.3$ GeV. Furthermore, just about $m_0 \simeq 1.3$ GeV, the c-quark threshold, the $S_0 - S_1$ mutual coupling constant $\eta_{01}^{(4)}$ starts at about 0.8, a value, while perturbative, that is roughly 80-fold larger than the mutual S_0 Higgs coupling constant $\lambda_0^{(4)}$. Then as the DM mass increases, $\eta_{01}^{(4)}$ decreases, steeply first, more slowly as we cross the τ mass toward the b mass. Just before $m_1/2$, the coupling $\eta_{01}^{(4)}$ hops onto another solution branch that is just emerging from negative territory, gets back to the first one at precisely $m_1/2$ as this latter carries now smaller values, and then jumps up again onto the second branch as the first crosses the m_0 axis down. It goes up this branch with a moderate slope until m_0 becomes equal to m_1, a value at which the S_1 annihilation channel opens. Just beyond m_1, there is a sudden fall to a value $\eta_{01}^{(4)} \simeq 0.0046$ that is about half the value of $\lambda_0^{(4)}$, and $\eta_{01}^{(4)}$ stays flat till $m_0 \simeq 45$ GeV where it starts increasing, sharply after 60 GeV. In the mass interval $m_0 \simeq 66$–79 GeV, there is a "desert" with no positive real solutions to the relic-density constraint, hence no viable dark matter candidate exists. Beyond $m_0 \simeq 79$ GeV, the mutual coupling constant $\eta_{01}^{(4)}$ keeps increasing monotonously, with a small notch at the W mass and a less noticeable one at the Z mass. As it increases, its values remain perturbative.

The second set of parameters we feature is still a small Higgs S_1 mixing angle $\theta = 10^o$, an increased S_0-Higgs mutual coupling constant $\lambda_0^{(4)} = 0.2$, and a moderate S_1 mass $m_1 = 20$ GeV. The behavior of the $S_0 - S_1$ mutual coupling constant $\eta_{01}^{(4)}$ versus the DM mass m_0 is displayed in **Figure 2**. Here too, no viable DM masses exist below roughly 1.4 GeV, at which value $\eta_{01}^{(4)}$ starts at 1.95. It decreases with a sharp change of slope at the b-quark threshold, then makes a sudden dive at about 5 GeV, a change of branch at $m_1/2$ down till about 12 GeV where it jumps up back onto the previous branch just before going to cross into negative territory. It drops

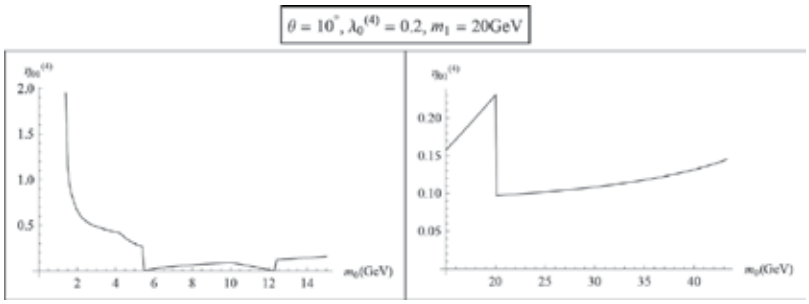

Figure 2. $\eta_{01}^{(4)}$ versus m_0 for small mixing, moderate m_1, and WIMP-Higgs coupling.

sharply at $m_0 = m_1$ and then increases slowly until $m_0 \simeq 43.3$ GeV. Then, no viable WIMP masses exist, a desert. As we see, for this set of parameters $(\theta, \lambda_0^{(4)}, m_1)$, the model constrains the dark matter mass inside the interval 1.6 GeV $\lesssim m_0 \lesssim$ 43.3 GeV, with perturbative coupling constants.

With the same mixing angle $\theta = 10^{o}$ and mutual coupling constant $\lambda_0^{(4)} = 0.2$, larger masses m_1 yield roughly the same behavior, but with values of $\eta_{01}^{(4)}$ that could be nonperturbative. For example, when $m_1 = 60$ GeV, the mutual coupling $\eta_{01}^{(4)}$ starts very high ($\simeq$85) at $m_0 \simeq 1.5$ GeV, and then decreases rapidly. There is a usual change of branches and a desert starting at about 49 GeV, a behavior that is peculiar in a way because the desert starts at a mass $m_0 < m_1$, that is, before the opening of the S_1 annihilation channel. In other words, the dark matter is annihilating into the light fermions only and the model is perturbatively viable in the range of 20–49 GeV.

4. Constraints from direct detection

Perhaps the most known constraints on a WIMP model are those coming from direct-detection experiments like the many we have cited in the introductory section. In such experiments, the signal sought for would typically come from the elastic scattering of a WIMP off a nonrelativistic nucleon target. However, as mentioned in the Introduction, until now, none of these direct-detection experiments have yielded an unambiguous dark matter signal. Rather, with increasing precision from one generation to the next, these experiments put increasingly stringent exclusion bounds on the dark matter-nucleon elastic-scattering total cross-section σ_{det} in terms of the dark matter mass m_0, and because of these constraints, many models can get excluded.

Therefore, a theoretical dark matter model like the two-singlet extension we discuss here has to satisfy these bounds to remain viable. For this purpose, we calculate σ_{det} as a function of m_0 for different values of the parameters $(\theta, \lambda_0^{(4)}, m_1)$ and compare its behavior against the experimental bounds. The calculation is carried out with sufficient details in Ref. [31], and the total cross-section for non-relativistic S_0-nucleon elastic scattering is given by

$$\sigma_{\rm det} = \frac{m_N^2\left(m_N - \frac{7}{9}m_B\right)^2}{4\pi(m_N+m_0)^2 v^2}\left[\frac{\lambda_0^{(3)}\cos\theta}{m_h^2} - \frac{\eta_{01}^{(3)}\sin\theta}{m_1^2}\right]^2. \tag{7}$$

In this relation, m_N is the nucleon mass and m_B is the baryon mass in the chiral limit. The mutual coupling constants $\lambda_0^{(3)}$ and $\eta_{01}^{(3)}$ are defined in Eq. (1). The relic-density constraint on the dark matter annihilation cross-section (6) has to be imposed throughout. In addition, we require now that the coupling constants be perturbative, and we do this by imposing the additional requirement $0 \le \eta_{01}^{(4)} \le 1$.

Generically, as m_0 increases, the detection cross-section $\sigma_{\rm det}$ starts from high values, slopes down to minima that depend on the parameters, and then picks up moderately. There are features and action at the usual mass thresholds, with varying sizes and shapes. Regions coming from the relic-density constraint and new ones originating from the additional perturbativity requirement are excluded.

For the purpose of illustration, we choose three indicative sets of values for the parameters $(\theta, \lambda_0^{(4)}, m_1)$. We start first with a Higgs-S_1 mixing angle $\theta = 10^{\rm o}$, a weak mutual S_0-Higgs coupling $\lambda_0^{(4)} = 0.01$, and an S_1 mass $m_1 = 20$ GeV. The behavior of $\sigma_{\rm det}$ versus m_0 is shown in **Figure 3**. There, we see that for the two mass intervals 20–65 GeV and 75–100 GeV, plus an almost singled-out dip at $m_0 = m_1/2$, the elastic scattering cross-section is below the sensitivity of SuperCDMS. However, XENON1T should probe all these masses, except $m_0 \simeq 58$ and 85 GeV.

Increasing m_1 has the effect of closing possibilities for very light dark matter and thinning the intervals as it drives the predicted masses to larger values. Indeed, in **Figure 4**, where

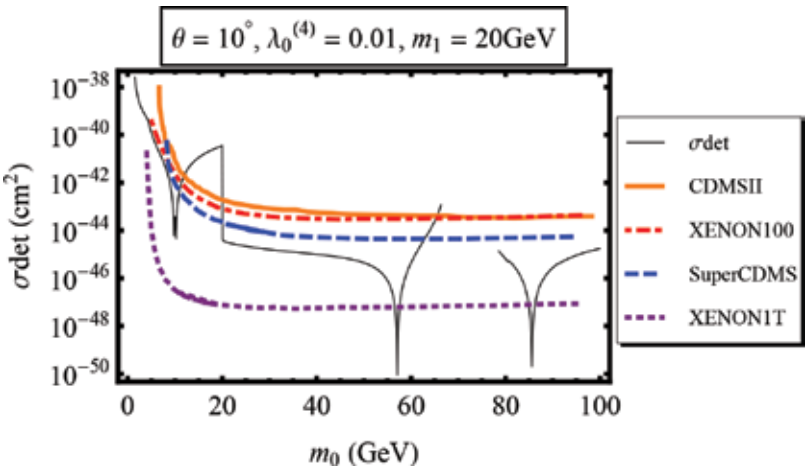

Figure 3. Elastic $N - S_0$ scattering cross-section as a function of m_0 for moderate m_1, small mixing, and small WIMP-Higgs coupling.

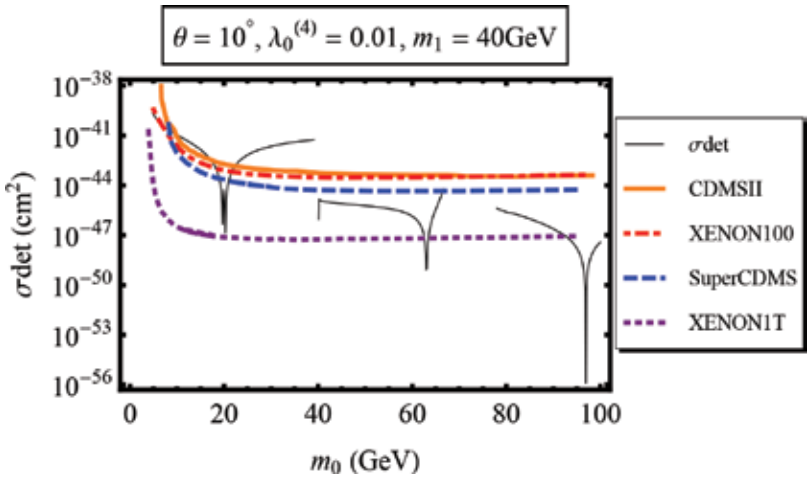

Figure 4. Elastic $N - S_0$ scattering cross-section as a function of m_0 for moderate m_1, small mixing, and small WIMP-Higgs coupling.

$m_1 = 40$ GeV, in addition to the dip at $m_1/2$ that crosses SuperCDMS but not XENON1T, we see acceptable masses in the ranges of 40–65 GeV and 78 GeV up. The intervals narrow as we descend, surviving XENON1T only as spiked dips at 62 GeV and around 95 GeV.

On the other hand, a larger mutual coupling constant $\lambda_0^{(4)}$ has the general effect of squeezing the acceptable intervals of m_0 by pushing the values of σ_{det} up, and it may even happen that at some point, the model has no predictability. This case is shown in **Figure 5**, where $\theta = 10^{\text{o}}$, $\lambda_0^{(4)} = 0.4$, and $m_1 = 60$ GeV. In this example, the effects of increasing the values of both $\lambda_0^{(4)}$ and m_1. As we see, the model cannot even escape Cryogenic Dark Matter Search II (CDMSII).

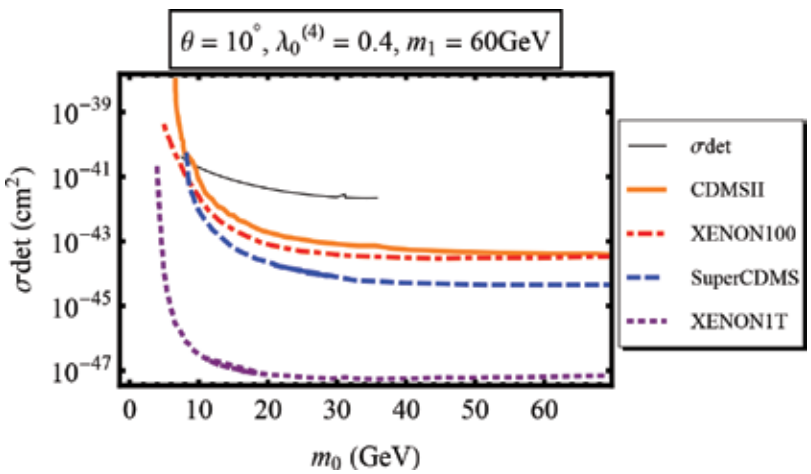

Figure 5. Elastic cross-section σ_{det} versus m_0 for heavy S_1, small mixing, and relatively large WIMP-Higgs coupling.

5. Constraints from particle phenomenology

If a dark matter model based on WIMP physics is not killed already by the constraints coming from cosmology, perturbativity, and direct detection, it has to undergo the tests of particle phenomenology. To see how this works, we discuss here the constraints on our two-singlet model that come from a small selection of low-energy processes, namely, the rare decays of Υ mesons. The forthcoming discussion is based on work done in Ref. [32]. There, the interested reader will find a fuller account of this study, together with relation to Higgs phenomenology. Note that the dark matter relic-density constraint in Eq. (6) and the perturbativity requirement $0 < \eta_{01}^{(4)} < 1$ are implemented systematically. Also, as in Ref. [32], we will restrict the discussion to light cold dark matter.

We therefore look at the constraints that come from the decay of the meson Υ in the state nS ($n = 1, 3$) into one photon γ and one particle S_1. For $m_1 \lesssim 8$ GeV, the branching ratio for this process is given by the relation:

$$\mathrm{Br}(\Upsilon_{nS} \to \gamma + S_1) = \frac{G_F m_b^2 \sin^2\theta}{\sqrt{2}\pi\alpha}\, x_n \left(1 - \frac{4\alpha_s}{3\pi} f(x_n)\right) \mathrm{Br}^{(\mu)}\, \Theta(m_{\Upsilon_{nS}} - m_1). \tag{8}$$

In the above expression, $x_n \equiv \left(1 - m_1^2/m_{\Upsilon_{ns}}^2\right)$ with the mass of $\Upsilon_{1(3)S}$ given by $m_{\Upsilon_{1(3)S}} = 9.46(10.355)$ GeV, the branching ratio $\mathrm{Br}^{(\mu)} \equiv \mathrm{Br}\left(\Upsilon_{1(3)S} \to \mu^+\mu^-\right) = 2.48(2.18) \times 10^{-2}$ [41], α is the QCD coupling constant, $\alpha_s = 0.184$ the QCD coupling constant at the scale $m_{\Upsilon_{nS}}$, the quantity G_F is the Fermi coupling constant, and m_b is the b-quark mass [38]. The function $f(x)$ incorporates the effect of QCD radiative corrections given in [42] and the step function is denoted by $\Theta(x)$. However, a rough estimate of the lifetime of S_1 indicates that the latter is likely to decay inside a typical particle detector, which means we should take into account its most dominant decay products. We first have a process by which S_1 decays into a pair of pions, with the following decay rate:

$$\begin{aligned}\Gamma(S_1 \to \pi\pi) \simeq \frac{G_F m_1}{4\sqrt{2}\pi} \sin^2\theta \Bigg[& \frac{m_1^2}{27}\left(1 + \frac{11 m_\pi^2}{2 m_1^2}\right)^2 \\ & \times \left(1 - \frac{4m_\pi^2}{m_1^2}\right)^{\frac{1}{2}} \Theta(m_1 - 2m_\pi)(2m_K - m_1)\Bigg] \\ & + 3\left(M_u^2 + M_d^2\right)\left(1 - \frac{4m_\pi^2}{m_1^2}\right)^{\frac{3}{2}} \Theta(m_1 - 2m_K)].\end{aligned} \tag{9}$$

Here, m_π is the pion mass and m_K is the kaon mass. Also, chiral perturbation theory is used below the kaon pair production threshold [43, 44], and the spectator-quark model above up to roughly 3 GeV, with the dressed u and d quark masses $M_u = M_d \simeq 0.05$ GeV. Note that this rate includes all pions, charged and neutral. Above the $2m_K$ threshold, there is the production of both a pair of kaons and η particles. The decay rate for K production is

$$\Gamma(S_1 \to KK) \simeq \frac{9}{13}\frac{3G_F M_s^2 m_1}{4\sqrt{2}\pi}\sin^2\theta\left(1-\frac{4m_K^2}{m_1^2}\right)^{\frac{3}{2}}\Theta(m_1-2m_K). \tag{10}$$

In the above rate, $M_s \simeq 0.45$ GeV is the s-quark mass in the spectator-quark model [45, 46]. For η production, replace m_K by m_η and 9/13 by 4/13.

The particle S_1 also decays into c and b quarks (mainly c). Including the radiative QCD corrections, the corresponding decay rates are given by

$$\Gamma(S_1 \to q\bar{q}) \simeq \frac{3G_F \overline{m}^{q2} m_1}{4\sqrt{2}\pi}\sin^2\theta\left(\frac{1-4\overline{m}_q^2}{m_h^2}\right)^{\frac{3}{2}}\left(1+5.67\frac{\overline{\alpha}_s}{\pi}\right)\Theta\left(m_1-2\overline{m}_q\right). \tag{11}$$

The dressed quark mass $\overline{m}_q \equiv m_q(m_1)$ and the running strong coupling constant $\overline{\alpha}_s \equiv \alpha_s(m_1)$ are defined at the energy scale m_1 [47]. There is also a decay into a pair of gluons, with the rate

$$\Gamma(S_1 \to gg) \simeq \frac{G_F m_1^3 \sin^2\theta}{12\sqrt{2}\pi}\left(\frac{\alpha'_s}{\pi}\right)^2\left[6-2\left(1-\frac{4m_\pi^2}{m_1^2}\right)^{\frac{3}{2}}-\left(1-\frac{4m_K^2}{m_1^2}\right)^{\frac{3}{2}}\right]\Theta(m_1-2m_K). \tag{12}$$

Here, $\alpha'_s = 0.47$ is the QCD coupling constant at the spectator-quark model scale, between roughly 1 and 3 GeV.

We then have the decay of S_1 into leptons, the corresponding rate given by

$$\Gamma\left(S_1 \to \ell^+\ell^-\right) = \frac{G_F m_\ell^2 m_1}{4\sqrt{2}\pi}\sin^2\theta\left(1-\frac{4m_\ell^2}{m_1^2}\right)^{\frac{3}{2}}\Theta(m_1-2m_\ell), \tag{13}$$

where m_ℓ is the lepton mass. Finally, S_1 can decay into a pair of dark matter particles, with a decay rate:

$$\Gamma(S_1 \to S_0 S_0) = \frac{\left(\eta_{01}^{(3)}\right)^2}{32\pi m_1}\sqrt{1-\frac{4m_0^2}{m_1^2}}\Theta(m_1-2m_0). \tag{14}$$

The coupling constant $\eta_{01}^{(3)}$ is given in Eq. (1). The branching ratio for Υ_{nS} decaying via S_1 into a photon plus X, where X represents any kinematically allowed final state, will be

$$\mathrm{Br}(\Upsilon_{nS} \to \gamma + X) = \mathrm{Br}(\Upsilon_{nS} \to \gamma + S_1) \times \mathrm{Br}(S_1 \to X). \tag{15}$$

In particular, $X \equiv S_0 S_0$ corresponds to a decay into invisible particles.

The best available experimental upper bounds on 1S-state branching ratios are (i) $\mathrm{Br}(\Upsilon_{1S} \to \gamma + \tau\tau) < 5 \times 10^{-5}$ for $3.5\ \mathrm{GeV} < m_1 < 9.2\ \mathrm{GeV}$ [48]; (ii) $\mathrm{Br}(\Upsilon_{1S} \to \gamma + \pi^+\pi^-) < 6.3 \times 10^{-5}$ for $1\ \mathrm{GeV} < m_1$ [49]; (iii) $\mathrm{Br}(\Upsilon_{1S} \to \gamma + K^+K^-) < 1.14 \times 10^{-5}$ for $2\ \mathrm{GeV} < m_1 < 3\ \mathrm{GeV}$ [50]. **Figure 6** displays the corresponding branching ratios of Υ_{1S} decays via S_1 as

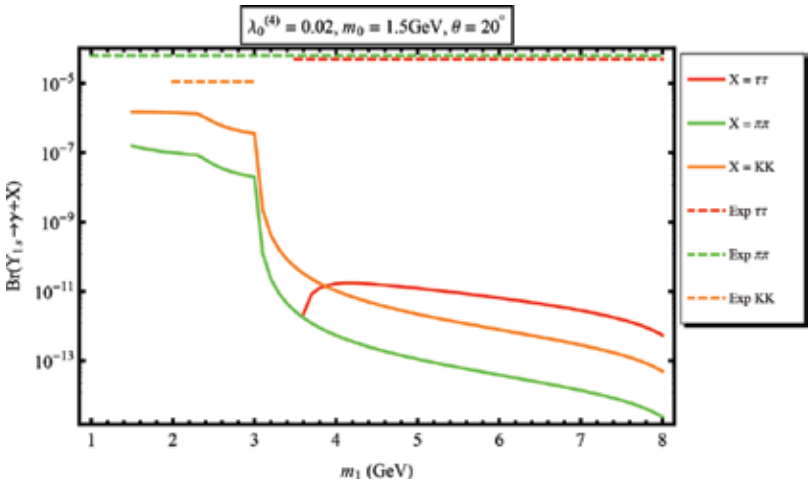

Figure 6. Typical branching ratios of Υ_{1S} decaying into τ's, charged pions, and charged kaons as functions of m_1. The corresponding experimental upper bounds are shown.

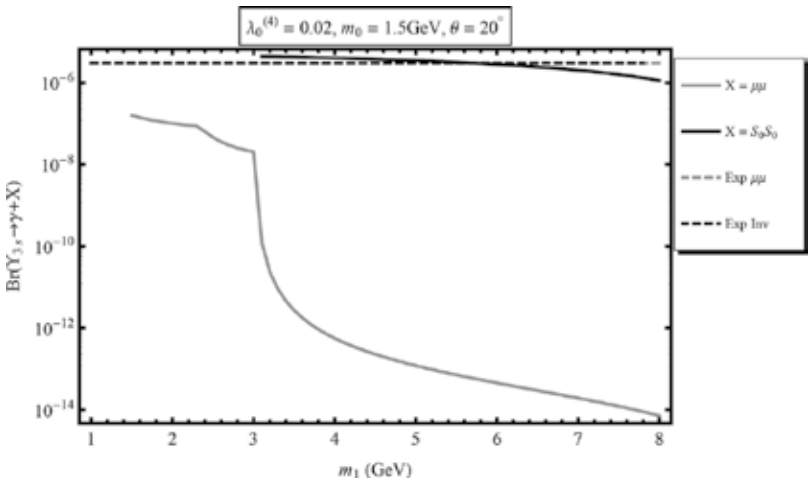

Figure 7. Typical branching ratios of Υ_{3S} decaying into muons and dark matter as functions of m_1. The corresponding experimental upper bounds are shown.

functions of m_1, together with these upper bounds. Also, the best available experimental upper bounds on Υ_{3S} branching ratios are: (i) $\text{Br}\left(\Upsilon_{3S} \to \gamma + \mu\mu\right) < 3 \times 10^{-6}$ for 1 GeV $< m_1 <$ 10 GeV; (ii) $\text{Br}(\Upsilon_{3S} \to \gamma + \text{invisible}) < 3 \times 10^{-6}$ for 1 GeV $< m_1 <$ 7.8 GeV [51]. Typical corresponding branching ratios are shown in **Figure 7**.

If we perform a systematic scan of the parameter space, we find that the main effect of the Higgs-dark matter coupling constant $\lambda_0^{(4)}$ and the dark matter mass m_0 is to exclude, via the relic-density and perturbativity constraints, regions of applicability of the model. This is shown in **Figures 6** and **7**, where the region $m_1 \lesssim 1.4$ GeV is excluded. Otherwise, these two

parameters have little effect on the shapes of the branching ratios themselves. The onset of the S_0S_0 channel for $m_1 \geq 2m_0$ abates sharply the other channels, and this one becomes dominant by far. The effect of the mixing angle θ is to enhance all branching ratios as it increases, due to the factor $\sin^2\theta$. The dark matter decay channel reaches the invisible upper bound already for $\theta \simeq 15^o$, for fairly small m_0, say, 0.5 GeV. The other channels find it hard to get to their respective experimental upper bounds, even for large values of θ. There are further constraints that come from particle phenomenology tests. The interested reader may refer to [32] for further details.

6. Internal constraints

Further constraints on a field-theory dark matter model come from internal consistencies. Indeed, one must ask how high in the energy scale the model is computationally reliable. To answer this question, one investigates the running of the coupling constants as a function of the scale Λ via the renormalization-group equations (RGE). One-loop calculations are amply sufficient. A detailed study of the RGE for our two-singlet model was carried out in Ref. [33]. The brief subsequent discussion is drawn from there, and the reader is referred to that article for more details.

In an RGE study, there are two standard issues to monitor, namely, the perturbativity of the scalar coupling constants and the vacuum stability of the theory. Imposing these two latter as conditions on the model will indicate at what scale Λ_m it is valid. As mentioned in the Introduction, it has been anticipated that new physics, such as supersymmetry would appear at the LHC at the scale $\Lambda \sim 1$ TeV. Present results from ATLAS and CMS indicate no such signs yet. One consequence of this is that the cutoff scale Λ_m may be higher. In this model, the RGE study suggests that it can be ~ 40 TeV. As ever, the DM relic-density constraint is systematically imposed, together with the somewhat less stringent perturbativity restriction $0 \leq \eta_{01}^{(4)} \leq \sqrt{4\pi}$.

Remember that the model is obtained by extending the Standard Model with two real, spinless, and $\mathbb{Z}_2$-symmetric SM-gauge-singlet fields. The potential function of the scalar sector *after* spontaneous breaking of the gauge and one of the $\mathbb{Z}_2$ symmetries is given in Eq. (1). The potential function *before* symmetry breaking is the one we need in this section. It is given in Eq. [31]:

$$\begin{aligned} U = & \frac{\tilde{m}_0^2}{2} S_0^2 - \mu^2 H^\dagger H - \frac{\mu_1^2}{2}\chi_1^2 \\ & + \frac{\eta_0}{24} S_0^4 + \frac{\lambda}{6}\left(H^\dagger H\right)^2 + \frac{\eta_1}{24}\chi_1^4 + \frac{\lambda_0}{2} S_0^2 H^\dagger H + \frac{\eta_{01}}{4} S_0^2\chi_1^2 + \frac{\lambda_1}{2} H^\dagger H\chi_1^2. \end{aligned} \tag{16}$$

The field S_0 is still the WIMP with unbroken $\mathbb{Z}_2$ symmetry, and χ_1 is the auxiliary field before spontaneously breaking its $\mathbb{Z}_2$ symmetry. Both fields interact with the SM particles via the Higgs doublet H. The masses $\tilde{m}_0^2$, μ^2, and μ_1^2 as well as all the coupling constants are real positive numbers.[1]

[1]The mutual couplings can be negative as discussed below, see (21).

A one-loop renormalization-group calculation yields the following β-functions for the above scalar coupling constants [33]:

$$\begin{aligned}
\beta_{\eta_0} &= \frac{3}{16\pi^2}\left(\eta_0^2 + \eta_{01}^2 + 4\lambda_0^2\right);\\
\beta_{\eta_1} &= \frac{3}{16\pi^2}\left(\eta_1^2 + \eta_{01}^2 + 4\lambda_1^2\right);\\
\beta_{\lambda} &= \frac{3}{16\pi^2}\left(\frac{4}{3}\lambda^2 + \lambda_0^2 + \lambda_1^2 - 48\lambda_t^4 + 8\lambda\lambda_t^2 - 3\lambda g^2 - \lambda g'^2 + \frac{3}{2}g^2 g'^2 + \frac{9}{4}g^4\right);\\
\beta_{\eta_{01}} &= \frac{1}{16\pi^2}\left(4\eta_{01}^2 + \eta_0\eta_{01} + \eta_1\eta_{01} + 4\lambda_0\lambda_1\right);\\
\beta_{\lambda_0} &= \frac{1}{16\pi^2}\left(4\lambda_0^2 + \lambda_0\eta_0 + 2\lambda_0\lambda + \eta_{01}\lambda_1 + 12\lambda_0\lambda_t^2 - \frac{9}{2}\lambda_0 g^2 - \frac{3}{2}\lambda_0 g'^2\right);\\
\beta_{\lambda_1} &= \frac{1}{16\pi^2}\left(4\lambda_1^2 + \lambda_1\eta_1 + 2\lambda_1\lambda + \eta_{01}\lambda_0 + 12\lambda_1\lambda_t^2 - \frac{9}{2}\lambda_1 g^2 - \frac{3}{2}\lambda_1 g'^2\right).
\end{aligned} \tag{17}$$

As usual, by definition $\beta_g \equiv dg/d\ln\Lambda$, where Λ is the running mass scale, starting from $\Lambda_0 = 100$ GeV. Note that the DM self-coupling constant η_0 has so far been decoupled from the other coupling constants, but not anymore in view of Eq. (17) now that the running is the focus. However, its initial value $\eta_0(\Lambda_0)$ is arbitrary and its β-function is always positive. This means $\eta_0(\Lambda)$ will only increase as Λ increases, quickly if starting from a rather large initial value, slowly if not. Therefore, without losing generality in the subsequent discussion, we fix $\eta_0(\Lambda_0) = 1$. Hence, here too we still effectively have four free parameters: $\lambda_0^{(4)}$, θ, m_0, and m_1.

Furthermore, the constants g, g', and g_s are the SM and strong gauge couplings, known [52] and given to one-loop order by the expression:

$$G(\Lambda) = \frac{G(\Lambda_0)}{\sqrt{1 - 2a_G\, G^2(\Lambda_0)\ln\left(\dfrac{\Lambda}{\Lambda_0}\right)}}, \tag{18}$$

where $a_G = \frac{-19}{96\pi^2}, \frac{41}{96\pi^2}, \frac{-7}{16\pi^2}$ and $G(\Lambda_0) = 0.65,\ 0.36, 1.2$ for $G = g, g', g_s$, respectively. The coupling constant λ_t is that between the Higgs field and the top quark. To one-loop order, it runs according to Ref. [52] the following expression:

$$\beta_{\lambda_t} = \frac{\lambda_t}{16\pi^2}\left(9\lambda_t^2 - 8g_s^2 - \frac{9}{4}g^2 - \frac{17}{12}g'^2\right), \tag{19}$$

with $\lambda_t(\Lambda_0) = \frac{m_t(\Lambda_0)}{v} = 0.7$, where v is the Higgs vacuum expectation value and m_t is the top mass. Note that we are taking into consideration the fact that the top-quark contribution is dominant over that of the other fermions of the Standard Model.

After the two spontaneous breakings of symmetry, we end up with the two vacuum expectation values: $v = 246$GeV for the Higgs field h, and v_1 for the auxiliary field S_1. In this section,

we take $v_1 = 150\text{GeV}$. Above v, the fields and parameters of the theory are those of (16). Below v_1, the fields and parameters are those of Eq. (1). We take the values of the physical parameters at the mass scale $\Lambda_0 = 100\text{GeV}$. The initial conditions for the coupling constants in (16) in terms of these physical free parameters are as follows:

$$\begin{aligned}
\eta_1(\Lambda_0) &= \frac{3}{2v_1^2}\left[m_1^2 + m_h^2 + |m_1^2 - m_h^2|\left(\cos(2\theta) + \frac{v}{2v_1}\sin(2\theta)\right)\right];\\
\lambda(\Lambda_0) &= \frac{3}{2v^2}\left[m_1^2 + m_h^2 - |m_1^2 - m_h^2|\left(\cos(2\theta) - \frac{v_1}{2v}\sin(2\theta)\right)\right];\\
\lambda_1(\Lambda_0) &= \frac{\sin(2\theta)}{2vv_1}|m_1^2 - m_h^2|;\\
\eta_{01}(\Lambda_0) &= \frac{1}{\cos(2\theta)}\left[\eta_{01}^{(4)}\cos^2\theta - \lambda_0^{(4)}\sin^2\theta\right];\\
\lambda_0(\Lambda_0) &= \frac{1}{\cos(2\theta)}\left[\lambda_0^{(4)}\cos^2\theta - \eta_{01}^{(4)}\sin^2\theta\right].
\end{aligned} \tag{20}$$

Note that, normally, as we go down the mass scale, we should seam quantities in steps: at v, v_1, and Λ_0. However, the corrections to (20) are of one-loop order times $\ln\frac{v}{v_1}$ or $\ln\frac{v_1}{\Lambda_0}$, small enough for our present purposes to neglect. The perturbativity constraint we impose on all dimensionless scalar coupling constants is $G(\Lambda) \le \sqrt{4\pi}$. Also, vacuum stability means that $G(\Lambda) \ge 0$ for the self-coupling constants η_0, λ, and η_1, and the conditions:

$$-\frac{1}{6}\sqrt{\eta_0\lambda} \le \lambda_0 \le \sqrt{4\pi}; \qquad -\frac{1}{6}\sqrt{\eta_0\eta_1} \le \eta_{01} \le \sqrt{4\pi}; \qquad -\frac{1}{6}\sqrt{\eta_1\lambda} \le \lambda_1 \le \sqrt{4\pi} \tag{21}$$

for the mutual couplings λ_0, η_{01}, and λ_1.

Figure 8 displays the behavior of the self-couplings under RGE for $\theta = 10^o$, $\lambda_0^{(4)} = 0.01$,$m_1 =$ 110 GeV, and $m_0 = 55$ GeV. The dramatic effect is on the Higgs self-coupling constant λ which quickly gets into negative territory, at about 15 TeV, thus rendering the theory unstable beyond this mass scale. This is better displayed in **Figure 9**, where the Renormalization Group (RG) behavior of λ is shown by itself. Such a negative slope for λ is expected, given the negative contributions to β_λ in (17). The coupling constant η_1 is dominant over the other couplings and controls perturbativity, leaving its region much later, at about 1600TeV. This seems to be a somewhat general trend: the non-Higgs SM particles seem to flatten the runnings of the scalar couplings.

The runnings of the mutual coupling constants for the same set of parameters' values are displayed in **Figure 10**. They also get flattened by the other SM particles, but they stay positive. They dwell well below the self-couplings. Increasing m_0 and m_1 will raise the mutual coupling η_{01} and not the two others, higher than η_1 in some regions.

Raising $\lambda_0^{(4)}$ will also make the self-couplings η_1 and η_0 run faster while affecting very little λ. It will also make the mutual coupling η_{01} starts higher, and so demarked from λ_0 and λ_1.

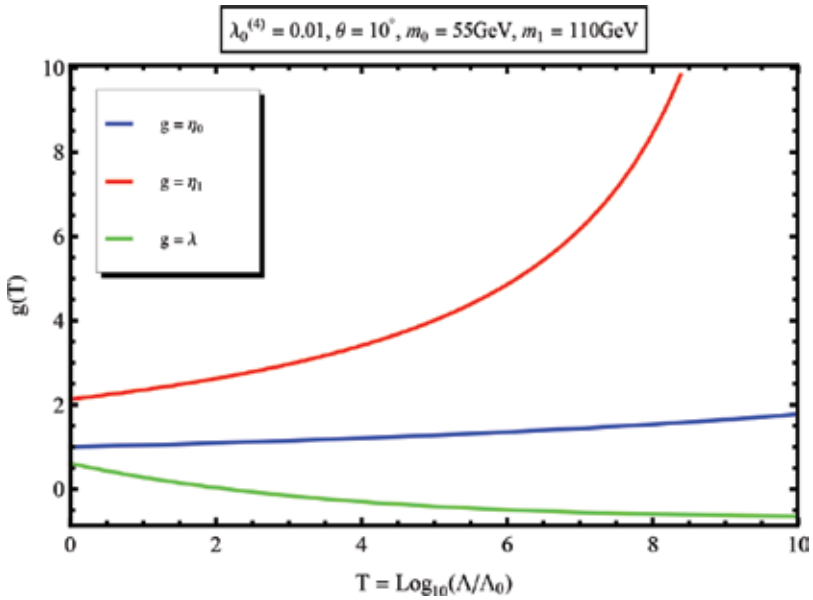

Figure 8. Running of the self-couplings. η_1 controls perturbativity and the Higgs coupling λ becomes negative quickly.

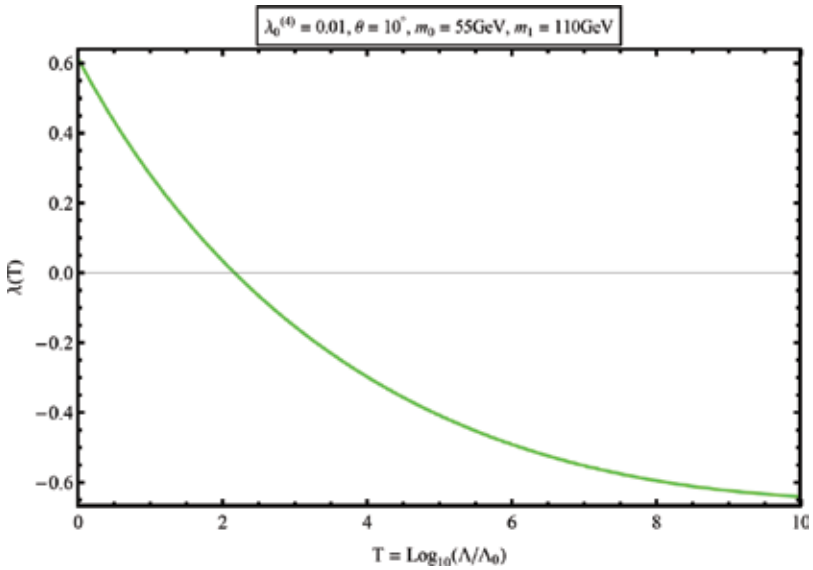

Figure 9. The running of the Higgs self-coupling λ. It becomes negative at about 15 TeV for this set of parameter values.

By contrast, the effect of θ is not very dramatic: the self-couplings are not much affected and the mutuals only evolve differently, without any particular boosting of η_{01}. Details and further comments are found in [33].

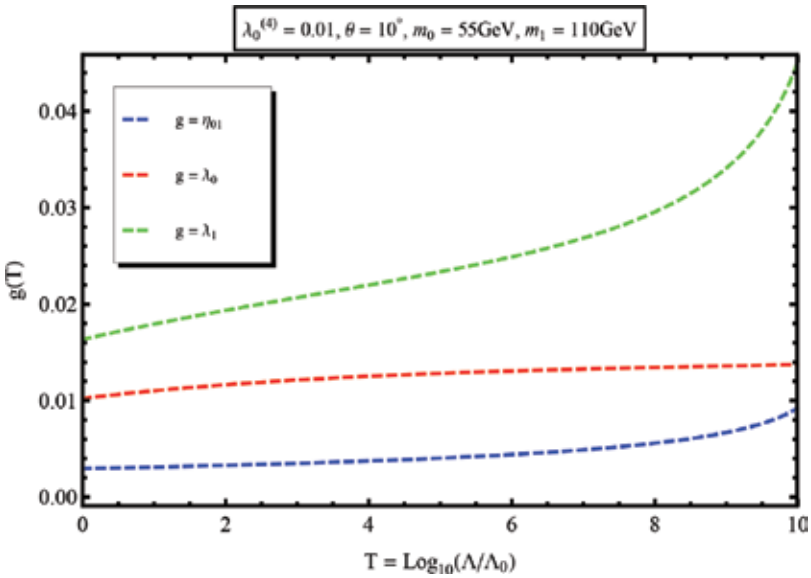

Figure 10. Running of the mutual couplings. The inclusion of the other SM particles flattens the runnings.

7. All constraints together: viability regions

The above RGE analysis taught us two lessons: (i) The two couplings η_1 and η_{01} control perturbativity. (ii) The change of sign of λ controls vacuum stability. Equipped with these indicators, we can try to systematically locate the regions in parameter space in which the model is viable. We have by now a number of tools at our disposal. First, the DM relic-density constraint (6), which has been and will continue to be applied throughout. We have the RGE analysis of the previous section. We will require both $\eta_1(\Lambda)$ and $\eta_{01}(\Lambda)$ to be smaller than $\sqrt{4\pi}$, and $\lambda(\Lambda)$ to be positive. From the phenomenological implications we deduced in Section 5, we will retain only two: the mixing angle θ and the physical self-coupling $\lambda_0^{(4)}$ are to be chosen small. Last, we want the model to comply with the experimental direct-detection upper bounds. The condition we impose is that σ_{det} of Eq. (7) be within the XENON 100 upper bounds [20]. We will vary $\lambda_0^{(4)}$ and θ and track the viability regions in the (m_0, m_1) plane. The relevant mass range for m_0 and m_1 is 1–160 GeV. This is because there are no reliable data to discuss below the GeV and beyond 160 GeV takes us outside the perturbativity region.[2]

One important issue must be addressed before we proceed: How far do we want the model to be perturbatively predictive and stable? The maximum value Λ_m for the mass scale Λ should not be very high. One reason, more conceptual, is that we want to allow the model to be intermediary between the current Standard Model and some possible higher structure at higher energies. Another one, more practical, is that a too high Λ_m is too restrictive for the

[2]In practice, m_0 is taken up to 200 GeV, but there are no additional features to report.

parameters themselves. From the results of the RGE analysis [33], a reasonable compromise is to set $\Lambda_m \simeq 40$ TeV.

With all this in mind, **Figure 11** displays the regions (blue) for which the model is viable when $\lambda_0^{(4)} = 0.01$ and $\theta = 1^o$. The mass m_1 is confined to the interval 116–138 GeV while the DM mass is confined mainly to the region above 118 GeV, the left boundary of which having a positive slope as m_1 increases. In addition, m_0 has a small showing in the narrow interval 57–68 GeV. The effect of increasing the mixing angle θ is to enrich the existing regions without relocating them. This is displayed in **Figure 12** for which θ is increased to 15^o. As θ increases, the region between the narrow band and the larger one to the right gets populated. This means more viable DM masses above 60 GeV, but m_1 stays in the same interval.

By contrast, increasing the Higgs-DM mutual coupling $\lambda_0^{(4)}$ has the opposite effect, that of shrinking existing viability regions. To see this, compare **Figure 13**, for which $\lambda_0^{(4)} = 0.1$ and $\theta = 15^o$, with **Figure 12**. We see indeed shrunk regions, pushed downward by a few GeVs, which is not a substantial relocation. This effect should be expected because increasing $\lambda_0^{(4)}$ raises $\eta_{01}(\Lambda_0)$, well enough above 1 so that we leave perturbativity sooner. Increasing $\lambda_0^{(4)}$ is also caught up by the relic-density constraint, which tends to shut down such larger values of $\lambda_0^{(4)}$ when m_0 is large. The direct-detection constraint has also a similar effect. Further comments can be found in [33].

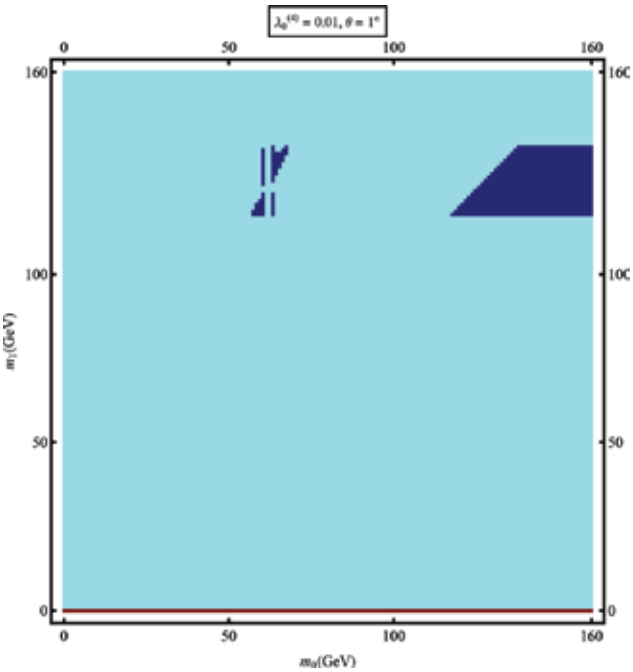

Figure 11. Regions of viability of the two-singlet model (in dark grey). Physical Higgs self-coupling $\lambda_0^{(4)}$ and mixing angle θ very small.

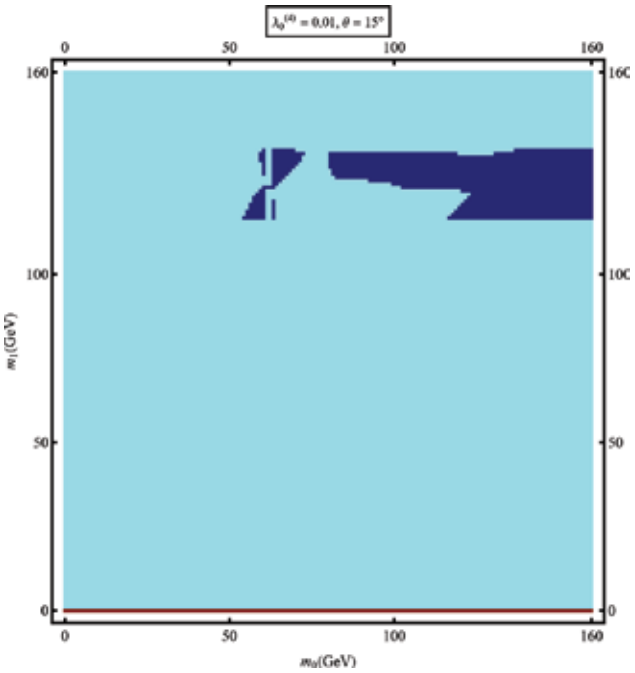

Figure 12. The region of viability (dark grey) is even richer for a larger mixing angle θ.

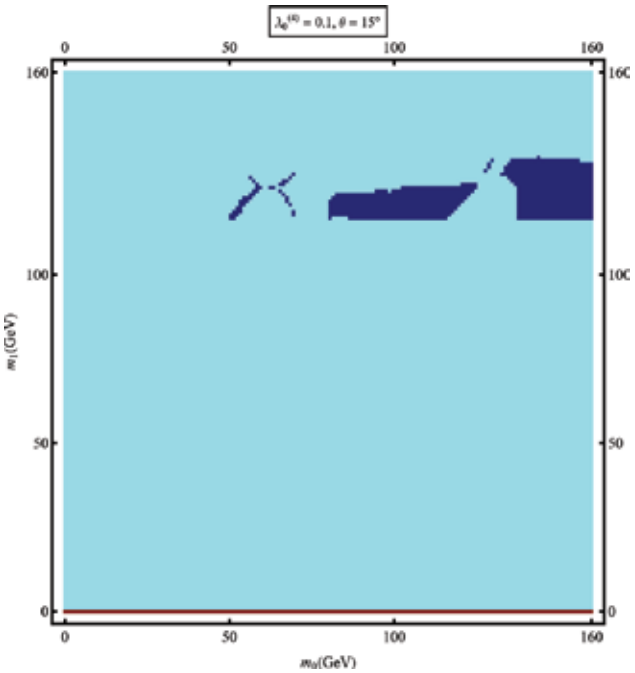

Figure 13. The physical Higgs self-coupling $\lambda_0^{(4)}$ shrinks the viability region (dark grey) as it increases.

8. Concluding remarks

The purpose of this chapter was to help the reader understand how modeling cold dark matter evolves from motivating the model itself to constraining the space of its parameters. We took as prototype a two-singlet extension to the Standard Model of elementary particles within the paradigm of weakly interacting massive particles.

The first set of constraints the model had to undergo came from cosmology and perturbativity. The model had to reproduce the known relic density of cold dark matter while being consistent with perturbation theory. The second set of tests came from direct detection, in the form of the total elastic cross-section of a WIMP scattering off a non-relativistic nucleon that had to satisfy bounds set by several direct-detection experiments. We have seen that the model is capable of satisfying all the existing bounds and will soon be probed by the coming XENON1t experiment. The third set of constraints came from particle phenomenology. We have seen how Υ rare decays constrain the predictions of the model for light cold dark matter. The fourth set of constraints came from internal consistency of the model, in the form of viability and stability under running coupling constants via a renormalization-group analysis. We have concluded that the model can still make sound predictions in important and useful physical regions. We then have investigated the regions in the space of parameters in which the model is viable when all these four sets of constraints are applied together with a maximum cutoff $\Lambda_m \simeq 40$ TeV, a scale at which heavy degrees of freedom may start to be relevant. We have deduced that for small $\lambda_0^{(4)}$ and θ, the auxiliary field mass m_1 is confined to the interval 116–138 GeV, while the DM mass m_0 is confined mainly to the region above 118 GeV, with a small showing in the narrow interval 57–68 GeV. Increasing θ enriches the existing viability regions without relocating them, while increasing $\lambda_0^{(4)}$ has the opposite effect, that of shrinking them without substantial relocation.

There is one aspect of the study we have not touched upon in this review, and that is the connection with and consequences from Higgs physics. This has been analyzed in Refs. [32, 33]. This aspect is important, of course, too important maybe to be just touched upon in this limited space. Such an analysis also needs to be reactualized in view of the many advances made in Higgs physics [53].

Despite all our efforts, dark matter stays elusive. Many models that tried to understand it have failed. The fate of the two-singlet model may not be different. But this will not be a source of disappointment. On the contrary, failure will only fuel motivation to try and explore new ideas.

Author details

Abdessamad Abada[1,2]* and Salah Nasri[3]

*Address all correspondence to: a.abada@uaeu.ac.ae

1 Physics Department, United Arab Emirates University, Al Ain, United Arab Emirates

2 Laboratoire de Physique des Particules et Physique Statistique, Ecole Normale Supérieure, Alger, Algeria

3 United Arab Emirates University, United Arab Emirates

References

[1] Planck Collaboration (Ade PAR, et al.). Astronomy and Astrophysics. 2016;**594**:A13. arXiv:1502.01589

[2] Brandt TD. The Astrophysical Journal. 2016;**824**:L31. arXiv:1605.03665

[3] Bulbul E, et al. ApJ. 2014;**789**:13. arXiv:1402.2301; Boyarsky A, et al. Physical Review Letters. 2014;**113**:251301. arXiv:1402.4119; Physical Review Letters. 2014;**115**:161301. arXiv:1408.2503; Urban O, et al. Monthly Notices of the Royal Astronomical Society. 2015;**451**:2447. arXiv:1411.0050; Iakubovskyi D, et al. arXiv:1508.05186; Franse J, et al. The Astrophysical Journal. 2016;**823**:94. arXiv:1604.01759; Jeltema T, Profumo S. Monthly Notices of the Royal Astronomical Society. 2015;**450**:2143; Ruchayskiy O, et al. Monthly Notices of the Royal Astronomical Society. 2016;**460**:1390. arXiv:1512.07217

[4] Schive HY, Chiueh T, Broadhurst T. Nature Physics. 2014;**10**:496. arXiv:1406.6586; Schive HY, et al. Physical Review Letters. 2014;**113**:261302. arXiv:1407.7762; Schwabe B, Niemeyer JC, Engels JF. Physical Review D. 2016;**94**:043513. arXiv:1606.05151; Marsh DJE. Physics Reports. 2016;**643**:1. arXiv:1510.07633; Hui L, Ostriker JP, Tremaine S, Witten E. arXiv:1610.08297

[5] Stern I, PoS ICHEP2016 (2016) 198, arXiv:1612.08296.

[6] CMS Collaboration. Physical Review Letters. 2017;**118**:021802. arXiv:1605.09305; The European Physical Journal C. 2014;**74**:3036. arXiv:1405.7570; Physics Letters B. 2016;**759**:9. arXiv:1512.08002; ATLAS Collaboration, JHEP. 2014;**04**:169. arXiv:1402.7029

[7] Munoz C, 6th Roma International Workshop on Astroparticle Physics (RICAP16), 21-24 Jun 2016, Roma, Italy, arXiv:1701.05259.

[8] Kahlhoefer F, Int.J.Mod.Phys. A32 (2017) 1730006, arXiv:1702.02430.

[9] Kane G, Shifman M. The Supersymmetric World: The Beginnings of the Theory. Singapore: World Scientific; 2000

[10] Englert F, Brout R. Physical Review Letter. 1964;**13**:321; Higgs PW. Physical Review Letter. 1964;**13**:508; Guralnik GS, Hagen CR, Kibble TWB. Physical Review Letter. 1964; **13**:585

[11] ATLAS Collaboration. Physics Letters B. 2012;**716**:1. arXiv:1207.7214; CMS Collaboration. Physics Letters B. 2012;**716**:30. arXiv:1207.7235

[12] Halkiadakis E, Redlinger G, Shih D. The Annual Review of Nuclear and Particle Science. 2014;**64**:319. arXiv:1411.1427; Flechl M (On behalf of the ATLAS and CMS collaborations), EPJ Web Conference. 2013;**60**:02005. arXiv:1307.4589

[13] Bernabei R, et al. Bled Workshops in Physics. 2016;**17**:1. arXiv:1612.01387

[14] Drukier KA, et al. Physical Review D. 1986;**33**:3495; Freese K, et al. Physical Review D. 1988;**37**:3388

[15] Aalseth CE, et al. arXiv:1401.3295

[16] CDMS Collaboration. Physical Review Letters. 2000;**84**:5699. arXiv:astro-ph/0002471

[17] CDMS Collaboration. Physical Review Letters. 2013;**111**:251301. arXiv:1304.4279

[18] Super CDMS Collaboration. Physical Review Letters. 2016;**116**:071301. arXiv:1509.02448

[19] Aprile E, et al. Astroparticle Physics. 2011;**34:**679. arXiv:1001.2834

[20] XENON100 Collaboration. Physical Review D. 2016;**94**:122001. arXiv:1609.06154; Science. 2015;**349**:851. arXiv:1507.07747; EPJ Web of Conferences. 2016;**121**:06006. arXiv:1501.03492

[21] The XENON Collaboration. Journal of Cosmology and Astroparticle Physics. 2016;**04**: 027. arXiv:1512.07501

[22] Akerib DS, et al. Physical Review Letters. 2016;**116**:161301. arXiv:1512.03506

[23] Akerib DS, et al. arXiv:1702.02646

[24] Jochum J, et al. [CRESST Collaboration], Physics of Atomic Nuclei. 2000;**63**:1242; Yadernaya Fizika. 2000;**63**:1315. arXiv:hep-ex/0005003

[25] Angloher G, et al. [CRESST II Collaboration], The European Physical Journal C. 2014;**74**:3184. arXiv:1407.3146; The European Physical Journal C. 2016;**76**:25. arXiv: 1509.01515; Physical Review Letters. 2016;**117**:021303. arXiv:1601.04447

[26] Armengaud E, et al. Journal of Cosmology and Astroparticle Physics. 2016;**05**:019. arxiv:1603. 05120

[27] Ackermann M, et al. [Fermi-LAT], Physical Review Letters. 2015;**115:**231301. arXiv: 1503.02641; Fermi-LAT Collaboration, The Astrophysical Journal. 2016;**819**:44. arXiv: 1511.02938; Karwin C, et al. arXiv:1612.05687

[28] Aguilar M, et al. [AMS Collaboration]. Physical Review Letters. 2016;**110:**141102; Aguilar M, et al. [AMS-02 Collaboration], Physical Review Letters. 2016;**117**:091103

[29] Adriani O, et al. [PAMELA Collaboration], Nature. 2009;**458**:607. arXiv:0810.4995; PAMELA Collaboration, Physical Review Letters. 2016;**111**:081102. arXiv:1308.0133; Adriani O, et al. [PAMELA collaboration]. Physics Reports. 2014;**544:**323

[30] ATLAS Collaboration. Physics Letters B. 2016;**763**:251. arXiv:1608.02372

[31] Abada A, Ghafor D, Nasri S. Physical Review D. 2011;**83**:095021. arXiv:1101.0365

[32] Abada A, Nasri S. Physical Review D. 2012;**85**:075009. arXiv:1201.1413

[33] Abada A, Nasri S. Physical Review D. 2013;**88**:016006. arXiv:1201.1413

[34] Autermann C. Progress in Particle and Nuclear Physics. 2016;**90**:125. arXiv:1609.01686

[35] Silveira V, Zee A. Physics Letters B. 1985;**161**:136

[36] McDonald J. Physical Review D. 1994;**50**:3637; Burgess CP, Pospelov M, ter Veldhuis T ter. Nuclear Physics B. 2001;**619**:709; Barger V, et al. Physical Review D. 2008;**77**:035005. arXiv:0706.4311; Gonderinger M, et al. JHEP. 2010;**053**:1001. arXiv:0910.3167

[37] He X, et al. Physical. Review D. 2009;**79**:023521. arXiv:0811.0658; Cai Y, He XG, Ren B. Physical Review D. 2011;**83**:083524. arXiv:1102.1522; Asano M, Kitano R. Physical Review D. 2010;**81**:054506. arXiv:1001.0486; Arina C, Tytgat MHG. Journal of Cosmology and Astroparticle Physics. 2011;**1101**:011. arXiv:1007.2765

[38] Patrignani C, et al. (Particle Data Group). Chinese Physics C. 2016;**40**:100001

[39] Kolb E, Turner MS. The Early Universe. Boston, MA: Addison-Wesley; 1998

[40] Weinberg S. Cosmology. Oxford: Oxford University Press; 2008

[41] Eidelman S, et al. Physics Letters B. 2004;**592**:1

[42] Nason P. Physics Letters B. 1986;**175**:223

[43] Chivukula RS, Cohen AG, Georgi H, Grinstein B, Manohar AV. Annals of Physics. 1989;**192**:93

[44] Voloshin MB. Soviet Journal of Nuclear Physics. 1986;**44**:478 [Yadernaya fizika **44**, 738 (1986)]

[45] Gunion JF, Haber HE, Kane G, Dawson S. The Higgs Hunters Guide. Cambridge, MA: Perseus Publishing; 1990

[46] McKeen D. Physical Review D. 2009;**79**:015007

[47] Djouadi A. Physics Reports. 2008;**459**:1

[48] Love W, et al. Physical Review Letters. 2008;**101:**151802

[49] Anastassov A, et al. [CLEO Collaboration]. Physical Review Letters. 1999;**82**:286

[50] Athar SB, et al. [CLEO Collaboration]. Physical Review D. 2006;**73**:032001

[51] Auber B, et al. [BABAR Collaboration]. Physical Review Letters. 2009;**103**:081803

[52] Ford C, Jones DRT, Stephenson PW, Einhorn B. Nuclear Physics B. 1993;**395**:17; Sher M. Physics Reports. 1989;**179**:273; Djouadi A. Physics Reports. 2008;**457**:1

[53] Work in progress

Chapter 3

Neutrino Interactions with Nuclei and Dark Matter

Paraskevi C. Divari

Additional information is available at the end of the chapter

http://dx.doi.org/10.5772/intechopen.68196

Abstract

Even though the combined laboratory, astrophysical and cosmological evidence implies that neutrinos have masses, neutrinos provide only a small cosmic dark matter component. The study of solar neutrinos provides important information on nuclear processes inside the Sun as well as on matter densities. Moreover, supernova neutrinos provide sensitive probes for studying supernova explosions, neutrino properties and stellar collapse mechanisms. Neutrino-nucleus reactions at energies below 100 MeV play essential roles in core-collapse supernovae, explosive and r-process nucleosynthesis, as well as observation of solar and supernova neutrinos by earthbound detectors. On the other hand, recent experimental data of high-energy extragalactic neutrinos at 1 PeV open a new window to probe non-standard neutrino properties, such as resonant effects in the oscillation probability.

Keywords: neutrino physics, neutrino oscillations, charge current neutrino-nucleus scattering, dark matter, sterile neutrino

1. Introduction

Neutrinos play a fundamental role in cosmology and astrophysics, two rapidly progressing fields. The origin of neutrino masses and the nature of dark matter (DM) are two most pressing open questions in modern astro-particle physics. We know from the observation of neutrino oscillations that neutrinos have masses [1, 2]. The smallness of neutrino masses relative to those of the standard model (SM) charged fermions remains a puzzle. The effect of small neutrino masses may be probed in precision cosmic microwave background (CMB) radiation observations [3–10] as well as large-scale galaxy surveys [11–13]. The absolute scale of neutrino mass may also affect the long-standing issue of cosmic structure formation. Furthermore, neutrinos govern big-bang nucleosynthesis so that neutrino properties can be inferred from the observed light-element abundances [14–16]. Massive neutrinos may also be responsible to account for the mystery of the matter to anti-matter asymmetry in the Universe. Finally, core-collapse supernovae are powerful 'laboratories' to probe neutrino properties if in the future

one were to observe a high-statistics neutrino signal. For example, a stellar core collapse in the Milky Way satellite galaxies may produce an enormous burst of neutrinos 'visible' by terrestrial detectors. Such an effect will carry important information in astrophysics, cosmology and particle physics [17, 18]. In addition, dedicated experiments are now planned involving intense accelerator-produced neutrino beams to study neutrino properties over long baselines. These will traverse the mantle or/and core of the Earth [19] so that the interpretation of the results will require geophysical details [20, 21].

Neutrinos could be key particles to unravel the nature of the DM in the Universe. The dark matter problem has been a long-standing one in physics [22, 23]. Even though we know that it must exist [24–27], we do not know much about its true nature. It is clear, though, that massive neutrinos and dark matter are both part of nature and should be incorporated in models of physics beyond the standard model. It may be that they are related to each other [28] and that, in addition, both originate from new physics at the TeV scale.

Several studies have noted that the existence of light sterile neutrinos would have important consequences for dark matter searches [29]. Moreover, MSW-enhanced transitions between active and sterile neutrinos would have a substantial impact on searches for neutrinos from dark matter annihilation in the Sun [30, 31]. Furthermore, if sterile neutrinos in addition to their mixing with the active neutrinos possess some new gauge interactions, they could lead to signals which appear to favour a dark matter interpretation. These can be used to investigate sterile states and may also generate strong signals in DM detectors [32–34]. Couplings between neutrino, either active or sterile, and dark matter have been studied in many different contexts [35–46].

Understanding the explosion of supernovae or the physics of the early universe, where neutrinos play an essential role, requires a solid theoretical background in astrophysics and cosmology and reliable input from nuclear physics. Neutrino-nucleus scattering at energies below 100 MeV plays an essential role in core-collapse supernova simulations in various interactions of neutrinos with the supernova environment. Based on the improved supernova simulations, it is found that inelastic neutrino-nucleus reactions will also allow for an additional mode of energy deposition to the matter ahead of the shock wave in the post-shock explosion phase, supporting the shock propagation.

A call for reliable neutrino-nucleus cross sections has also been made in the context of explosive nucleosynthesis, occurring when the shock wave passes through the exploding star and leads to fast nuclear reactions. It has also been pointed out that neutrino-induced reactions in the outer layers of the star can actually be the major source for the production of certain nuclides in nature. This is the so-called ν-process. Such ν-process is sensitive to those neutrinos, which are detectable at the new generation of supernova neutrino detectors. The latter can distinguish the incoming neutrino types and hence will probe the supernova neutrino distributions. An analysis of the events observed by these detectors requires detailed calculations of the interaction of neutrinos with the detector material. Such accurate determination of the neutrino-nucleus cross sections for nuclei, like ^{12}C (KamLAND, Borexino) [47–49], ^{16}O (SNO, Super-Kamiokande) [50, 51], ^{40}Ar (ICARUS) [52], ^{208}Pb (OMNIS) [53, 54], ^{56}Fe (MINOS) [55], ^{114,116}Cd (COBRA) [56, 57], ^{132}Xe (XENON) [58], will be especially useful for present or near future experiments.

Recently, the IceCube Collaboration has reported the detection of ultra-high energy (UHE) neutrino events coming from extraterrestrial sources, that is, neutrinos with energies in the range TeV–PeV [59–61]. The most plausible sources that these events are connected are from unique high-energy cosmic ray accelerators like semi-relativistic hypernova remnants (HNRs) [62–64], and remnants from gamma ray bursts in star-burst galaxies, which can produce primary cosmic rays with the required energies and abundance [65]. Neutrino interactions with DM could have strong implications at cosmological scales, such as reduction of the relic neutrino density, modification of the CMB spectra [37] or even a connection between the smallness of neutrino mass and a MeV-mass scalar field DM [66]. Many DM candidates have been proposed in this context: heavy neutrinos as dark matter, lightest supersymmetric particles (LSP) and MeV-mass scalar field. Furthermore, sterile neutrinos appear in models attempting to explain the dark matter problem either as the main component for the dark matter content or as an additional subleading component of a multiparticle dark matter model. Those particles interact with matter through mixing with the active neutrino states. If there is a mixing between active and sterile neutrinos, UHE neutrinos interacting with dark matter may experience an enhancement in the oscillation probability when they propagate in a DM medium. This is a mechanism that could be tested from future UHE experimental data.

The chapter has been organized as follows. In Section 2, we outline the basic formalism used in the evaluation of neutrino-nucleus cross sections. Section 3 presents original cross section calculations for charged current (CC) neutrino and antineutrino scattering off targets from ^{12}C to ^{208}Pb, at energies below 100 MeV. Illustrative test calculations are performed for CC (anti)neutrino reactions on ^{56}Fe and ^{40}Ar, and the results are compared with other previous theoretical studies. Such cross section calculations provide us with significant information regarding the range of efficiency of these isotopes in low-energy neutrino searches. The event estimates are made by convolving the calculated cross sections with two different distributions: the Fermi-Dirac (FD) flux and the Livermore one. In Section 4, results are presented concerning the interaction potential of extragalactic neutrinos, at ultra-high energies, with dark matter, which might induce resonant effects in the oscillation survival probability. Finally, in Section 5, the main conclusions extracted from the present work are summarized.

2. Charge current neutrino-nucleus cross-section formalism

Let us consider a neutrino-nucleus interaction in which a low or intermediate energy neutrino (or antineutrino) is scattered inelastically from a nucleus (A, Z) being in its ground state.

The standard model effective Hamiltonian in a charge current interaction can be written as:

$$\mathcal{H} = \frac{G\, cos\boldsymbol{\theta}_c}{\sqrt{2}} j_\mu(x) J^\mu(x), \tag{1}$$

Here, $G = 1.1664 \times 10^{-5} GeV^{-2}$ denotes the Fermi weak coupling constant and $\theta_c \simeq 13^o$ is the Cabibbo angle. According to V-A theory, the leptonic current takes the form:

$$j_\mu = \overline{\psi}_{\nu_\ell}(x)\gamma_\mu(1-\gamma_5)\psi_{\nu_\ell}(x)\,, \tag{2}$$

where, Ψ_{ν_ℓ} are the neutrino/antineutrino spinors. The hadronic current of vector, axial-vector and pseudo-scalar components is written as:

$$J_\mu = \overline{\psi}_N\left[F_1(q^2)\gamma_\mu + F_2(q^2)\frac{i\sigma_{\mu\nu}q^\nu}{2M_N} + F_A(q^2)\gamma_\mu\gamma_5 + F_P(q^2)\frac{1}{2M_N}q_\mu\gamma_5\right]\psi_N \tag{3}$$

(M_N stands for the nucleon mass and ψ_N denotes the nucleon spinors). By the conservation of the vector current (CVC), the vector form factors $F_{1,2}(q^2)$ can be written in terms of the proton and neutron electromagnetic form factors [67]. The axial-vector form factor $F_A(q^2)$ is assumed to be of dipole form [68]:

$$F_A = -g_A(1-q^2/M_A^2)^{-2}\,, \tag{4}$$

where $M_A = 1.05$ GeV is the axial cut-off mass and g_A is the static value (at $q = 0$) of the axial form factor. Recently, it has been shown in modelling the GT^+ and GT^- transition strengths that in both channels the quenching factor 0.8 in the axial vector coupling constant is necessary to describe the experimentally measured GT strengths. Therefore, in our work, the effective quenched static value g_A = 1.0 is employed [69]. Moreover, the pseudoscalar form factor $F_P(q^2)$ is obtained from the Goldberger-Treiman relation [70]:

$$F_P(q^2) = \frac{2M_N F_A(q^2)}{m_\pi^2 - q^2} \tag{5}$$

where $m_\pi = 139.57$ MeV represents the mass of the charged pion. The strangeness contributions are not taken into account since the energy region considered here is below the quasi-elastic region where the contributions from strangeness can be neglected [71].

In the convention we used in the present work q^2, the square of the four-momentum transfer $q \equiv (q_0,\mathbf{q})$ is written as:

$$q^2 = q^\mu q_\mu = \omega^2 - \mathbf{q}^2 = (\varepsilon_f - \varepsilon_i)^2 - (\mathbf{p}_f - \mathbf{p}_i)^2 < 0\,, \tag{6}$$

where $\omega = -q_0 = \varepsilon_i - \varepsilon_f$ is the excitation energy of the nucleus. ε_i denotes the energy of the incoming lepton and ε_f that of the outgoing lepton. $\mathbf{p}_i$ and $\mathbf{p}_f$ are the corresponding 3-momenta of the incoming and outgoing leptons, respectively.

The neutrino/antineutrino-nucleus differential cross section, after applying a multipole analysis of the weak hadronic current, is written as:

$$\sigma(\varepsilon_i) = \frac{2G^2 cos^2\theta_c}{2J_i+1}\sum_f |\mathbf{p}_f|\varepsilon_f \int_{-1}^{1} d(\cos\theta)F(\varepsilon_f,Z_f)\left(\sum_{J=0}^{\infty}\sigma_{CL}^J + \sum_{J=1}^{\infty}\sigma_T^J\right) \tag{7}$$

θ denotes the lepton scattering angle. The summations in Eq. (7) contain the contributions σ_{CL}^J, for the Coulomb $\widehat{\mathcal{M}}_J$ and longitudinal $\widehat{\mathcal{L}}_J$, and σ_T^J, for the transverse electric $\widehat{\mathcal{T}}_J^{el}$ and magnetic

$\widehat{T}_J^{mag}$ multipole operators [72]. These operators include both polar-vector and axial-vector weak interaction components.

The contributions of σ_{CL}^J and σ_T^J are written as:

$$\begin{aligned}\sigma_{CL}^J &= (1 + a\cos\theta)\left|\langle J_f||\hat{\mathcal{M}}_J||J_i\rangle\right|^2 + (1 + a\cos\theta - 2b\sin^2\theta)\left|\langle J_f||\hat{\mathcal{L}}_J||J_i\rangle\right|^2 \\ &+ \left[\frac{\varepsilon_i - \varepsilon_f}{q}(1 + a\cos\theta) + c\right] 2\,\Re e\langle J_f||\hat{\mathcal{L}}_J||J_i\rangle\langle J_f||\hat{\mathcal{M}}_J||J_i\rangle^*\end{aligned} \tag{8}$$

$$\begin{aligned}\sigma_T^J &= (1 - a\cos\theta + b\sin^2\theta)\left[\left|\langle J_f||\hat{\mathcal{T}}_J^{mag}||J_i\rangle\right|^2 + \left|\langle J_f||\hat{\mathcal{T}}_J^{el}||J_i\rangle\right|^2\right] \\ &\mp \left[\frac{(\varepsilon_i + \varepsilon_f)}{q}(1 - a\cos\theta) - c\right] 2\,\Re e\,\langle J_f||\hat{\mathcal{T}}_J^{mag}||J_i\rangle\,\langle J_f||\hat{\mathcal{T}}_J^{el}||J_i\rangle^*\end{aligned} \tag{9}$$

where $b = \varepsilon_i\varepsilon_f a^2/|\mathbf{q}|^2$, $a = |\mathbf{p}_f|/\varepsilon_f$ and $c = (m_f c^2)^2/(|\mathbf{q}|\varepsilon_f)$. In Eq. (9), the $(-)$ sign corresponds to neutrino scattering and the (+) sign to antineutrino. The absolute value of the three-momentum transfer is given by:

$$|\mathbf{q}| = \sqrt{\omega^2 + 2\varepsilon_f\varepsilon_i(1 - a\cos\theta) - (m_f c^2)^2} \tag{10}$$

For charge current (CC) reactions, the cross section of Eq. (7) must be corrected for the distortion of the outgoing lepton wave function by the Coulomb field of the daughter nucleus [73] and references therein.

3. Original cross sections

Development of large mass detectors for low energy neutrinos and dark matter may allow supernova detection via neutrino-nucleus scattering (elastic or inelastic). An analysis of the events observed by these detectors requires a detailed calculation of the interaction cross sections of neutrinos with the detector material. Especially interesting is modelling the reaction cross sections of neutrinos scattering on nuclei that can be used as targets for SN neutrino detectors. The target materials include a range of isotopes from ^{4}He to ^{208}Pb. In this chapter, we report results concerning the cross sections of charge current (CC) (anti)neutrino-nucleus reactions for some isotopes of astrophysical interest. The results refer to the target isotopes ^{12}C, ^{16}O, ^{18}O, ^{40}Ar, ^{56}Fe, ^{114}Cd, ^{116}Cd, ^{132}Xe and ^{208}Pb. The nuclear matrix elements entering in Eqs. (8) and (9) have been calculated in the framework of pnQRPA [73–75]. The respective cross sections are listed in **Tables 1** and **2** for various incoming (anti)neutrino energies E_ν below 100 MeV. Cross-section results for ^{208}Pb are taken from Ref. [76]. The reliability of our calculations is justified from the comparison of the CC neutrino-nucleus cross sections with other calculations. In **Figure 1**, we compare our calculated cross sections for the reactions $\nu_e/\overline{\nu}_e - {}^{56}Fe$ and $\nu_e/\overline{\nu}_e - {}^{40}Ar$ with those of Refs. [76] and [77], respectively.

	$\sigma_{tot}(10^{-42}$ cm$^2)$								
E_{ν_e} (MeV)	^{12}C	^{16}O	^{18}O	^{40}Ar	^{56}Fe	^{114}Cd	^{116}Cd	^{132}Xe	^{208}Pb
7.5			2.72(0)	1.29(0)	3.34(−1)	1.73(+1)	3.40(+1)	1.07(0)	2.47(−4)
10.0			5.72(0)	4.59(0)	2.10(0)	6.24(+1)	9.93(+1)	2.09(+1)	8.49(0)
5.0			1.75(+1)	2.25(+1)	2.03(+1)	2.55(+2)	3.32(+2)	1.97(+2)	1.75(+2)
20.0	4.80(−1)	4.48(−2)	3.86(+1)	5.90(+1)	6.23(+1)	5.58(+2)	6.73(+2)	6.27(+2)	8.53(+2)
25.0	2.02(0)	2.95(−1)	7.10(+1)	1.17(+2)	1.28(+2)	9.45(+2)	1.10(+3)	1.30(+3)	2.86(+3)
30.0	5.8(0)	8.91(−1)	1.17(+2)	1.98(+2)	2.18(+2)	1.29(+3)	1.41(+3)	1.82(+3)	4.90(+3)
40.0	2.78(+1)	8.20(0)	2.60(+2)	4.42(+2)	4.74(+2)	1.92(+3)	2.07(+3)	2.76(+3)	7.13(+3)
50.0	7.89(+1)	3.97(+1)	4.88(+2)	8.07(+2)	8.25(+2)	2.65(+3)	2.83(+3)	3.74(+3	1.13(+4)
60.0	1.71(+2)	1.19(+2)	8.29(+2)	1.30(+3)	1.27(+3)	3.43(+3)	3.65(+3)	4.76(+3)	1.63(+4)
70.0	3.07(+2)	2.74(+2)	1.30(+3)	1.89(+3)	1.81(+3)	4.21(+3)	4.46(+3)	5.75(+3)	2.20(+4)
80.0	4.87(+2)	5.33(+2)	1.91(+3)	2.55(+3)	2.42(+3)	4.94(+3)	5.22(+3)	6.63(+3)	2.83(+4)
90.0	7.06(+2)	9.17(+2)	2.65(+3)	3.27(+3)	3.07(+3)	5.65(+3)	5.95(+3)	7.32(+3)	3.50(+4)
100.0	9.95(+2)	1.43(+3)	3.51(+3)	4.03(+3)	3.75(+3)	6.33(+3)	6.65(+3)	7.78(+3)	4.16(+4)

The cross sections are given in units of 10^{-42} cm^2, exponents are given in parentheses.

Table 1. Total cross sections σ_{tot} for the indicated neutrino-nucleus charge current reactions as a function of the incoming neutrino energy.

Charge current interactions proceed through interaction of ν_e and $\overline{\nu}_e$ with neutrons and protons, respectively, in nuclei $\nu_e + (N,Z) \rightarrow (N-1,Z+1) + e^-$ and $\overline{\nu}_e + (N,Z) \rightarrow (N+1,Z-1) + e^+$. The kinematic threshold is $E_{thres} = \frac{M_f^2 + m_e^2 + 2M_f m_e - M_i^2}{2M_i} \sim M_f - M_i + m_e$, where M_f and M_i are the initial- and final-state nuclear masses and m_e is the electron mass. The corresponding thresholds for CC reactions on the above target isotopes are given in **Table 3**. Note that at supernova energies, ν_μ and ν_τ are below the CC interaction threshold and thus are kinematically unable to produce their partner leptons.

An important application of microscopic models of neutrino-nucleus reactions is the calculation of cross sections for supernova neutrinos. Thus, in order to estimate the response of a nucleus to a specific source of neutrinos, the calculated cross sections given in **Tables 1** and **2** must be folded with a specific supernova neutrino energy distribution. The neutrino spectrum of a core-collapse supernova is believed to be similar to a Fermi-Dirac (FD) spectrum, with temperatures in the range 3–8 MeV [78]. The FD energy distribution is given by:

$$\eta_{FD} = \frac{N_2(\alpha)}{T^3} \frac{E_\nu^2}{1 + exp[(E_\nu/T) - \alpha]} \tag{11}$$

where T is the neutrino temperature and α being a degeneracy parameter. $N_2(\alpha)$ denotes the normalization factor depending on α given from

	$\sigma_{tot}(10^{-42}$ cm$^2)$								
$E_{\bar{\nu}_e}$ (MeV)	^{12}C	^{16}O	^{18}O	^{40}Ar	^{56}Fe	^{114}Cd	^{116}Cd	^{132}Xe	^{208}Pb
7.5					1.68(0)	6.30(−1)	1.30(−1)	8.78(−3)	1.37(−6)
10.0				4.07(−1)	6.04(0)	3.37(0)	1.41(0)	1.63(−1)	8.36(−3)
5.0	1.23(−1)	2.26(−2)	1.30(0)	4.62(0)	2.07(+1)	2.19(+1)	1.57(+1)	2.46(0)	2.44(−1)
20.0	8.43(−1)	1.88(−1)	5.66(0)	1.73(+1)	4.48(+1)	5.72(+1)	4.70(+1)	1.75(+1)	1.11(0)
25.0	2.29(0)	6.00(−1)	1.58(+1)	4.10(+1)	7.95(+1)	1.07(+2)	9.38(+1)	4.75(+1)	3.05(0)
30.0	7.77(0)	1.78(0)	3.31(+1)	7.71(+1)	1.24(+2)	1.69(+2)	1.54(+2)	8.69(+1)	1.53(0)
40.0	3.35(+1)	1.23(+1)	9.38(+1)	1.91(+2)	2.40(+2)	3.21(+2)	3.07(+2)	1.77(+2)	5.65(0)
50.0	9.05(+1)	4.23(+1)	1.95(+2)	3.62(+2)	3.80(+2)	4.98(+2)	4.87(+2)	3.93(+2)	3.48(+1)
60.0	1.88(+2)	1.03(+2)	3.45(+2)	5.83(+2)	5.33(+2)	7.93(+2)	6.87(+2)	6.92(+2)	8.29(+1)
70.0	3.28(+2)	2.07(+2)	5.47(+2)	8.42(+2)	6.94(+2)	1.27(+3)	8.96(+2)	9.83(+2)	1.46(+2)
80.0	5.04(+2)	3.62(+2)	8.04(+2)	1.12(+3)	8.64(+2)	1.82(+3)	1.10(+3)	1.24(+3)	2.16(+2)
90.0	7.09(+2)	5.72(+2)	1.11(+3)	1.43(+3)	1.04(+3)	2.42(+3)	1.31(+3)	1.47(+3)	2.91(+2)
100.0	9.34(+2)	8.38(+2)	1.48(+3)	1.76(+3)	1.23(+3)	3.02(+3)	1.50(+3)	1.69(+3)	3.67(+2)

The cross sections are given in units of 10^{-42} cm^2, exponents are given in parentheses

Table 2. Total cross sections σ for the indicated antineutrino-nucleus charge current reactions as a function of the incoming neutrino energy.

$$N_k(\alpha) = \left(\int_0^\infty \frac{x^k}{1 + e^{x-\alpha}} dx \right)^{-1} \tag{12}$$

for $k = 2$. The degeneracy parameter α is called the chemical potential parameter. Characteristic of the FD energy distribution is that the peak shifts to higher neutrino energies and the width increases as the neutrino temperature increases (**Figure 2**).

Following Ref. [79], the average neutrino energy $\langle E_\nu \rangle$ can be written in terms of the functions of Eq. (12) as:

$$\langle E_\nu \rangle = \frac{N_2(\alpha)}{N_3(\alpha)} T \tag{13}$$

Some characteristic values of $\langle E_\nu \rangle$ are listed in **Table 4**.

For a connection of the present theoretical results with the neutrino experiments and the neutrino sources, we carry out the folding (convolution) of the calculated cross sections given in **Tables 1** and **2** with the distribution η_{FD} and estimate the response of the given isotopes to the corresponding spectrum. These responses (signals to the detector) are evaluated by:

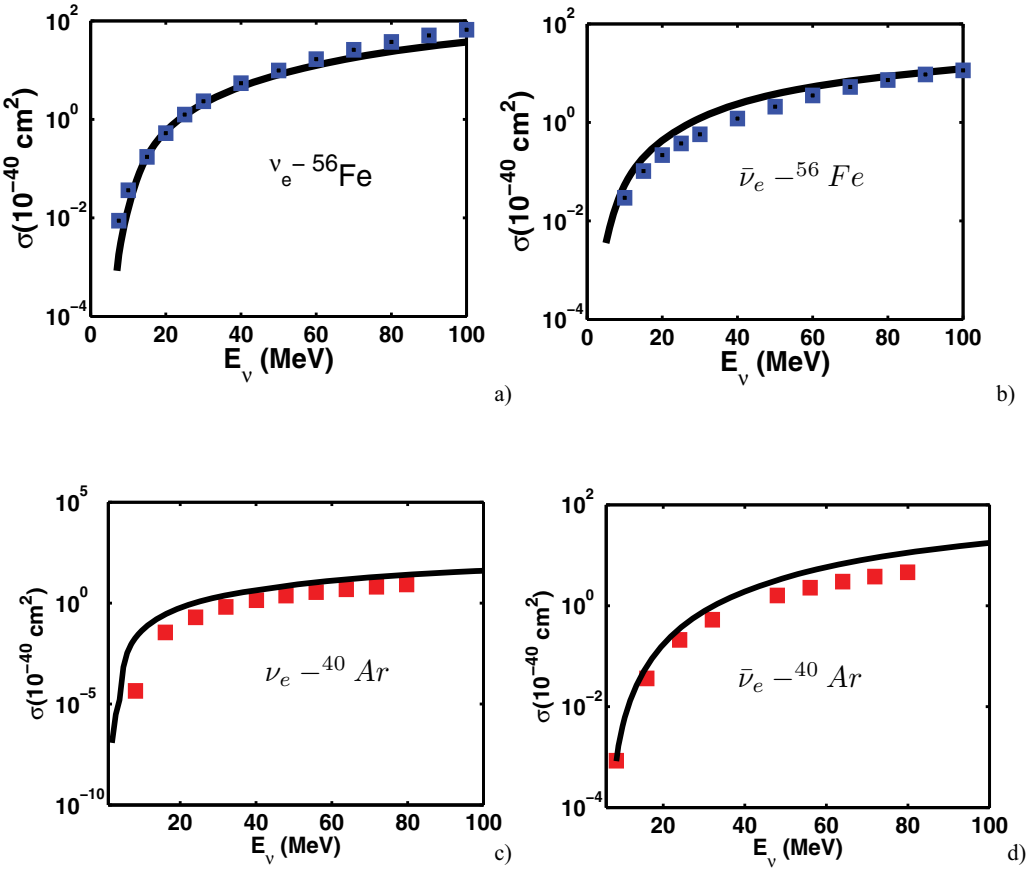

Figure 1. Cross sections for relevant neutrino (antineutrino) reactions on isotopes ^{56}Fe and ^{40}Ar. The results denoted by square symbols are taken from Refs. [76] and [77].

$$\langle\sigma\rangle = \int_0^\infty \sigma(E_\nu)\eta_{FD}(E_\nu)dE_\nu \tag{14}$$

In **Figure 3**, we compare the respective neutrino flux-averaged cross sections for some of target nuclei given in **Table 1**.

We close this subsection by exploiting our predictions of total cross sections to estimate the number of expected electron (anti)neutrino events in a detector. For current detectors [80], typical event yields are a few hundred events per kt of detector material for a core-collapse event at $D = 10$ kpc (3.1×10^{22} cm) away from the Earth. A supernova radiates via neutrinos, an amount of total energy 3×10^{53} erg in about 10*s*. Assuming an equal partition of energy among neutrinos, the supernova radiates $N_{\nu_e} = 3.0 \times 10^{57}$ electron neutrinos and $N_{\overline{\nu}_e} = 2.1 \times 10^{57}$ electron antineutrinos. The neutrino fluence $\Phi(E_\nu)$ for electron neutrinos/antineutrinos is given by the relation:

Interaction	E_{thres}(MeV)
$^{12}C(\nu_e,e^-)^{12}N$	17.34
$^{12}C(\overline{\nu}_e,e^+)^{12}B$	14.39
$^{16}O(\nu_e,e^-)^{16}F$	15.42
$^{16}O(\overline{\nu}_e,e^+)^{16}N$	11.42
$^{18}O(\nu_e,e^-)^{18}F$	1.65
$^{18}O(\overline{\nu}_e,e^+)^{18}N$	14.91
$^{40}Ar(\nu_e,e^-)^{40}K$	1.50
$^{40}Ar(\overline{\nu}_e,e^+)^{40}Cl$	8.50
$^{56}Fe(\nu_e,e^-)^{56}Co$	4.56
$^{56}Fe(\overline{\nu}_e,e^+)^{56}Mn$	4.71
$^{114}Cd(\nu_e,e^-)^{114}In$	1.45
$^{114}Cd(\overline{\nu}_e,e^+)^{114}Ag$	6.09
$^{116}Cd(\nu_e,e^-)^{116}In$	0.46
$^{116}Cd(\overline{\nu}_e,e^+)^{116}Ag$	7.11
$^{132}Xe(\nu_e,e^-)^{132}Cs$	2.12
$^{132}Xe(\overline{\nu}_e,e^+)^{132}I$	4.60
$^{208}Pb(\nu_e,e^-)^{208}Bi$	2.90
$^{208}Pb(\overline{\nu}_e,e^+)^{208}Tl$	6.01

Table 3. Thresholds values E_{thres} (in MeV) for charge current antineutrino-nucleus interactions.

$$\Phi(E_\nu) = \frac{N_{\nu_e/\overline{\nu}_e}}{4\pi D^2}\eta_{FD}(E_\nu) \tag{15}$$

Two examples of supernova models are used to predict the neutrino flux: (i) the model based on the FD distribution with a single temperature (3.5 MeV for neutrinos and 5 MeV for antineutrinos) and zero chemical parameter ($\alpha = 0$) and (ii) the numerical simulation of supernova neutrino emission model called Livermore [81], which assumes the FD spectra with $\alpha = 0$ and with the average energies indicated as a function of time integrated from 0 to 14 seconds after the core collapse. The Livermore energy spectrum for the ν_e and $\overline{\nu}_e$ flavour components is shown in **Figure 4**. The nature of the neutrino spectra and their time evolution depend on mass, oscillation parameters, such as θ_{13} and the mass hierarchy. Furthermore, the chance that the supernova neutrinos will traverse Earth matter on their way to a detector is not negligible [82] and oscillations in the Earth modulate the supernova neutrino spectrum for either ν_e or $\overline{\nu}_e$ [83–85]. In a single detector, an Earth matter-induced spectral modulation may give information about oscillations, involving probably sterile neutrino states (e.g., [19, 86]).

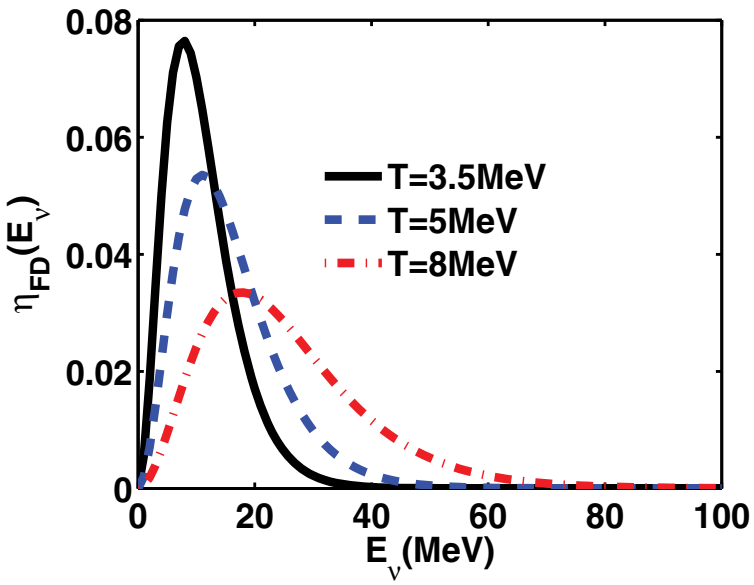

Figure 2. The normalized unity Fermi-Dirac spectrum for $\alpha = 0$.

	< *Eν* > (MeV)		
α	**T = 3.5MeV**	**T = 5MeV**	**T = 8MeV**
0	11.03	15.76	25.21
0.76	11.46	16.37	26.19
1.52	12.10	17.28	27.65
2.28	12.96	18.52	29.63
3.04	14.03	20.05	32.08
4.56	16.66	23.80	38.09
5.76	19.06	27.23	43.58

Table 4. The average supernova neutrino energies as a function of the parameters α and T.

If the mass of the target material is m_t, corresponding to N_{at} atoms, then the number of expected events per energy are:

$$\frac{dN_{events}}{dE_\nu} = N_{at}\Phi(E_\nu)\sigma_{tot}(E_\nu) \tag{16}$$

where $\sigma_{tot}(E_\nu)$ is the total cross section (see **Tables 1** and **2**). **Figure 5** shows the event rates in 1 kt of the target material for the Livermore model. The total number of events per kiloton for each of the two neutrino fluxes are listed in **Table 5**. The actual detected number of events may

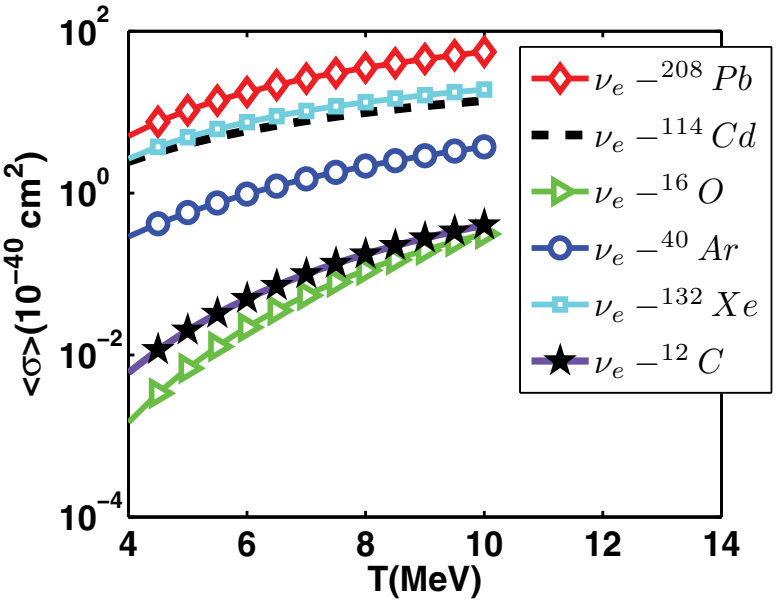

Figure 3. Temperature dependence of the energy-weighted cross section for charge current neutrino-nucleus reactions, whose neutrino spectra obey the Fermi-Dirac distribution with chemical parameter $\alpha = 0$.

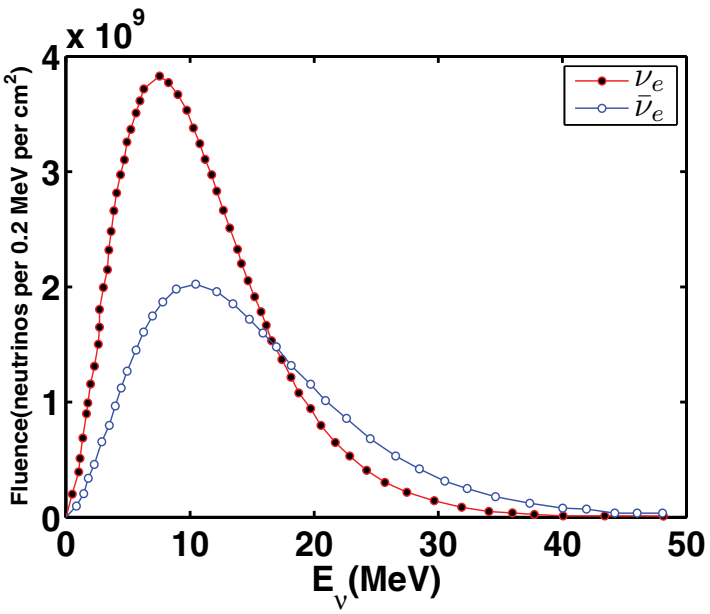

Figure 4. Livermore fluence for ν_e and $\bar{\nu}_e$ flavour components, assuming Fermi-Dirac spectra with the average energies indicated as a function of time and zero chemical potential, integrated from core collapse till about 14 seconds later.

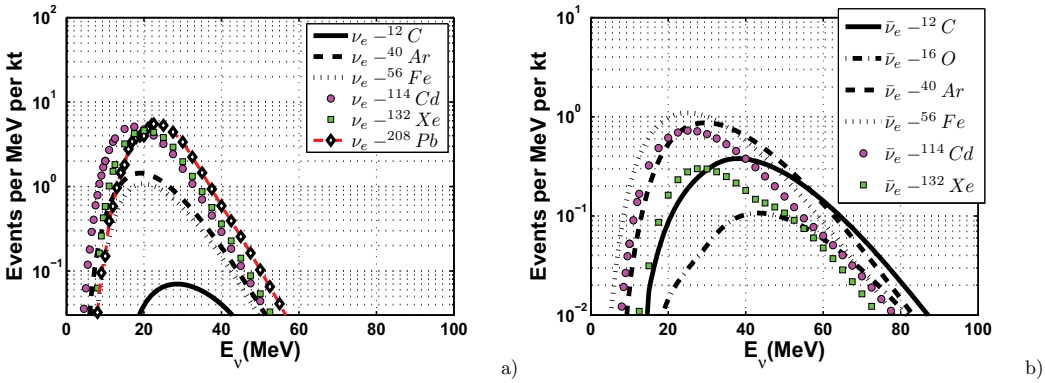

Figure 5. Event rates in 1 kt of the target isotope for the Livermore model. The event rates of $\nu_e - {}^{16}O$ and $\overline{\nu}_e - {}^{208}Pb$, which are less than 10^{-2}, are not shown.

Channel	N_{events}	N_{events}
	Fermi-Dirac	**Livermore**
$\nu_e + {}^{12}\mathrm{C} \rightarrow e^- + {}^{12}\mathrm{N}^{(*)}$	3	2
$\overline{\nu}_e + {}^{12}\mathrm{C} \rightarrow e^+ + {}^{12}\mathrm{B}^{(*)}$	15	13
$\nu_e + {}^{16}\mathrm{O} \rightarrow e^- + {}^{16}\mathrm{F}^{(*)}$	1	1
$\overline{\nu}_e + {}^{16}\mathrm{O} \rightarrow e^+ + {}^{16}\mathrm{N}^{(*)}$	4	4
$\nu_e + {}^{40}\mathrm{Ar} \rightarrow e^- + {}^{40}\mathrm{K}^*$	71	28
$\overline{\nu}_e + {}^{40}\mathrm{Ar} \rightarrow e^+ + {}^{40}\mathrm{Cl}^*$	40	26
$\nu_e + {}^{56}\mathrm{Fe} \rightarrow e^- + {}^{56}\mathrm{Co}^*$	48	20
$\overline{\nu}_e + {}^{56}\mathrm{Fe} \rightarrow e^+ + {}^{56}\mathrm{Mn}^*$	58	31
$\nu_e + {}^{114}\mathrm{Cd} \rightarrow e^- + {}^{114}\mathrm{In}^*$	229	88
$\overline{\nu}_e + {}^{114}\mathrm{Cd} \rightarrow e^+ + {}^{114}\mathrm{Ag}^*$	35	20
$\nu_e + {}^{132}\mathrm{Xe} \rightarrow e^- + {}^{132}\mathrm{Cs}^*$	198	78
$\overline{\nu}_e + {}^{132}\mathrm{Xe} \rightarrow e^+ + {}^{132}\mathrm{I}^*$	12	8
$\nu_e + {}^{208}\mathrm{Pb} \rightarrow e^- + {}^{208}\mathrm{Bi}^*$	219	89
$\overline{\nu}_e + {}^{208}\mathrm{Pb} \rightarrow e^+ + {}^{208}\mathrm{Tl}^*$	0	0

We consider the Fermi-Dirac distribution with temperature T = 3.5 MeV for neutrinos and T = 5 MeV for antineutrinos (second column) and the Livermore numerical simulation for supernova neutrino emission (third column). No detector efficiency (detector threshold, energy response, background effects, etc.) is taken into account.

Table 5. Number of supernova events per kt at 10 kpc away from the Earth, on different targets relevant for existing detector types.

be significantly fewer, if the detector energy threshold, detector efficiency and other background contamination effects coming from radioactive isotopes are taken into account. The results show that there is no considerable variation in the total antineutrino events between the two supernova models used in the calculation.

4. Interaction of neutrinos with dark matter

Dark matter particles (hereafter generically denoted by χ) may interact with ordinary matter through Z boson exchanges. Therefore, they have to be heavy, or else they would have been pair-produced in Z decays. A light dark matter candidate should have no significant direct coupling to the Z boson, but it could still interact with ordinary matter through the exchanges of other spin-1 gauge bosons or of spin-0 Higgs bosons.

If there is a mixing between active and sterile neutrinos, high-energy neutrinos interacting with dark matter may suffer a kind of MSW effect when they propagate in a dark matter medium. In a simplified model, which includes ordinary and dark matter potentials, the evolution equation with one sterile ν_s and an active one ν_α is written as:

$$i\frac{\mathrm{d}}{\mathrm{d}t}\begin{pmatrix}\nu_\alpha\\ \nu_s\end{pmatrix} = (UH_0U^\dagger + V)\begin{pmatrix}\nu_\alpha\\ \nu_s\end{pmatrix}, \tag{17}$$

with

$$H_0 = \frac{1}{2E}\ \mathrm{diag}\ \{0,\Delta m^2_{\alpha 4}\} \tag{18}$$

$$\mathcal{V} = \mathrm{diag}\ \{V_{\nu_\alpha f} + V_{\nu_\alpha \chi}, V_{\nu_s \chi}\} \tag{19}$$

and

$$U = \begin{pmatrix}\cos\theta_0 & -\sin\theta_0\\ \sin\theta_0 & \cos\theta_0\end{pmatrix}, \tag{20}$$

where E is the neutrino energy, $\Delta m^2_{\alpha 4} = m^2_4 - m^2_\alpha$ is the mass-squared splitting and θ_0 is the vacuum mixing angle between the sterile and the active neutrino. The matter potentials are defined as:

$$V_{\nu_\alpha f} = \sqrt{2}G_F(N_\alpha - N_n/2)\,; \tag{21}$$

$$V_{\nu_\alpha \chi} = \varepsilon_{\nu_\alpha \chi} G_F N_\chi\,; \tag{22}$$

$$V_{\nu_s \chi} = \varepsilon_{\nu_s \chi} G_F N_\chi\,, \tag{23}$$

where N_α, N_n and N_χ are, respectively, the number density of leptons, neutrons and dark matter particles interacting with neutrinos. The parameters $\varepsilon_{\nu_{\alpha,s}\chi}$ account for the coupling strength in terms of Fermi constant $G_F = 1.166\times10^{-5}$ GeV^{-2}. A list of values is given in [87]. Considering an

astrophysical environment where $N_e \approx N_n/2$ and $N_\mu \approx N_\tau \approx 0$, the contribution, $V_{\nu_{e,\mu,\tau}f}$, from electron, tau and muon neutrinos is negligible in comparison with the neutrino and dark matter interactions $V_{\nu_\alpha\chi}$ and $V_{\nu_s\chi}$. The dark matter number density, N_χ, can be written as $N_\chi = \rho_\chi/m_\chi$, where m_χ being the dark matter particle mass and ρ_χ the dark matter density. Around our galactic halo, it is expected that $\rho_\chi = 0.3\ \text{GeV}\cdot\text{cm}^{-3}$ [88]. Even though there exists firm indirect evidence for a halo of dark matter in galaxies from the observed rotational curves, see for example the review [89], it is essential to directly detect such matter. The possibility of such detection, however, depends on the nature of the dark matter constituents and their interactions. There are quite a few dark matter candidates such as WIMPs (weakly interacting massive particles), superWIMPs, light gravitinos, hidden dark matter, sterile neutrinos, Kaluza-Klein particles and axions. We will pay special attention to WIMPs. WIMPs have masses m_χ in the range of few GeV to few TeV [90–94]. In this context, we take m_χ = 20 GeV.

It is interesting to compute the survival probability $P(\nu_\alpha \to \nu_\alpha)$ for active neutrinos for various values of $\sin^2(2\theta_0)$. **Figure 6** depicts $P(\nu_\alpha \to \nu_\alpha)$ as a function of neutrino energy E_ν with a coupling $|\varepsilon_\chi| = |\varepsilon_{\nu_\alpha\chi} - \varepsilon_{\nu_s\chi}| = 3\times10^{11}$. As it is seen, a resonant effect happens at the energy around 0.4 PeV which corresponds to an oscillation length $L = \frac{4\pi E}{\sin(2\theta_0)\Delta m^2} \sim 10^{18}$ Km in accordance with the expected dark matter halo dimension. This suggests that the high-energy spectrum of extragalactic neutrinos could be affected by the existence of sterile neutrino and its interaction with dark matter. If the various experiments such as IceCube [59, 60, 95–97]

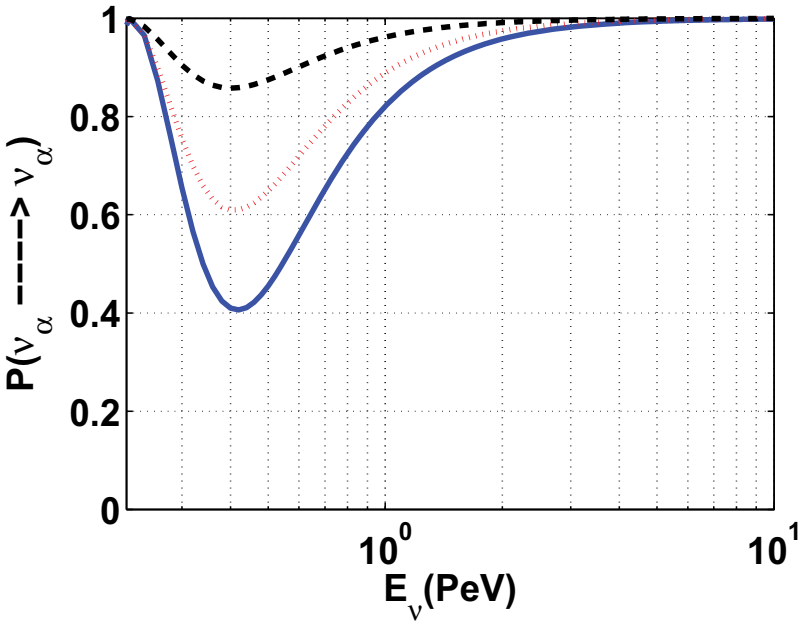

Figure 6. Survival probability $P(\nu_\alpha \to \nu_\alpha)$ as a function of the neutrino energy E_ν, considering the galactic halo average dark matter density. The (black) dashed line corresponds to $\sin^2(2\theta_0) = 0.05$, the (red) dotted line to 0.15 while the (blue) solid line to $\sin^2(2\theta_0) = 0.25$. The neutrino squared mass difference is taken $\Delta m^2 = 7\times10^{-13}\ \text{eV}^2$.

collect in future sufficient data, it might be possible to observe the MSW mechanism for dark matter as a distortion in the UHE neutrino spectrum. Resonance enhancement in the oscillation probability can also be found considering a more realistic halo density profile of the form:

$$\rho(r) = \frac{\rho_0}{(r/R)^{\delta}[1+(r/R)^{\alpha}]^{(\beta-\delta)/\alpha}} \ , \tag{24}$$

where the parameters α, β, δ and R (in kpc) depend on the specific model to be considered. A list of parameters is given in **Table 6** for various model density profiles [98–101]. The left panel of **Figure 7** illustrates the four different density profiles, whereas the right one depicts the corresponding survival probability as a function of neutrino energy for constant density and as an example of the survival probability corresponding to the density profile [101].

Ref.	α	β	δ	R(kpc)
[98]	1	3	1	20
[99]	2	3	0.4	10
[100]	1.5	3	1.5	28
[101]	2	3	0	3.5

Table 6. Model parameters for some known halo density profiles.

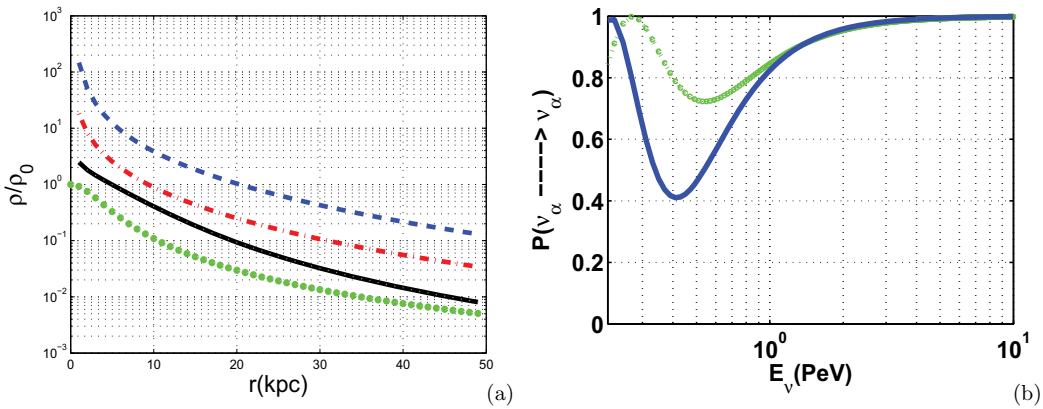

Figure 7. Left panel: Dark matter density profiles, Ref. [98] (red) dot-dashed line, Ref. [99] (black) solid line, Ref. [100] (blue) dashed line, and Ref. [101] (green) dotted line. Right panel: Survival probabilities for constant ρ (blue) solid line and for the density profile [101] (green) dotted line.

5. Conclusions

The study of neutrino scattering with nuclei provides the most attractive mechanism to detect or distinguish neutrinos of different flavour and to investigate the basic structure of weak interactions. Further studies involving neutrino-induced transitions between discrete nuclear

states may help us to explore the structure of the weak hadronic currents and also constitute good sources of explanation for neutrino properties.

Neutrino-induced reactions are of particular significance in view of studies on modern detectors, based on neutrino scattering on various isotopes. So far, experimental neutrino cross sections are not available for modest energies below 100 MeV, with the exception of ^{12}C and, with large uncertainty, ^{56}Fe. These are rather important for astrophysical and cosmological applications and must be calculated. In this chapter, we have presented neutrino(antineutrino)-nucleus reactions via charge current related to a range of targets from ^{12}C to ^{208}Pb. The calculated cross sections are tabulated for a set of neutrino energies which are relevant for supernova neutrinos. The rather low neutrino energies involved introduce, however, some sensitivity to nuclear structure effects and, in particular, for neutrinos with energies lower than 20 MeV, where state-of-the-art nuclear models must be employed which describe the many-body correlations in the nucleus accurately. The model of choice is the pnQRPA yielding to reasonable cross sections in a wide range of nuclear isotopes. The nuclear responses of these isotopes (used in common detector materials) to supernova neutrinos have been studied for two neutrino flux models. The two-parameter Fermi-Dirac neutrino energy model with zero chemical potential and the Livermore model assuming Fermi-Dirac spectra with average neutrino energies indicated as a function of time integrated over 14 seconds burst. The expected number of events per kt are predicted for supernova-detector distance 10 kpc. The results show that there is no considerable variation in the total antineutrino events between the two supernova models used in the calculation.

Furthermore, we also present results concerning the interaction potential of extragalactic neutrinos, at high energies 1 PeV, with DM in the presence of sterile neutrino state. High-energy neutrinos interacting with DM may suffer a kind of MSW effect when propagating in DM medium. The resonance effect happens at around 0.4–0.6 PeV for various density DM profiles. The existence of light sterile neutrinos can impact existing and future dark matter searches. The mechanism of MSW effect in the UHE neutrino survival probability may be tested in future experimental searches using experimental data, for instance, as those taken from IceCube operation.

Author details

Paraskevi C. Divari

Address all correspondence to: pdivari@gmail.com

Department of Physical Sciences and Applications, Hellenic Army Academy, Attica, Greece

References

[1] D. Forero, M. Tortola and J. Valle, Phys. Rev. D 86, 073012 (2012).

[2] F. Capozzi *et al*., Phys. Rev. D 89, 093018 (2014).

[3] P. Ade *et al*., (Planck Collaboration) Planck 2013 results: XV. CMB power spectra and likelihood (arXiv: 1303.5075).

[4] P. Ade *et al*., (Planck Collaboration) Planck 2013 results. I. Overview of products and scientific results (arXiv: 1303.5062).

[5] P. Ade *et al*., (Planck Collaboration) 2014 Planck 2013 results. XVI. Cosmological parameters, Astron. Astrophys. (arXiv: 1303.5076).

[6] C. Bennett *et al*., (WMAP Collaboration) Astrophys. J. Suppl. 208, 20 (2013).

[7] G. Hinshaw *et al*., (WMAP Collaboration) Astrophys. J. Suppl. 208, 19 (2013).

[8] S. Das *et al*., J. Cosmol. Astropart. Phys. JCAP04, 014 (2014).

[9] J.L. Sievers *et al*., J. Cosmol. Astropart. Phys. JCAP10, 060 (2013).

[10] K. Story *et al*., Astrophys. J. 779 86 (2013).

[11] L. Anderson *et al*., (BOSS Collaboration) arXiv:1312.4877.

[12] D. Parkinson *et al*., Phys. Rev. D 86, 103518 (2012).

[13] B.A. Reid *et al*., Mon. Not. Roy. Astron. Soc. 404, 60 (2010).

[14] R. Cooke, M. Pettini, R.A. Jorgenson, M.T. Murphy and C.C. Steidel, arXiv:1308.3240.

[15] F. Iocco, G. Mangano, G. Miele, O. Pisanti and P.D. Serpico, Phys. Rept. 472, 1 (2009).

[16] Y. Izotov, G. Stasinska and N. Guseva, arXiv:1308.2100.

[17] Amol Dighe. Physics potential of future supernova neutrino observations. J. Phys. Conf. Ser., 136:022041 (2008).

[18] K. Scholberg, Ann. Rev. Nucl. Part. Sci. 62, 81 (2012).

[19] P.C. Divari and J.D. Vergados, Int. J. Mod. Phys. A 31, 1650123 (2016).

[20] A.M. Dziewonski and D.L. Anderson, Physics of the Earth and Planetary Interiors, 25, 297 (1981).

[21] E. Lisi and D. Montanino, Phys. Rev. D 56, 1792 (1997).

[22] J.H. Oort, Bull. Astron. Inst. Neth. 6, 249 (1932).

[23] F. Zwicky, Helv. Phys. Acta 6, 110 (1933).

[24] E. Komatsu *et al*., (WMAP Collaboration) Astrophys. J. Suppl. 180, 330 (2009).

[25] E. Komatsu *et al*., (WMAP Collaboration) Astrophys. J. Suppl. 192, 18 (2011).

[26] G. Hinshaw, D. Larson, E. Komatsu, D.N. Spergel, C. Bennett *et al*., Nine-Year Wilkinson Microwave Anisotropy Probe (WMAP) Observations: Cosmological Parameter Results (2012), arXiv:1212.5226 [astro-ph.CO].

[27] P.A.R. Ade *et al*., (Planck Collaboration) Planck 2013 results. XVI. Cosmological parameters (2013), arXiv:1303.5076 [astro-ph.CO].

[28] D. Restrepo, O. Zapata, and C. Yaguna. JHEP 1311, 011 (2013).

[29] A. Merle, Int. J. Mod. Phys. D 22, 1330020 (2013).

[30] A. Esmaili and O.L. Peres, arXiv:1202.2869 [hep-ph] (2012).

[31] C.A. Arguelles and J. Kopp, arXiv:1202.3431 [hep-ph] (2012).

[32] M. Pospelov, Phys.Rev. D84, 085008 (2011).

[33] R. Harnik, J. Kopp, and P.A. Machado, (2012) arXiv:1202.6073 [hep-ph] (2012).

[34] M. Pospelov and J. Pradler, arXiv:1203.0545 [hep-ph] (2012).

[35] J. Huang and A.E. Nelson, Phys. Rev. D 88, 033016 (2013).

[36] L.G. van den Aarssen, T. Bringmann and C. Pfrommer, Phys. Rev. Lett. 109, 231301 (2012).

[37] G. Mangano, A. Melchiorri, P. Serra, A. Cooray and M. Kamionkowski, Phys. Rev. D 74, 043517 (2006).

[38] P. Fayet, Phys. Rev. D 75, 115017 (2007).

[39] C. Boehm and P. Fayet, Nucl. Phys. B 683, 219 (2004).

[40] P.J. Fox and E. Poppitz, Phys. Rev. D 79, 083528 (2009).

[41] Z.G. Berezhiani and R.N. Mohapatra, Phys. Rev. D 52, 6607 (1995).

[42] Z.G. Berezhiani, A.D. Dolgov and R.N. Mohapatra, Phys. Lett. B 375, 26 (1996).

[43] R. Laha, B. Dasgupta and J.F. Beacom, Phys. Rev. D 89, 093025 (2014).

[44] I.M. Shoemaker, Phys. Dark Univ. 2, no. 3, 157 (2013).

[45] B. Dasgupta and J. Kopp, Phys. Rev. Lett. 112, no. 3, 031803 (2014).

[46] S. Hannestad, R.S. Hansen and T. Tram, Phys. Rev. Lett. 112, no. 3, 031802 (2014).

[47] K. Eguchi *et al*., Phys. Rev. Lett. 90, 021802 (2003).

[48] L. Cadonati, F.P. Calaprice and M.C. Chen, Astropart. Phys. 16, 361 (2002).

[49] M.E. Monzani, Nuovo Cim. C29, 269 (2006).

[50] A. Kibayashi *et al*., 0909.5528 (2009).

[51] J. Boger *et al*., Nucl. Instrum. Meth. A449, 172 (2000).

[52] A. Bueno, I. Gil Botella and A. Rubbia, hep-ph/0307222 (2003).

[53] R.N. Boyd, A.S.J. Murphy and R.L. Talaga, Nucl. Phys. A718, 222 (2003).

[54] S. Elliott, Phys. Rev. C62, 065802 (2000).

[55] R. Maschuw, KARMEN Collaboration, Prog. Part. Nucl. Phys. 40, 183 (1998).

[56] K. Zuber, Prog. Part. Nucl. Phys. 57, 235 (2006).

[57] K. Zuber, J. Phys. Conf. Ser. 203, 012070 (2010).

[58] E. Aprile *et al*., New Astronomy Reviews, 49, no. 2-3, 289, (2005).

[59] M.G. Aartsen *et al*., (IceCube Collaboration), Phys. Rev. Lett. 111, 021103 (2013).

[60] M.G. Aartsen *et al*., (IceCube Collaboration), Science 342, no. 6161, 1242856 (2013).

[61] M.G. Aartsen *et al*., (IceCube Collaboration), Phys. Rev. D 91, 022001 (2015).

[62] H.N. He, T. Wang, Y.Z. Fan, S.M. Liu and D.M. Wei, Phys. Rev. D 87, 063011 (2013).

[63] K. Murase, M. Ahlers and B.C. Lacki, Phys. Rev. D 88, 121301 (2013).

[64] R.Y. Liu, X.Y. Wang, S. Inoue, R. Crocker and F. Aharonian, Phys. Rev. D 89, 083004 (2014).

[65] S. Dado and A. Dar, Phys. Rev. Lett. 113, 191102 (2014).

[66] C. Boehm *et al*., Phys. Rev. D 77 (2008).

[67] M.S. Athar, S. Ahmad and S.K. Singh, Nucl. Phys. A 764, 551 (2006).

[68] S.K. Singh, Nucl. Phys. B (Proc. Suppl.) 112, 77 (2002).

[69] N. Paar, T. Suzuki, M. Honma, T. Marketin and D. Vretenar, Phys. Rev. C 84, 047305 (2011).

[70] J.D. Walecka, *Theoretical Nuclear and Subnuclear Physics* (Oxford University Press, New York, 1995), p.531.

[71] A. Meucci, C. Giusti, and F.D. Pacati, Nucl. Phys. A 744, 307 (2004).

[72] T.W. Donnelly and J.D. Walecka, Nucl. Phys. A 201, 81 (1973).

[73] P.C. Divari, J. Phys. G: Nucl. Part. Phys. 40, 125201 (2013).

[74] P.C. Divari, Advances in High Energy Physics Volume 2013, Article ID 143184.

[75] P.C. Divari, Advances in High Energy Physics Volume 2012, Article ID 379460.

[76] R. Lazauskas and C. Volpe, Nucl. Phys. A 792, 219 (2007).

[77] M. Cheoun, E. Ha and T. Kajino, Phys. Rev. C 83, 028801 (2011).

[78] H.T Janka, Astrophys. J. 590, 971 (2003).

[79] M.S Athar, S. Ahmad and S.K. Singh, Phys. Rev. C 71, 045501 (2005).

[80] K. Scholberg, Ann. Rev. Nucl. Part. Sci. 62, 81 (2012).

[81] T. Totani, K. Sato, H.E. Dalhed and J.R. Wilson, Astrophys. J. 496, 216 (1998).

[82] A. Mirizzi, G.G.Raffelt and P.D.Serpico, JCAP 0605, 012 (2006).

[83] C. Lunardini and A.Y.Smirnov, Nucl. Phys. B 616, 307 (2001).

[84] K. Takahashi and K. Sato, Phys. Rev. D 66, 033006 (2002).

[85] K. Takahashi and K. Sato, Prog. Theor. Phys. 109, 919 (2003).

[86] J. Fetter, G.C. McLaughlin, A.B. Balantekin and G.M. Fuller, Astropart. Phys. 18, 433 (2003)

[87] O.G. Miranda, C.A. Moura and A. Parada, Phys. Lett. B 744, 55 (2015).

[88] R. Foot, Phys. Rev. D 86, 023524 (2012).

[89] P. Ullio and M. Kamioknowski, JHEP 0103, 049 (2001).

[90] G. Jungman, M. Kamionkowski and K. Griest, Phys. Rep. 267, 195 (1996).

[91] L. Bergstrom, Rep. Prog. Phys. 63, 793 (2000).

[92] G. Bertone, D. Hooper and J. Silk, Phys. Rep. 405, 279 (2005).

[93] D. Hooper and S. Profumo, Phys. Rep. 453, 29 (2007).

[94] Particle Dark Matter: Observations, Models and Searches, edited by G. Bertone (Cambridge University Press, Cambridge, England, 2010).

[95] P. Abreu *et al*., (The Pierre Auger Collaboration), arXiv:1107.4805 [astro-ph.HE].

[96] S. Biagi, Nucl. Phys. Proc. Suppl. 212-213, 109 (2011).

[97] R. Abbasi *et al*., (IceCube Collaboration), Nature 484, 351 (2012).

[98] J.F. Navarro, C.S. Frenk and S.D.M. White, Astrophys. J. 462, 563 (1996).

[99] A.V. Kravtsov, A.A. Klypin, J.S. Bullock and J.R. Primack, Astrophys. J. 502, 48 (1998).

[100] B. Moore, T.R. Quinn, F. Governato, J. Stadel and G. Lake, Mon. Not. Roy. Astron. Soc. 310, 1147 (1999).

[101] L. Bergstrom, P. Ullio and J.H. Buckley, Astropart. Phys. 9, 137 (1998).

Chapter 4

Relativistic Celestial Metrology: Dark Matter as an Inertial Gauge Effect

Luca Lusanna and Ruggero Stanga

Additional information is available at the end of the chapter

http://dx.doi.org/10.5772/68115

Abstract

In canonical tetrad gravity, it is possible to identify the gauge variables, describing relativistic inertial effects, in Einstein general relativity. One of these is the York time, the trace of the extrinsic curvature of the instantaneous non-Euclidean 3-spaces (global Euclidean 3-spaces are forbidden by the equivalence principle). The extrinsic curvature depends both on gauge variables and on dynamical ones like the gravitational waves after linearization. The fixation of these gauge variables is done by relativistic metrology with its identification of time and space. Till now, the International Celestial Reference Frame ICRF uses Euclidean 3-spaces outside the Solar System. It is shown that York time and non-Euclidean 3-spaces may explain the main signatures of dark matter in ordinary space-time before using cosmology. Also dark energy may be connected to these inertial gauge effects, because both red-shift and luminosity distance depend on them.

Keywords: dark matter

1. Introduction

An extremely important, till now not explicitly clarified, point in Einstein general relativity (GR) (and in every generally covariant theory of gravity), whose gauge group is the group of diffeomorphisms of the Lorentzian 4-dimensional space-time,[1] is that the fixation of the gauge freedom is nothing else than *the establishment of conventions for relativistic metrology,* an operation performed from atomic physicists, NASA engineers and astronomers [2] with the introduction of a notion of clock synchronization and with a definition of the axes for the 4-coordinates in each point, that is, with the identification of a non-inertial frame of the space-time (global inertial frames are forbidden by the equivalence principle). See Ref. [3, 4] for a review of the existing conventions in the Solar System.

[1]See Ref. [1] for theoretical considerations concerning the nature of space and time in GR.

According with the International Astronomic Union IAU inside the Solar System, the choice of the 4-coordinates is *solved at the experimental level by the choice of a convention for the description of matter* based on special post-Newtonian (PN) solutions of linearized Einstein equations in a fixed given harmonic gauge [2–4]: (a) for satellites near the Earth (like the GPS ones) one uses NASA 4-coordinates compatible with the reference frames of the International Terrestrial Reference System ITRS2003[2] and of the Geocentric Celestial Reference System GCRS IAU2000; (b) for planets in the Solar System one uses the frame of the Barycentric Celestial Reference System BCRS-IAU2000.

These frames are compatible with the usual interpretation as *quasi-inertial frames* in Minkowski space-time and are metrology choices like the choice of a certain atomic clock as standard of time. However, already in the Solar System, the instantaneous 3-spaces are not Euclidean in the selected solutions, but the existing technology is not yet able to show it, being a property of order $O(1/c^2)$[3]

In astronomy, data like luminosity, light spectrum and angles are used to determine the positions of stars and galaxies and their temporal evolution in a 4-dimensional nearly Galilei space-time with the International Celestial Reference System ICRS [2, 3], a frame considered as a "quasi-inertial frame" and with all galactic dynamics described by PN gravity.

This is in accord with the smallness of the intrinsic 3-curvature of the 3-spaces as implied by the CMB data, a property included in the standard Friedmann-Lemaitre-Robertson-Walker (FLRW) Λ CDM cosmological model with its isotropy and homogeneity symmetries. However, to reconcile all the existing data with this 4-dimensional description, one must postulate the existence of *dark matter and dark energy* as the dominant components of the classical universe [6–8] after the recombination 3-surface (before it quantum mechanics is entering in the description and there is no acceptable description for the transition from quantum to classical astrophysics) already within galaxies before making the transition to cosmology and the replacement of ordinary space-time with the standard cosmological FLWR one, whose points describe a mean over a volume of 100 Mega-parsecs of the ordinary space-time. The attempts to avoid the appearance of "darkness" have led to many proposals of modifications of GR like MOND [9], $f(R)$ gravity [10–12] and the ones analyzed in Refs. [6–8].

After a description of ICRS and of the measurements in ordinary astrophysics (not cosmology) of quantities like luminosity distance, rotation curves of galaxies, gravitational lensing,…. implying "darkness," we will study canonical ADM tetrad gravity and its gauge freedom after a suitable but arbitrary $3+1$ splitting of the space-time in a family of Einstein space-times able to include the extension of the models of particle physics to GR. We will identify which are the *gauge variables* to be fixed with astrophysical metrology and how the interpretation of "dark

[2]A relativistic version of ITRS is not yet existing, so that one cannot yet connect the time of the atomic clocks in different laboratories to the clock on the Space Station with a suitable Lorentz transformations.

[3]See however the LATOR proposal [5] of measuring the deviation from 2π of the sum of the three angles of a triangle formed by the Space Station and two spacecrafts behind the Sun. When this non-Euclidean nature will be measured, one will have to redefine the standard of length measurements [2].

http://dx.doi.org/10.5772/68115

matter" and probably also of "dark energy" depends on the fixation of these gauge variables in a family of gauge-fixings different from the harmonic ones used in the IAU conventions. Therefore, our suggestion is that "*darkness*" *may be interpreted as a relativistic inertial effect* and that ICRS should be reformulated in a suitable relativistic way.

2. Astrophysical metrology

Reference data for positional astronomy, such as the data in astrometric star catalogs, are specified in the International Celestial Reference System ICRS [2, 3] with origin in the solar system barycenter and with kinematically non-rotating spatial axes fixed with respect to space according to the IAU conventions [2, 3]. It is based on the position of extragalactic radio sources that are distant enough to be considered stationary, in the limit of today's capabilities, and whose position is known with a precision of 0.001 arcsec, thanks to the Very Long Baseline Interferometry technique [13]. These sources are assumed to have no observable intrinsic angular momentum. The International Celestial Reference Frame ICRF is a realization of ICRS obtained by supposing that the origin is a quasi-inertial observer and that we have a quasi-inertial (essentially non-relativistic) reference frame with rectangular 3-coordinates in a nearly Galilean space-time whose 3-spaces are Euclidean.

However, a number of different categories of astronomical observations are explained in the usual Euclidean 3-space only in terms of so far undetermined dark matter and dark energy: rotational curves of galaxies [14–17], gravitational lensing [18–20], application of the virial theorem to galaxy clusters [21–23] and the acceleration of the expansion of the universe [24–29]. This already happens before the transition from the ordinary space-time to the cosmological one, the FLWR space-time which is not a Galilean space-time but has nearly internally flat 3-spaces and uses a theoretical cosmic time. What is still not explored is the possibility that in Einstein GR one can use non Euclidean 3-spaces with small internal 3-curvature, but with an extrinsic curvature (as 3-submanifolds of the space-time) depending on the gauge variables, namely on the metrology conventions.

In all the astronomical observations, the distance of the objects needs to be known. Measuring distances in astronomy is a difficult task, especially when dealing with extragalactic objects. Different methods must be applied at increasing distances, which need to be inter-calibrated appropriately. To get relevant quantities like distances and absolute luminosity of stars from the directly measured quantities, that is, apparent luminosity, angles and red-shift, it is important to know the geometry of the 3-spaces crossed by the propagating rays of light on null 4-geodesics of the space-time.

The most important methods rely on the absolute intrinsic luminosity L of a *standard candle* compared to the apparent brightness F as measured on Earth. In terms of these quantities, one defines the *luminosity distance* [6, 18–20] of a luminous object $d_L = \sqrt{L/4\,\pi\,F}$, which is the proper distance of an object at rest with respect to the observer in a Euclidean stationary universe. In an expanding universe, the luminosity distance is dependent on the red-shift z of the light arriving on the Earth from the object and to the comoving distance r_1. If a_o is the scale

factor, H_o is the Hubble constant, $\dot{H}_o$ its time derivative, and if one keeps only the first-order terms in the expansion, one has

$$d_L = a_o\, r_1\, (1+z) = \frac{z}{H_o}\, [1 + (1 + \frac{\dot{H}_o}{2\, H_o^2})\, z], \tag{1}$$

Also used is the *angular diameter distance* $d_A = D/\theta$, where θ is the angular diameter of the source as measured by the observer and D is the diameter of well-known close galaxies. Also the angular diameter distance depends on the red-shift: $d_A = \frac{a_o\, r_1}{1+z} = \frac{z}{H_o}\, \left[1 - (1 - \frac{\dot{H}_o}{2\, H_o^2})\, z\right]$.

In both luminosity distance and angular diameter distance, the terms which depart from Euclidean geometry enter only at higher orders, which depend on the rate of expansion of the universe and on the curvature parameter. For the galaxies with the most reliable rotation curves that are within a range of a few tens of Mega-parsec, they can be neglected, and we can consider the 3-space to be Euclidean. Higher order terms need instead to be considered when the objects have a distance of hundreds of Mega-parsec or more.

For larger z, one has to take into account a model of cosmology: In a FLWR metric, one has $F = L/[4\,\pi\, (a_o\, r_1)^2\, (1+z)^2]$ with $a_o = 1/(1+z)$ and with r_1 depending also on z.

Assuming that all supernovae (SN) Ia have the same intrinsic luminosity, it was found [26–29] that the SN1a's at $z \leq 0.5$ are about 10 per cent fainter than expected, and this has been interpreted as evidence of an accelerated expansion of the universe and dark energy has been invoked to take care of the accelerated expansion.

3. Einstein general relativity

We shall use the formulation of Einstein GR in a 4-dimensional Lorentzian space-time (the one used in classical astrophysics, not in cosmology, after the recombination surface for the propagation of light) with the Lagrangian description implied by the ADM action principle [30, 31], because it allows to make the transition to the canonical formalism and to use Dirac theory of constraints [32], in particular to use the Shanmugadhasan canonical transformation [33, 34] to find canonical bases adapted to the constraints (see Ref. [35] for reviews). Light and visible stars and galaxies constitute the matter.

We will restrict ourselves to *globally hyperbolic, topologically trivial* and *asymptotically Minkowskian space-times*, in the absence of Killing symmetries (see Ref. [36] for their inclusion as Dirac constraints) and with the asymptotic SPI symmetries at spatial infinity of Ref. [37] restricted to the asymptotic ADM Poincaré group [38] by eliminating the super-translations with suitable boundary conditions on the 4-metric. This framework is defined in Refs. [39–43], where the matter consists of electrically charged positive-energy scalar point particles plus the electromagnetic field. In the limit of vanishing Newton constant ($G = 0$), the asymptotic Poincare' group becomes the Poincare' group of particle physics, where elementary particles are always considered as irreducible representations of this group.

http://dx.doi.org/10.5772/68115

While in the family of spatially compact without spatial boundary space-times[4], considered in loop quantum gravity [44, 45], the Dirac Hamiltonian is a combination of constraints because the canonical Hamiltonian vanishes, in our space-times there is not a frozen picture, because the canonical Hamiltonian is the weak ADM energy $\hat{E}_{ADM}$[5] plus a combination of constraints. In the absence of matter, Christodoulou-Klainermann space-times [46] are compatible with this description.

In the ADM Lagrangian, the basic variable is the 4-metric ${}^4g_{\mu\nu}(x)$ of the space-time (x^μ are local 4-coordinates with an arbitrary origin): it determines the dynamical chrono-geometrical structure of space-time by means of the line element $ds^2 = {}^4g_{\mu\nu}(x)\, dx^\mu\, dx^\nu$, and it teaches to massless particles which are the allowed trajectories in each point.

However, to include the coupling of gravity to the spin of fermions, we must use ADM *tetrad gravity*: the 10 components of the 4-metric appearing in the ADM Lagrangian are decomposed on a set of cotetrads [31] $E^{(\alpha)}_\mu(x)$, ${}^4g_{\mu\nu}(x) = E^{(\alpha)}_\mu(x)\, \eta_{(\alpha)(\beta)}\, E^{(\beta)}_\nu(x)$.[6] This leads to an interpretation of gravity based on a congruence of time-like observers endowed with orthonormal tetrads $E^\mu_{(\alpha)}(x)$ (i.e., the inverse of the cotetrads $E^\mu_{(\alpha)}(x)\, E^{(\beta)}_\mu(x) = \delta^{(\beta)}_{(\alpha)}$): in each point of space-time, the time-like axis is the unit 4-velocity of a time-like observer, whereas the spatial axes are a (gauge) convention for the three gyroscopes of the observer.

A. Metrology as the Fixation of the Gauge Freedom of General Relativity

While the ADM action for metric gravity is invariant under space-time diffeomorphisms, the decomposition of the 4-metric on the cotetrads gives an ADM action [30] invariant not only under the space-time diffeomorphisms but also on a local O(3,1) Lorentz group describing the freedom in the orientation and transport of the gyroscopes along the time-like world lines of observers. Let us remark that the same gauge freedoms are present in all the generally covariant formulations of GR proposed as modifications of Einstein GR.

In electromagnetism and in Yang-Mills theories, the Lagrangian description in terms of potentials implies the presence of a gauge group acting on an internal space and implying the gauge nature of certain scalar and longitudinal components of the potentials: the gauge fixings imply the description of physics in terms of electric and magnetic fields or of their non-abelian analogues. Instead, in the metric formulation of GR, the gauge freedom is connected with the freedom in the choice of the metrology conventions, described in the previous section, for the definitions of clocks (i.e., time) and 3-space in each point of the space-time. As we shall see a metrology convention implies the fixation of 8 of the 10 components of the 4-metric, so that the remaining two components describe the physical degrees of freedom of the gravitational field

[4]Therefore, it is not possible to define a Poincare' group and to find a connection with particle physics.

[5]It is a volume integral over 3-space of a coordinate-dependent energy density. It is weakly equal to the *strong* ADM energy, which is a flux through a 2-surface at spatial infinity.

[6](α) are flat indices and $\eta_{(\alpha)(\beta)}$ is the flat 4-metric of Minkowski space-time. The signature of the 4-metrics is $\epsilon = \pm$ so that $\eta_{(\alpha)(\beta)} = \epsilon\,(1; -1, -1, -1)$. $\epsilon = 1$ is the convention of particle physics, whereas $\epsilon = -1$ is the convention usually used in GR

(the gravitational waves (GW) of its linearization in the case of weak fields). In tetrad gravity, we have 16 fields, but the extra 6 fields are fixed by metrology conventions on the orientation of three gyroscopes and on their transport along time-like world lines in each point of the space-time.

In special relativity, the metrology conventions amount to the choice of a standard atomic clock and of the instantaneous Euclidean 3-spaces of a *global inertial frame*, whose extension to *global non-inertial frames* was done in Ref. [47] with an application to relativistic atomic physics described in Ref. [48].

In GR, due to the equivalence principle forbidding the existence of global inertial frames, one has to use the cited theory of global non-inertial frames in the form of the so-called *3+1 point of view*[7]: one gives the world line of a time-like observer and a nice foliation of the space-time whose leaves are the instantaneous 3-spaces. Instead of standard local 4-coordinates x^μ centered in a point of the observer world line, one uses *4-scalar observer-dependent radar 4-coordinates*[8] $\sigma^A = (\tau; \sigma^r)$, where τ is an arbitrary increasing function of the observer proper time and σ^r is curvilinear 3-coordinates on the 3-spaces Σ_τ (diffeomorphic to R^3) with the observer as origin.

The inverse transformation $\sigma^A \mapsto x^\mu = z^\mu(\tau, \sigma^r)$ defines the embeddings of the 3-spaces Σ_τ into the space-time and the induced 4-metric is $g_{AB}[z(\tau,\sigma^r)] = z^\mu_A(\tau,\sigma^r)\, z^\nu_B(\tau,\sigma^r)\, g_{\mu\nu}(z(\tau,\sigma^r))$, where $z^\mu_A = \partial z^\mu / \partial \sigma^A$, while the cotetrads take the form $E^{(\alpha)}_A(\tau,\sigma^r) = z^\mu_A(\tau,\sigma^r)\, E^{(\alpha)}_\mu(z(\tau,\sigma^r))$. As shown explicitly in Ref. [51], the use of the 4-scalar radar 4-coordinates implies that *the ten components* ${}^4g_{AB}(\tau,\sigma^r)$ *and the sixteen components* $E^{(\alpha)}_A(\tau,\sigma^r)$ *are 4-scalars of the space-time*. Also, all the components of *radar tensors* (i.e., tensors expressed in radar 4-coordinates) are 4-scalars of the space-time.

While the 4-vectors $z^\mu_r(\tau,\sigma^u)$ are tangent to Σ_τ, so that in each point of the 3-space, the unit normal $l^\mu(\tau,\sigma^u)$ is proportional to $\epsilon^\mu{}_{\alpha\beta\gamma}\, z^\alpha_1(\tau,\sigma^r)\, z^\beta_2(\tau,\sigma^r)\, z^\gamma_3(\tau,\sigma^u)$, we have $z^\mu_\tau(\tau,\sigma^r) = N(\tau,\sigma^r)\, l^\mu(\tau,\sigma^r) + N^r(\tau,\sigma^r)\, z^\mu_r(\tau,\sigma^r)$, where $N(\tau,\sigma^r) = \epsilon\, z^\mu_\tau(\tau,\sigma^r)\, l_\mu(\tau,\sigma^r)$ and $N_r(\tau,\sigma^r) = -\epsilon g_{\tau r}(\tau,\sigma^r)$ are the lapse and shift functions of canonical GR.

In the chosen family of space-times, the foliation needed for the 3+1 splitting is nice and admissible if the lapse function satisfies $N(\tau,\sigma^r) > 0$ in every point of Σ_τ,[9] if $\epsilon^4 g_{\tau\tau}(\tau,\sigma^r) > 0$[10] and if the positive-definite 3-metric ${}^3g_{rs}(\tau,\sigma^u) = -\epsilon\, {}^4g_{rs}(\tau,\sigma^u)$ has three positive eigenvalues. These are the Møller conditions [52, 53].

Moreover, all the 3-spaces Σ_τ must tend to the same space-like hyperplane at spatial infinity. Due to the imposed absence of super-translations [39, 40], the non-Euclidean 3-spaces are orthogonal to the conserved ADM 4-momentum at spatial infinity; therefore, each 3-space is a

[7]Instead the usually used 1+3 point of view using the world line of a time-like observer leads only to local coordinate systems like the Riemann and Fermi ones valid only in a neighborhood of a time-like world line, because locally the 3-spaces are identified with the tangent spaces orthogonal to the observer 4-velocity so that they intersect each other.

[8]They were introduced by Bondi in Ref. [49, 50].

[9]Therefore, the 3-spaces never intersect, avoiding the coordinate singularity of Fermi coordinates.

[10]This property avoids the coordinate singularity of the rotating disk.

non-inertial rest frame [39–41] of the 3-universe with vanishing ADM 3-momentum, and there are asymptotic inertial observers with spatial axes identified by means of the fixed stars of star catalogues. In each 3-space Σ_τ, there are cotriads ${}^3e_{(a)r}(\tau,\sigma^r) = \sum_b R_{(a)(b)}(\alpha_{(c)}(\tau,\sigma^r))\,{}^3\overline{e}_{(a)r}(\tau,\sigma^r)$ defined modulo rotations ($R_{(a)(b)}$ are rotation matrices and $\alpha_{(a)}(\tau,\sigma^r)$ are angles).

In Refs. [39–43], there is a parametrization of tetrads, cotetrads and 4-metric in the framework of the 3+1 splitting of space-time. The basic configuration variables, that is, the cotetrads, are connected to cotetrads adapted to the 3+1 splitting of space-time (so that the adapted time-like tetrad is the unit normal to the 3-space Σ_τ) by standard Wigner boosts $L^{(\alpha)}{}_{(\beta)}$ for time-like vectors depending upon boost parameters $\varphi_{(a)}(\tau,\sigma^r)$: ${}^4E^{(\alpha)}_A = L^{(\alpha)}{}_{(\beta)}(\varphi_{(a)})\,{}^4E^{\rm o}_A(\beta)$. The adapted tetrads and cotetrads have the expression[11],[12]

$$
\begin{aligned}
&{}^4E^A_{(\alpha)} \stackrel{def}{=} {}^4\mathring{E}^{\,A}_{(\beta)}\, L^{(\beta)}{}_{(\alpha)}(\varphi_{(a)}) \stackrel{def}{=} {}^{\mathring{}A}\overline{E}_{(o)}\, L^{(o)}{}_{(\alpha)}(\varphi_{(c)}) + \\
&\quad + \sum_{ab} {}^{\mathring{}A}\overline{E}_{(b)}\, R^T_{(b)(a)}(\alpha_{(c)})\, L^{(a)}{}_{(\alpha)}(\varphi_{(c)}), \\
&{}^4g_{AB} = E^{(\alpha)}_A\, {}^4\eta_{(\alpha)(\beta)}\, E^{(\beta)}_B = \\
&\quad = {}^4\mathring{E}^{(\alpha)}_A\, {}^4\eta_{(\alpha)(\beta)}\, {}^4\mathring{E}^{(\beta)}_B = {}^4\overline{E}^{(\alpha)}_A\, {}^4\eta_{(\alpha)(\beta)}\, {}^4\overline{E}^{(\beta)}_B, \\
&{}^4\overline{E}^{\mathring{}A}_{(o)} = {}^4\mathring{E}^{\,A}_{(o)} = \frac{1}{1+n}\,(1;\, -\sum_a \overline{n}_{(a)}\, {}^3\overline{e}^r_{(a)}) = l^A, \qquad {}^4\overline{E}^{\mathring{}A}_{(a)} = (0; {}^3\overline{e}^r_{(a)}), \\
&{}^4\overline{E}^{\mathring{}(o)}_A = {}^4\mathring{E}^{(o)}_A = (1+n)\,(1;\, \vec{0}) = \epsilon l_A, \qquad {}^4\overline{E}^{\mathring{}(a)}_A = (\overline{n}_{(a)}; {}^3\overline{e}_{(a)r}), \\
&{}^4\mathring{E}^{(a)}_A = \sum_b R_{(a)(b)}\,(\overline{n}_{(b)}; {}^3\overline{e}_{(b)r}), \\
&{}^4g_{\tau\tau} = \epsilon\,[(1+n)^2 - \sum_a \overline{n}^2_{(a)}], \qquad {}^4g_{\tau r} = -\epsilon\, n_r = -\epsilon \sum_a \overline{n}_{(a)}\, {}^3\overline{e}_{(a)r}, \\
&{}^4g_{rs} = -\epsilon\, {}^3g_{rs} = -\epsilon \sum_a {}^3\overline{e}_{(a)r}\, {}^3\overline{e}_{(a)s}, \qquad \sqrt{-g} = \sqrt{|{}^4g|} = \frac{\sqrt{{}^3g}}{\sqrt{\epsilon\, {}^4g^{\tau\tau}}} = \sqrt{\gamma}\,(1+n).
\end{aligned}
\tag{2}
$$

From Eq. (5.5) of the third paper in Ref. [43], we assume the following (direction-independent, so to kill super-translations) boundary conditions at spatial infinity ($r = \sqrt{\sum_r (\sigma^r)^2}$; $\epsilon > 0$; $M = const.$): $n(\tau,\sigma^r) \to_{r\to\infty} O(r^{-(2+\epsilon)})$, $\pi_n(\tau,\sigma^r) \to_{r\to\infty} O(r^{-3})$, $n_{(a)}(\tau,\sigma^r) \to_{r\to\infty} O(r^{-\epsilon})$, $\pi_{n_{(a)}}(\tau,\sigma^r) \to_{r\to\infty} O(r^{-3})$, $\varphi_{(a)}(\tau,\sigma^r) \to_{r\to\infty} O(r^{-(1+\epsilon)})$, $\pi_{\varphi_{(a)}}(\tau,\sigma^r) \to_{r\to\infty} O(r^{-2})$, ${}^3e_{(a)r}(\tau,\sigma^r) \to_{r\to\infty} \left(1+\frac{M}{2r}\right)\delta_{ar} + O(r^{-3/2})$, ${}^3\pi^r_{(a)}(\tau,\sigma^r) \to_{r\to\infty} O(r^{-5/2})$.

---

[11] $N(\tau,\sigma^r) = 1 + n(\tau,\sigma^r)$ and $n_{(a)}(\tau,\sigma^r) = (N^r\, {}^3e^r_{(a)})(\tau,\sigma^r) = \sum_b R_{(a)(b)}(\alpha_{(c)}(\tau,\sigma^r))\,\overline{n}_{(b)}(\tau,\sigma^r)$ are the lapse and shift functions respectively.

[12] ${}^4\mathring{E}^{\,A}_{(\beta)}$ and ${}^4\overline{E}^{\,A}_{(o)}$ are tetrads adapted to the 3+1 splitting.

As shown in Refs. [[39–43], due to the existence of the asymptotic ADM Poincare' group, the isolated system *gravitational field plus matter*, namely the 3-universe, has the mass given by the ADM weak energy and the spin by the ADM angular momentum. Therefore, at each time, the 3-universe can be described as a decoupled non-covariant non-observable external pseudo-particle (the center of mass of the 3-universe) carrying a pole (the mass)-dipole (the spin) structure. Since the ADM 3-momentum vanishes due to the rest-frame condition, the conjugate non-observable internal center of mass of the 3-universe may be eliminated from the observable variables by imposing the vanishing of the ADM Lorentz boosts.

As a conclusion to fix the gauge in GR with a metrology convention, so to visualize the associated gauge-dependent inertial effects, we need to separate the gauge variables from the dynamical ones, the so-called Dirac observables (DO), and only the Hamiltonian formalism has the tools to face this problem. The usual criticism that this can be done only in a non-covariant coordinate-dependent way is avoided due to the use of the radar coordinates implying the existence of 4-scalar tensors.

B. Canonical ADM Tetrad Gravity and Its Gauge Variables

The parametrization of cotetrads given in the previous subsection for ADM tetrad gravity implies [40] that the ADM action may be considered function of the 16 configurational variables $\varphi_{(a)}$, $1 + n$, $n_{(a)}$, ${}^3e_{(a)r}$. At the Hamiltonian level, there is a phase space spanned by these 16 configuration variables and their conjugated 16 momenta, and there are *14 first class constraints*. Ten of them are primary constraints (the vanishing of the 7 momenta of boosts, lapse and shift variables plus three constraints describing the gauge freedom in the rotation on the flat indices (a) of the cotriads), whereas four are secondary ones (the super-Hamiltonian and super-momentum constraints). Therefore, there are 14 gauge variables describing *inertial effects* and 2 canonical pairs of physical degrees of freedom describing the *tidal effects* of the gravitational field (namely GW in the weak field limit).

The basis of canonical variables for this formulation of tetrad gravity, naturally adapted to 7 of the 14 first-class constraints, is (only the momenta ${}^3\pi^r_{(a)}$ conjugated to the cotriads are not vanishing)

$$\begin{array}{cccc} \varphi_{(a)} & n & \overline{n}_{(a)} & {}^3e_{(a)r} \\ \pi_{\varphi_{(a)}} \approx 0 & \pi_n \approx 0 & \pi_{n_{(a)}} \approx 0 & |{}^3\pi^r_{(a)} \end{array} \tag{3}$$

In Ref. [42], a York canonical basis, adapted to 10 first-class constraints (not to the super-Hamiltonian and super-momentum ones, whose solution is unknown), was identified by means of a Shanmugadhasan canonical transformation [33, 34]; this allows *for the first time to get the explicit identification of the inertial and tidal variables*. It implements the York map of Ref. [54] and diagonalizes the York-Lichnerowicz approach [55]. Its final form is[13]

[13]G is Newton constant. The set of numerical parameters $\gamma_{\bar{a}\bar{a}}$ satisfies $\sum_u \gamma_{\bar{a}u} = 0$, $\sum_u \gamma_{\bar{a}u}\,\gamma_{\bar{b}u} = \delta_{\bar{a}\bar{b}}$, $\sum \bar{a}\,\gamma_{\bar{a}u}\,\gamma_{\bar{a}v} = \delta_{uv} - \frac{1}{3}$. Each solution of these equations defines a different York canonical basis.

http://dx.doi.org/10.5772/68115

$$\begin{array}{lllllll} \varphi_{(a)} & \alpha_{(a)} & n & \overline{n}_{(a)} & \theta^r & \tilde{\phi} & R_{\bar{a}} \\ \pi_{\varphi_{(a)}} \approx 0 & \pi^{(\alpha)}_{(a)} \approx 0 & \pi_n \approx 0 & \pi_{\overline{n}_{(a)}} \approx 0 & \pi^{(\theta)}_r & \pi\tilde{\phi} = \dfrac{c^3}{12\pi G}\, {}^3K & \Pi_{\bar{a}} \end{array} \tag{4}$$

$$\begin{aligned} & {}^3e_{(a)r} = \sum_b R_{(a)(b)}(\alpha_{(c)})\, V_{rb}(\theta^i)\, \tilde{\phi}1/3\, e^{\sum_{\bar{a}}^{1,2}\gamma_{\bar{a}a} R_{\bar{a}}}, \\ & {}^4g_{\tau\tau} = \epsilon[(1+n)^2 - \sum_a \overline{n}^2_{(a)}], \\ & {}^4g_{\tau r} = -\epsilon\, \overline{n}_{(a)}\, V_{ra}(\theta^i)\, \tilde{\phi}1/3\, e^{\sum_{\bar{a}}^{1,2}\gamma_{\bar{a}a} R_{\bar{a}}}, \\ & {}^4g_{rs} = -\epsilon\, {}^3g_{rs} = -\epsilon\, \tilde{\phi}2/3 \sum_a V_{ra}(\theta^i)\, V_{sa}(\theta^i)\, e^{\sum_{\bar{a}}^{1,2}\gamma_{\bar{a}a} R_{\bar{a}}}, \\ & \tilde{\phi} = \sqrt{det\, {}^3g_{rs}}, \end{aligned} \tag{5}$$

In this York canonical basis, the *inertial effects* are described by the arbitrary gauge variables[14] $\alpha_{(a)}$, $\varphi_{(a)}$, $1+n$, $\overline{n}_{(a)}$, θ^i, ${}^3K$, whereas the *tidal effects*, that is, the physical degrees of freedom of the gravitational field (the two polarizations of GW in the linearized theory), by the two canonical pairs $R_{\bar{a}}$ and $\Pi_{\bar{a}}$, $\overline{a} = 1, 2$ ($R\overline{a}$ are eigenvalues of the 3-metric with determinant one).

The momenta $\pi^{(\theta)}_r(\tau, \sigma^r)$ and the 3-volume element $\tilde{\phi}(\tau, \sigma^r) = \sqrt{det\, {}^3g_{rs}(\tau, \sigma^u)}$ have to be found as solutions of the super-momentum ($\mathcal{H}_{(a)}(\tau, \sigma^r) \approx 0$) and super-Hamiltonian (i.e., the Lichnerowicz equation [55] $\mathcal{H}(\tau, \sigma^r) \approx 0$) constraints, respectively.

Instead, the DO's (gauge invariant under the Hamiltonian gauge transformations generated by all the first class constraints; see Ref. [51]) of the gravitational field are not known[15]; they would be the two pairs of 4-scalar tidal variables in a Shanmugadhasan canonical basis adapted to all the 14 first class constraints.

The extra O(3,1) gauge freedom of the tetrads[16] is described by the gauge variables $\alpha_{(a)}(\tau, \sigma^r)$, $\varphi_{(a)}(\tau, \sigma^r)$. In the *Schwinger time gauges*, one imposes the gauge fixings $\varphi_{(a)}(\tau, \sigma^r) \approx 0$, $\alpha_{(a)}(\tau, \sigma^r) \approx 0$ so that the time-like tetrad coincides with the unit normal to the 3-space and the space-like ones became tangent to it (namely the tetrads become adapted to the 3+1 splitting).

[14] $\alpha_{(a)}$, $\varphi_{(a)}$, θ^i and ${}^3K$ are the primary gauge variables, whereas n and $\overline{n}_{(a)}$ are the secondary ones, which are determined as a consequence of the gauge fixing of the primary ones.

[15] $R_{\bar{a}}$, $\Pi_{\bar{a}}$ are not gauge invariant under the Hamiltonian gauge transformations generated by the super-Hamiltonian and super-momentum constraints.

[16] The gauge freedom for each observer to choose three gyroscopes as spatial axes and to choose the law for their transport along the time-like world line.

The gauge angles $\theta^i(\tau,\sigma^r)$[17] describe the freedom in the choice of the axes for the 3-coordinates σ^r on each 3-space: their fixation implies the determination of the shift gauge variables $\overline{n}_{(a)}$, namely the appearances of gravitomagnetism in the chosen 3-coordinate system [55]. The *3-orthogonal gauges* are defined by the gauge fixings $\theta^i(\tau,\sigma^r)\approx 0$: in them, the 3-metric ${}^3g_{rs}(\tau,\sigma^u) = -\epsilon\, {}^4g_{rs}(\tau,\sigma^u) = \delta_{rs}\,\tilde{\phi}2/3\, e^2 \sum_{\overline{a}}^{1,2} \gamma_{\overline{a}r}\, R_{\overline{a}}$ is diagonal.

Only one momentum is a gauge variable (a reflection of the Lorentz signature): the *York time* [56, 57], that is, the trace ${}^3K(\tau,\sigma^r)$ of the *extrinsic curvature* of the non-Euclidean 3-spaces as 3-submanifolds of space-time.[18] This inertial effect describes the GR version of the special-relativistic gauge freedom in clock synchronization [47, 48] when one has to describe physics in non-inertial frames. Its fixation determines the lapse function.

The Dirac Hamiltonian is $H_D = \frac{1}{c}\,\hat{E}_{ADM} + \int d^3\sigma\, [n\,\mathcal{H} - \overline{n}_{(a)}\,\mathcal{H}_{(a)}](\tau,\sigma^u) + \int d^3\sigma\, [\lambda_n\,\pi_n + \lambda_{\overline{n}_{(a)}}\,\pi_{\overline{n}_{(a)}} + \lambda_{\varphi_{(a)}}\,\pi_{\varphi_{(a)}} + \lambda_{\alpha(a)}\,\pi^{(\alpha)}_{(a)}](\tau,\sigma^u)$, where the weak ADM energy is an explicit function of all the variables, and the λ's are arbitrary Dirac multipliers (to be determined as a consequence of the gauge fixings).

In the family of Schwinger time gauges, the fixation of the primary gauge variables ${}^3K(\tau,\sigma^r)$, $\theta^i(\tau,\sigma^r)$ implies elliptic equations on the instantaneous 3-space Σ_τ for the determination of the lapse and shift functions (the secondary gauge variables) and then of their Dirac multipliers λ's. Instead in the usually used harmonic gauges, one imposes the primary gauge fixing $\chi^A(\tau,\sigma^r) = \partial_\tau \left((1 + n(\tau,\sigma^r))\, {}^3e(\tau,\sigma^r)\, {}^4g^{\tau A}(\tau,\sigma^r) \right) \approx 0$, whose stability in time, that is, $\partial_\tau\, \chi^A(\tau,\sigma^r) \approx 0$, implies hyperbolic equations for the lapse and shift functions, namely the necessity of Cauchy conditions in the past for these metrology gauge variables.

This parametrization of canonical tetrad gravity clarifies the meaning of the metrology conventions.

The fixation of the York time determines the sequence of instantaneous non-Euclidean 3-spaces Σ_τ of the 3+1 splitting of space-time centered on an observer either on the Earth or on the Space Station[19]: all the clocks on each 3-space are synchronized with the atomic clock (τ is its proper time) of the observer at the intersection of the 3-space with the observer world line. This time metrology convention implies also the determination of the lapse function, which describes how the unit of time of the atomic clock changes when one goes from a 3-space to an infinitesimally near successive one. The metrology conventions on the choice of the three space coordinates σ^r also imply the determination of the shift functions, which say in which point of the infinitesimally near next 3-space there are the same 3-coordinates of the chosen point on the original 3-space.

---

[17] They identify the direction cosines of the tangents to the three coordinate lines in each point of the 3-space Σ_τ.

[18] It is absent in the Galilean space-time of Newtonian gravity with its absolute notions of time and Euclidean 3-space.

[19] The detailed structure of these non-Euclidean 3-spaces depends on the extrinsic curvature 3-tensor ${}^3K_{rs}$, which depends not only from all the gauge variables but also on the tidal variables, so that it is determined by the chosen solution of Einstein equations.

http://dx.doi.org/10.5772/68115

C. Einstein Hamilton Equations of Tetrad Gravity and their Linearization

In the York canonical basis, the Hamilton equations generated by the Dirac Hamiltonian $H_D = \hat{E}_{ADM} + (constraints)$ are divided into four groups after the fixation of the O(3,1) gauge variables with the Schwinger time gauges:

A. Four contracted Bianchi identities, namely the evolution equations for $\tilde{\phi}$ and $\pi_i^{(\theta)}$ (they say that given a solution of the constraints on a Cauchy surface, it remains a solution also at later times).

B. Four evolution equation for the four basic primary gauge variables θ^i and ${}^3K$: these equations determine the lapse and the shift functions once four gauge fixings for the basic gauge variables are added.

C. four evolution equations for the tidal variables $R\bar{a}$, $\Pi\bar{a}$;

D. the Hamilton equations for matter, when present.

The Hamilton equations become completely deterministic after a fixation of the gauge freedom. In the York canonical basis, it is convenient to use a family of *non-harmonic 3-orthogonal Schwinger time gauges* $\alpha_{(a)}(\tau,\sigma^r) \approx 0$, $\varphi_{(a)}(\tau,\sigma^r) \approx 0$, $\theta^i(\tau,\sigma^r) \approx 0$, ${}^3K(\tau,\sigma^r) \approx F(\tau,\sigma^r)$ parametrized by the numerical values $F(\tau,\sigma^r)$ of the York time ${}^3K(\tau,\sigma^r)$ and having the 3-metric in the 3-spaces diagonal and well determined lapse and shift functions. In these gauges, given a solution of the super-momentum and super-Hamiltonian constraints, one can find a solution of Einstein's equations in radar 4-coordinates adapted to a time-like observer giving the Cauchy data on an initial 3-space only for the tidal variables. This happens in the associated 3+1 splitting of space-time with dynamically selected instantaneous 3-spaces in accord with Ref. [1]. Then, one can pass to adapted world 4-coordinates ($x^\mu = z^\mu(\tau,\sigma^r) = x_o^\mu + \epsilon_A^\mu\ \sigma^A$) and can describe the solution in every 4-coordinate system by means of 4-diffeomorphisms.

In Ref. [43], this class of asymptotically Minkowskian space-times without super-translations is used to study the coupling of N charged scalar point particles (with the inertial and gravitational masses equal as required by the equivalence principle) plus the electromagnetic field to ADM tetrad gravity. The use of Grassmann-valued electric charges and the signs of the energy of the particles allows to regularize the self-energies. The theory can be reformulated in terms of transverse electromagnetic fields by using the non-covariant radiation gauge; this allows to extract the generalization of the Coulomb interaction among the particles in the Riemannian instantaneous 3-spaces of global non-inertial frames.

From the Hamilton equations in the York canonical basis [43], followed by a Hamiltonian Post-Minkowskian (HPM) linearization (disregarding terms of order $O(G^2)$ in the Newton constant and using an ultra-violet cutoff for matter) with the asymptotic flat Minkowski 4-metric at spatial infinity as background, it has been possible to develop a theory of GW's with asymptotic background propagating in the non-Euclidean 3-spaces Σ_τ of a family of *non-harmonic 3-orthogonal Schwinger time gauges* $\alpha_{(a)}(\tau,\sigma^r) \approx 0$, $\varphi_{(a)}(\tau,\sigma^r) \approx 0$, $\theta^i(\tau,\sigma^r) \approx 0$, ${}^3K(\tau,\sigma^r) \approx F(\tau,\sigma^r)$ parametrized by the numerical values $F(\tau,\sigma^r)$ of the York time ${}^3K(\tau,\sigma^r)$ and having the 3-metric in the 3-spaces diagonal and well-determined lapse and shift functions.

Since the celestial reference frame ICRS has diagonal 3-metric, our 3-orthogonal Schwinger time gauges are a good choice for celestial metrology.

The open problem is that the GCRS and BCRS conventions in the Solar System are using the special harmonic gauge of IAU [2, 3], in which the lapse function satisfies a hyperbolic equation like the tidal variables and needs initial data in the past, differently from what happens in the 3-orthogonal Schwinger time gauges. See Subsection 3.3 of the third paper in Ref. [43] for the comparison of the IAU harmonic gauge for BCRS with the 3-orthogonal gauges and Subsection 3.3 of the second paper in Ref. [43] for the equations identifying the 4-coordinate transformation from the 3-orthogonal gauges to the harmonic ones after the linearization, which have to be solved to get the reformulation of IAU conventions in our gauges.

4. Dark matter as a relativistic inertial effect

The linearized HPM Hamilton equations for point particles of mass m_i, $i = 1, .., N$[20], whose world lines $x^\mu_i(\tau) = z^\mu(\tau, \eta^r_i(\tau))$ are identified by radar 3-coordinates $\eta^r_i(\tau)$ due to the 3+1 splitting, and for the electromagnetic field coupled to tetrad gravity have been written explicitly in Refs. [43]: among the forces acting on matter, there are both the inertial potentials and the GW's.

In the third paper of Ref. [43], electro-magnetism is eliminated and there is a detailed studied of the HPM equations of motion of the particles. Then, the PN expansion of these regularized HPM equations of motion for the particles was studied, and it was shown that the particle 3-coordinates $\eta^r_i(\tau = ct) = \tilde{\eta}^r_i(t)$ (coinciding with the Newtonian coordinates of the world lines at this level of approximation) satisfy the equation of motion

$$\begin{aligned} &\frac{d}{dt}\left[m_i \left(1 + \frac{1}{c}\,\frac{d}{dt}\,{}^3\tilde{\mathcal{K}}_{(1)}(t, \vec{\tilde{\eta}}_i\,(t))\right) \frac{d\,\tilde{\eta}^r_i(t)}{dt}\right] \stackrel{\circ}{=} \\ &-G\,\frac{\partial}{\partial\,\tilde{\eta}^r_i} \sum_{j\neq i} \eta_j\,\frac{m_i\,m_j}{|\vec{\tilde{\eta}}_i\,(t) - \vec{\tilde{\eta}}_j\,(t)|} + \mathcal{O}(G^2). \end{aligned} \tag{6}$$

where at the lowest order, there is the standard Newton gravitational force

$$\vec{F}_{i(Newton)}(t) = -m_i\,G\,\frac{\partial}{\partial\,\tilde{\eta}^r_i} \sum_{j\neq i} \frac{m_j}{|\vec{\tilde{\eta}}_i\,(t) - \vec{\tilde{\eta}}_j\,(t)|} = -m_i\,\frac{\partial\,\Phi(t, \vec{\tilde{\eta}}_i(t))}{\partial\,\tilde{\eta}^r_i}. \tag{7}$$

Since Eqs. (4) imply

$$\epsilon^4 g_{\tau\tau}(\tau = ct, \sigma^r) - 1 = 2\,n(\tau = ct, \sigma^r) + O(G^2) = 2\,\frac{\Phi(t, \sigma^r)}{c^2} - \frac{2}{c}\,\frac{\partial}{\partial\,t}\,{}^3\tilde{\mathcal{K}}_{(1)}(\tau = ct, \sigma^r) + O(G^2), \tag{8}$$

[20] m_i is both the inertial and the gravitational mass, since they coincide in Einstein GR due to the equivalence principle.

http://dx.doi.org/10.5772/68115

there is a 0.5 PN *inertial effect* (hidden in the lapse function) not existing in the Newton theory where the Euclidean 3-space is an absolute notion like the Newtonian time. It does not depend on the York time ${}^3K_{(1)}$ but on the *non-local York time* (Δ is the Laplacian associated to the asymptotic Minkowski 4-metric)

$$ {}^3\tilde{\mathcal{K}}_{(1)}(\tau,\sigma^r) = \left(\frac{1}{\Delta}\,{}^3K_{(1)}\right)(\tau,\sigma^r). \tag{9} $$

If we put ${}^3K_{(1)} = 0$, the standard results about binaries are reproduced.

The term in the non-local York time can be *interpreted* as the introduction of an *effective (time-, velocity- and position-dependent) inertial mass term* for the kinetic energy of each particle:

$$ m_i \mapsto m_i \left(1 + \frac{1}{c}\,\frac{d}{dt}\,{}^3\tilde{\mathcal{K}}_{(1)}(t,\vec{\tilde{\eta}}_i(t))\right) \tag{10} $$

in each instantaneous 3-space. Since, in the Newton potential, there are the gravitational masses m_i of the particles, the effect is due to a modification of the effective inertial mass in each non-Euclidean 3-space depending on its shape as a 3-submanifold of space-time. Therefore, we find *it is the equality of the inertial and gravitational masses of Newtonian gravity to be violated* in a gauge-dependent way in Einstein GR!

In the two-body case, one gets that for Keplerian circular orbits of radius r the modulus of the relative 3-velocity can be written in the form $\sqrt{\frac{G\,(m+\Delta\,m(r))}{r}}$ with $\Delta\,m(r)$ function only of ${}^3\tilde{\mathcal{K}}_{(1)}$.

The data on the *rotation curves of spiral galaxies* [14–17] imply that the relative 3-velocity goes to constant for large r instead of vanishing like in Kepler theory. As shown in Subsection 6.4 of the third paper in Ref. [43], this result can be simulated by fitting $\Delta\,m(r)$ (i.e., the non-local York time) to the experimental data with $\Delta\,m(r)$ interpreted as a *dark matter halo* around the galaxy.

Therefore, this dark matter can be explained as a *relativistic inertial gauge effect* consequence of the non-trivial shape of the non-Euclidean 3-space as a 3-submanifold of space-time. There is the concrete possibility to explain the rotation curves of galaxies [14–17] as a *relativistic inertial effect inside Einstein GR* (choice of a non-local York time compatible with observations) without modifications: (a) of Newton gravity like in MOND [9]; (b) of GR like in $f(R)$ theories [10–12]; (c) of particle physics with the introduction of WIMPS [58].

A similar interpretation (see Subsections 6.2 and 6.3 of the third paper in Ref. [43]) can be given for the other two main signatures of the existence of dark matter in the observed masses of galaxies and clusters of galaxies, namely *the mass determination with weak and strong gravitational lensing*[21] [18–20] and *the mass determination with the virial theorem* [21–23].

---

[21]In the case of gravitational lensing Einstein's deflection angle, $\alpha = 4\,G\,M/c^2\,\xi$ (ξ is the impact parameter of the ray of light deflected at the position of the mass M) has $M = M_{baryon} + M_{DM}$ with the dark matter term given by $G\,M_{DM} = -2\,c^2\,|\,\vec{\sigma}\,|\,\partial_\tau\,{}^3\tilde{\mathcal{K}}_{(1)}(\tau,\sigma^u)$.

Therefore, there is the possibility of describing part (or maybe all) dark matter as a *relativistic inertial effect*.

The quoted three main experimental signatures of dark matter are well-defined functional of the time and space derivatives of the non-local York time[22] the inertial gauge variable describing the general relativistic remnant of the gauge freedom in clock synchronization.

Since the time evolution of the signatures of dark matter is not known, at best from the data, we can extract information only on a *mean value in time* of the time- and space derivatives of the non-local York time. Since from Eq. (7), we see that $-\partial_\tau\, {}^3\tilde{\mathcal{K}}_{(1)}(\tau,\sigma^r)$ is a modification of the Newton potential, we can assume that in Einstein GR the gauge variable non-local York time can be equated to the time-independent potentials $V(\sigma^r)$ used either in phenomenology or in modified theories of GR to describe dark matter in either galaxies or cluster of galaxies. Then, we can make the ansatz ${}^3\tilde{\mathcal{K}}_{(1)}(\tau,\sigma^r) = -\tau\, V(\sigma^r)$ and find the local York time ${}^3K_{(1)}(\tau,\sigma^r) = \Delta\, {}^3\tilde{\mathcal{K}}_{(1)}(\tau,\sigma^r)$ connected with the dark matter of the chosen either galaxy or cluster of galaxies.

Since there is no indication of dark matter in the voids existing among the clusters of galaxies, we can get an idea on the form of the local York time in the 3-space Σ_τ (i.e., the whole 3-universe) by summing its value for all the known galaxies and clusters of galaxies. This would produce an indication of which could be a metrology convention on the inertial gauge variable describing the general relativistic gauge freedom in clock synchronization in the Einstein space-time outside the Solar System. One expects that, with this metrology convention, the resulting 3-spaces (each one with all the clocks synchronized) are nearly Euclidean except where there is need of introducing dark matter.

In Ref. [59], there is a first attempt to fit some data of dark matter by using a Yukawa-like ansatz on the non-local York time of a galaxy. In each galaxy, the Yukawa-like potential of $f(R)$ theories [10–12] is put equal to a contribution to the extra potential depending on the non-local York time present in the lapse function appearing in Eq. (8); in this way, the good fits of the rotation curves of galaxies obtainable with $f(R)$ theories can be reproduced inside Einstein's GR as an inertial gauge effect.

5. Metrology against darkness

In conclusion, a suitable metrology convention on the inertial gauge variable York time could reduce or maybe eliminate the necessity of introducing dark matter in the classical universe and in its extension to classical cosmology after the recombination surface.

A needed natural proposal is now to define a *Post-Minkowskian ICRS* with non-Euclidean 3-spaces, whose intrinsic 3-curvature (due essentially to GW and matter) is small, in such a way

---

[22] $\partial_\tau\, {}^3\tilde{\mathcal{K}}_{(1)}(\tau,\sigma^r)$ in the gravitational lensing case, $\frac{d}{dt}\, {}^3\tilde{\mathcal{K}}_{(1)}(c\,t,\vec{\tilde{\eta}}_i(t)) = (\frac{\partial}{\partial t} + \dot{\vec{\tilde{\eta}}}_i(t)\cdot\frac{\partial}{\partial\, \vec{\tilde{\eta}}_i})\, {}^3\tilde{\mathcal{K}}_{(1)}(c\,t,\vec{\tilde{\eta}}(t))$ in the rotation curve case and $\frac{d^2}{dt^2}\, {}^3\tilde{\mathcal{K}}_{(1)}(c\,t,\vec{\tilde{\eta}}_i\,(t))$ in the virial theorem case.

that the York time be (at least partially) fitted to the observational data implying the presence of dark matter. As a consequence, BCRS would be its quasi-Minkowskian approximation for the Solar System.[23] Let us remark that the 3-spaces can be quasi-Euclidean (i.e. with a small internal 3-curvature tensor), as required by CMB data in the astrophysical context, even when their shape as 3-submanifolds of space-time is not trivial and is described by a not-small York time.

In this way, one would get a solution to the gauge problem for the PM space-times of GR: one chooses a reference system of 4-coordinates in a 3-orthogonal gauge selected by the observational conventions for matter. A PM definition of ICRS will be also useful for the ESA-GAIA mission [60] (cartography of the Milky Way) and for the possible anomalies (different from the already explained Pioneer one) inside the Solar System [5].

Regarding *dark energy* in cosmology [24–29], we can remark that in the FLRW cosmological solution, the Killing symmetries connected with homogeneity and isotropy imply (τ is the cosmic time, $a(\tau)$ the scale factor) ${}^3K(\tau) = -\frac{\dot{a}(\tau)}{a(\tau)} = -H$, namely the York time is no more a gauge variable but coincides with the Hubble constant. However, in cosmological perturbation theory, we have ${}^3K = -H + {}^3K_{(1)}$ at the first order with ${}^3K_{(1)}$ being again an inertial gauge variable.

Let us also remark that in Szekeres space-times [61–63], that is, in inhomogeneous space-times without Killing symmetries, the York time remains an inertial gauge variable.

As said in Section 2, the red-shift and luminosity distance of SNIa is a signal of *dark energy*. In Section 3 of the third paper in Ref. [43], there is the evaluation of the dependence on the non-local York time of the PM time-like geodesics, whereas in Section 4 of that paper, there is evaluated the dependence on it of the PM null geodesics, of the PM red-shift, of the PM geodesics deviation equation, of the PM luminosity distance and of the Hubble old red-shift distance relation (becoming the Hubble law if cosmology in introduced in the description). Like in the case of dark matter, one has a dependence on the second derivatives ∂_τ^2, $\partial_\tau \partial_r$ and $\partial_r \partial_s$ of the non-local York time now concentrated along the either time- or null geodesics. Therefore, also, this indication of dark energy is metrology dependent!

Let us also remark that in the back-reaction approach [64–69], in which to take into account the inhomogeneity of the observed universe when trying to get a cosmological description of it, one considers spatial mean values on large scales, dark energy in cosmology is a byproduct of the nonlinearities of GR. In this approach, one gets that the spatial average of the 4-scalar gauge variable York time gives the effective Hubble constant of this approach.

Finally, as shown in Eq. (10) of the last paper in Ref. [35], it can be shown that the York time is responsible for the negative terms in the kinetic energy term in the ADM energy, whose existence was known but whose explicit form could be given only in the York canonical basis. It is therefore possible that the connected Landau-Lifschitz energy-momentum pseudo-tensor [70] of GR could be reformulated as the energy-momentum tensor of a viscous pseudo-fluid,

[23] To test this possibility, one has to study the transition from harmonic gauges to 3-orthogonal ones in linearized Einstein GR.

which could have a negative pressure for certain choices of the York time like the dark energy fluid in FLWR cosmology.

In conclusion, the York time has a central position in all the cases where darkness is required to fit the data!

Author details

Luca Lusanna[1]* and Ruggero Stanga[2]

*Address all correspondence to: lusanna@fi.infn.it

1 Retired Research Director of Sezione INFN di Firenze, Sesto Fiorentino (FI), Italy

2 Dipartimento di Fisica e Astronomia, Firenze Univ., and Sezione INFN di Firenze, Sesto Fiorentino (FI), Italy

References

[1] L. Lusanna and M. Pauri, *Explaining Leibniz equivalence as difference of non-inertial Appearances: Dis-solution of the Hole Argument and physical individuation of point-events*, History and Philosophy of Modern Physics 37, 692 (2006) (arXiv gr-qc/0604087); *The Physical Role of Gravitational and Gauge Degrees of Freedom in General Relativity. I: Dynamical Synchronization and Generalized Inertial Effects; II: Dirac versus Bergmann Observables and the Objectivity of Space-Time*, Gen. Rel. Grav. 38, 187 and 229 (2006) (arXiv gr-qc/0403081 and 0407007); *Dynamical Emergence of Instantaneous 3-Spaces in a Class of Models of General Relativity,* in *Relativity and the Dimensionality of the World*, ed. V. Petkov (Springer Series Fundamental Theories of Physics, Berlin, 2007) (arXiv gr-qc/0611045).

[2] M. Soffel, S.A. Klioner, G. Petit, P. Wolf, S.M. Kopeikin, P. Bretagnon, V.A. Brumberg, N. Capitaine, T. Damour, T. Fukushima, B. Guinot, T. Huang, L. Lindegren, C. Ma, K. Nordtvedt, J. Ries, P.K. Seidelmann, D. Vokroulicky', C. Will and Ch. Xu, *The IAU 2000 Resolutions for Astrometry, Celestial Mechanics and Metrology in the Relativistic Framework: Explanatory Supplement*. Astron. J., 126, pp.2687–2706, (2003) (astro-ph/0303376).

[3] *IERS Conventions (2003)*, eds. D.D. McCarthy and G. Petit, IERS TN 32 (2004), Verlag des BKG. G.H. Kaplan, *The IAU Resolutions on Astronomical Reference Systems, Time Scales and Earth Rotation Models*, U.S.Naval Observatory circular No. 179 (2005) (astro-ph/0602086).

[4] L. Lusanna, *Relativistic Metrology: from Earth to Astrophysics*, In-Tech E-Book *Modern Metrology Concerns*, 2012 (ISBN 978-953-51-0584-8).

[5] S.G. Turishev, M. Shao and K.L. Nordtvedt, *Experimental Design of the LATOR Mission*, arXiv gr-qc/0410044 (2004). S.G. Turyshev and V.T. Toth, *The Pioneer Anomaly* Living Rev. Rel. 13, n.4 (2010) (arXiv1001.3686).

[6] M. Bartelmann, *The Dark Universe*, Rev. Mod. Phys. 82, 331 (2010)(arXiv0906.5036).

[7] K. Freese, *Status of Dark Matter in the Universe*, (arXiv1701.01840) (2017).

[8] Planck Collaboration, *Planck 2015 results: XIV. Dark energy and modified gravity, AeA*594, A14 (2016).

[9] M. Milgrom, *New Physics at Low Accelerations (MOND): An Alternative to Dark Matter*, (aXiv0912.2678) (2009).

[10] S. Capozziello and M. de Laurentis, *The Dark Matter Problem from f(R) Gravity Viewpoint*, Annalen der Physik524, 545 (2012).

[11] S. Capozziello, V.F. Cardone and A. Troisi, *Low Surface Brightness Galaxy Rotation Curves in the Low Energy Limit of R^n Gravity: No Need for Dark Matter?*, Mon. Not. R. Astron. Soc. 375, 1423 (2007) (arXivastro-ph/0603522).

[12] S. Capozziello, E. De Filippis and V. Salzano, *Modelling Clusters of Galaxies by $f(R)$ Gravity*, Mon.Not.R.Astron.Soc. 394, 947 (2009) (arXiv0809.1882).

[13] A. Fey, G. Gordon and C. Jacobs (eds), The Second Realization of the International Celestial Reference Frame by Very Long Baseline Interferometry, IERS Technical Notes 35 (2009).

[14] E. Battaner and E. Florido, *The Rotation Curve of Spiral Galaxies and its Cosmological Implications*, Fund.Cosmic Phys. 21, 1 (2000).

[15] D.G.Banhatti, *Disk Galaxy Rotation Curves and Dark Matter Distribution*, Current Science 94, 986 (2008).

[16] W.J.G. de Blok and A. Bosma, *High Resolution Rotation Curves of Low Surface Brightness Galaxies*, Astron. Astrophys. 385, 816 (2002) (arXivastro-ph/0201276).

[17] P. Bhattacharjee, S. Chaudhury and S. Kundu, *Rotation Curves of the Milky Way out to $\sim 200Kpc$*, Astrophys. J. 785, 63 (2014) (arXiv1310.2659).

[18] P. Schneider, J. Ehlers and E.E. Falco, *Gravitational Lenses* (Springer, Berlin, 1992). M. Ross, *Dark Matter: the Evidence from Astronomy, Astrophysics and Cosmology* (arXiv1001.0316).

[19] K. Garret and G. Duda, *Dark Matter: A Primer* (arXiv1006.2483).

[20] M. Bartelmann and P. Schneider, *Weak Gravitational Lensing*, Phys. Rep. 340, 291 (2001) (arXivastro-ph/9912508).

[21] M.S. Longair, *Galaxy Formation* (Springer, Berlin, 2008).

[22] M. Ross, *Dark Matter: the Evidence from Astronomy, Astrophysics and Cosmology* (arXiv1001.0316).

[23] K. Garret and G. Duda, *Dark Matter: A Primer*, Adv. Astron. 2011, 968283 (2011) (arXiv1006.2483).

[24] R. Durrer, *What do we really Know about Dark Energy?*, Phil.Trans.R.Soc. A369, 5102 (2011) (arXiv1103.5331).

[25] C. Bonvin and R. Durrer, *What Galaxy Surveys Really Measure*, Phys. Rev. D84, 063505 (2011) (arXiv1105.5280).

[26] A.V. Filippenko, *Type Ia supernovae and cosmology*, in *White Dwarfs: Cosmological and Galactic Probes*, eds. E. Sion, S. Vennes and H. Shipman, Astrophs. Space Sci. Libr. 332, 97 (2005).

[27] J.A. Frieman, M.S. Turner and D. Huterer, *Dark Energy and the Accelerating Universe*, Annu. Rev. Astron. Astrophys. 46, 385 (2008).

[28] S. Perlmutter et al. (The Supernova Cosmology Project), *Measurements of* Ω *and* Λ *from 42 High-Redshift Supernovae*, Astrophys. J. 517, 565 (1999) (arXivastro-ph/9812133).

[29] A.G. Riess et al., *Observational evidence from Supernovae for an Accelerating Universe and a Cosmological Constant*, Astron. J 116, 1009 (1998) (arXivastro-ph/9805201).

[30] R. Arnowitt, S. Deser and C.W. Misner, *The Dynamics of General Relativity*, ch.7 of *Gravitation: an Introduction to Current Research*, ed. L. Witten (Wiley, New York, 1962) (arXiv gr-qc/0405109).

[31] S. Deser and C.J. Isham, *Canonical Vierbein Form of General Relativity*, Phys. Rev. D14, 2505 (1976).

[32] P.A.M. Dirac, *Lectures on Quantum Mechanics*, Belfer Graduate School of Science, Monographs Series (Yeshiva University, New York, N.Y., 1964); *Gauge Invariant Formulation of Quantum Electrodynamics*, Can. J. Phys. 33, 650 (1955).

[33] S. Shanmugadhasan, *Canonical Formalism for Degenerate Lagrangians*, J. Math. Phys. 14, 677 (1973).

[34] L. Lusanna, *The Shanmugadhasan Canonical Transformation, Function Groups and the Second Noether Theorem*, Int. J. Mod. Phys. A8, 4193 (1993); *The Relevance of Canonical Transformations in Gauge Theories and General Relativity*, Lecture Notes of "SeminarioInterdisciplinare di Matematica" (Basilicata Univ.) 5, 125 (2006).

[35] L. Lusanna, *From Clock Synchronization to Dark Matter as a Relativistic Inertial Effect*, Lecture at the *Black Objects in Supergravity* School BOSS2011, Frascati, 9-13 May 2011 (arXiv1205.2481), Springer Proc. Phys. 144, pp. 267–343 (Spinger, Berlin, 2013); *Non-Inertial Frames in Special and General Relativity*, to appear in the Proceedings of the School *Gravity: where do we stand?*, 11–15 May 2009, Villa Olmo, Como, Italy, eds. R. Peron, M. Colpi, V. Gorini and U. Moschella (Springer, Berlin, 2016) (arXiv:1310.4465); *Canonical ADM Tetrad Gravity: from Metrological Inertial Gauge Variables to Dynamical Tidal Dirac Observables*, Int. J. Geom. Meth. Mod. Phys. 12, 1530001 (2015) (arXiv1401.1375).

[36] L. Lusanna, *Killing Symmetries as Hamiltonian Constraints*, Int. J. Geom. Meth. Mod. Phys. *13*, 1650044 (2016) (arXiv1511.05829).

[37] A. Ashtekar, *Asymptotic Structure of the Gravitational Field at Spatial Infinity*, in *General Relativity and Gravitation*, Vol. 2, ed. A. Held (Plenum, New York, 1980).

http://dx.doi.org/10.5772/68115

[38] R. Beig and Ó Murchadha, *The Poincar Group as the Symmetry Group of Canonical General Relativity*, Ann. Phys. (N.Y.) 174, 463 (1987).

[39] L. Lusanna, *The Rest-Frame Instant Form of Metric Gravity*, Gen. Rel. Grav. 33, 1579 (2001) (arXiv gr-qc/0101048).

[40] L. Lusanna and S. Russo, *A New Parametrization for Tetrad Gravity*, Gen. Rel. Grav. 34, 189 (2002) (arXiv gr-qc/0102074).

[41] R. DePietri, L. Lusanna, L. Martucci and S. Russo, *Dirac's Observables for the Rest-Frame Instant Form of Tetrad Gravity in a Completely Fixed 3-Orthogonal Gauge*, Gen. Rel. Grav. 34, 877 (2002) (arXiv gr-qc/0105084).

[42] D. Alba and L. Lusanna, *The York Map as a Shanmugadhasan Canonical Transformationn in Tetrad Gravity and the Role of Non-Inertial Frames in the Geometrical View of the Gravitational Field*, Gen. Rel. Grav. 39, 2149 (2007) (arXiv gr-qc/0604086, v2).

[43] D. Alba and L. Lusanna, *The Einstein-Maxwell-Particle System in the York Canonical Basis of ADM Tetrad Gravity: (I) The Equations of Motion in Arbitrary Schwinger Time Gauges.*, Canad. J. Phys. 90, 1017 (2012) (arXiv0907.4087); *(II) The Weak Field Approximation in the 3-Orthogonal Gauges and Hamiltonian Post-Minkowskian Gravity: the N-Body Problem and Gravitational Waves with Asymptotic Background.*, Canad. J. Phys. 90, 1077 (2012) (arXiv1003.5143); *(III) The Post-Minkowskian N-Body Problem, its Post-Newtonian Limit in Non-Harmonic 3-Orthogonal Gauges and Dark Matter as an Inertial Effect.*, Canad. J. Phys. 90, 1131 (2012) (arXiv1009.1794).

[44] T. Thiemann, Modern Canonical Quantum General Relativity (Cambridge Univ. Press, Cambridge, 2007).

[45] C. Rovelli, *Quantum Gravity* (Cambridge University Press, Cambridge, 2004).

[46] D. Christodoulou and S. Klainerman, *The Global Nonlinear Stability of the MinkowskiSpace* (Princeton, Princeton, 1993).

[47] D. Alba and L. Lusanna, *Charged Particles and the Electro-Magnetic Field in Non-Inertial Frames: I. Admissible 3+1 Splittings of MinkowskiSpacetime and the Non-Inertial Rest Frames*, Int.J.Geom.Methods in Physics 7, 33 (2010) (arXiv0908.0213) and *II. Applications: Rotating Frames, Sagnac Effect, Faraday Rotation, Wrap-up Effect*, Int. J. Geom. Methods in Physics, 7, 185 (2010) (arXiv0908.0215); *Generalized Radar 4-Coordinates and Equal-Time Cauchy Surfaces for Arbitrary Accelerated Observers* (2005), Int. J. Mod. Phys. D16, 1149 (2007) (arXiv gr-qc/0501090).

[48] D. Alba, H.W. Crater and L. Lusanna, *Towards Relativistic Atom Physics. I. The Rest-Frame Instant Form of Dynamics and a Canonical Transformation for a system of Charged Particles plus the Electro-Magnetic Field*, Canad.J.Phys. 88, 379 (2010) (arXiv0806.2383) and *II. Collective and Relative Relativistic Variables for a System of Charged Particles plus the Electro-Magnetic Field*, Canad. J. Phys. 88, 425 (2010) (arXiv0811.0715).

[49] H. Bondi, *Assumption and Myth in Physical Theory* (Cambridge University Press, Cambridge, 1967).

[50] R. D'Inverno, *Introducing Einstein Relativity* (Oxford University Press, Oxford, 1992).

[51] L. Lusanna and M. Villani, *Hamiltonian Expression of Curvature Tensors in the York Canonical Basis:I) Riemann Tensor and Ricci Scalars*, Int. J. Geom. Meth. Mod. Phys. 11, 1450052 (2014) (arXiv1401.1370); *II) Weyl Tensor, Weyl Scalars, Weyl Eigenvalues and the Problem of the Observables of the Gravitational Field*, Int. J. Geom. Meth. Mod. Phys. 11, 1450053 (2014) (arXiv1401.1375).

[52] C.M. Møller, *The Theory of Relativity* (Oxford Univ. Press, Oxford, 1957).

[53] C. Møller, *Sur la dinamique des syste'mesayant un moment angulaire interne*, Ann. Inst. H. Poincare' 11, 251 (1949).

[54] J. Isenberg and J.E. Marsden, *The York Map is a Canonical Transformation*, J. Geom. Phys. 1, 85 (1984).

[55] I. Ciufolini and J.A. Wheeler, *Gravitation and Inertia* (Princeton Univ. Press, Princeton, 1995).

[56] J.W. York Jr, *Gravitational Degrees of Freedom and the Initial Value Problem*, Phys. Rev. Lett. 26, 1656 (1971); *Role of Conformal Three Geometry in the Dynamics of Gravitation*, Phys.Rev. Lett.28, 1082 (1972); *Kinematics and Dynamics of General Relativity*, in *Sources of Gravitational Radiation*, Battelle-Seattle Workshop 1978, ed. L.L. Smarr (Cambridge Univ. Press, Cambridge, 1979).

[57] A. Qadir and J.A. Wheeler, *York's Cosmic Time Versus Proper Time*, in *From SU(3) to Gravity*, Y. Ne'eman's festschrift, eds. E. Gotsma and G. Tauber (Cambridge Univ. Press, Cambridge, 1985).

[58] J.L. Feng, *Dark Matter Candidates from Particle Physics and Methods of Detection*, Ann. Rev. Astron. Astrophys. 48, 495 (2010) (arXiv1003.0904).

[59] M. Villani, *Constraints on ADM tetrad gravity parameter space from S2 star in the center of the Galaxy and from the Solar System*, 2015 (arXiv:1502.06801).

[60] S. Jordan, *The GAIA Project: Technique, Performance and Status*, Astron. Nachr. 329, 875 (2008) (doi:10.1002/asna.200811065).

[61] W.B. Bonnor, A.H. Sulaiman and N. Tanimura, *Szekeres's Space-Times have no Killing Vectors*, Gen. Rel. Grav. 8, 549 (1977).

[62] B.K. Berger, D.M. Eardley and D.W. Olson, *Notes on the Spacetimes of Szekeres*, Phys. Rev. D16, 3086 (1977).

[63] A. Nwankwo, M. Ishak and J. Thomson, *Luminosity Distance and Redshift in the Szekeres Inhomogeneous Cosmological Models*, JCAP 1105, 028 (2011) (arXiv1005.2989).

[64] T. Buchert, *Dark Energy from Structure: a Status Report*, Gen. Rel. Grav. 40, 467 (2008) (arXiv0707.2153).

http://dx.doi.org/10.5772/68115

[65] A. Wiegand and T. Buchert, *Multiscale Cosmology and Structure-Emerging Dark Energy: a Plausibility Analysis*, Phys. Rev. D82, 023523 (2010) (arXiv1002.3912).

[66] J. Larena, *Spatially Averaged Cosmology in an Arbitrary Coordinate System*, Phys. Rev. D79, 084006 (2009) (arXiv0902.3159).

[67] R.J. van den Hoogen, *Averaging Spacetime: Where do we go from here ?*, The Twelfth Marcel Grossmann Meeting: *On Recent Developments in Theoretical and Experimental General Relativity, Astrophysics and Relativistic Field Theories*, eds. T. Damour, R.T. Jantzen and R. Ruffini, (World Scientific, 2012), pp. 578–588 (arXiv1003.4020).

[68] T. Clifton, Back-Reaction in Relativistic Cosmology, Int. J. Mod. Phys. D22, 133004 (2013) (arXiv1302.6717).

[69] T. Buchert, M. Carfora, G. F. R. Ellis, E. W. Kolb, M. A. H. MacCallum, J. J. Ostrowski, S. Räsänen, B. F. Roukema, L. Andersson, A. A. Coley and D.L. Wiltshire, *Is there proof that backreaction of inhomogeneities is irrelevant in cosmology?*, Clas. Quan. Grav. 32, 215021 (2015) (arXiv1505.07800).

[70] L. D. Landau and E. M. Lifshitz, The Classical Theory of Fields, 2nd ed. (Reading, Mass.: Addison-Wesley, 1962).

Chapter 5

Superfluid Quantum Space and Evolution of the Universe

Valeriy I. Sbitnev and Marco Fedi

Additional information is available at the end of the chapter

http://dx.doi.org/10.5772/68113

Abstract

We assume that dark energy and dark matter filling up the whole cosmic space behave as a special superfluid, here named "superfluid quantum space." We analyze the relationship between intrinsic pressure of SQS (dark energy's repulsive force) and gravity, described as an inflow of dark energy into massive particles, causing a negative pressure gradient around massive bodies. Since no superfluid has exact zero viscosity, we analyze the consequences of SQS's viscosity on light propagation, and we show that a static Universe could be possible, by solving a modified Navier-Stokes equation. Indeed, Hubble's law may actually refer to tired light, though described as energy loss due to SQS's nonzero viscosity instead of Compton scattering, bypassing known historical problems concerning tired light. We see that SQS's viscosity may also account for the Pioneer anomaly. Our evaluation gives a magnitude of the anomalous acceleration $a_P = -H_\Lambda c = -8.785^\circ 10^{-10}$ ms^{-2}. Here, H_Λ is the Hubble parameter loaded by the cosmological constant Λ. Furthermore, the vorticity equation stemming from the modified Navier-Stokes equation gives a solution for flat profile of the orbital speed of spiral galaxies and discloses what one might call a breathing of galaxies due to energy exchange between the galactic vortex and dark energy.

Keywords: gravity, dark energy, Hubble's law, tired light, Pioneer anomaly, flat profile

1. Introduction

A recent view of the evolution of the Universe suggests that it pre-existed the Big Bang. What we now observe seems, however, to be the result of such event. The Universe apparently continues to expand at an accelerated pace, as evidenced by the Doppler redshift of light coming from distant sources. To explain this accelerated expansion, scientists resort to dark energy. In addition, it turns out that spiral galaxies demonstrate a flat profile of orbital speeds.

Dark matter is used to explain this riddle [1]. Current evaluations of the presence of dark energy and dark matter in the cosmos say that the former is of about 69.1% and the latter about 25.9%. In total, they are about 95% of the whole energy matter in the Universe. The residue of 5% corresponds to baryon matter, which is the constituent material of all observed galaxies, stars, planets, etc. At present, space as a mere container of matter is therefore being revised. It is not an empty vessel: On the contrary, it may act as a quantum superfluid, named by us "superfluid quantum space" (SQS) [2]. It consists of dark energy and dark matter whose hydrodynamics generates perennially fluctuating particle-antiparticle pairs, which annihilate and newly arise, forming a dark fluid whose features are similar to a Bose-Einstein condensate [3–7]. Within this concept, the repulsive action of dark energy may be simply explained as the internal pressure of the SQS. It should be noted that there are scientists [8–12] who do not agree with a concept of Universe based on Big Bang, inflation and Doppler redshift. They explain its evolution without calling into play any "Deus ex machina" as cosmic inflation. On the contrary, they believe that light loses energy as a function of the traveled distance. We assert that this happens because of a nonzero viscosity of the SQS, in perfect agreement with the empirical Hubble's law. This could be interpreted as a revised phenomenon of tired light, different from that proposed in 1929 by F. Zwicky. In effect, while Zwicky's hypothesis based on light scattering [13] may be disproved, for example, by the absent blurring of distant cosmic objects, tired light due to SQS's viscosity is a more robust concept, which seems not to conflict with the current observations. In addition, while a viscosity-related tired light would let us observe a Doppler-alike redshift, pressure phenomena of opposite sign, that is, repulsion caused by SQS's internal pressure and gravity as an inflow of dark energy into massive particles [14], could balance and permit a not expanding Universe.

It is interesting to note the critical opinion of a greatest theorist of our time, of Roger Penrose. In his recently published book "Fashion, Faith, and Fantasy in the New Physics of the Universe" [15], he argues that most of the current imaginary ideas about the origins of the Universe could be not true. We agree with Penrose, being unsatisfied with the current mainstream. In this key, we speculate and analyze a different framework.

At the beginning, in Section 2, we present as much detail as possible on our idea of space as superfluid quantum space, including a short historical overview about the concept of ether, vacuum, and physical space. In Section 3, we introduce a general relativistic hydrodynamic equation, and we analyze the corresponding equation in non-relativistic limit, as a modified Navier-Stokes equation. Here, we discuss the issue of tired light, and we evaluate the Pioneer anomaly according to the nonzero viscosity of SQS. Section 4 deals with solutions of the vorticity equation derived from the modified Navier-Stokes equation. We obtain exact formulas for the flat profile of orbital speeds of spiral galaxies. Section 5 gives concluding remarks and a look on the overall issue of a superfluid Universe.

2. Space, vacuum and ether: toward a Superfluid Quantum Space

The issue concerning the concepts of space, time, motion and the existence, or not, of a real vacuum has accompanied the human knowledge all along [16]. The most distinct form of

http://dx.doi.org/10.5772/68113

representation about space and time has developed in the form of two dialectically opposite ideas, later known as the conceptions of Democritus-Newton and Aristotle-Leibniz. According to Democritus everything is formed of "atoms," each of them is considered indivisible. Between atoms, we have empty space. Philosophical views of Sir Isaac Newton were focused on the idea that all material bodies move in Absolute Space and Absolute Time. Such a philosophy is extremely convenient in the analysis of motion based on Newton's mechanics [17]. Huygens championed a different concept, according to which, the whole space is filled with a special substance, the ether [18]. In his view, each point in space was a virtual source of light waves. This implied the homogeneity of space, a feature which is important also in modern quantum field theory (QFT), where wave functions propagate along all available paths.

Exactly QFT has triggered the current concept of a not inert vacuum, seen as the scene of continuous, frantic physical events. What John Wheeler named quantum foam [19]. A sea of particle-antiparticle pairs which arise and annihilate according to Heisenberg's principle of uncertainty, in a vacuum where energy can't be always and surely zero. These pairs perform an endless dance by infinitely arising and annihilating. In Dirac's opinion, the new theory of electrodynamics, which implies a vacuum filled with virtual particles, forces us to take into account the existence of an ether. In 1951, he stated [20]: "If one examines the question in the light of present-day knowledge, one finds that the aether is no longer ruled out by relativity, and good reasons can now be advanced for postulating an aether." His new ether model was based on a stochastic covariant distribution of subquantum motion, which generates a vacuum dominated by fluctuations and randomness.

De Broglie stated that: "any particle, even isolated, has to be imagined as in continuous energetic contact with a hidden medium" [21]. The hydrodynamics of this medium could explain the outcome of the double slit experiment using electron beams, where the leptons interfere as waves, probably driven through the aether by pressure waves, generated by their motion, exactly as pressure waves forming the same patterns are involved in the case of sound propagating through a double slit. De Broglie-Bohm's pilot-waves could be then explained as aether waves, which guide the electrons and show analogies with Faraday waves guiding a bouncing droplet along a surface of silicon oil [22]. Petroni and Vigier stated that: "one can deduce the De Broglie waves as real collective Markov processes on the top of Dirac's aether" [23].

Robert Betts Laughlin, Nobel Laureate for the fractional quantum Hall effect, in his work [24], writes: "Studies with large particle accelerators have now led us to understand that space is more like a piece of window glass than ideal Newtonian emptiness. It is filled with "stuff" that is normally transparent but can be made visible by hitting it sufficiently hard to knock out a part. The modern concept of the vacuum of space, confirmed every day by experiment, is a relativistic ether. But we do not call it this because it is taboo." Laughlin also tells us that this false vacuum can be treated with the laws of fluid dynamics: "About the time relativity was becoming accepted, studies of radioactivity began showing that the empty space had spectroscopic structure similar to that of ordinary quantum solids and fluids."

In summary, it seems that any phenomenon occurring in quantum mechanics needs to interact with the vacuum, which consequently possesses a quantum physical structure, rather than

being real empty (zero-energy) space. Thus, a single unbound particle is always and anyway connected to its environment. We believe that this fact might also facilitate the explanation to quantum entanglement, in which quantum information would be transmitted from a particle to the other through, and thanks to, the quantum structure of space. Petroni and Vigier debate that: "the quantum potential associated with this ether's modification, by the presence of EPR photon pairs, yields a relativistic causal action at a distance which interprets the superluminal correlations recently established by Aspect et al." [23].

In our opinion, this is also the case of gravitational waves, for which the asserted space-time deformation could be actually interpreted as a negative pressure wave traveling through a superfluid quantum space (SQS) from the source up to a measuring point due to a mechanism that we call superfluid quantum gravity (SQG) [14], a quantum fluid dynamic explanation of gravity. In a few words, gravitational waves could be a hydrodynamic phenomenon in a SQS instead of a deformation of space. After all, it is unlikely that a deformation occurs in a non-solid substance. If space is not solid, we can then only observe fluid dynamic events, which can, indeed, fully replace and better justify any effect of SR and GR [14]. SQS also shares interesting analogies with Higgs field, being an ubiquitous fundamental scalar field with non-zero viscosity, which gives mass to particles. In our case, thanks to quantum fluid dynamic perturbations of the field, with formation of superfluid quantum vortices, akin to what happens in superfluid He-4.

This suggests to even reconsider the pre-existence of a quantum space (as quantized dark energy) even before the Big Bang. By assuming that what we know to be the ubiquitous dark energy is a quantum superfluid, it could exactly correspond to our idea of SQS in a state of rest. Since dark energy still pervades the cosmos, corresponding to 69.1% of its energy, thinking that the Big Bang has rather been a perturbation event occurred in a previously quiet sea of dark energy, seems to be reasonable. From then on, cascade perturbations at Planck scale would have generated any existing particle as superfluid vortices or as pulses. Since no fluid or superfluid has real zero-viscosity, vortex-particles could attract the surrounding quanta, causing gravity as a fluid dynamic phenomenon. If the attracted space's quanta were packed and re-emitted as virtual photons, stable particles could exist, and the link gravity-electromagnetism would be clear [2]. In such a view, quantum gravity is an apparent force which does not accelerate bodies by directly acting on them thanks to gravitons, they are rather dragged by the superfluid quantum space in which they are immersed that flows toward the site where greater absorption is exerted, i.e. toward the greater mass of a gravitational system, according to Newton's law of universal gravitation. Cahill came to a similar conclusion in 2003, describing gravity as an inflow of quantum foam [25], though we consider more likely absorption of quantized dark energy.

Compared to QFT's quantum vacuum, SQS would be at the lowest level (we believe that it is the very fundamental scalar field in nature) made up of dark energy's quanta, whose hydrodynamic perturbation produces the continuous fluctuations which allow the formation and annihilation of particle-antiparticle pairs. In addition, Bohm and Vigier, moving from Dirac's ether model, introduced in 1954 the idea of a sub-quantum medium, a hidden medium which all particles of the microphysical level constantly interact with [26]. The surface level of SQS, that is, the currently defined quantum foam or quantum vacuum, has to possess superfluid features as well and may act as a special Bose-Einstein condensate. The historical problem of vacuum's infinite energy is solved by the infinite extent of the SQS.

http://dx.doi.org/10.5772/68113

As far as the Michelson-Morley test run in 1887 is concerned, we could wonder whether light interacts with the SQS, if it really exists, that is, if light interacts with dark energy. That test hypothesized a static ether and took into account Earth's motion. However, if we change the premise, by supposing that the Earth absorbs the ether, since massive particles absorb dark energy, we deal with a radial ether wind, independent of Earth's motion through the space, an ether wind which transports any object pointing toward the center of the Earth. In the hypothesis of fluid quantum gravity, this vertical ether wind exactly corresponds to the gravitational field [14]. This view would explain all the relativistic effects due to curved space-time, for example, the gravitational lensing and the Lense-Thirring precession. The correspondence between ether wind and gravitational field seems to be confirmed in a test run in 2009 by Martin Grusenick, who used a vertically placed Michelson's interferometer [27]. Maxwell's idea of an electromagnetic ether should be then revisited since, if a SQS exists, light could be a mechanical wave which propagates through an ether and its speed would merely correspond to the speed of sound through that specific fluid medium (i.e. of a pulse through dark energy) analogously to the case of sound through the air and for any other mechanical wave. In the case of light, this pulse would spin[1] and its velocity would arise from SQS's parameters such as density and compressibility [2, 14]. In short, a photon would be a spinning phonon through superfluid dark energy, whose mechanical interaction with dark energy's quanta would excite them, producing the photon's electromagnetic field. By starting from the formula which indicates the speed of a mechanical wave through a fluid, $a = \sqrt{K/\rho}$, in which $K = V^{dP}/_{dV}$ is the bulk modulus, calculated by dividing the pressure increment, dP, by relative increment of the volume, dV/V, and ρ is the mass density and by putting $\beta_S = 1/K$ as isentropic compressibility, we have $a = 1/\sqrt{\beta_S \rho}$. If we consider $\beta_S = \beta_0$ as SQS's compressibility and ρ_0 as its mass density, we get

$$a = \frac{1}{\sqrt{\beta_0 \rho_0}}, \tag{1}$$

expressing the speed of a photon as a phonon through the SQS, mathematically analogous to

$$c = \frac{1}{\sqrt{\varepsilon_0 \mu_0}}, \tag{2}$$

as resulting from Maxwell's equations. The nonzero viscosity of the superfluid medium (SQS) would compel light to undergo redshift over very large distances: the more distant a galaxy the more stronger the observed redshift. This is fully compatible with Hubble's law, letting us doubt that an accelerated expansion of the Universe is really occurring.

3. Hydrodynamics of SQS

General relativity describes the Universe with a curved space-time metric due to presence of mass and energy. Observations show that the Universe, nevertheless, is flat at large distances

[1]Spinning sound waves have already been demonstrated [57], and thus, we can think of a photon as a spinning phonon through a superfluid medium.

and long times [28]. It means that the curvature tensor in the Einstein's field equations has to be omitted. In fact, as discussed below, we believe that what is supposed to be the curvature of space-time is rather a pressure force acting in a fluid, flat space, whose effect is compatible with that of general relativity's differential geometry. We come then to the general relativistic hydrodynamic equations [29, 30] containing the local conservation laws of the stress-energy tensor (the Bianchi identities) and of matter current density (the continuity equation) [5]:

$$\partial_\mu T^{\mu\nu} = 0, \tag{3}$$

$$\partial_\mu J^\mu = 0. \tag{4}$$

Here, ∂_μ is the covariant derivative associated with the four-dimensional space-time metric $\eta^{\mu\nu}$ having the signature $(-+++)$. The density current is given by $J^\mu = \rho_m u^\mu$, where u^μ is the fluid 4-velocity and ρ_m is the rest-mass density in a locally inertial reference frame:

$$\rho_m = m\rho = m\frac{N_B}{\Delta V} = \frac{M}{\Delta V}. \tag{5}$$

Here, ρ is the density distribution of N particles within the unit volume ΔV, where each of them has mass m. So, $M = mN_B$ represents the bulk mass of the fluid occupying this volume.

The stress-energy tensor, $T^{\mu\nu}$, is expressed in units of pressure, whereas we need it in units of energy. Indeed, we further adopt the expression $T^{\mu\nu}/\rho$ in order to have the possibility of getting the quantum potential $Q = P_Q/\rho$, where P_Q is the internal quantum pressure arising in SQS under influence of the external environment. We consider an incompressible, viscous fluid along with the gravitational potential φ. So, Eq. (3) reads [5]:

$$\partial_\mu\left(\frac{T^{\mu\nu}}{\rho}\right) = \partial_\mu\left(\frac{\varepsilon + p}{\rho}\gamma u^\mu u^\nu\right) + \partial^\nu Q - \partial^\nu\varphi + \partial_\mu\Big(\mu(t)/\rho\Big)\pi^{\mu\nu} = 0. \tag{6}$$

Here, ε and p are functions per unit volume. Divided by ρ, the sum $\varepsilon + p$ has the dimension of energy. The term $\mu(t)$ is the dynamic viscosity coefficient having the dimension of [N s/m^2]. Divided by ρm, this function represents the kinetic viscosity coefficient $\nu(t)$, having the dimension of [m^2/s]. In our case, viscosity is a fluctuating-about-zero function of time. We suppose that its expectation vanishes in time but the variance is not zero. That is, we suppose the following average quantities:

$$\langle\mu(\mathrm{t})\rangle = \varepsilon \to 0_+, \langle\mu(t)\mu(0)\rangle > 0. \tag{7}$$

Here, 0_+ is an arbitrarily close-to-zero positive value, which describes the energy exchange with the zero-point energy of the SQS. The term $\pi^{\mu\nu}$ reads:

$$\pi^{\mu\nu} = c(\partial^\mu u^\nu + \partial^\nu u^\mu) - c\frac{2}{3}\partial^\mu u_\mu \eta^{\mu\nu}. \tag{8}$$

In order to bring Eq. (6) to the relativistic Navier-Stokes equation, we shall repeat the computations of van Holten [31]. These calculations are reproduced also in Ref. [5].

http://dx.doi.org/10.5772/68113

We shall further consider only the non-relativistic limit, since the orbital speeds of galaxies and of many intergalactic bodies are predominantly much lower than the speed of light [32]. The factor γ in Eq. (6) is a sign of relativistic/non-relativistic limit. When it tends to infinity, we have the relativistic limit. In this case, also the mass m tends to infinity. On the other hand, when γ converges to unit, it denotes a non-relativistic limit. In this case, the mass m becomes the rest mass. For the sake of simplicity, we further take into account only shear viscosity. Given the quantum and granular nature of the SQS, a dilatant behavior under a linear, great increase of shear stress would be plausible and that would help to explain the upper limit to the acceleration of a body in the Universe [14]: The more acceleration is supplied the much more resistance is encountered, following Lorentz factor. In the non-relativistic limit, the viscosity term can be cut up to $\left(\mu(t)/\rho\right)\partial_i\partial^i c v^i \rightarrow \left(\mu(t)/\rho\right)\nabla^2\vec{v}$. As a result, we come to the following non-relativistic modified Navier-Stokes equation:

$$\rho_m \frac{d\vec{v}}{dt} = -\rho_m \nabla\varphi + \rho\nabla\Sigma Q + \mu(t)\nabla^2\vec{v}. \tag{9}$$

Here, ΣQ calculates the contributions of the quantum potential within SQS. The gravitational potential, φ, is a function coming from a continuous mass distribution ρ_m [33]. Gravity by itself described as an inflow of SQS obeys Gauss's law for gravity (gravity as an incoming flux), which in differential form is $(\nabla \cdot \vec{g}) = -4\pi G\rho_m$. In our view, the classical gravitational potential $\varphi = GM/r$ of the absorbing body, associated to the radial field in each point, that is, $\vec{g} = -\nabla\varphi$, can be interpreted [14] as a quantum potential expressed as the ratio of the pressure P_G of the incoming flux to mass density, ρ_m:

$$\varphi = -G\int_V \frac{\rho_m(\vec{r})}{r} dV = \frac{P_G}{\rho_m}. \tag{10}$$

Here, G is the Newtonian gravitational constant, and r is the distance from the volume element dV to a point in the field, and the integration is performed in the entire volume of the body, creating a field. We note that the gravitational constant in the rightmost part of Eq. (10) is absent, and we cleanly look at gravity as a quantum phenomenon driven by the ratio pressure/density. The continuous mass distribution $\rho_m(\vec{r})$ can be expressed using the Laplace operator, Δ:

$$\rho_m(\vec{r}) = \frac{1}{4\pi G}\Delta\varphi. \tag{11}$$

We note that the mass density, in addition, submits to the continuity equation

$$\frac{\partial\rho_m}{\partial t} + (\nabla \cdot \vec{v})\rho_m = 0. \tag{12}$$

We can express from Eqs. (10) and (11) the gravitational pressure P_G as a function of the gravitational potential φ:

$$P_G = \frac{\varphi \cdot \Delta\varphi}{4\pi G} = \frac{\varphi^2}{4\pi G}((\nabla \ln\varphi)^2 + \nabla^2 \ln\varphi). \tag{13}$$

We now see that in Eq. (9) two opposite quantum potentials act:

$$\rho_m \frac{d\vec{v}}{dt} = -\rho_m \nabla\left(\frac{P_G}{\rho_m}\right) + \rho\nabla\Sigma\left(\frac{P_Q}{\rho}\right) + \mu(t)\nabla^2\vec{v} \tag{14}$$

The Navier-Stokes equation is written above in the modified form [34]. The modification is due to (a) presence of the quantum potentials $Q = P_Q/\rho$ and $Q_\varphi = M\varphi = MP_G/\rho_m = P_G/\rho$ (M is the mass of Universe, about 10^{53} kg) and (b) existence of the dynamic viscosity coefficient $\mu(t)$ that fluctuates about zero. In other words, we accept that there is an energy exchange between baryon matter and the SQS. The pair of Eqs. (12) and (14) represents a full set of equations, sufficient for describing the motion of baryon matter through SQS in the non-relativistic limit of the Euclidean geometry.

Referring to Eq. (14), we believe that baryon matter is reciprocally attracted due to the gravitational quantum potential $Q_\varphi = P_G/\rho$ that we suppose justified by a hydrodynamic interaction occurring between SQS and baryon matter (attraction of dark energy's quanta toward vortex-particles, causing decrease of pressure and a consequent apparent attractive force [14]). On the contrary, the quantum potential $Q = P_Q/\rho$ existing in SQS causes reciprocal repulsion of the baryon matter on large distance.

By omitting from consideration the viscous term in Eq. (14), we assume $\mu = 0$ and we obtain Newton's second law describing variations of the acceleration $\vec{a} = d\vec{v}/dt$ under the action of the two opposite quantum forces described above, ∇Q_φ and $\nabla\Sigma Q$:

$$\begin{aligned}\rho_m \frac{d\vec{v}}{dt} &= -\rho_m \nabla\left(\frac{P_G}{\rho_m}\right) + \rho\nabla\Sigma\left(\frac{P_Q}{\rho}\right) = -\rho\nabla Q_\varphi + \rho\nabla\Sigma Q \\ &= -\nabla P_G + \nabla P_Q + \Big(P_G\nabla\ln(\rho) - P_Q\nabla\ln(\rho)\Big) = f_{QG}.\end{aligned} \tag{15}$$

We generally consider the volume of the whole visible Universe, $\Delta V \to V$, so the rest mass density $\rho_m = mN_B/V = M/V$, where $M = mN_B$ is the total mass of the Universe (about 10^{53} kg). Here, f_{GQ} is the force density. It arises from the superposition of two forces within the considered volume, which are expressed through the gradient of the gravitational potential and that of the intrinsic quantum potential of SQS. They are represented by a negative pressure gradient around baryonic bodies, ∇P_G (Superfluid Quantum Gravity) [14], and the quantum pressure gradient acting on SQS, ∇P_Q.

The acceleration, $\vec{a} = d\vec{v}/dt$, vanishes if both potentials, Q_φ and Q, are uniformly distributed across the space. The uniformity of the potentials can be justified according to the reports of the Planck Observatory [28]. So that $\mathcal{E} = -Q_\varphi/m + \Sigma Q/m$ reads

$$\mathcal{E} = G\int_V \frac{\rho_m(\vec{r})}{r}dV + N_D D^2\left(\frac{\nabla^2\rho_m}{\rho_m} - \frac{1}{2}\frac{(\nabla\rho_m)^2}{\rho_m^2}\right). \tag{16}$$

http://dx.doi.org/10.5772/68113

It should be constant at least within the visible Universe. The first term follows from Eq. (10) that is $\varphi = P_G/\rho_m = Q_\varphi/M$ and the second term is the intrinsic quantum potential of SQS [5, 34] divided by mass. The integer multiplier N_D is equal to the sum of all the quantum potentials, which arise from the contribution of all dark energy and dark matter in SQS. This value is calculated from the fact that about 95% of mass-energy in the Universe accounts for this dark fluid, respectively, 69.1% dark energy and 25.9% dark matter. So, from here, we find $N_D = 95/(100-95)\cdot N_B = 19\cdot M/m$.The number $N_B = M/m$ follows from Eq. (5).

As for the mass density distribution ρ_m under the integral, we permit the existence of a static spherically symmetric Gaussian density of baryon matter

$$\rho_m(r) = \frac{M}{(\sigma\sqrt{2\pi})^3}\exp\left\{-\frac{r^2}{2\sigma^2}\right\}. \tag{17}$$

By accepting this result, Eq. (16) gives the following solution:

$$\varepsilon = \frac{GM}{r}\mathrm{erf}\left\{\frac{r}{\sigma\sqrt{2}}\right\} + N_D D^2\left(\frac{r^2}{2\sigma^4} - \frac{1}{\sigma^2}\right) \tag{18}$$

The expression of ε reduced to dimensionless form by multiplying by c^{-2} (c is the speed of light) is shown as a function of r in **Figure 1**. We see that there is a *flat potential plateau* of baryon matter ranging in the radius of the visible Universe $r < \sigma \approx 4.5\cdot 10^{26}\mathrm{m} \approx 14.6$ Gpc. The negative pressure arising among the baryon bodies determines the attraction.

On the other hand, the repulsion is due to the quantum vacuum fluctuations in SQS. This repulsion is conditioned by the quantum potential Q represented by the second term In Eq. (18). In this case, the diffusion coefficient D reads

$$D = \frac{\hbar}{2m} \tag{19}$$

In the case of the proton mass, m, that is, about $1.67\cdot 10^{-27}$kg, we have $D \approx 4.6\cdot 10^{-8}\mathrm{m}^2\cdot\mathrm{s}^{-1}$. The term $N_D D^2$ in Eq. (18), however, reaches the enormous value of about $10^{65}\mathrm{m}^4\cdot\mathrm{s}^{-2}$.

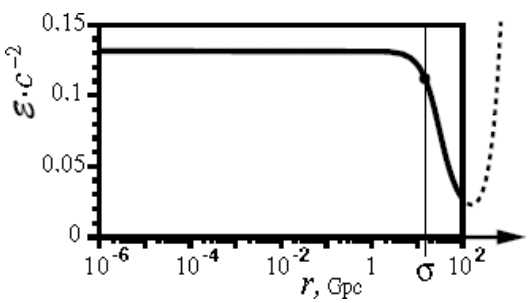

Figure 1. Function ε reduced to dimensionless form by multiplying by c^{-2} (c is the speed of light) as a function of r, where σ is the radius of the visible Universe. A flat plateau ranging from 0 to about 10 Gpc tells us that the expansion of the Universe is almost absent. Dotted curve outside the chart shows divergence due to the quadratic term $r^2/2\sigma^4$ in the quantum potential.

Therefore, the quantum potential outside the visible horizon gives divergence because of the quadratic term $r^2/2\sigma^4$ in its representation. In **Figure 1**, this divergence is shown by a dotted curve.

3.1. Viscosity of SQS: tired-light and the Pioneer anomaly

Let us return to the relativistic hydrodynamic equation [5] by considering the Klein-Gordon equation, loaded by the viscosity term. The kinetic energy of a relativistic particle, in this case, can be written as follows:

$$E = E_0 - 2m\nu(t)\frac{d\ln(\rho_m)}{dt} = E_0 - E_0\frac{2}{c^2}\nu(t)\frac{d\ln(\rho_m)}{dt}. \tag{20}$$

Here, $\nu(t) = \mu(t)/\rho_m$ is the kinematic viscosity coefficient. Its dimension is $\mathrm{m}^2 \cdot \mathrm{s}^{-1}$. The second term here describes energy exchange with vacuum fluctuations during a particle's motion through SQS. Here, we took into account that $E_0 = mc^2$. By adopting $E_0 = \hbar\omega_0$, we can write a suitable wave function for a photon coming from a distant source:

$$\Psi(t) = \exp\left\{-i\omega_0 t\left(1 - \frac{2}{t}\int_0^t \frac{\nu(\tau)}{c^2}\frac{d\ln(\rho_m)}{dt}d\tau\right)\right\}. \tag{21}$$

We let the integral under the exponent be linked with the expanded Hubble parameter H_Λ, as follows:

$$H_\Lambda = \frac{2}{t^2}\int_0^t \frac{\nu(\tau)}{c^2}\frac{d\ln(\rho_m)}{dt}d\tau = \frac{\dot{a}}{a} = \sqrt{\frac{8\pi G\rho_m}{3} - k\frac{c^2}{a^2} + \Lambda\frac{c^2}{3}}. \tag{22}$$

The rightmost terms under root in (22) result from the first Friedmann equation. Here, Λ is the cosmological constant (which refers to dark energy, i.e., to the SQS itself, being $\Lambda = \kappa\rho_{sqs}$, where $\kappa = (8\pi G)/c^2$ is Einstein's constant), a the dimensionless scale factor, and k its Gaussian curvature. We further consider the case of a flat Universe, $k = 0$:

$$H_\Lambda = \sqrt{H_0^2 + \frac{\Lambda c^2}{3}}, \qquad H_0 = \sqrt{\frac{8\pi G\rho_m}{3}}. \tag{23}$$

Being Λ omitted, the parameter H_Λ degenerates to H_0. We may evaluate H_0 at the known critical density $\rho_c = \rho_m \approx 10^{-26}$ kg·m^{-3} and knowing G [33]. We find $H_0 \approx 2.36 \cdot 10^{-18}\mathrm{s}^{-1}$ in SI unit, while, in units adopted in astrophysics, it is about 73 km $\cdot$ Mpc$^{-1} \cdot$ s^{-1}. H_0 fits well within the confidence interval estimated by Friedmann and others in [35] (see **Figure 2**).

We know that, to justify a ratio of the actual density to the critical density corresponding to a flat Universe, that is, $\Omega = \rho_m/\rho_c = 1$, we have to solve the flatness problem ($|\Omega - 1| < 10^{-62}$ at the Planck era [36]). Its solution, as well known, is given by the theory of cosmic inflation, to

http://dx.doi.org/10.5772/68113

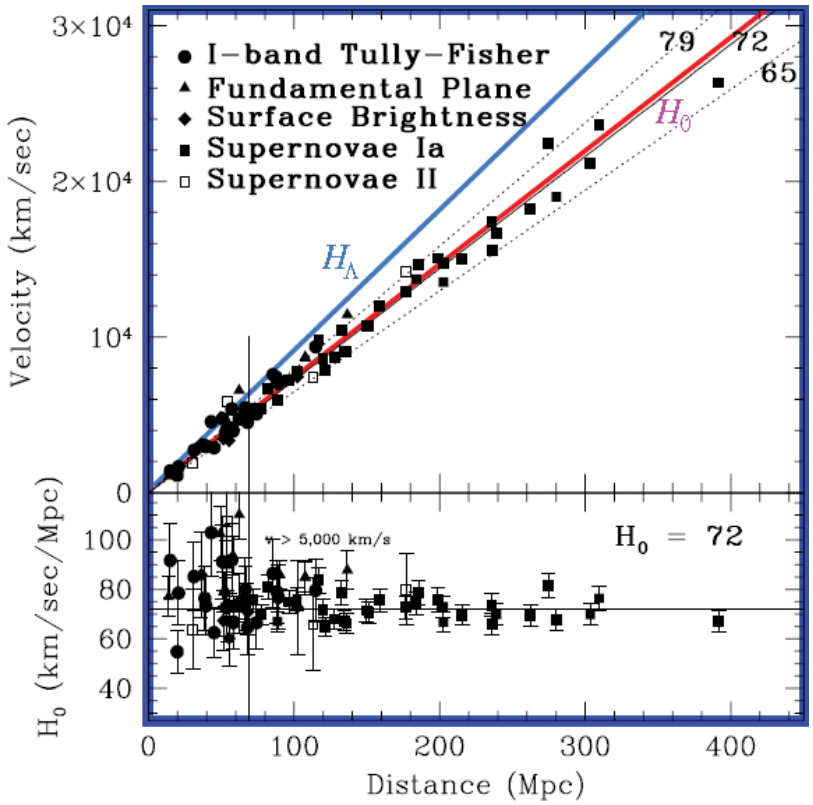

Figure 2. A Hubble diagram of distance versus velocity for secondary distance indicators, calibrated to Cepheids. Figure is taken from Ref. [35] and modified by adding the parameter H_Λ. Note that H0 belongs to the confidence interval, whereas H_Λ lies beyond it.

which many of the scientific community resort also to solve the magnetic-monopole problem and the homogeneity problem. In accordance with what above, we believe that no accelerating Universe exists, and consequently, the Doppler effect does not influence the observed redshift. We identify the cause of the redshift in the phenomenon of tired light, which in our case is due to the weak viscosity of SQS that leads to Eq. (21). The frequency ω shifted with respect to the initial frequency ω_0 after the time t will be [37]:

$$\omega = \omega_0 e^{-H_0 t} \tag{24}$$

Cosmic inflation appears to us as a *deus ex machina*, which could actually hide the effect of viscosity on photons traveling through the SQS. As follows from Eq. (22), tired light occurs due to the existence of a tiny viscosity of SQS, in which photons are subject to by traveling through the cosmos. Fluctuations of the space-time metric (fluid dynamic fluctuations of dark energy, in our case) at the Planck scale [38] give a crucial contribution to the viscosity effect.

From Eq. (22), we can evaluate $H_\Lambda \approx 2.93 \cdot 10^{-18} \mathrm{s}^{-1}$ (about 90 km $\cdot$ Mpc$^{-1} \cdot$ s^{-1}) at the adopted value of $\Lambda = 10^{-52} m^{-2}$. We observe that this parameter lies far outside the confidence interval,

marked in **Figure 2**. It means that the parameter H_Λ, most possibly, plays another role different from the Hubble constant H_0. Let us compute the acceleration of an object, $\vec{a} = d\vec{v}/dt$ traveling through the Universe. It can be found from Eq. (9), by setting $\nabla(m\varphi + \Sigma Q) = 0$:

$$\vec{a} = \nu(t)\nabla^2\vec{v} = -\nu(t)\nabla(d\ln(\rho_m)/dt). \tag{25}$$

The term $\nabla\vec{v} = -d\ln(\rho_m)/dt$ comes from the continuity Eq. (12). Now, by multiplying Eq. (22) by $t^2/2$ and differentiating it with respect to t, we gain:

$$\frac{\nu(t)}{c^2}\frac{d\ln(\rho_m)}{dt} = \frac{1}{2}\frac{d}{dt}t^2\sqrt{\frac{8\pi G\rho_m}{3} + \Lambda\frac{c^2}{3}} = tH_\Lambda + \frac{t^2}{4H_\Lambda}\left(\frac{8\pi G\rho_m}{3}\right)\frac{d\ln(\rho_m)}{dt}. \tag{26}$$

Then, by multiplying by c^2 and by applying the operator ∇, we get

$$a = -\frac{d}{d\ell}tc^2H_\Lambda - \frac{d}{d\ell}\frac{t^2c^2}{4H_\Lambda}(H_0^2)\frac{d\ln(\rho_m)}{dt}. \tag{27}$$

Here, the operator $\nabla = d/d\ell$ calculates a gradient along the increment $d\ell$. Let us suppose that $d\ell/dt$ represents an updated rate for the cosmic microwave background (CMB) fluctuations at the frequency $\Omega_{CMB} = \omega_0$, that is, the speed of light $d\ell/dt = \lambda_{\mathrm{CMB}}\Omega_{\mathrm{CMB}} = c$. By substituting c into Eq. (27) instead of $d\ell/dt$, we get:

$$a = -H_\Lambda c\left(1 + \frac{H_0^2}{H_\Lambda^2}\cdot\left(\frac{1}{4}\frac{t}{\rho_m}\frac{d\rho_m}{dt}\right)\right). \tag{28}$$

We observe that the first term, $H_\Lambda c$, is equal to $8.785\cdot10^{-10}\mathrm{m}\cdot\mathrm{s}^{-2}$. This indicates a good agreement with the acceleration $a_P = (8.74\ \pm 1.33)\cdot10^{-10}\mathrm{m}\cdot\mathrm{s}^{-2}$ which became known as the Pioneer anomaly [39–41]. From this, we have the fact that the term in second brackets vanishes, namely, $d\rho_m/dt = 0$, as follows from the continuity Eq. (12). It means that $\rho_m = \rho_c = const.$ Eq. (28) suggests that the Pioneer anomaly is due to the presence of non-zero energy density (dark energy) of the vacuum, as reflected in the cosmological constant $\Lambda \approx 10^{-52}\mathrm{m}^{-2}$ in metric units.

The Hubble parameters, H_0 and H_Λ, concern different manifestations of SQS. The first parameter is due to presence of the tiny non-zero, positive viscosity of the SQS, whereby light undergoes loss of energy (redshift) proportional to the traveled distance. The Hubble diagram in **Figure 2** shows in fact the relationship with distance expressed by our hypothesis, in which the role of the recessional velocity in causing the cosmological redshift has to be however substituted by that of energy dissipation. Since in our analysis (see Ch.2 and [14]) photons are phonons through the SQS, i.e. waves carrying a momentum, in agreement with the concept of photon, they lose energy while traveling huge distances, as no superfluid has perfectly zero viscosity.

As for the parameter $H_{\Lambda,}$ it results from the trigonometric shear of the Hubble parameter H_0 by adding the contribution of the cosmological constant Λ, see Eq. (23). The calculated acceleration (28), excellently close to the acceleration a_P of the Pioneer apparatus, is due to the contribution of the SQS (i.e., of dark energy and of its hydrodynamic perturbations) expressed by the

cosmological constant [42, 43]. Indeed, we know that the relationship between Λ and the energy density of free space is $\Lambda = \kappa\rho_0$, where $\kappa = 8\pi G c^{-2}$ is Einstein's constant and ρ_0 is vacuum's (i.e., SQS's) energy density. Thus, by considering the SQS as a ubiquitous sea of quantized, perturbed dark energy, partially condensed as dark matter (25.9%), we see that its mass is $m_{darkenergy} = \rho_0(t)V(t) = E_{darkenergy}c^{-2} = \beta_0\rho_0 E_{darkenergy}$. Where $V(t)$ is the volume of the Universe at an instant t (even in an expanding/shrinking Universe, we have $\rho_0 V = const$, so at any moment dark energy is neither created nor annihilated) and $c^{-2} = \beta_0\rho_0$ from Eq. (1), where β_0 and ρ_0 are physical parameters of dark energy, responsible for a small non-zero, positive viscosity of free space and, consequently, for the investigated anomalous deceleration.

4. Vorticity equation and solutions for orbital speeds of spiral galaxies

The modified Navier-Stokes Eqs. (9) and (14) can exhibit a manifestation of long-lived vortices in SQS. The last term in this equation is dissipative due to the presence of a weak viscosity of the medium fluctuating about zero. If the viscosity coefficient μ is a fluctuating function of time, we can assume (see Eq. (7)) that (a) time-averaged, the viscosity coefficient vanishes; (b) its variance is not zero. Therefore, the viscosity coefficient is a function fluctuating about zero. We suppose that such fluctuations determine energy exchange between the existing baryon matter and the zero-point fluctuations of the superfluid physical vacuum [44].

Note first that the total derivative of $\vec{v}$ with respect to t in the Navier-Stokes equation (9), rewritten through the partial derivatives reads:

$$\frac{d\vec{v}}{dt} = \frac{\partial\vec{v}}{\partial t} + (\vec{v}\cdot\nabla)\vec{v}. \tag{29}$$

Let us apply now the curl operator to the Navier-Stokes equation. We come to the equation for vorticity $\vec{\omega} = [\nabla \times \vec{v}]$ [45]:

$$\frac{\partial\vec{\omega}}{\partial t} + (\vec{v}\cdot\nabla)\vec{\omega} = \nu(t)\nabla^2\vec{\omega}. \tag{30}$$

Here, $\nu(t) = \mu(t)/\rho_m$ is the kinematic viscosity coefficient. The vector $\vec{\omega}$ is directed along the rotation axis. In order to simplify this task, let us move to the coordinate system in which the rotation occurs in the plane (x, y) and the z-axis lies along the vorticity, **Figure 3**.

Under this transformation, the vorticity equation takes a particularly simple form:

$$\frac{\partial\omega}{\partial t} = \nu(t)\left(\frac{\partial^2\omega}{\partial r^2} + \frac{1}{r}\frac{\partial\omega}{\partial r}\right). \tag{31}$$

A general solution of this equation has the following view [5, 46]:

$$\omega(r,t) = \frac{\Gamma}{4\Sigma(\nu,t,\sigma)}\exp\left\{-\frac{r^2}{4\Sigma(\nu,t,\sigma)}\right\}, \tag{32}$$

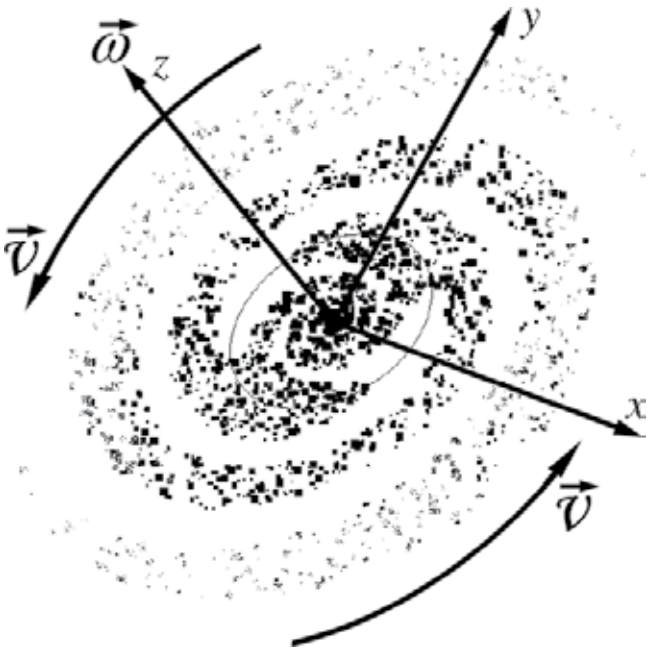

Figure 3. A simulation of a rotating spiral galaxy: the orbital velocity $\vec{v}$ lies in the plane (x, y). The vorticity vector $\vec{\omega}$ is oriented perpendicular to this plane.

$$v(r,t) = \frac{1}{r}\int_0^r \omega(r',t)r'dr' = \frac{\Gamma}{2r}\left(1 - \exp\left\{-\frac{r^2}{4\Sigma(\nu,t,\sigma)}\right\}\right). \tag{33}$$

The first function is vorticity; the second is the orbital speed. We do not mark the arrows above the letters ν and ω since the orbital velocity lies in the (x, y) plane and vorticity lies on z-axis. The denominator $\Sigma(\nu, t, \sigma)$ in these formulas reads:

$$\Sigma(\nu,t,\sigma) = \int_0^t \nu(\tau)d\tau + \sigma^2. \tag{34}$$

Here, σ is an arbitrary constant such that the denominator is always positive.

Taking into account $\langle \nu(t) \rangle = 0_+$, see Eq. (7), we can see that the integral in Eq. (34) tends to zero and solutions of (32) and (33) in the limit of $t \to \infty$ reduce to

$$\omega_{Gcvc}(r,t) = \frac{\Gamma}{4\sigma^2}\exp\left\{-\frac{r^2}{4\sigma^2}\right\}, \tag{35}$$

$$v_{Gcvc}(r,t) = \frac{\Gamma}{2r}\left(1 - \exp\left\{-\frac{r^2}{4\sigma^2}\right\}\right). \tag{36}$$

http://dx.doi.org/10.5772/68113

That is, vorticity and angular speed are permanent in time. Here, the circulation Γ and the average radius σ are initially existing. The extra parameter σ comes from the Gaussian coherent vortex cloud [47]. The subscript G_{cvc} indicates the *Gaussian coherent vortex cloud*. The vortex cloud represents localized concentration of vorticity energy with a lifetime tending to infinity [48]. It does not significantly interact with any form of matter and exists in itself as long as possible.

4.1. Flat profile of the orbital speed (evaluations)

Solution (36) gives no flat profile. The function monotonically decreases with $r \to \infty$. This velocity is shown by curve 1 in **Figure 4**.

Let us begin to search for a solution of Eq. (31) by perturbing the solution (32) through a function $g(r)$ not equal to one, that is, $\omega(r, t) \cdot g(r)$. When we substitute this function into Eq. (31), we get:

$$g\frac{\partial\omega}{\partial t} = g\nu(t)\left(\frac{\partial^2\omega}{\partial r^2} + \frac{1}{r}\frac{\partial\omega}{\partial r}\right) + \nu(t)\left(\omega\frac{\partial^2 g}{\partial r^2} + \left(2\frac{\partial\omega}{\partial r} + \frac{1}{r}\omega\right)\frac{\partial g}{\partial r}\right). \tag{37}$$

Here, we obtain two independent differential equations. The first one is for the function $\omega(r, t)$. We return to the same solution (32). While the second equation for the function $g(r)$ becomes equal to zero. In this case, we introduce an auxiliary function $\varphi = \partial g/\partial r$ for which this equation takes the form:

$$\frac{\partial\varphi}{\partial r} + \left(\frac{2}{\omega}\frac{\partial\omega}{\partial r} + \frac{1}{r}\right)\varphi = \frac{\partial\varphi}{\partial r} + \left(-\frac{r}{\Sigma} + \frac{1}{r}\right)\varphi = 0. \tag{38}$$

In the second part instead of $(2/\omega) \cdot \partial\omega/\partial r$, we put its solution $-r/\Sigma$. For the sake of simplicity, we write Σ instead of $\Sigma(\nu, t, \sigma)$. The function $g(r)$ stemming from the solution of Eq. (38) reads:

$$g(r) = \int_0^r \frac{1}{\xi}\exp\left\{\frac{\xi^2}{2\Sigma}\right\}d\xi. \tag{39}$$

Next, we find the orbital speed

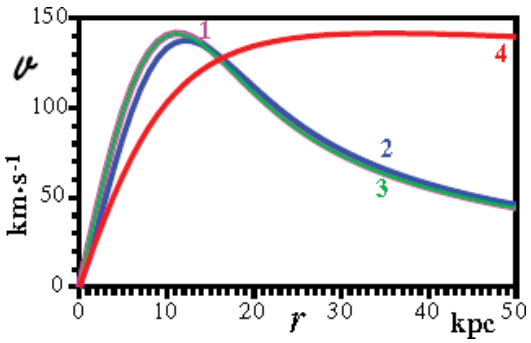

Figure 4. (1, 2, 3) are monotonically decreasing profiles with $r \to \infty$; 4 is an example of flat profile for large *r*, but when *r* tends to infinity, the curve vanishes.

$$v'(r,t)=\frac{1}{r}\int_0^r \omega(r',t)\cdot g(r')\cdot r'dr'. \tag{40}$$

This speed is shown as curve 2 in **Figure 4**. We have to observe, however, that the weight function $g(r)$ can be approximated by the continued fraction [49]

$$E_1(x)=\cfrac{e^{-x}}{x+\cfrac{1}{1+\cfrac{1}{x+\cfrac{2}{1+\cfrac{2}{x+\cfrac{3}{1+\cfrac{3}{x+\cfrac{4}{1+\cfrac{4}{\cdots}}}}}}}}}}. \tag{41}$$

In this way, we find an approximated function of the orbital speed

$$v''(r,t)=\frac{1}{r}\int_0^r \omega(r',t)\cdot E_1\left(\frac{r'}{2\Sigma}\right)\cdot r'dr'. \tag{42}$$

This speed is shown as curve 3 in **Figure 4**. One can see that all curves, 1, 2, and 3, accurate to the scaling, show good accordance with each other.

As for the curve 4 in this figure, it follows from the function

$$v'''(r,t)=\frac{\Gamma}{r}\sum_{n=1}^{N}\frac{1}{4\sigma_n^2}\int_0^r E_1\left(\left(\frac{r'}{2\sigma_n}\right)^2\right)\cdot r'dr'. \tag{43}$$

This function is drawn with linear growth of σ_n when n goes on, $\sigma_n=10\cdot n$. For n large enough, it shows a good outcome for the flat profile at $r\gg 1$.

4.2. Flat profile of the orbital speed (a general case)

A rich gallery of galactic rotation curves showing output on a flat profile is presented in [50].

These flat profiles of the orbital speeds are here rearranged, and they are shown in **Figure 5**. The curves draw approximations of these profiles.

Equation (43) gives a hint for getting flat profiles of orbital speeds, which are typical for spiral galaxies. In this section, we present formulas which show the formation of flat profiles evolving in time. First, we hypothesize that the above-mentioned Gaussian coherent vortex clouds (see Eqs. (35) and (36)) have a long-term memory, and they can therefore manifest themselves as dark matter. As shown in **Figure 4** by the curve 4, the clouds can support flat profiles for a long time through their superposition (see Eq. (43)). For the sake of demonstration, let us set [46]

http://dx.doi.org/10.5772/68113

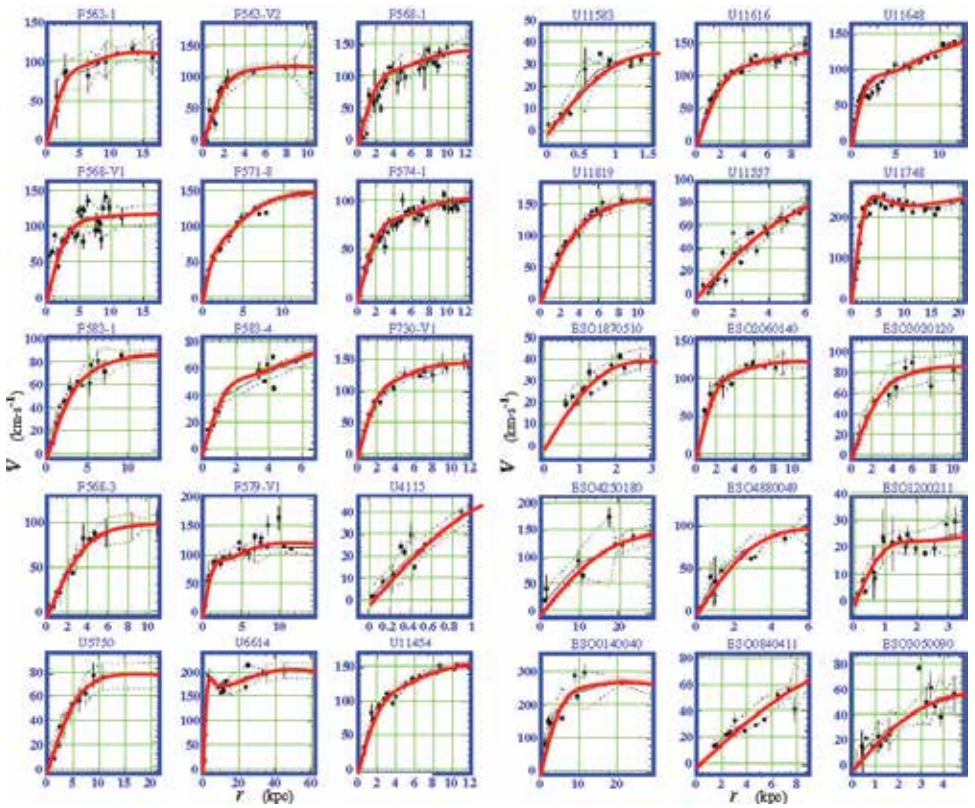

Figure 5. Families F#, U#, and ESO# of the flat profiles of the orbital speeds taken from [50]. The curves approximate these profiles marked by the black points.

$$v(t) = v\frac{e^{i\Omega t} + e^{-t\Omega t}}{2} = v\cos(\Omega t). \tag{44}$$

In this case $\Sigma(v, t, \sigma) = (v/\Omega)\sin(\Omega t) + \sigma^2 = (v/\Omega)\Big(\sin(\Omega t) + \zeta\Big), \sigma^2 = (v/\Omega)\cdot\zeta$ and $\zeta > 1$. Note first that the Gaussian coherent vortex clouds show self-similarity.

From this view, let us assume that the fluctuating viscosity reads as follows [5]:

$$\nu_n(t) = \frac{c^2}{\Omega_n}\cos(\Omega_n t). \tag{45}$$

The kinetic viscosity coefficient c^2/Ω_n has dimension [$m^2{\cdot}s^{-1}$]. Here, c is the speed of light, and Ω_n is the angular frequency of a vacuum oscillation. That is, there is a periodic exchange of energy $\hbar\Omega_n = n^{-1}$ with SQS. The energy tends to zero at n going to infinity, whereas the viscosity goes to infinity. It can mean that SQS acquires a high viscosity on very small frequencies of the vortex energy exchange. Note, however, that $\langle\nu_n(t)\rangle = 0_+$ for any n.

Let us compute the flat profile for the orbital speed of a spiral galaxy guided by the rule formulated above. To see its formation, we perform computations of sets collected from modes

(45), $n = 1,\ 2, \cdots, N$. Let us substitute the expression (45) into the integral (34). After computing it, we get the following view of the denominator $\Sigma(v, t, \sigma)$:

$$\Sigma_n(t) = \frac{c^2}{\Omega_n^2}\Big(\sin(\Omega_n t) + \zeta\Big). \tag{46}$$

Since $\Omega_n = n^{-1}$, the coefficient $\Sigma_n = c^2/\Omega_n^2$ tends to infinity as Ω_n goes to zero while n increases. From here, it follows that the expression $1 - \exp\{-r^2/4\Sigma_n\}$ in Eq. (33) reaches 1 the more slowly with increasing r, the larger is Σ_n. As a result, the set of coefficients Σ_n for $n = 1, 2, \cdots$ can give output to the flat profile of the orbital speed. Let us, therefore, compute a sum of possible orbital speeds of galaxies for all entangled modes for which baryon matter is allowed to exchange energy with the SQS. Our statistical sum reads as follows:

$$V(r, t) = \frac{\Gamma}{2r}\sum_{n=1}^{N}\left(1 - \exp\left\{-\frac{r^2}{4\Sigma_n(t)}\right\}\right). \tag{47}$$

The orbital speed $V(r, t)$ versus r and t is shown in **Figure 6**. Here, for the evaluated calculations, we used $\Gamma = 3 \cdot 10^{25}\text{m}^2 \cdot \text{s}^{-1}$ and the angular frequency Ω_n ranges from 10^{-11} s^{-1} to $1.667^{\circ}10^{-13}$ s^{-1} as n runs from 1 to 60. The angular frequencies are extremely small, while the wavelengths, $\lambda_n = c/\Omega_n$, are in the range from 0.97 to 58.3 kpc. These oscillating modes cover areas from the galactic core up to the size of the galaxy itself.

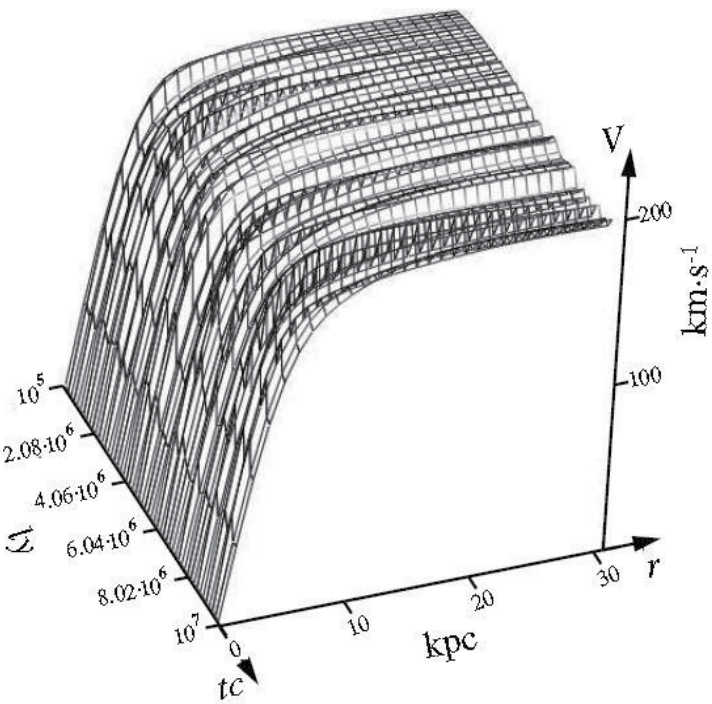

Figure 6. Orbital speed V is a function of the radius r from the galactic center (in kiloparsec) and time t (in light years). Variations of the orbital speed in time are evident.

http://dx.doi.org/10.5772/68113

Figure 6 shows that the orbital speed experiences small fluctuations in time, resembling the breathing of the galaxy. This trembling of galaxies within the $1/f$ spectrum is caused by the exchange of vortex energy with the SQS on the ultra-low frequencies Ω_n.

De Broglie wavelength, $\lambda_n = c/\Omega_n$, by changing in the range from about 20 kpc to 2 Mpc covers all galactic scales. One can evaluate the mass of axion-like particles [51],

$$m = \frac{\hbar\Omega_n}{c^2}. \tag{48}$$

It ranges from about 10^{-62} kg to $5^{\circ}10^{-66}$ kg. They are in the range shown in Ref. [52]. These particles may correspond to dark energy's quanta and be responsible for exchange phenomena among baryon objects in the frequency range from $\Omega_n = 10^{-11}\mathrm{s}^{-1}$ to $\Omega_n \approx 5 \cdot 10^{-15}\mathrm{s}^{-1}$. We note that the frequency Ω_c is $2.2 \cdot 10^{-18}\mathrm{s}^{-1}$. We obtain $c/\Omega_c \approx 1.36 \cdot 10^{26}$m, which is close enough to the Compton wavelength evaluated for the visible Universe in [53]. This corresponds to the radius of the Hubble sphere $r_{HS} = c/H_0$, which is about $4 \cdot 10^3$Mpc (at the Hubble constant $H_0 = 73\ \mathrm{km} \cdot (\mathrm{s} \cdot \mathrm{Mpc})^{-1}$). On these cosmological scales, we can evaluate the mass of a graviton (or more likely of a quantum of dark energy, since we don't need gravitons in superfluid quantum gravity [2, 14]), by resorting to a wavelength that is commensurable with the radius of the Universe stated above. An extreme mass of the axion-like particle for the observable Universe is $m_g = \hbar\Omega/c^2 \approx 2.6 \cdot 10^{-69}$ kg. This value finds a good agreement with the evaluation that comes from the holographic screen model to be the boundary of the visible Universe [52]. This evaluation is also in agreement with the graviton mass given in Ref. [54], here interpreted as a quantum of dark energy. We finally add that ultra-light dark matter particles produced in the vacuum have been predicted in Ref. [10].

We can continue the calculation of the orbital speed (44) up to the point $\Omega_c = 2.2 \cdot 10^{-18}\mathrm{s}^{-1}$. This would allow us to affirm that the observable Universe rotates about some center with an orbital speed, which has a flat profile through enormous distances. Excepting a central region where the orbital speed grows from zero to the maximal value corresponding to the profile level. This rotation possibly takes place around the richest Super Cluster in the Sloan Great Wall, SCl~126, and especially around its core, resembling a very rich filament [55].

5. Conclusion

We have shown that the fluid dynamics of SQS could explain the astrophysical observations without resorting to far-fetched auxiliary concepts, such as cosmic inflation and accelerated expansion.

In general, the fluid dynamics of SQS is described by the conservation equations of energy, momentum, orbital momentum, etc. In the non-relativistic limit, these equations are reduced to the modified Navier-Stokes equation and to the continuity equation of mass density. The modification leads to the emergence of a quantum potential, $Q(t)$, and reduces the viscosity coefficient, $\mu(t)$, to a weak term fluctuating about zero, $\langle\mu(t)\rangle = 0_+$, $\langle\mu(t)\mu(0)\rangle > 0$. Because

of that, this term acquires an absolutely different physical meaning. Firstly, an active exchange of energy between cosmological structures and SQS takes place and extends their lifetime.

We applied the modified Navier-Stokes equation to describe a balance within the visible Universe between the gravitational potential, φ, expressed as the quantum potential $Q_\varphi = P_G/\rho_m$ and the intrinsic quantum potential, Q, of SQS. Outside this range, strong repelling forces act (see dotted curve in **Figure 1**), probably due to osmotic expansion of dark energy in a really empty space. Figuratively speaking, baryon matter in the Universe is similar to a hydrophobic droplet floating in a hydrophilic medium filling the vast space. However, there is a difference between a "droplet model" and the Universe, since the latter consists of numerous clumps of baryonic matter separated by vast voids. These baryonic clumps are concentrated on vortex filaments that permeate the whole Universe and form an intricate cosmic web [56] with galaxies strung on these filaments.

Since $\langle \mu(t) \rangle = 0_+$ (it differs from zero to a tiny value), light coming from distant stars shows a frequency shift due to a loss of energy when traveling through the SQS. We therefore introduce an updated concept of tired light without resorting to Compton scattering and overcoming in this way the known objections to the classical concept of tired light.

The Pioneer anomaly has a lot in common with the revised tired light effect. The same loss of energy due to motion through the SQS most likely led to a deceleration of the space apparatus. An essential contribution to the deceleration comes from a non-zero small correction of the Hubble parameter thanks to the cosmological constant, which refers to dark energy, i.e., to SQS itself). This correction gives a value of the negative acceleration of the cosmic apparatus $a = -H_\Lambda c = -c\sqrt{H_0^2 + \Lambda c^2/3} \approx -8.785 \cdot 10^{-10} \mathrm{m \cdot s^{-2}}$, which acceptably falls within the measured anomalous acceleration of the Pioneer probes 10 and 11.

Eventually, the considered superfluid dark medium is capable of explaining the flat profile of the orbital speed of spiral galaxies, due to their interactions with the SQS. We can observe flat profile solutions by putting (46) as denominator in Eqs. (30) and (31), with $\sigma_0 > 1$, where the set of coefficients Σ_n for $n = 1,\ 2, \cdots$ shows the flat profile.

Author details

Valeriy I. Sbitnev[1,2]* and Marco Fedi[3]

*Address all correspondence to: valery.sbitnev@gmail.com

1 Petersburg B. P. Konstantinov Nuclear Physics Institute, NRC Kurchatov Institute, Gatchina, Russia

2 Department of Electrical Engineering and Computer Sciences, University of California, Berkeley, CA, USA

3 Ministero dell'Istruzione, dell'Università e della Ricerca (MIUR), Italy

References

[1] Rubin VC. A brief history of dark matter. in Livio Mn editor The Dark Universe: Matter, Energy and Gravity. Cambridge. Cambridge University Press. 2004, pp. 1–13.

[2] Fedi M. Gravity as a fluid dynamic phenomenon in a superfluid quantum space. Fluid Quantum Gravity and Relativity. 2016. URL: https://hal.archives-ouvertes.fr/hal-01248015

[3] Ardey A. Dark fluid: A complex scalar field to unify dark energy and dark matter. Phys. Rev. D, 2006; **74**: 043516. doi:10.1103/PhysRevD.74.043516

[4] Hajdukovic DS. Quantum vacuum and dark matter. Astrophys. Space Sci. 2011; **337**: 9–14. doi:10.1007/s10509-011-0938-9

[5] Sbitnev VI. Hydrodynamics of the physical vacuum: dark matter is an illusion. Mod. Phys. Lett. A. 2015; **30**: 1550184. doi:10.1142/S0217732315501849

[6] Albareti FD, Cembranos JAR, Maroto AL. Vacuum energy as dark matter. Phys. Rev. D. 2014; **90**: 123509. doi:10.1103/PhysRevD.90.123509

[7] Das S, Bhaduri RK. Dark matter and dark energy from Bose-Einstein condensate. Class. Quant. Grav. 2015; **32**: 105003. doi:10.1088/0264-9381/32/10/105003

[8] Baum L, Frampton PH. Entropy of Contracting Universe in Cyclic Cosmology. Mod. Phys. Lett. A. 2008; **23**: 33-36. doi:10.1142/S0217732308026170

[9] Gurzadyan VG, Penrose R. Concentric circles in WMAP data may provide evidence of violent pre-Big-Bang activity. 2010. URL: http://arxiv.org/abs/1011.3706

[10] Chefranov SG, Novikov EA. Hydrodynamic vacuum sources of dark matter self-generation in an accelerating universe without a Big Bang. JETP. 2010; **111**: 731–743.

[11] Crawford DF. Observational evidence favors a static universe. 2014. URL: http://arxiv.org/abs/1009.0953

[12] López-Corredoira M, Melia F, Lusso E, Risaliti G. Cosmological test with the QSO Hubble diagram. Int. J. Mod. Phys. D 2016; **25**: 1650060. doi:10.1142/S0218271816500607

[13] Zwicky F. On the Red Shift of Spectral Lines through Interstellar Space. PNAS. 1929; **15**: 773–779. doi:10.1073/pnas.15.10.773

[14] Fedi M. Quantum gravity as dark energy inflow, 2016, URL: https://hal.archives-ouvertes.fr/hal-01423134

[15] Penrose R. Fashion, Faith, and Fantasy in the New Physics of the Universe. Princeton and Oxford. Princeton University Press. 2016.

[16] Stanford Encyclopedia of Philosophy. Absolute and Relational Theories of Space and Motion. 2015. URL: http://plato.stanford.edu/entries/spacetime-theories/

[17] Motte A. Axioms or Laws of Motion (translation of Newton's Principia (1687)). Published by Daniel Adee, 45 Liberty str., N. Y. 1846.

[18] Huygens C. Treatise on light. London. Macmillan and Co. Ltd. 1912.

[19] Wheeler JA, Ford K. Geons, Black Holes, and Quantum Foam. Norton & Co. 1995.

[20] Dirac PAM. Is there an Aether? Nature. 1951; **168**; 906–907.

[21] De Broglie L. Interpretation of quantum mechanics by the double solution theory. Annales de la Fondation Louis de Broglie. 1987; **12**; 1–22.

[22] Couder Y, Protiére S, Fort E, Boudaoud A. Dynamical phenomena—walking and orbiting droplets. Nature. 2005; **473**: 208. doi:10.1038/437208a

[23] Petroni NC, Vigier JP. Dirac's aether in relativistic quantum mechanics. Foundations of Physics. 1983; **13**: 253–286.

[24] Laughlin RB. A Different Universe: Reinventing Physics from the Bottom Down, N. Y.: Basic Books, 2005.

[25] Cahill RT. Gravity as quantum foam in-flow. 2004. URL: https://arxiv.org/abs/physics/0307003

[26] Bohm D, Vigier JP. Model of the causal interpretation of quantum theory in terms of a fluid with irregular fluctuations. Phys. Rev. 1954; **96**: 208–216. doi:10.1103/PhysRev.96.208

[27] Grusenick M. Extended Michelson-Morley Interferometer experiment. 2009. URL: https://www.youtube.com/watch?v=7T0d7o8X2-E

[28] Planck Collaboration: Ade PAR, Aghanim N, et al. (260 co-authors). Planck 2015 results. XIII. Cosmological parameters. 2015. URL: http://arxiv.org/abs/1502.01589

[29] Font JA. Numerical Hydrodynamics and Magnetohydrodynamics in General Relativity. Living Rev. Relat. 2008; 11: 1–131. doi:10.12942/lrr-2008-7

[30] Romatschke P. New Developments in Relativistic Viscous Hydrodynamics. Int. J. Mod. Phys. E. 2010; **19**: 1–53. doi:10.1142/S0218301310014613

[31] Van Holten JW. Relativistic fluid dynamics. NIKHEF. Amsterdam NL. 2006. Available from: http://www.nikhef.nl/~t32/relhyd.pdf

[32] Parkhomov AG. Dark matter: its role in cosmo-terrestrial interactions. Consciousness and Physical Reality. 1998; **3**: 24–35.

[33] Ryden B. Introduction to Cosmology. The Ohio State University. 2006.

[34] Sbitnev VI. Hydrodynamics of the physical vacuum: I. Scalar quantum sector. Foundations of Physics. 2016; **46**: 606–619. doi:10.1007/s10701-015-9980-8

[35] Freedman WL, et al. (14 co-authors). Final Results from the Hubble Space Telescope Key Project to Measure the Hubble Constant. Astrophys. J. 2001; **553**: 47–72. doi:10.1086/320638

[36] Spergel DN, et al. (21 co-authors). Wilkinson Microwave Anisotropy Probe (WMAP) Three Year Results: Implications for Cosmology. Astrophys. J. Suppl. 2007; **170**: 337–408. doi:10.1086/513700

[37] Khaidarov KA. Galilean Interpretation of the Hubble Constant. GALILEAN ELECTRODYNAMICS. 2005; **16**: 103–105.

[38] Crowell LB. Quantum fluctuations of spacetime. Singapore. World Scientific. Co. Pte. Ltd. 2005.

[39] Anderson JD, Laing PA, Lau EL, Liu AS, Nieto MM, Turyshev SG. Indication from Pioneer 10/11, Galileo, and Ulysses Data, of an Apparent Anomalous, Weak, Long-Range Acceleration. Phys. Rev. Lett. 1998; **81**: 2858–2861. doi:10.1103/PhysRevLett.81.2858

[40] Page GL, Dixon DS, Wallin JF. Can minor planets be used to assess gravity in the outer solar system? Astrophys. J. 2006; **642**: 606–614. doi:10.1086/500796

[41] Turyshev SG, Toth VT, Kinsella G, Lee S-Ch, Lok SM, Ellis J. Support for the thermal origin of the Pioneer anomaly. Phys. Rev. Lett. 2012; **108**: 241101. doi:10.1103/PhysRevLett.108.241101

[42] Mukhopadhyay U. et al. Generalized Model for Λ-Dark Energy. URL: arXiv:0802.1032, Int. J. Mod. Phys. 2009; D18: 389–396. doi:10.1142/S021827180901456X

[43] Zhao H. An Uneven Vacuum Energy Fluid as Λ, Dark Matter, MOND and Lens. 2008. URL: arXiv:0802.1775, Mod. Phys. Lett. A23:555–568, 2008. doi:10.1142/S021773230802656X

[44] Sbitnev VI. Dark matter is a manifestation of the vacuum Bose-Einstein condensate. 2016. URL: http://arxiv.org/abs/1601.04536

[45] Sbitnev VI. Hydrodynamics of the physical vacuum: II. Vorticity dynamics. Found. of Physics. 2016; 1–15. URL: http://rdcu.be/kdon. doi: 10.1007/s10701-015-9985-3

[46] Sbitnev VI. Physical vacuum is a special superfluid medium. In: Pahlavani MR, editor. Selected Topics in Applications of Quantum Mechanics. Rijeka: InTech; 2015. pp. 345–373. doi:10.5772/59040

[47] Kevlahan NK-R, Farge M. Vorticity filaments in two-dimensional turbulence: creation, stability and effect. J. Fluid Mech. 1997; 346: 49–76. doi:10.1017/S0022112097006113

[48] Provenzale A, Babiano A, Bracco A, Pasquero C, Weiss JB. Coherent vortices and tracer transport. Lect. Notes Phys. 2008; **744**: 101–116. doi:10.1007/978-3-540-75215-8 5

[49] Tseng P-H, Lee T-C. Numerical evaluation of exponential integral: Theis well function approximation. J. Hydrol. 1998; 205: 38–51. doi:10.1016/S0022-1694(97)00134-0

[50] De Blok WJG, McGaugh SS, Rubin VC. High-resolution rotation curves of low surface brightness galaxies. II. Mass models. Astron. J. 2001; **122**: 2396–2427. doi:10.1086/323450

[51] Mielczarek J, Stachowiak T, Szydlowski M. Vortex in axion condensate as a dark matter halo. Int. J. Mod. Phys. D. 2010; **19**: 1843–1855. doi:10.1142/S0218271810018037

[52] Mureika JR, Mann RB. Does entropic gravity bound the masses of the photon and graviton? Mod. Phys. Lett. A. 2011; **26**: 171–181. doi:10.1142/S0217732311034840

[53] Goldhaber AS, Nieto MM. Photon and graviton mass limits. Rev. Mod. Phys. 2010; **82**: 939–979. doi:10.1103/RevModPhys.82.939

[54] Triple S. A simplified treatment of gravitational interaction on galactic scales. JKAS. 2013; **46**: 41–47. doi:10.5303/JKAS.2013.46.1.41

[55] Einasto E, et al. (10 co-authors). The Sloan Great Wall. Morphology and galaxy content. Astrophys. J. 2011; **736**: 25 p. doi:10.1088/0004-637X/736/1/51

[56] Laigle C, Pichon C, et al. (10 co-authors). Swirling around filaments: are large-scale structure vortices spinning up dark haloes? MNRAS. 2013; **446**: 2744–2759. doi:10.1093/mnras/stu2289

[57] Santillán AO, Volke-Sepúlveda K. A demonstration of rotating sound waves in free space and the transfer of their angular momentum to matter. Am. J. Phys. 2009; 77: 209–215. doi:10.1119/1.3056580

Section 3

Gravity, Dark Energy and Black Holes

Chapter 6

Modified Gravity Theories: Distinguishing from ΛCDM Model

Koichi Hirano

Additional information is available at the end of the chapter

http://dx.doi.org/10.5772/intechopen.68281

Abstract

The method and probability of distinguishing between the Λ cold dark matter (ΛCDM) model and modified gravity are studied from future observations for the growth rate of cosmic structure (Euclid redshift survey). We compare the mock observational data to the theoretical cosmic growth rate by modified gravity models, including the extended Dvali–Gabadadze–Porrati (DGP) model, kinetic gravity braiding model, and Galileon model. In the original DGP model, the growth rate $f\sigma_8$ is suppressed in comparison with that in the ΛCDM model in the setting of the same value of the today's energy density of matter $\Omega_{m,0}$, due to suppression of the effective gravitational constant. In the case of the kinetic gravity braiding model and the Galileon model, the growth rate $f\sigma_8$ is enhanced in comparison with the ΛCDM model in the same value of $\Omega_{m,0}$, due to enhancement of the effective gravitational constant. For the cosmic growth rate data from the future observation (Euclid), the compatible value of $\Omega_{m,0}$ differs according to the model. Furthermore, $\Omega_{m,0}$ can be stringently constrained. Thus, we find the ΛCDM model is distinguishable from modified gravity by combining the growth rate data of Euclid with other observations.

Keywords: accelerated expansion, gravitational theory, dark energy, observational test, cosmic growth rate

1. Introduction

Cosmological observations, including type Ia supernovae (SNIa) [1, 2], cosmic microwave background (CMB) anisotropies, and baryon acoustic oscillations (BAO), indicate that the universe is undergoing an accelerated phase of expansion. This late-time acceleration is one of the biggest mysteries in current cosmology. The standard explanation is that this acceleration is

caused by dark energy [3–6]. This would mean that a large part of components in the universe is unknown. The cosmological constant is a candidate of dark energy. To explain the late-time accelerated expansion of the universe, the cosmological constant must be a very small value. However, its value is not compatible with a prediction from particle physics, and it has fine-tuning and coincidence problems.

An alternative explanation for the current acceleration of the universe is to modify general relativity to be a more general theory of gravity at a long-distance scale. Several modified gravity theories have been studied, such as $f(R)$ gravity (for reviews, see, e.g., [7]), scalar-tensor theories [8–10], and the Dvali–Gabadadze–Porrati (DGP) braneworld model [11–13].

Furthermore, as an alternative to general relativity, Galileon gravity models have been proposed [14–22]. These models are built by introducing a scalar field with a self-interaction whose Lagrangian, which is invariant under Galileon symmetry $\partial_\mu\phi \to \partial_\mu\phi + b_\mu$, keeps the field equation of motion as a second-order differential equation. This avoids presenting a new degree of freedom, and perturbation of the theory is free from ghost or instability problems. The simplest term of the self-interaction is $\Box\phi(\nabla\phi)^2$, which induces decoupling of the Galileon field from gravity at small scales via the Vainshtein mechanism [23]. Therefore, the Galileon theory recovers general relativity at scales around the high-density region, as is not inconsistent with solar system experiments.

Galileon theory has been covariantized and studied in curved backgrounds [24, 25]. Although Galileon symmetry cannot be maintained in the case that the theory is covariantized, it is possible to preserve the equation of motion at second order, which means that the theory does not raise ghost-like instabilities. Galileon gravity induces self-accelerated expansion of the current universe. Thus, inflation models inspired by the Galileon gravity theory have been studied [26–28]. In Ref. [29], the parameters of the generalized Galileon cosmology were constrained from the observational data of SNIa, CMB, and BAO. The evolution of matter density perturbations for Galileon cosmology has also been investigated [16–18, 30, 31].

Almost 40 years ago, Horndeski derived the action of most general scalar-tensor theories with second-order equations of motion [32]. His theory received much attention as an extension of covariant Galileons [14, 24, 25, 33]. One can show that the four-dimensional action of generalized Galileons derived by Deffayet et al. [34] is equivalent to Horndeski's action under field redefinition [35]. Because Horndeski's theory contains all modified gravity models and single-field inflation models with one scalar degree of freedom as specific cases, considerable attention has been paid to various aspects of Horndeski's theory and its importance in cosmology.

Recently, more general modified gravity theories have been studied, including Gleyzes-Langlois-Piazza-Vernizzi (GLPV) theories [36, 37] and eXtended Galileon with 3-space covariance (XG3) [38].

In this chapter, the probability of distinguishing between the Λ cold dark matter (ΛCDM) model and modified gravity is studied by using future observations for the growth rate of cosmic structure (e.g., Euclid redshift survey [39]). We computed the growth rate of matter density perturbations in modified gravity and compared it with mock observational data. Whereas the background expansion history in modified gravity is almost identical to that of dark energy

models, the evolution of matter density perturbations of modified gravity is different from that of dark energy models. Thus, it is important to study the growth history of perturbations to distinguish modified gravity from models based on the cosmological constant or dark energy.

Although past observations of the growth rate of matter density perturbations have been used to study modified gravity [40], we focus on future observations of the growth rate by Euclid. We adopt the extended DGP model [41], kinetic gravity braiding model [30], and Galileon model [16, 17] as modified gravity models. The kinetic gravity braiding model and the Galileon model are specific aspects of Horndeski's theory.

This chapter is organized as follows. In the next section, we present the background evolution and the effective gravitational constant in modified gravity models. In Section 3, we describe the theoretical computations and the mock observational data of the growth rate of matter density perturbations. In Section 4, we study the probability of distinguishing between the ΛCDM model and modified gravity by comparing the predicted cosmic growth rate by models to the mock observational data. Finally, conclusions are given in Section 5.

2. Modified gravity models

2.1. Extended DGP model

In the DGP model [11], it is assumed that we live on a 4D brane embedded in a 5D Minkowski bulk. Matter is trapped on the 4D brane, and only gravity experiences the 5D Minkowski bulk.

The action is

$$S = \frac{1}{16\pi} M_{(5)}^3 \int_{bulk} d^5x \sqrt{-g_{(5)}} R_{(5)} + \frac{1}{16\pi} M_{(4)}^2 \int_{brane} d^4x \sqrt{-g_{(4)}} (R_{(4)} + L_m), \tag{1}$$

where quantities of the 4D brane and the 5D Minkowski bulk are represented with subscripts (4) and (5), respectively. M is the Planck mass, and L_m is the Lagrangian of matter confined on the 4D brane. The transition between 4D and 5D gravity occurs at the crossover scale r_c.

$$r_c = \frac{M_{(4)}^2}{2M_{(5)}^3}. \tag{2}$$

At scales larger than r_c, gravity appears in 5D. At scales smaller than r_c, gravity is effectively bound to the brane, and 4D Newtonian dynamics is recovered to a good approximation. r_c is a parameter in this model, which has the unit of length [42].

Under spatial homogeneity and isotropy, a Friedmann-like equation is obtained on the brane [43, 44]:

$$H^2 = \frac{8\pi G}{3}\rho + \varepsilon \frac{H}{r_c}, \tag{3}$$

where ρ represents the total fluid energy density on the 4D brane. The DGP model has two

branches ($\varepsilon = \pm 1$). The choice of $\varepsilon = +1$ is called the self-accelerating branch. In this branch, the accelerated expansion of the universe is induced without dark energy, since the Hubble parameter comes close to a constant $H = 1/r_c$ as time passes. By contrast, $\varepsilon = -1$ is the normal branch. In this case, the expansion cannot accelerate without a dark energy component. Therefore, in the following, we adopt the self-accelerating branch ($\varepsilon = +1$).

The original DGP model, however, is plagued by the ghost problem [45] and is incompatible with cosmological observations [46].

Dvali and Turner [41] phenomenologically extended the Friedmann-like equation of the DGP model (Eq. (3)). This model interpolates between the original DGP model and the ΛCDM model by adding the parameter α. The modified Friedmann-like equation is

$$H^2 = \frac{8\pi G}{3}\rho + \frac{H^\alpha}{{r_c}^{2-\alpha}}. \tag{4}$$

For $\alpha = 1$, this is equivalent to the original DGP Friedmann-like equation, whereas $\alpha = 0$ leads to an expansion history identical to ΛCDM cosmology. This is important for distinguishing the ΛCDM model from the original DGP model between $\alpha = 0$ and 1. In the extended DGP model, the crossover scale r_c can be expressed as follows:

$$r_c = (1 - \Omega_{m,0})^{\frac{1}{\alpha-2}} H_0^{-1}. \tag{5}$$

Thus, the independent parameters of the cosmological model are α and today's energy density parameter of matter $\Omega_{m,0}$. The effective gravitational constant of the extended DGP model is given in order to interpolate between ΛCDM and the original DGP model. The effective gravitational constant is as follows.

$$\frac{G_{\text{eff}}}{G} = 1 + \frac{1}{3\beta}, \tag{6}$$

where

$$\beta \equiv 1 - \frac{2(r_c H)^{2-\alpha}}{\alpha}\left[1 + \frac{1}{3}\frac{(2-\alpha)\dot{H}}{H^2}\right]. \tag{7}$$

G_{eff} / G is the effective gravitational constant normalized to Newton's gravitational constant, and an overdot represents differentiation with respect to cosmic time t.

2.2. Kinetic gravity braiding model

The kinetic gravity braiding model [30] is proposed as an alternative to the dark energy model. One can say that the kinetic gravity braiding model is a specific aspect of Horndeski's theory [32].

The most general four-dimensional scalar-tensor theories keeping the field equations of motion at second order are described by the Lagrangian [32–35, 47]

$$\mathcal{L} = \sum_{i=2}^{5} \mathcal{L}_i, \tag{8}$$

where

$$\mathcal{L}_2 = K(\phi, X), \tag{9}$$

$$\mathcal{L}_3 = -G_3(\phi, X)\Box\phi, \tag{10}$$

$$\mathcal{L}_4 = G_4(\phi, X)R + G_{4,X}[(\Box\phi)^2 - (\nabla_\mu\nabla_\nu\phi)(\nabla^\mu\nabla^\nu\phi)], \tag{11}$$

$$\begin{aligned}\mathcal{L}_5 = {} & G_5(\phi, X)G_{\mu\nu}(\nabla^\mu\nabla^\nu\phi) - \frac{1}{6}G_{5,X}[(\Box\phi)^3 - 3(\Box\phi)(\nabla_\mu\nabla_\nu\phi)(\nabla^\mu\nabla^\nu\phi) \\ & + 2(\nabla^\mu\nabla_\alpha\phi)(\nabla^\alpha\nabla_\beta\phi)(\nabla^\beta\nabla_\mu\phi)].\end{aligned} \tag{12}$$

Here, K and G_i (i = 3, 4, 5) are functions of the scalar field ϕ and its kinetic energy $X = -\partial^\mu\phi\partial_\mu\phi/2$ with the partial derivatives $G_{i,X} \equiv \partial G_i/\partial X$. R is the Ricci scalar, and $G_{\mu\nu}$ is the Einstein tensor. The above Lagrangian was first derived by Horndeski in a different form Ref. [32]. This Lagrangian (Eqs. (8)–(12)) is equivalent to that derived by Horndeski [35]. The total action is then given by

$$S = \int d^4x\sqrt{-g}(\mathcal{L} + \mathcal{L}_m), \tag{13}$$

where g represents a determinant of the metric $g_{\mu\nu}$, and $\mathcal{L}_m$ is the Lagrangian of non-relativistic matter.

Variation with respect to the metric produces the gravity equations, and variation with respect to the scalar field ϕ yields the equation of motion. By using the notation $K \equiv K(\phi,X)$, $G \equiv G_3(\phi,X)$, $F \equiv \frac{2}{M_{\rm pl}^2}G_4(\phi,X)$, and assuming $G_5(\phi,X) = 0$ for Friedmann–Robertson–Walker spacetime, the gravity equations give

$$3M_{\rm pl}^2FH^2 = \rho_m + \rho_r - 3M_{\rm pl}^2H\dot{F} - K + 2XK_{,X} + 6H\dot{\phi}XG_{,X} - 2XG_{,\phi}, \tag{14}$$

$$-M_{\rm pl}^2F(3H^2 + 2\dot{H}) = p_r + 2M_{\rm pl}^2H\dot{F} + M_{\rm pl}^2\ddot{F} + K - 2XG_{,X}\ddot{\phi} - 2XG_{,\phi}, \tag{15}$$

and the equation of motion for the scalar field gives

$$\begin{aligned}&(K_{,X} + 2XK_{,XX} + 6H\dot{\phi}G_{,X} + 6H\dot{\phi}XG_{,XX} - 2XG_{,\phi X} - 2G_{,\phi})\ddot{\phi} \\ &+(3HK_{,X} + \dot{\phi}K_{,\phi X} + 9H^2\dot{\phi}G_{,X} + 3\dot{H}\dot{\phi}G_{,X} + 6HXG_{,\phi X} - 6HG_{,\phi} - G_{,\phi\phi}\dot{\phi})\dot{\phi} \\ &-K_{,\phi} - 6M_{\rm pl}^2H^2F_{,\phi} - 3M_{\rm pl}^2\dot{H}F_{,\phi} = 0.\end{aligned} \tag{16}$$

Here, an overdot denotes differentiation with respect to cosmic time t, and $H = \dot{a}/a$ is the Hubble expansion rate. Note that we use the partial derivative notation $K_{,X} \equiv \partial K/\partial X$ and

$K_{,XX} \equiv \partial^2 K/\partial X^2$ and a similar notation for other variables. Also, ρ_m and ρ_r are the energy densities of matter and radiation, respectively, and p_r is the pressure of the radiation.

In the kinetic gravity braiding model [30], the functions in Horndeski's theory are given as follows:

$$K(\phi,X) = -X, \tag{17}$$

$$G_3(\phi,X) = M_{\rm pl}\left(\frac{r_c^2}{M_{\rm pl}^2}X\right)^n, \tag{18}$$

$$G_4(\phi,X) = \frac{M_{\rm pl}^2}{2}, \tag{19}$$

$$G_5(\phi,X) = 0. \tag{20}$$

$M_{\rm pl}$ is the reduced Planck mass related to Newton's gravitational constant by $M_{\rm pl} = 1/\sqrt{8\pi G}$, and r_c is called the crossover scale in the DGP model [42]. The kinetic braiding model we study is characterized by parameter n in Eq. (18). For n = 1, this corresponds to Deffayet's Galileon cosmological model [22]. For n equal to infinity, the background expansion of the universe of the kinetic braiding model approaches that of the ΛCDM model. This helps distinguish the kinetic braiding model from the ΛCDM model.

In the case of the kinetic braiding model using the Hubble parameter as the present epoch H_0, the crossover scale r_c is given by

$$r_c = \left(\frac{2^{n-1}}{3n}\right)^{1/2n}\left[\frac{1}{6(1-\Omega_{m,0}-\Omega_{r,0})}\right]^{(2n-1)/4n} H_0^{-1}, \tag{21}$$

where $\Omega_{r,0}$ is the density parameter of the radiation at the present time. Thus, the independent parameters of the cosmological model are n and $\Omega_{m,0}$. The effective gravitational constant normalized to Newton's gravitational constant $G_{\rm eff}$ / G of the kinetic braiding model is given by

$$\frac{G_{\rm eff}}{G} = \frac{2n + 3n\Omega_m - \Omega_m}{\Omega_m(5n-\Omega_m)}, \tag{22}$$

where Ω_m is the matter energy density parameter defined as $\Omega_m = \rho_m/3M_{\rm pl}^2H^2$. Here, we used the attractor condition. Although the background evolution for large n approaches the ΛCDM model, the growth history of matter density perturbations is different due to the time-dependent effective gravitational constant.

2.3. Galileon model

The Galileon gravity model is proposed as an alternative to the dark energy model. It is thought that the Galileon model studied in Refs. [16, 17] is a specific aspect of Horndeski's theory [32].

http://dx.doi.org/10.5772/intechopen.68281

In the Galileon model [16, 17], the functions in the Lagrangian (Eqs. (8)–(12)) of the Horndeski's theory are given as follows:

$$K(\phi,X) = 2\frac{\omega}{\phi}X, \tag{23}$$

$$G_3(\phi,X) = 2\xi(\phi)X, \tag{24}$$

$$G_4(\phi,X) = \phi, \tag{25}$$

$$G_5(\phi,X) = 0, \tag{26}$$

where ω is the Brans–Dicke parameter and $\xi(\phi)$ is a function of ϕ.

In this case, the Friedmann-like equations, Eqs. (14) and (15), can be written in the following forms, respectively:

$$3H^2 = \frac{1}{M_{\rm pl}^2}(\rho_m + \rho_r + \rho_\phi), \tag{27}$$

$$-3H^2 - 2\dot{H} = \frac{1}{M_{\rm pl}^2}(p_r + p_\phi), \tag{28}$$

where the effective dark energy density ρ_ϕ is defined as

$$\rho_\phi = 2\phi\left[-3H\frac{\dot{\phi}}{\phi} + \frac{\omega}{2}\left(\frac{\dot{\phi}}{\phi}\right)^2 + \phi^2\xi(\phi)\left\{3H + \frac{\dot{\phi}}{\phi}\right\}\left(\frac{\dot{\phi}}{\phi}\right)^3\right] + 3H^2(M_{\rm pl}^2 - 2\phi), \tag{29}$$

and the effective pressure of dark energy p_ϕ is

$$p_\phi = 2\phi\left[\frac{\ddot{\phi}}{\phi} + 2H\frac{\dot{\phi}}{\phi} + \frac{\omega}{2}\left(\frac{\dot{\phi}}{\phi}\right)^2 - \phi^2\xi(\phi)\left\{\frac{\ddot{\phi}}{\phi} - \left(\frac{\dot{\phi}}{\phi}\right)^2\right\}\left(\frac{\dot{\phi}}{\phi}\right)^2\right] - (3H^2 + 2\dot{H})(M_{pl}^2 - 2\phi). \tag{30}$$

The equation of motion for the scalar field is given by Eq. (16).

For the numerical analysis, we adopt a specific model in which

$$\xi(\phi) = \frac{r_c^2}{\dot{\phi}^2}, \tag{31}$$

where r_c is the crossover scale [15]. This Galileon model extends the Brans–Dicke theory by adding the self-interaction term, $\xi(\phi)(\nabla\phi)^2\Box\phi$. Thus, ω of this model is not exactly the same as the original Brans–Dicke parameter. The evolution of matter density perturbations of this model was computed in Refs. [16, 17].

At early times, we set the initial condition $\phi \simeq M_{\rm pl}^2/2$ to recover general relativity. Using these initial conditions reduces the Friedmann equations (Eqs. (27) and (28)) to their usual forms: $3H^2 = (\rho_m + \rho_r)/M_{\rm pl}^2$ and $-3H^2 - 2\dot{H} = p_r/M_{\rm pl}^2$. This is the cosmological version of the Vainshtein effect [23], which is a method to recover general relativity below a certain scale. At present, to induce cosmic acceleration, the value of r_c must be fine tuned.

The energy density parameter of matter at present in this model is defined as $\Omega_{m,0} = \rho_{m,0}/3H_0^2\phi_0$. Therefore, in the numerical analysis, the value of r_c is fine tuned so that $\Omega_{m,0}$ becomes an assumed value. Thus, the independent parameters of the cosmological model are ω and $\Omega_{m,0}$. For the Galileon model specified by Eqs. (23)–(26) and (31), the effective gravitational constant is given by

$$G_{\rm eff} = \frac{1}{16\pi\phi}\left[1 + \frac{(1+\xi(\phi)\dot{\phi}^2)^2}{J}\right], \tag{32}$$

where

$$J \equiv 3 + 2\omega + \phi^2\xi(\phi)\left[4\frac{\ddot{\phi}}{\phi} - 2\frac{\dot{\phi}^2}{\phi^2} + 8H\frac{\dot{\phi}}{\phi} - \phi^2\xi(\phi)\frac{\dot{\phi}^4}{\phi^4}\right]. \tag{33}$$

The effective gravitational constant $G_{\rm eff}$ is close to Newton's constant G at early times, but increases at later times.

3. Cosmic growth rate

3.1. Density perturbations

Under the quasistatic approximation on sub-horizon scales, the evolution equation for cold dark matter over-density δ in linear theory is given by

$$\ddot{\delta} + 2H\dot{\delta} - 4\pi G_{\rm eff}\rho\delta \simeq 0, \tag{34}$$

where $G_{\rm eff}$ represents the effective gravitational constant of the modified gravity models described in the previous section.

We set the same initial conditions as in the conventional ΛCDM case ($\delta \approx a$ and $\dot{\delta} \approx \dot{a}$) because we trace the difference between the evolution of the matter perturbations in modified gravity and the evolution in the ΛCDM model. From the evolution equation, we numerically obtain the growth factor δ / a for modified gravity models. The linear growth rate is written as

$$f = \frac{d\ln\delta}{d\ln a}. \tag{35}$$

where δ is the matter density fluctuations and a is the scale factor. The growth rate can be parameterized by the growth index γ, defined by

$$f = \Omega_m^{\gamma}. \tag{36}$$

Refs. [48, 49] showed that the growth rate f in the Galileon model specified by Eqs. (23)–(26) and (31) is enhanced compared with the ΛCDM model for the same value of $\Omega_{m,0}$ due to enhancement of the effective gravitational constant.

3.2. Euclid

Euclid [39] is a European Space Agency mission that is prepared for a launch at the end of 2020. The aim of Euclid is to study the origin of the accelerated expansion of the universe. Euclid will investigate the distance-redshift relationship and the evolution of cosmic structures by measuring shapes and redshifts of galaxies and the distribution of clusters of galaxies over a large part of the sky. Its main subject of research is the nature of dark energy. However, Euclid will cover topics including cosmology, galaxy evolution, and planetary research.

In this study, Euclid parameters are adopted as the growth rate observations. The growth rate can be parameterized by using the growth index γ, defined by $f = \Omega_m{}^{\gamma}$. Mock data of the cosmic growth rate are built based on the 1σ marginalized errors of the growth rate by Euclid. These data are listed in Table 4 in the paper by Amendola et al. [39]. **Table 1** shows the 1σ marginalized errors for the cosmic growth rates with respect to each redshift in accordance with Table 4 in [39]. In **Figure 1**, the mock data of the cosmic growth rate used in this study are plotted.

The mock data are used to compute the statistical χ^2 function. The χ^2 function for the growth rate is defined as

$$\chi_f^2 = \sum_{i=1}^{14} \frac{\left(f_{theory}(z_i) - f_{obs}(z_i)\right)^2}{\sigma_{f_g}(z_i)^2} \tag{37}$$

where $f_{obs}(z_i)$ is the future observational (mock) data of the growth rate. The theoretical growth rate $f_{theory}(z_i)$ is computed as Eq. (35). In Ref. [50], constraints on neutrino masses are estimated based on future observations of the growth rate of the cosmic structure from the Euclid redshift survey.

The estimated errors from the observational technology of Euclid are known, but the center value of future observations is not known. Therefore, the purpose of this study is not to validate the ΛCDM model or modified gravity but to find ways and probabilities to distinguish between the ΛCDM model and modified gravity.

Experiment	z	σ_{f_g} (ref.)
Euclid [39]	0.7	0.011
	0.8	0.010
	0.9	0.009
	1.0	0.009
	1.1	0.009
	1.2	0.009
	1.3	0.010
	1.4	0.010
	1.5	0.011
	1.6	0.012
	1.7	0.014
	1.8	0.014
	1.9	0.017
	2.0	0.023

Here, z represents the redshift and σ_{f_g} represents the 1σ marginalized errors of the growth rates.

Table 1. 1σ marginalized errors for the growth rates in each redshift bin based on Table 4 in the study by Amendola et al. [39].

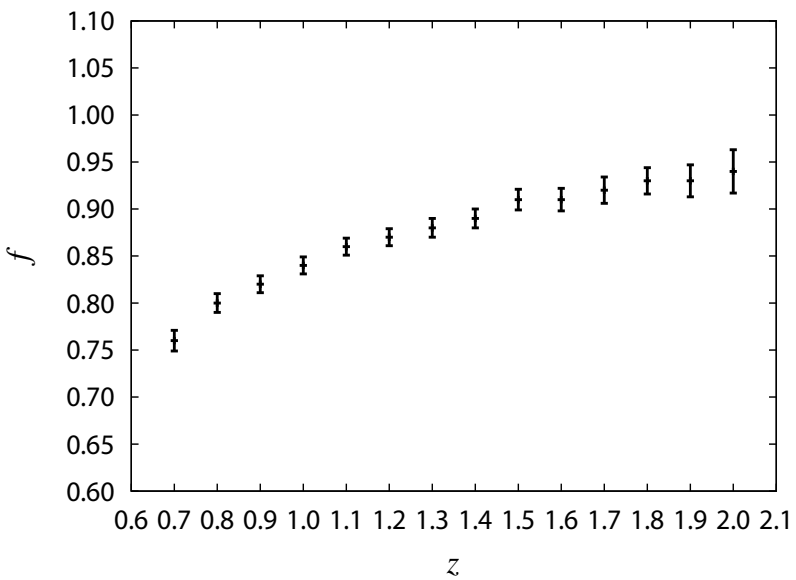

Figure 1. Plot of mock data of the cosmic growth rate.

http://dx.doi.org/10.5772/intechopen.68281

4. Comparison with observations

4.1. Extended DGP model

In **Figure 2**, we plot the probability contours in the (α, σ_8)-plane in the extended DGP model from the observational (mock) data of the cosmic growth rate by Euclid. The blue (dark) and light blue (light) contours show the 1σ (68.3%) and 2σ (95.0%) confidence limits, respectively. Part of $\alpha = 0$ for the horizontal axis corresponds to the ΛCDM model, and part of $\alpha = 1$ corresponds to the original DGP model. σ_8 is the root mean square (rms) amplitude of over-density at the comoving $8\,h^{-1}$ Mpc scale (where h is the normalized Hubble parameter $H_0 = 100\,h\mathrm{kmsec}^{-1}\mathrm{Mpc}^{-1}$). In **Figures 3–5**, we demonstrate why σ_8 is stringently constrained.

We plot $f\sigma_8$ (the product of growth rate and σ_8) in the extended DGP model as a function of redshift z for various values of the energy density parameter of matter at the present $\Omega_{m,0}$ in **Figures 3–5**. In **Figure 3**, the parameters are fixed by $\alpha = 1$, $\sigma_8 = 0.6$. For the various values of $\Omega_{m,0}$, the theoretical curves seem to revolve around the dashed circle. Hence, the value of $\sigma_8 = 0.6$ is incompatible with the observational (mock) data.

In **Figure 4**, the parameters are fixed by $\alpha = 1$, $\sigma_8 = 1.0$. For the various values of $\Omega_{m,0}$, the theoretical curves seem to revolve around the dashed circle. Hence, the value of $\sigma_8 = 1.0$ is incompatible with the observational (mock) data.

In **Figure 5**, the parameters are fixed by $\alpha = 1$, $\sigma_8 = 0.855$. For the various values of $\Omega_{m,0}$, although the theoretical curves seem to revolve around the dashed circle, some theoretical curves are comparatively close to the observational (mock) data. Hence, the value of $\sigma_8 = 0.855$ is compatible with the observational (mock) data in the original DGP model ($\alpha = 1$).

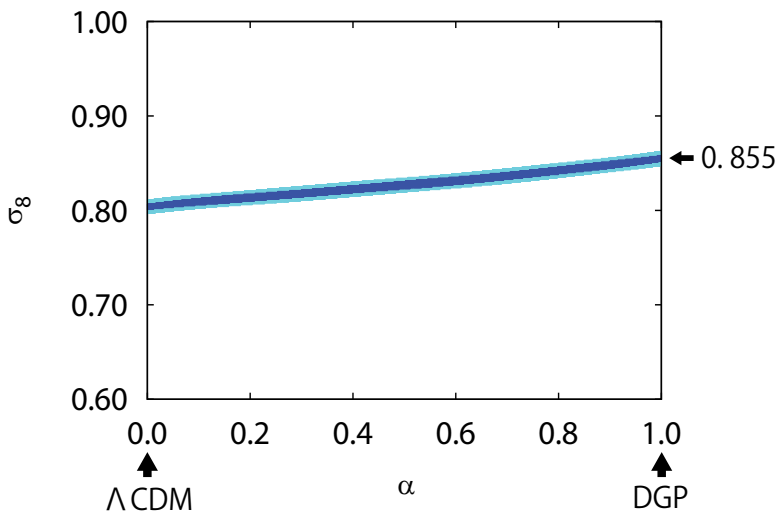

Figure 2. Probability contours in the (α, σ_8)-plane for the extended DGP model from the observational (mock) data of the cosmic growth rate by Euclid. The contours show the 1σ (68.3%) and 2σ (95.0%) confidence limits.

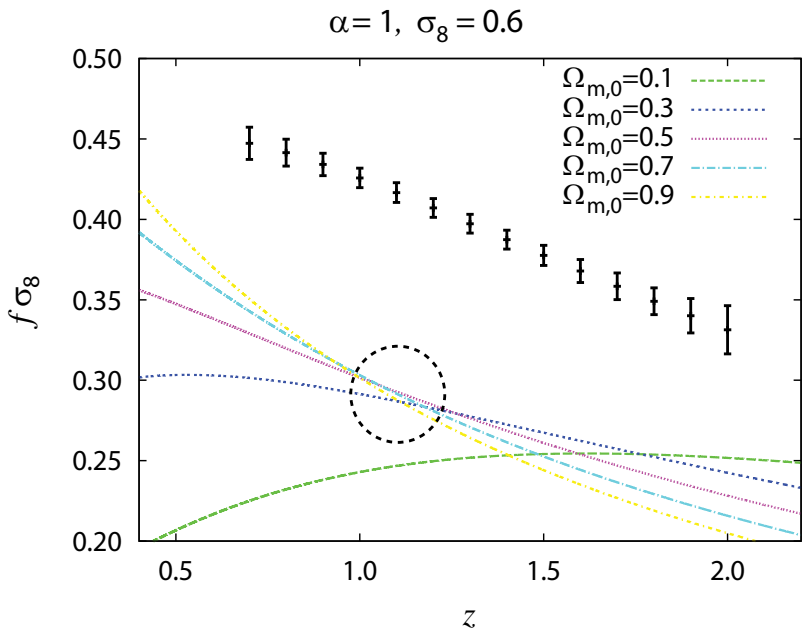

Figure 3. $f\sigma_8$ (the product of growth rate and σ_8) in the extended DGP model as a function of redshift z for various values of $\Omega_{m,0}$. The parameters are fixed by $\alpha = 1$, $\sigma_8 = 0.6$.

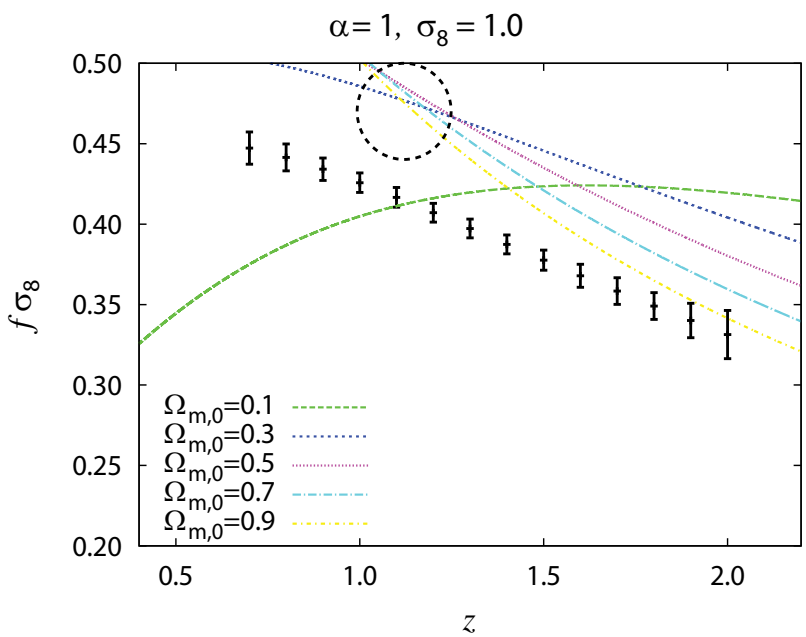

Figure 4. $f\sigma_8$ in the extended DGP model as a function of redshift z for various values of $\Omega_{m,0}$. The parameters are fixed by $\alpha = 1$, $\sigma_8 = 1.0$.

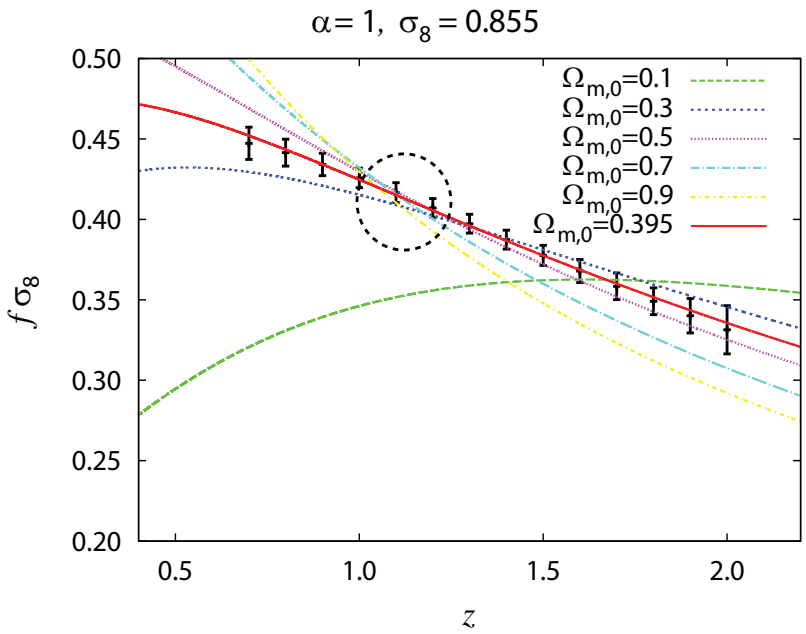

Figure 5. $f\sigma_8$ in the extended DGP model as a function of redshift z for various values of $\Omega_{m,0}$. The parameters are fixed by $\alpha = 1$, $\sigma_8 = 0.855$.

In **Figure 6**, we plot the probability contours in the (α, $\Omega_{m,0}$)-plane in the extended DGP model from the observational (mock) data of the cosmic growth rate by Euclid. The red (dark) and pink (light) contours show the 1σ (68.3%) and 2σ (95.0%) confidence limits, respectively. We demonstrate why $\Omega_{m,0}$ is positively correlated with α in **Figure 7**.

We plot $f\sigma_8$ in the extended DGP model as a function of redshift z in **Figure 7**. The red (solid) line is the theoretical curve for the best-fit parameter in the ΛCDM model ($\alpha = 0$, $\Omega_{m,0} = 0.257$, $\sigma_8 = 0.803$). In the case of changing only α =1, the growth rate $f\sigma_8$ is suppressed due to suppression of the effective gravitational constant (green (dashed) line: $\alpha = 1$, $\Omega_{m,0} = 0.257$, $\sigma_8 = 0.803$). For $\alpha = 1$, by tuning the value of $\Omega_{m,0}$ and σ_8, the theoretical curve is compatible with the observational (mock) data again (blue (dotted) line: $\alpha = 1$, $\Omega_{m,0} = 0.395$, $\sigma_8 = 0.855$).

In **Figure 8**, we add constraints on $\Omega_{m,0}$ for the extended DGP model from the combination of CMB, BAO, and SNIa data (black solid lines) [46] to the probability contours in the (α, $\Omega_{m,0}$)-plane by the growth rate (mock) data by Euclid of **Figure 6**.

Because $\Omega_{m,0}$ is stringently constrained by the cosmic growth rate data from Euclid, we find the ΛCDM model is distinguishable from the original DGP model by combining the growth rate data of Euclid with other observations.

4.2. Kinetic gravity braiding model

In **Figure 9**, we plot the probability contours in the (n, $\Omega_{m,0}$)-plane in the kinetic gravity braiding model from the observational (mock) data of the cosmic growth rate by Euclid. The red (dark) and pink (light) contours show the 1σ (68.3%) and 2σ (95.0%) confidence limits, respectively.

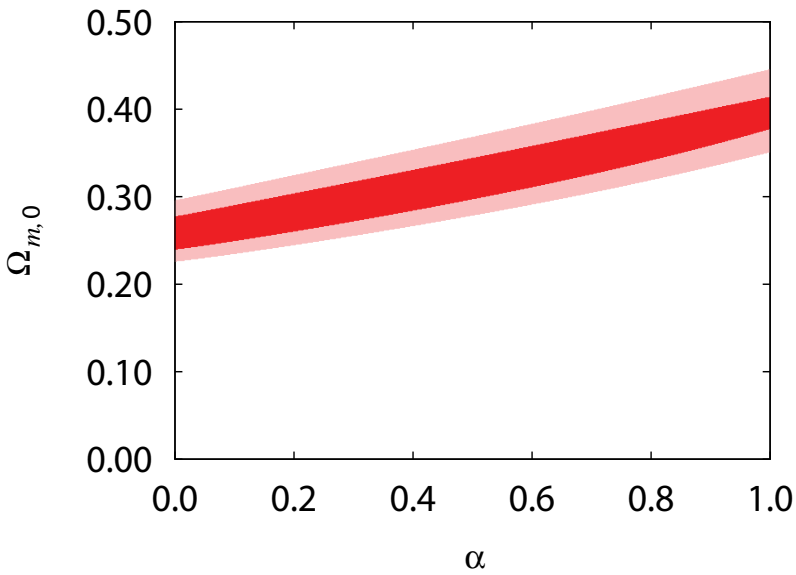

Figure 6. Probability contours in the (α, $\Omega_{m,0}$)-plane for the extended DGP model from the observational (mock) data of the cosmic growth rate by Euclid. The contours show the 1σ (68.3%) and 2σ (95.0%) confidence limits.

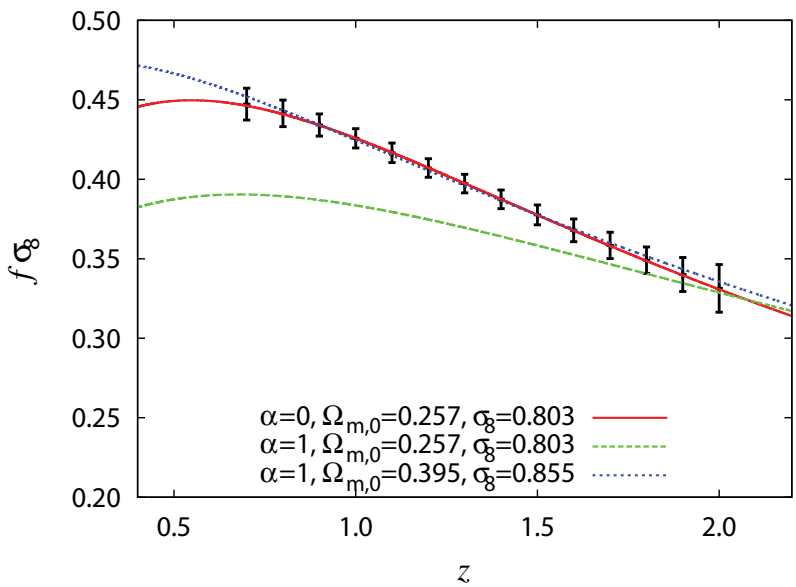

Figure 7. $f\sigma_8$ in the extended DGP model as a function of redshift z. The values of the parameters are as follows. Red (solid) line: $\alpha = 0$, $\Omega_{m,0} = 0.257$, $\sigma_8 = 0.803$. Green (dashed) line: $\alpha = 1$, $\Omega_{m,0} = 0.257$, $\sigma_8 = 0.803$. Blue (dotted) line: $\alpha = 1$, $\Omega_{m,0} = 0.395$, $\sigma_8 = 0.855$.

http://dx.doi.org/10.5772/intechopen.68281

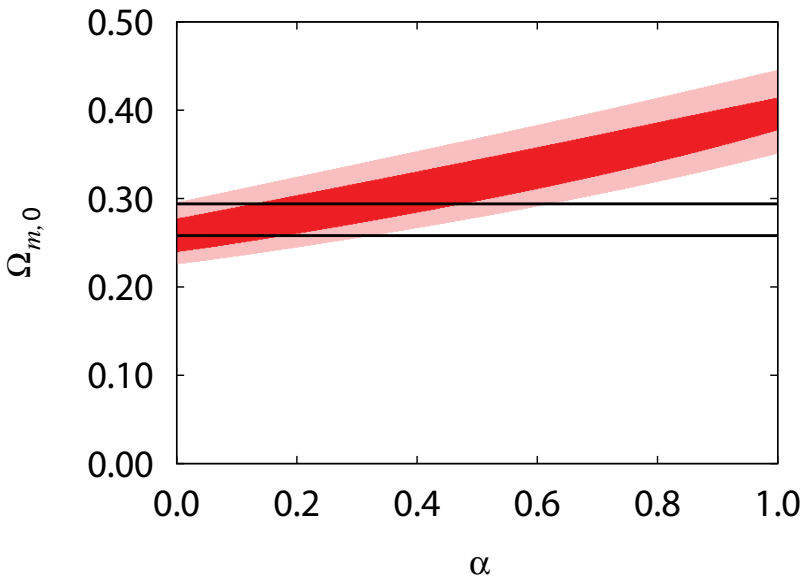

Figure 8. Addition of constraints on $\Omega_{m,0}$ for the extended DGP model from CMB, BAO and SNIa data [46] to the data in **Figure 6**.

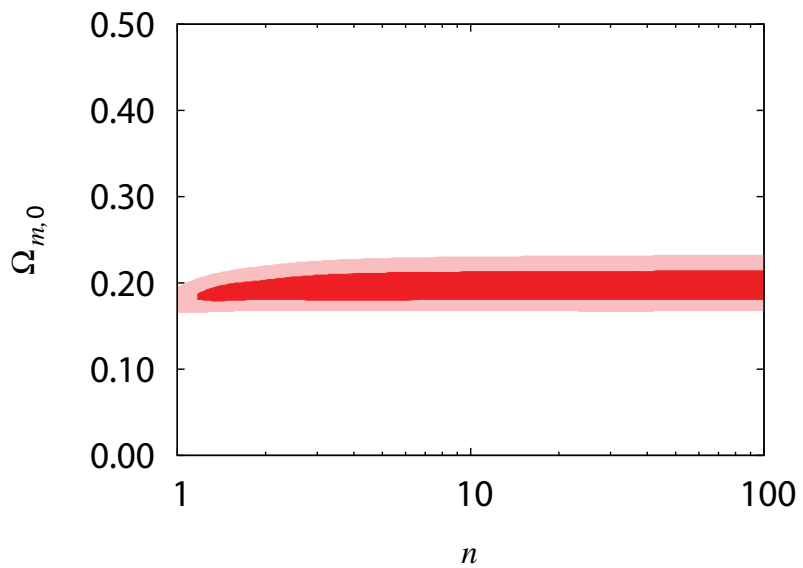

Figure 9. Probability contours in the (n, $\Omega_{m,0}$)-plane for the kinetic gravity braiding model from the observational (mock) data of the cosmic growth rate by Euclid. The contours show the 1σ (68.3%) and 2σ (95.0%) confidence limits.

We plot $f\sigma_8$ in the kinetic gravity braiding model as a function of redshift z in **Figure 10**. The red (solid) line is the theoretical curve for the best-fit parameter in the ΛCDM model ($\Omega_{m,0} = 0.257$, $\sigma_8 = 0.803$). In the case of the kinetic gravity braiding model for $n = 1$, the growth rate $f\sigma_8$ is enhanced due to enhancement of the effective gravitational constant (Green (dashed) line: $n = 1$, $\Omega_{m,0} = 0.257$, $\sigma_8 = 0.803$). For $n = 100$, by tuning the value of $\Omega_{m,0}$ and σ_8, the theoretical curve is compatible with the observational (mock) data again (blue (dotted) line: $n = 100$, $\Omega_{m,0} = 0.196$, $\sigma_8 = 0.820$).

In **Figure 11**, we add constraints on $\Omega_{m,0}$ for the kinetic gravity braiding model from CMB (black dashed lines) and from SNIa (black solid lines) [30], respectively, to the probability contours in the (n, $\Omega_{m,0}$)-plane by the growth rate (mock) data by Euclid of **Figure 9**.

In the kinetic gravity braiding model, the allowed parameter region obtained by using only the growth rate data does not overlap with the allowed parameter region obtained from CMB or from SNIa data.

4.3. Galileon model

In **Figure 12**, we plot the probability contours in the (ω, $\Omega_{m,0}$)-plane in the Galileon model from the observational (mock) data of the cosmic growth rate by Euclid. The red (dark) and pink (light) contours show the 1σ (68.3%) and 2σ (95.0%) confidence limits, respectively. We also plot the constraints on $\Omega_{m,0}$ for the Galileon model from the combination of CMB, BAO, and SNIa (black solid lines) [49].

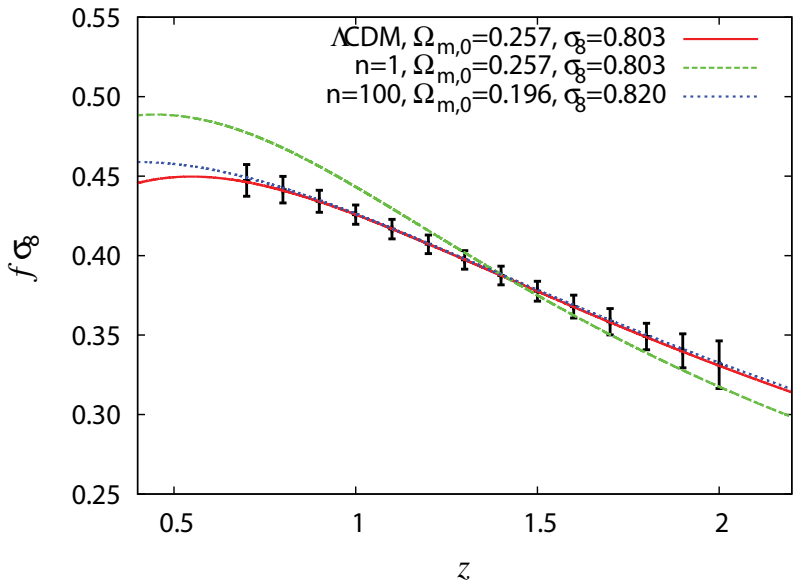

Figure 10. $f\sigma_8$ in kinetic gravity braiding model as a function of redshift z. The values of the parameters are as follows. Red (solid) line: ΛCDM, $\Omega_{m,0} = 0.257$, $\sigma_8 = 0.803$. Green (dashed) line: $n = 1$, $\Omega_{m,0} = 0.257$, $\sigma_8 = 0.803$. Blue (dotted) line: $n = 100$, $\Omega_{m,0} = 0.196$, $\sigma_8 = 0.820$.

http://dx.doi.org/10.5772/intechopen.68281

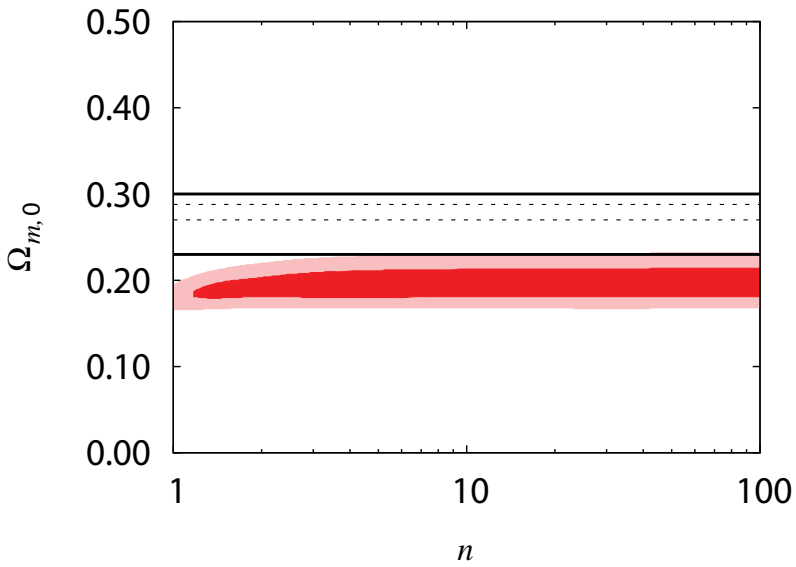

Figure 11. Addition of constraints on $\Omega_{m,0}$ for the kinetic gravity braiding model from CMB (black dashed lines) and from SNIa (black solid lines), respectively, [30] to **Figure 9**.

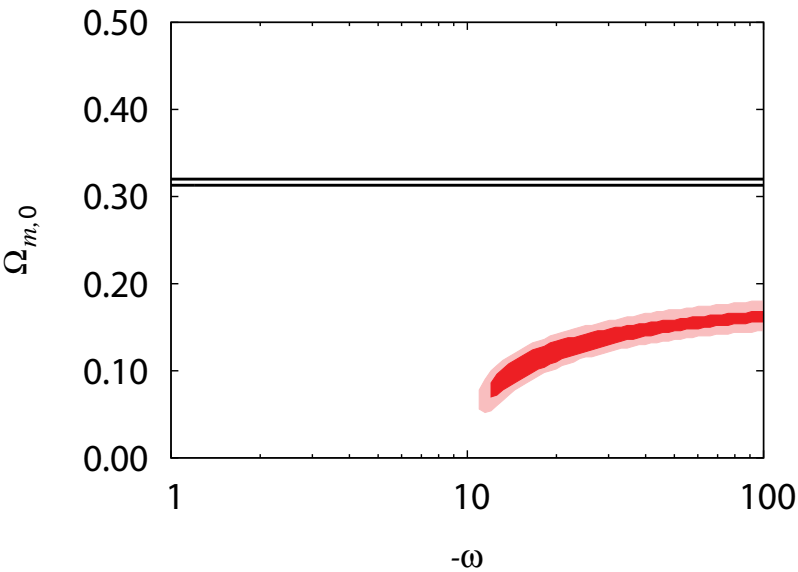

Figure 12. Probability contours in the (ω, $\Omega_{m,0}$)-plane for the Galileon model from the observational (mock) data of the cosmic growth rate by Euclid. The contours show the 1σ (68.3%) and 2σ (95.0%) confidence limits. The added constraints on $\Omega_{m,0}$ for the Galileon model are from the combination of CMB, BAO, and SNIa (black solid lines) [49].

In the Galileon model, the allowed parameter region obtained by using only the growth rate data do not overlap at all with the allowed parameter region obtained from the combination of CMB, BAO, and SNIa data.

5. Conclusions

The growth rate $f\sigma_8$ in the original DGP model is suppressed in comparison with that in the ΛCDM case in the setting of the same value of $\Omega_{m,0}$ due to suppression of the effective gravitational constant. In the case of the kinetic gravity braiding model and the Galileon model, the growth rate $f\sigma_8$ is enhanced in comparison with the ΛCDM case in the same value of $\Omega_{m,0}$ due to enhancement of the effective gravitational constant. For the cosmic growth rate data from the future observation, compatible values of $\Omega_{m,0}$ differ according to the model. Furthermore, values of $\Omega_{m,0}$ can be stringently constrained. Thus, we find the ΛCDM model is distinguishable from modified gravity by combining the growth rate data of Euclid with other observations.

The estimated errors from the observational technology of Euclid are known, but the center value of future observations is not known. If the center value of the cosmic growth rate of future observations is different from that of this chapter, the valid model can differ from that of this chapter. However, the methods in this chapter are useful for distinguishing between the ΛCDM model and modified gravity.

In this chapter, assuming the function $G_5(\phi, X)$ in Horndeski's theory $G_5(\phi, X) = 0$, we compute the linear matter density perturbations for the growth rate. In future work, we will study the model having non-zero function $G_5(\phi, X)$ in Horndeski's theory and investigate the nonlinear effect.

Acknowledgements

This work was supported by a Grant-in-Aid for Scientific Research from the Japan Society for the Promotion of Science (Grant Number 25400264).

Author details

Koichi Hirano

Address all correspondence to: k_hirano@tsuru.ac.jp

Department of Primary Education, Tsuru University, Yamanashi, Japan

References

[1] Riess AG, et al. Observational evidence from supernovae for an accelerating universe and a cosmological constant. The Astronomical Journal. 1998;**116**:1009–1038. DOI: 10.1086/300499

[2] Perlmutter S, et al. Measurements of Ω and Λ from 42 high-redshift supernovae. The Astrophysical Journal. 1999;**517**:565–586. DOI: 10.1086/307221

[3] Ratra B, Peebles PJE. Cosmological consequences of a rolling homogeneous scalar field. Physical Review D. 1988;**37**:3406–3427. DOI: 10.1103/PhysRevD.37.3406

[4] Caldwell RR. A phantom menace? Cosmological consequences of a dark energy component with super-negative equation of state. Physics Letters B. 2002;**545**:23–29. DOI: 10.1016/S0370-2693(02)02589-3

[5] Komiya Z, Kawabata K, Hirano K, Bunya H, Yamamoto N. Galaxy merging and number vs. apparent magnitude relation for the universe with a time-decaying cosmological term. Astronomy & Astrophysics. 2006;**449**:903–916. DOI: 10.1051/0004-6361:20054406

[6] Komiya Z, Kawabata K, Hirano K, Bunya H, Yamamoto N. Constraints on Λ-decaying cosmology from observational point of view. Journal of Korean Astronomical Society. 2005;**38**:157–160. DOI: 10.5303/JKAS.2005.38.2.157

[7] De Felice A, Tsujikawa S. f(R) Theories. Living Reviews in Relativity. 2010;**13**:3. DOI: 10.12942/lrr-2010-3

[8] Hirano K, Komiya Z. Observational tests for oscillating expansion rate of the Universe. Physical Review D. 2010;**82**:103513. DOI: 10.1103/PhysRevD.82.103513

[9] Hirano K, Kawabata K, Komiya Z. Spatial periodicity of galaxy number counts, CMB anisotropy, and SNIa Hubble diagram based on the universe accompanied by a non-minimally coupled scalar field. Astrophysics and Space Science. 2008;**315**:53–72. DOI: 10.1007/s10509-008-9794-7

[10] Hartnett JG, Hirano K. Galaxy redshift abundance periodicity from Fourier analysis of number counts N(z) using SDSS and 2dF GRS galaxy surveys. Astrophysics and Space Science. 2008;**318**:13–24. DOI: 10.1007/s10509-008-9906-4

[11] Dvali G, Gabadadze G, Porrati M. 4D gravity on a brane in 5D Minkowski space. Physics Letters B. 2000;**485**:208–214. DOI: 10.1016/S0370-2693(00)00669-9

[12] Hirano K, Komiya Z. Crossing the phantom divide in extended Dvali-Gabadadze-Porrati gravity. General Relativity and Gravitation. 2010;**42**:2751–2763. DOI: 10.1007/s10714-010-1030-4

[13] Hirano K, Komiya Z. Observational constraints on phantom crossing DGP gravity. International Journal of Modern Physics. 2011;**D20**:1–16. DOI: 10.1142/S0218271811018585

[14] Nicolis A, Rattazzi R, Trincherini E. Galileon as a local modification of gravity. Physical Review D. 2009;**79**:064036. DOI: 10.1103/PhysRevD.79.064036

[15] Chow N, Khoury J. Galileon cosmology. Physical Review D. 2009;**80**:024037. DOI: 10.1103/PhysRevD.80.024037

[16] Silva FP, Koyama K. Self-accelerating universe in Galileon cosmology. Physical Review D. 2009;**80**:121301. DOI: 10.1103/PhysRevD.80.121301

[17] Kobayashi T, Tashiro H, Suzuki D. Evolution of linear cosmological perturbations and its observational implications in Galileon-type modified gravity. Physical Review D. 2010;**81**:063513. DOI: 10.1103/PhysRevD.81.063513

[18] Kobayashi T. Cosmic expansion and growth histories in Galileon scalar-tensor models of dark energy. Physical Review D. 2010;**81**:103533. DOI: 10.1103/PhysRevD.81.103533

[19] Gannouji R, Sami M. Galileon gravity and its relevance to late time cosmic acceleration. Physical Review D. 2010;**82**:024011. DOI: 10.1103/PhysRevD.82.024011

[20] De Felice A, Tsujikawa S. Cosmology of a covariant Galileon field. Physical Review Letters. 2010;**105**:111301. DOI: 10.1103/PhysRevLett.105.111301

[21] De Felice A, Tsujikawa S. Generalized Galileon cosmology. Physical Review D. 2011;**84**: 124029. DOI: 10.1103/PhysRevD.84.124029

[22] Deffayet C, Pujolas O, Sawicki I, Vikman A. Imperfect dark energy from kinetic gravity braiding. Journal of Cosmology and Astroparticle Physics. 2010;**1010**:026. DOI: 10.1088/1475-7516/2010/10/026

[23] Vainshtein AI. To the problem of nonvanishing gravitation mass. Physics Letters B. 1972;**39**:393–394. DOI: 10.1016/0370-2693(72)90147-5

[24] Deffayet C, Esposito-Farese G, Vikman A. Covariant Galileon. Physical Review D. 2009;**79**:084003. DOI: 10.1103/PhysRevD.79.084003

[25] Deffayet C, Deser S, Esposito-Farese G. Generalized Galileons: All scalar models whose curved background extensions maintain second-order field equations and stress tensors. Physical Review D. 2009;**80**:064015. DOI: 10.1103/PhysRevD.80.064015

[26] Kobayashi T, Yamaguchi M, Yokoyama J. Inflation driven by the Galileon field. Physical Review Letters. 2010;**105**:231302. DOI: 10.1103/PhysRevLett.105.231302

[27] Mizuno S, Koyama K. Primordial non-Gaussianity from the DBI Galileons. Physical Review D. 2010;**82**:103518. DOI: 10.1103/PhysRevD.82.103518

[28] Kamada K, Kobayashi T, Yamaguchi M, Yokoyama J. Higgs G inflation. Physical Review D. 2011;**83**:083515. DOI: 10.1103/PhysRevD.83.083515

[29] Nesseris S, De Felice A, Tsujikawa S. Observational constraints on Galileon cosmology. Physical Review D. 2010;**82**:124054. DOI: 10.1103/PhysRevD.82.124054

[30] Kimura R, Yamamoto K. Large scale structures in the kinetic gravity braiding model that can be unbraided. Journal of Cosmology and Astroparticle Physics. 2011;**1104**:025. DOI: 10.1088/1475-7516/2011/04/025

[31] De Felice A, Kase R, Tsujikawa S. Matter perturbations in Galileon cosmology. Physical Review D. 2011;**83**:043515. DOI: 10.1103/PhysRevD.83.043515

[32] Horndeski GW. Second-order scalar-tensor field equations in a four-dimensional space. International Journal of Theoretical Physics. 1974;**10**:363–384. DOI: 10.1007/BF01807638

[33] Charmousis C, Copeland EJ, Padilla A, Saffin PM. General second-order scalar-tensor theory and self-tuning. Physical Review Letters. 2012;**108**:051101. DOI: 10.1103/PhysRevLett.108.051101

[34] Deffayet C, Gao X, Steer DA, Zahariade G. From k-essence to generalized Galileons. Physical Review D. 2011;**84**:064039. DOI: 10.1103/PhysRevD.84.064039

[35] Kobayashi T, Yamaguchi M, Yokoyama J. Generalized G-inflation: Inflation with the most general second-order field equations. Progress of Theoretical Physics. 2011;**126**:511–529. DOI: 10.1143/PTP.126.511

[36] Gleyzes J, Langlois D, Piazza F, Vernizzi F. New class of consistent scalar-tensor theories. Physical Review Letters. 2015;**114**:211101. DOI: 10.1103/PhysRevLett.114.211101

[37] Gleyzes J, Langlois D, Piazza F, Vernizzi F. Exploring gravitational theories beyond Horndeski. Journal of Cosmology and Astroparticle Physics. 2015;**1502**:018. DOI: 10.1088/1475-7516/2015/02/018

[38] Gao X. Unifying framework for scalar-tensor theories of gravity. Physical Review D. 2014;**90**:081501. DOI: 10.1103/PhysRevD.90.081501

[39] Amendola L, et al. Cosmology and fundamental physics with the Euclid satellite. Living Reviews in Relativity. 2013;**16**:6. DOI: 10.12942/lrr-2013-6

[40] Okada H, Totani T, Tsujikawa S. Constraints on f(R) theory and Galileons from the latest data of galaxy redshift surveys. Physical Review D. 2013;**87**:103002. DOI: 10.1103/PhysRevD.87.103002

[41] Dvali G, Turner MS. Dark energy as a modification of the Friedmann equation. 2003. arXiv:astro-ph/0301510

[42] Koyama K, Maartens R. Structure formation in the Dvali-Gabadadze-Porrati cosmological model. Journal of Cosmology and Astroparticle Physics. 2006;**0601**:016. DOI: 10.1088/1475-7516/2006/01/016

[43] Deffayet C. Cosmology on a brane in Minkowski bulk. Physics Letters B. 2001;**502**:199–208. DOI: 10.1016/S0370-2693(01)00160-5

[44] Deffayet C, Dvali G, Gabadadze G. Accelerated universe from gravity leaking to extra dimensions. Physical Review D. 2002;**65**:044023. DOI: 10.1103/PhysRevD.65.044023

[45] Koyama K. Ghosts in the self-accelerating universe. Classical and Quantum Gravity. 2007;**24**:R231–R253. DOI: 10.1088/0264-9381/24/24/R01

[46] Xia JQ. Constraining Dvali-Gabadadze-Porrati gravity from observational data. Physical Review D. 2009;**79**:103527. DOI: 10.1103/PhysRevD.79.103527

[47] De Felice A, Kobayashi T, Tsujikawa S. Effective gravitational couplings for cosmological perturbations in the most general scalar-tensor theories with second-order field equations. Physics Letters B. 2011;**706**:123–133. DOI: 10.1016/j.physletb.2011.11.028

[48] Hirano K. Observational tests of Galileon gravity with growth rate. General Relativity and Gravitation. 2016;**48**:138. DOI: 10.1007/s10714-016-2129-z

[49] Hirano K, Komiya Z, Shirai H. Constraining Galileon gravity from observational data with growth rate. Progress of Theoretical Physics. 2012;**127**:1041–1056. DOI: 10.1143/PTP.127.1041

[50] Hirano K. Neutrino masses from CMB B-mode polarization and cosmic growth rate. International Journal of Modern Physics. 2015;**A30**:1550001. DOI: 10.1142/S0217751X15500013

Chapter 7

The Impact of Baryons on the Large-Scale Structure of the Universe

Weiguang Cui and Youcai Zhang

Additional information is available at the end of the chapter

http://dx.doi.org/10.5772/68116

Abstract

Numerical simulations play an important role in current astronomy researches. Previous dark-matter-only simulations have represented the large-scale structure of the Universe. However, nowadays, hydro-dynamical simulations with baryonic models, which can directly present realistic galaxies, may twist these results from dark-matter-only simulations. In this chapter, we mainly focus on these three statistical methods: power spectrum, two-point correlation function and halo mass function, which are normally used to characterize the large-scale structure of the Universe. We review how these baryon processes influence the cosmology structures from very large scale to quasi-linear and non-linear scales by comparing dark-matter-only simulations with their hydro-dynamical counterparts. At last, we make a brief discussion on the impacts coming from different baryon models and simulation codes.

Keywords: large-scale structure, simulation, statistical methods, hydro-dynamical simulation, baryonic models

1. Introduction

The core of current research foci in cosmology is to interpret the distribution and properties of observed galaxies in the sky and to understand their formation and evolution. The current standard cosmology model—lambda-cold-dark-matter (ΛCDM) paradigm—provides a general explanation for the galaxy formation and evolution: matter is dominated by the dark matter, which only subjects to gravitational interactions; inside dark matter halo that acts as a gravitational potential well, baryonic matters go through a series of physical processes, such as gas cooling, star forming and death with Supernova feedback.

From the cosmic micro background (CMB) observation, such as WMAP [1] and Plank [2], matters occupy roughly one-fourth of total energy of the Universe. The rest comes from dark energy. Dark matter is about 20% of the total energy, while baryons only occupy 5% (see more accurate fractions from [3]). At the CMB time ($z \sim 1100$), matters are distributed nearly 'homogeneous' in the Universe with little fluctuations at small scales. Started from that time, dark matter and baryons are assembled by the gravitational force. They follow a pattern of hierarchical structure formation, where the smaller structures form first, then merge to build massive ones. At very large scale, this structure formation process can be roughly described by the Zel'dovich approximation [4]. However, the formation of structures with gravity is a nonlinear process, which cannot be fully described analytically, especially at small scales. Therefore, building these structures and tracing their evolutions require numerically solving the gravitational equation.

Combining with modern computers, this problem can be solved with numerical methods—N-body simulations, which boosts a new area of research in astronomy. Initially, different numerical methods are developed to simulate only dark matter component, such as particle-mesh (PM), particle-particle/particle-mesh (P3M) and tree-PM algorithms. Dark matter is described numerically by data points/particles that trace a mass element corresponding to a volume element of the early 'homogeneous' universe. Those methods successfully describe the formation of structures by implementing gravitational interactions. Thus, over decades, such simulations have been widely used with little variation in term of physics. Combined with ever decreasing limitations of computer resources and vast improvement in terms of implementations, larger volumes can be explored with increasing resolution to reserve the small-scale information. The properties of cosmology structures (such as cosmic web, voids), halos and even subhaloes are well understood.

However, these simulations cannot give any information of galaxies, which are resident inside dark matter halos.

To connect these theoretical investigation results with observed galaxies, numerous methods are developed. They can be roughly separated into these three approaches:

i. Much simpler approaches are halo occupation distribution (HOD) models, where observed galaxies are assigned to halos by matching both the halo mass and stellar mass functions (e.g. [5–10]). Such methods are tuned to directly link the luminosity functions with halo mass functions. Thus, they are successful in defining the stellar mass halo mass (SMHM) relation. However, this method cannot provide useful individual galaxy information. Furthermore, the scatter in this relation still remains uncertain and difficult to interpret. It can be constrained by comparing specific galaxies, their environments, the inter galactic medium (IGM) and their full formation history.

ii. Other less computationally intensive methods involve applying sub-grid models on the scale of dark matter halos, starting from the accretion of gas by the potential well, following recipes of gas cooling, star forming, supernova (SN) and active galactic nuclei (AGN) feedbacks, at last galaxies are formed and evolved under the halo merger tree. These semi-analytical models (SAMs) have been successfully applied to halo catalogues

http://dx.doi.org/10.5772/68116

extracted from N-body simulations (e.g. [11–17]). Interested readers are encouraging to find the differences between these models (including HOD models) in the nIFTy cosmology comparison project [18] and their following works. As the formation of halos can be traced in the form of halo merger trees, both the formation and interaction of galaxies can be explored within the time frame and the mass resolution explored by the simulation. Although these methods can provide more physical views of galaxy formation, they are still lacking the consistency of co-evolving between baryon and dark matter.

iii. Hydro-dynamical simulations are the only way to overcome the problem faced by SAMs. They can directly solve the physical processes of the baryonic component on top of the dark matter one, which can provide consistent co-evolution with the same gravitational force. These hydro-simulations require complex implementations of baryonic models with gas described either as (a) numerical data points with associated density (smooth particles hydrodynamics (SPH): [19–22], etc.), (b) grid cells fixed in the volume (cells are refined and unrefined as required to explore highest gas density while neglecting low-density regions with nested mesh or adaptive mesh refinement (AMR): [23–25], etc.) or (c) moving mesh (the gas element is associated with a numerical point within a volume defined from the distribution of nearby mesh point through Voronoi tessellation) [26]. The key aspect is the description of the physical processes within these gas elements. These recipes from SAM can be implanted in hydro-dynamical simulations with moderate modifications. However, hydro-dynamical simulation is suffered from its time-consuming computation, with which the numerous free parameters from these sub-grid baryonic models cannot be easily tuned to represent these observational relations as they are in SAM.

Although hydro-dynamical simulations are the heaviest and most time-consuming tool for connecting the dark part with the luminous part in the Universe, they are irreplaceable in investigating/understanding galaxy formations in a full picture. Those HOD and SAM models, which are used to create mock galaxy catalogues, have been quite successfully in reproducing the observational statistical features, such as the two-point correlation functions, luminosity functions, colour distributions and star formation rates. Nevertheless, they are based on the assumption that baryon processes are independent of dark matter halo formation, which is apparently not true [27–29]. As both observation and simulation are becoming more and more accurate, the back reaction of baryons to dark matter cannot be ignored. Thanks to the Morse's law, more and more efforts are being put in these areas in recent years, for example, [30, 31], the OWLS project [32], the EAGLE project [33], the Illustris project [34] and the Horizon-AGN simulation [35] for these cosmological simulations; the NIHAO project [36] and the FIRE project [37] for these zoom-in simulations. Interested readers refer to the Aquila project [38], the AGORA project [39] and the nIFTy cluster comparison project [40–44] for the comparison of different hydro-dynamical simulation codes. A number of studies based on cosmological hydro-dynamic simulations have been recently carried out to analyse in detail the effect of baryonic processes on different properties of the total mass distribution, such as the power spectrum of matter density fluctuations (e.g. [45–48]), the halo correlation functions (e.g. [49, 50]), the halo density profiles (e.g. [29, 51–53]), concentration (e.g. [54, 55]) and shape (e.g. [56, 57]) and the halo mass function (e.g. [30, 31, 58–61]).

In this chapter, we will focus on the impacts of baryons through these comparisons between hydro-dynamical simulations with dark-matter-only simulations and summarize the results in these three aspects: power spectrum, two-point correlation function (2-PCF) and halo mass function (HMF).

2. Chapter

In the last decade, dark-matter-only simulations have been vastly used to theoretically investigate the large-scale structure of the Universe. Through different statistical methods, such as power spectrum, two-point correlation function, halo mass function and so on, the formation and evolution of the large-scale structures have been clearly characterized by those cosmological dark-matter-only simulations. However, the observed Universe can only show the distribution of baryonic matters at such scales. To connect these theoretical understanding with observations of the large-scale structure of the Universe, we need hydro-dynamical simulations, which can provide a consistent evolution driving by the gravitational force for both dark matter and baryons. With these hydro-simulations, we can directly compare simulations with observations through mock techniques (e.g. [62–64]); explore the galaxy formation process in details; correct and improve our understanding of these baryon models, and so on. In this chapter, we only concentrate on one simple question: How do the baryon processes react on dark matter? This is a question, which these simplified analytical models such as HOD and SAM with ad hoc parameters lack the ability to deal with. As baryons occupy only a small fraction of total matter, we are expecting a very weak effect on the dark matter structures. Nevertheless, baryons dominate at small scales such as in galaxies, where the effect cannot be ignored anymore. Thus, we will address this question with different statistical quantities at different scales, which are listed in Sections 2.1, 2.2 and 2.3.

2.1. Power spectrum

The power spectrum P(k) (here k is the comoving wavenumber corresponding to a comoving spatial scale $\lambda = 2\frac{\pi}{k}$) is one of the most powerful and basic statistical measurements that describes the distribution of mass in the Universe, and one of the most thoroughly investigated quantities in modelling the structure formation process. Due to the large amount of data from both observation and simulation, the power spectra are measured mostly using the fast Fourier transform (FFT) technique. Lots of methods are used to improve the accuracy of the measurement for power spectrum especially at nonlinear scale, for example [65, 66]. However, such algorithm improvements cannot deal with the power spectrum changes caused by the physical models.

Using the OWSL simulations, [46] studied the influence of baryonic models on matter power spectrum through a comparison between a dark-matter-only (DMONLY) one and hydro-dynamical simulations (REF and AGN). Starting from the same initial condition, these simulations from various models are listed in **Table 1**.

http://dx.doi.org/10.5772/68116

Simulation	Description
REF	Reference simulation, includes radiative cooling and heating, star forming with the Chabrier (2003) stellar initial mass function and SN feedback with wind mass loading $\eta = 2$ and velocity $v_w = 600$ km s^{-1}
AGN	Includes AGN (in addition to SN feedback)
DMONLY	No baryons, CDM only
DBLIMFV1618	Top-heavy IMF at high pressure, extra SN energy in wind velocity
NOSN	No SN energy feedback
NOSN_NOZCOOL	No SN energy feedback and cooling assumes primordial abundances
NOZCOOL	Cooling assumes primordial abundances
WDENS	Wind mass loading and velocity depend on gas density (SN energy as REF)
WML1V848	Wind mass loading $\eta = 1$, velocity $v_w = 848$ km s^{-1} (SN energy as REF)
WML4	Wind mass loading $\eta = 4$ (twice the SN energy of REF)

Table 1. Different variations on the reference simulation that are compared in the chapter. Unless noted otherwise, all simulations use a set of cosmological parameters derived from the WMAP3 results and use identical initial conditions.

In **Figure 1**, they showed the dimensionless matter power spectrum $\Delta^2(k) = k^3 P(k)/2\pi^2$ on the upper panel and the relative difference to the DMONLY run on the lower panel. It is clear that the contribution of the baryons is significant: they decrease the power by more than 1% for $k \approx 0.8$–5 h Mpc^{-1} by comparing the DMONLY simulation with the REF simulation; the power is greatly increased at smaller scales < 1 h^{-1} Mpc ($k \geq 6$ h Mpc^{-1}). The decreased power is caused by the gas pressure, which smooths the density field relative to that expected from dark matter alone. While, the increased power in the REF simulation is because radiative cooling enables gas to cluster on smaller scales than the dark matter. These results confirm the findings of previous studies, at least qualitatively (e.g. [45, 67, 68]). However, with the AGN feedback, which is required to match observations of groups and clusters, its effect on the power spectrum is enormous: the power is reduced by ≥10% for $k \geq 1$ h Mpc^{-1}. This could be caused by that large amounts of gas are moved to large radii due to the AGN feedback (see also [43]). Because the AGN normally reside in massive and thus strongly clustered objects, the power is suppressed out to scales, where the removed gas can reach.

In **Figure 2**, they showed power spectra from the REF (left panel) and AGN (right panel) simulations at z = 0. As indicated on the top left of each panel, different components are shown by different colour lines. The power spectrum for DMONLY (dashed black lines) is shown as a reference. The power spectra on top row is calculated with $\delta_i \equiv (\rho_i - \overline{\rho_i})/\overline{\rho_i}$. This definition guarantees that all power spectra from component i converge on large scales, thus enabling a straightforward comparison of their shapes. The bottom row, on the other hand, shows the

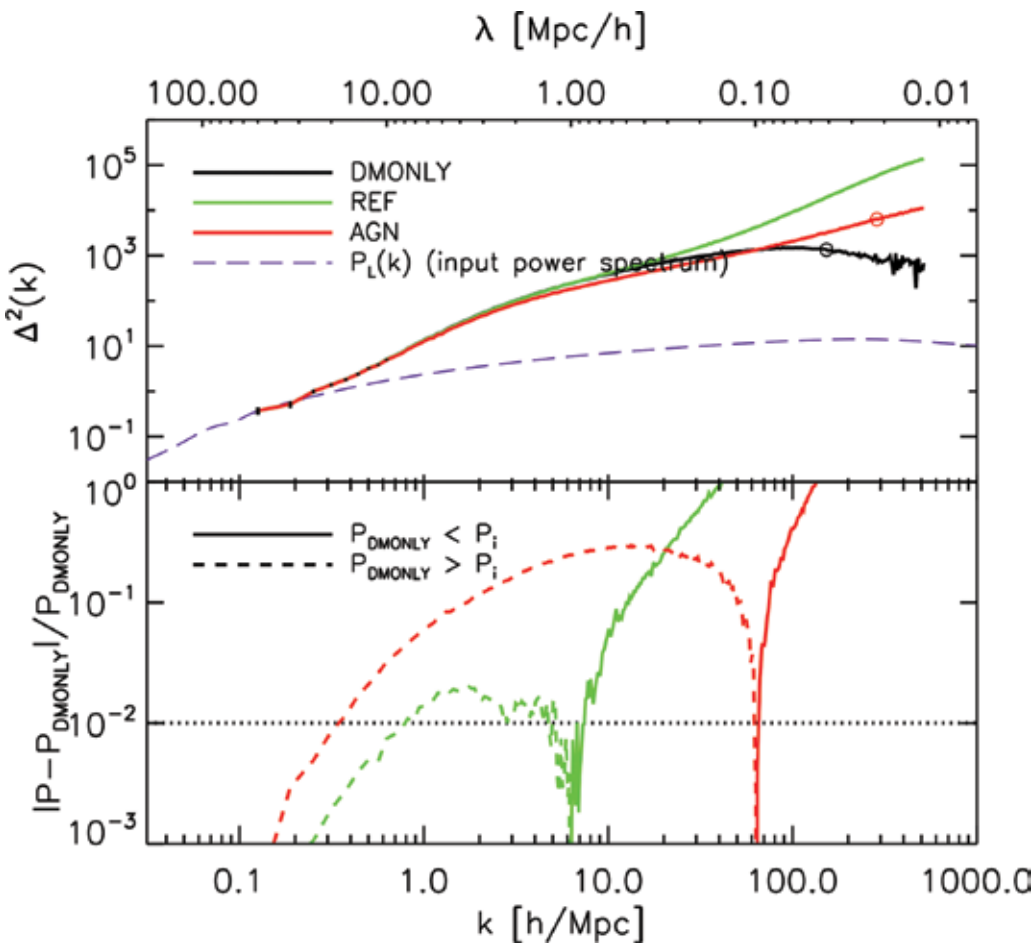

Figure 1. Upper panel: the total matter power spectra of REF (top solid line with highest value at k ~ 500), AGN (middle solid line) and DMONLY (bottom solid line), at redshift z = 0. Lower panel: the power spectrum difference between the two hydro runs and the DMONLY one; solid (dashed) curves indicate that the power is higher (lower) than for DMONLY. The dotted, horizontal line indicates the 1% level. This figure is from Ref. [46]. (note: Please refer to the online publication for a colorful figure).

power spectra of $\delta_i \equiv (\rho_i - \overline{\rho_{tot}})/\overline{\rho_{tot}}$, which allows one to estimate the contributions of different components to the total matter power spectrum. From the top-left panel, the baryonic components trace the dark matter well at the largest scales. However, significant differences exist for $\lambda \leq 10\ h^{-1}$ Mpc. At scales of several hundred kpc and smaller, the difference between the CDM component (also the total component) of the reference simulation and DMONLY exceeds the change between the latter and the analytic models. This is caused by the back-reaction of the baryons on the dark matter. On the bottom left panel of **Figure 2**, it is clear that CDM dominates the power spectrum on large scales. While the contribution of baryons is significant for $\lambda \leq 0.1\ h^{-1}$ kpc and dominates below $0.06\ h^{-1}$ Mpc. The strong small-scale baryonic clustering is a direct consequence of gas cooling and galaxy formation. For the baryonic component, the baryonic power spectrum is dominated by gas component on large scales, which has a flatter power for $\lambda \leq 1\ h^{-1}$ Mpc (corresponding to the virial radii of groups of galaxies) and a slightly

http://dx.doi.org/10.5772/68116

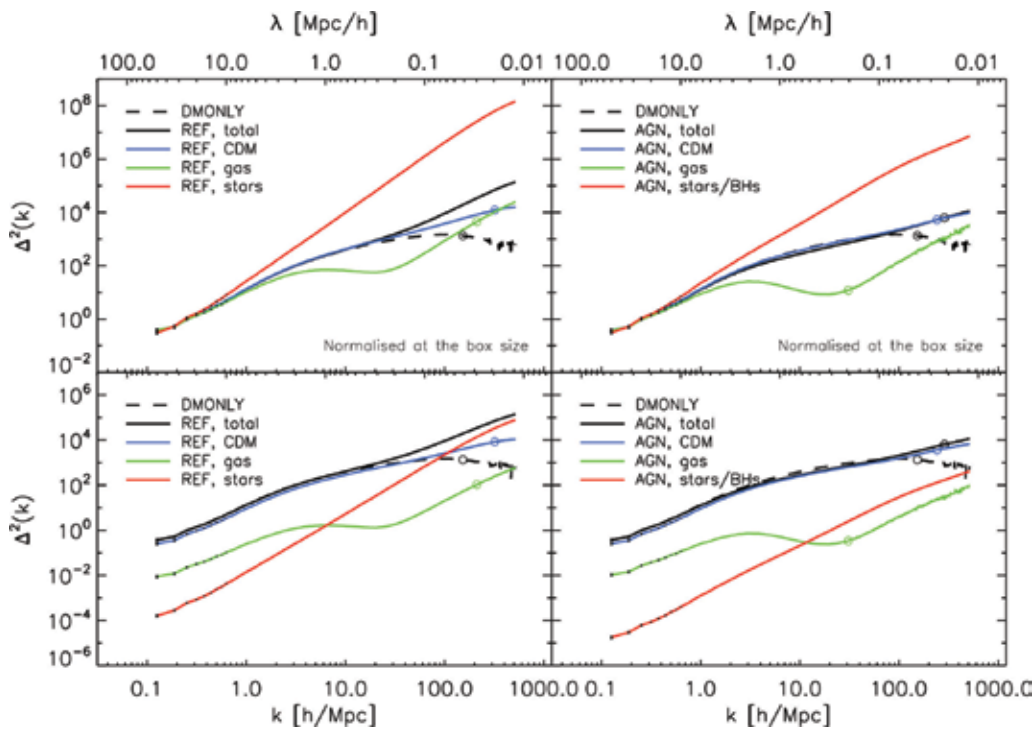

Figure 2. Decomposing the z = 0 total power spectra into the contributions from different components. The left- and right-hand columns show results for REF and AGN. For reference, the power spectrum for DMONLY is shown with dashed black lines. This figure is from Ref. [46].

steeper power again for $\lambda \leq 0.1\ h^{-1}$ Mpc (galaxy scales). While the stellar power spectrum takes control for $\lambda \leq 1\ h^{-1}$ Mpc. The inclusion of AGN feedback greatly impacts the matter power spectrum on a wide range of scales. Comparing the top panels of **Figure 2**, the power in both the gas and stellar components is decreased by AGN feedback for $\lambda \leq 1\ h^{-1}$ Mpc. Through comparing the two bottom panels, the stellar power spectrum is reduced the most: about an order of magnitude on the largest scales; more than two orders of magnitude on the smallest scales. This is an expected result of the AGN feedback, which suppresses star formation, as required to solve the overcooling problem. The gas power spectrum is also dramatically dropped as a consequence of the AGN feedback. The suppression of baryonic structure by AGN feedback also makes the dominant dark matter component of the power spectrum on small scales down.

In addition, different baryonic models investigated in [46] (see more details in their **Figure 3**) showed significant changes of power spectrum at non-linear scale. It means that these baryonic models need very subtle tuning of their parameters to represent the observational results.

2.2. Two-point correlation function

The correlation function, $\xi(r)$, through the calculation of the excess probability to a random distribution to find the possibility of two objects at a given separation r. It is a very useful

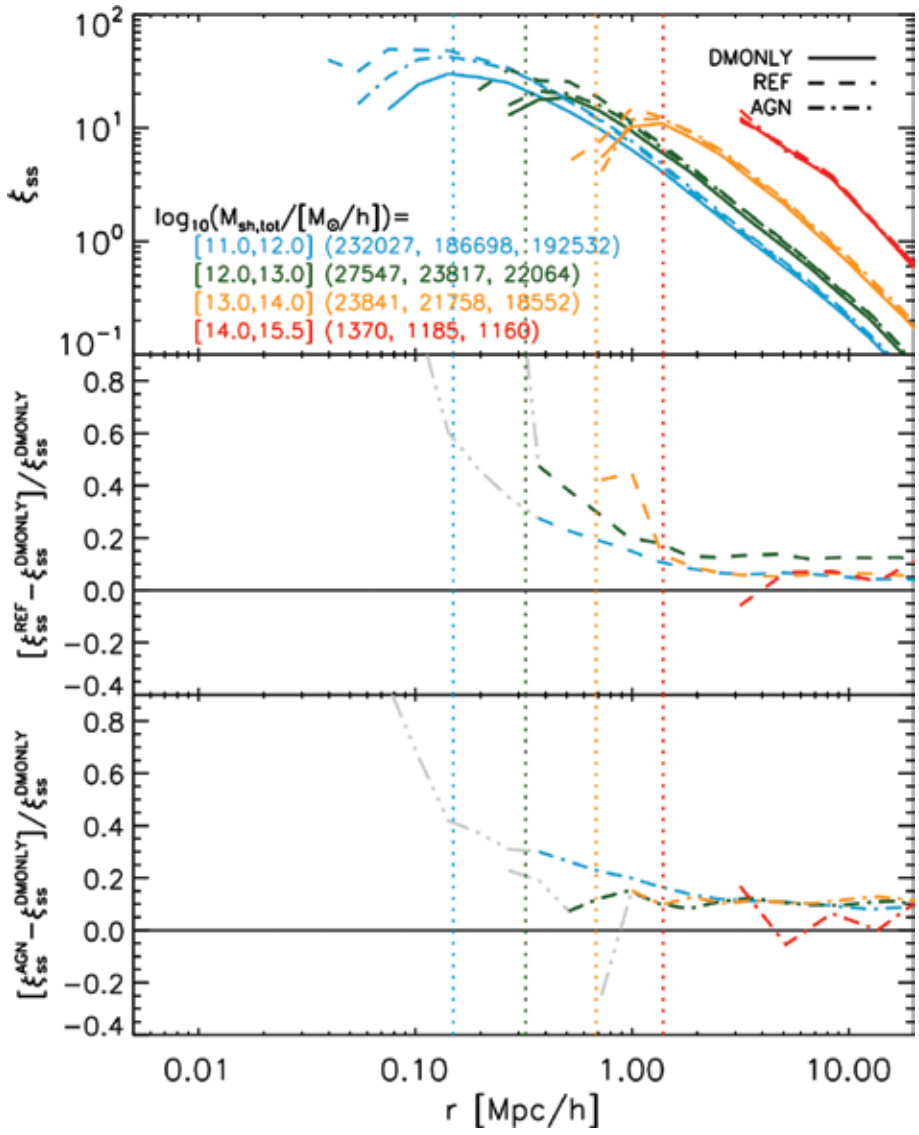

Figure 3. Upper panel: the subhalo autocorrelation function for the three simulations: DMONLY (solid), REF (dashed) and AGN (dot-dashed lines). Different total subhalo masses results are shown with different colours, and the number of objects in each bin is indicated in the legend. The median r_{vir} of the subhaloes are indicated by vertical dotted lines. Middle panel: the relative difference of subhalo clustering between REF and DMONLY. For radii, may biased due to subhalo non-detections, the curves are shown in grey. Bottom: similar to middle panel but for AGN and DMONLY. Both REF and AGN show increased clustering with a stronger effect on smaller scales. This figure is from Ref. [50].

measure of the clustering of these objects as a function of scale. Comparing power spectrum, correlation can provide different views of cosmological structures. Using galaxy as a tracer, it can be used to investigate the clustering of dark matter halo, for example, [69, 70].

Following their work on power spectrum [46], they studied the baryon effect on two-point correlation functions in [50] with the OWLS simualtions. A parallelized brute force approach

http://dx.doi.org/10.5772/68116

is used to calculate the correlation function. Through simple pair counts, $\xi(r)$ can be easily expressed as:

$$\varepsilon_{XY}(r) = \frac{DD_{XY}(r)}{RR_{XY}(r)} - 1. \quad (1)$$

Here, X and Y denote two (not necessarily distinct) sets of objects (e.g. subhaloes and particles or haloes and haloes), $DD_{XY}(r)$ is the number of unique pairs consisting of an object from set X and an object from set Y separated by a distance r, and $RR_{XY}(r)$ is the expected number of pairs at this separation if the positions of the objects in these sets were random.

Subhalos from their simulations are identified by the SUBFIND algorithm [71, 72] inside Friends-of-Friends haloes. Interested readers refer to Ref. [73] for the comparison of different subhalo finding codes, as well as the effect from the included baryonic models. Top panel of **Figure 3** shows the subhalo autocorrelation function, $\xi_{ss}(r)$, for three different simulations: DMONLY, REF and AGN. Different colours indicate different subsamples, selected by the total mass of the subhaloes, $M_{sh,tot}$. The median virial radii of subhaloes in each mass bin are indicated by vertical dotted lines. These radii are similar to the scales at which the subhalo correlation functions for DMONLY turn over. It is clear that subhalo clustering in the dark-matter-only simulation behaves quite differently from that in the baryonic models, especially on small scales ($r \leq 1\ h^{-1}$ Mpc).

The middle and bottom panels show the relative 2-PCF difference between REF (middle)/AGN (bottom) and DMONLY simulation. All subhaloes in the baryonic simulations are typically ~10% more strongly clustered on large scales than their dark-matter-only counterparts. This difference is due to the reduction of subhalo mass caused by baryonic processes. For the larger subhaloes, $10^{13} < M_{sh,tot}/[M_{\odot}/h] < 10^{14}$, this offset is somewhat larger when AGN feedback is included, because supernova feedback alone cannot change the subhalo mass by as much as it can for lower halo masses [74]. The differences between the baryonic and dark-matter-only simulations increase rapidly for $r < 2r_{vir}$, at least for $M_{sh,tot} < 10^{14}\ h^{-1}M_{\odot}$. Subhaloes from the REF simulation show significant larger clustering signal on small scales than from the AGN simulation. This seems to contradict to the results from the previous section. This is because at fixed mass range, subhaloes from the AGN simulation are less compact compared with these from the REF simulation. Due to the additional form of feedback in the AGN run, more material from the centre are pushed into outer radii, which results in a lower concentration. Similar to the subhalo 2-PCF, the galaxy 2-PCFs ($\xi_{gg}(r)$) are very similar between REF and AGN at smaller galaxy mass bins. However, it is worth to note that there is a significant difference at the largest halo mass bin, which is shown in [50].

Figure 4 shows the subhalo-mass 2-PCF, $\xi_{sm}(r)$ on the upper panel; the fractional difference between $\xi^{REF}_{sm}(r)$ and $\xi^{DMONLY}_{sm}(r)$ on the middle panel; the fractional difference between the $\xi^{AGN}_{sm}(r)$ and $\xi^{DMONLY}_{sm}(r)$ on the bottom panel. Again, subhaloes are generally more strongly clustered with matter in the REF and AGN than in DMONLY for scales $r > r_{vir}$. There is also a constant ~5% difference in favour of both REF and AGN simulations on large scales, regardless of subhalo mass. The largest differences can be up to 40% (20% for AGN) higher on intermediate scales for the lowest mass subhaloes. If sufficiently small scales are considered, this difference can be much higher for any subhalo mass. The AGN run does show a stronger

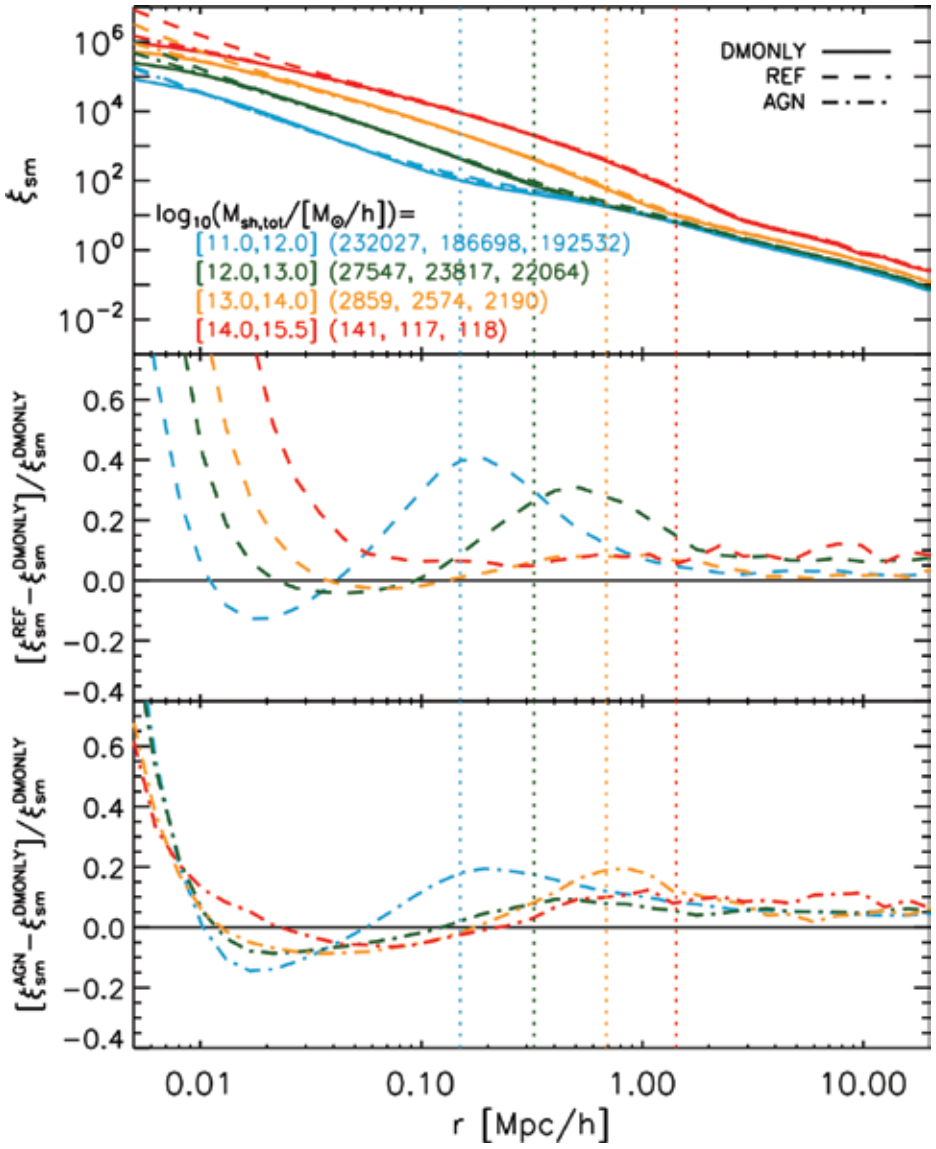

Figure 4. As Figure 3, but now for the subhalo-mass cross-correlation function, $\xi_{sm}(r)$. This figure is from Ref. [50].

decrease in clustering up to scales r ~ 0.1 h^{-1} Mpc. While the $\xi_{sm}(r)$ at smaller mass bins from REF also show similar decrease. It is worth to note the strongly non-monotonic changes of the subhalo-mass 2-PCF between the two baryonic runs and the DMONLY one. This can be caused by the interplay between the changes in both the total subhalo mass and its mass profile. On the one hand, the lowered halo masses in the baryonic simulations tend to increase clustering at fixed mass on all scales. On the other hand, galaxy formation dissipates smoothed gas component and causes the inner halo profile to steepen (increasing clustering on small scales);

the associated feedback causes the outer layers of the halo to expand (decreasing clustering on intermediate scales). These conclusions are proved in Ref. [50] through the 2-PCF $\xi_{sm}(r)$ that have been linked between a baryonic simulation and DMONLY which are selected based on their mass in the latter. This procedure removes the effects of changes in the subhalo masses, leaving only the effect on the mass profiles and the changes in the positions of the subhaloes.

Through these comparisons, the major reason for the increased clustering in the hydro-dynamical simulations is the lowering of the mass of objects due to galaxy formation with strong feedback. However, secondary effects, such as the resulting changes in the dynamics and density profiles of haloes, are also expected to be significant. Interestingly, Despali and Vegetti [75] find that the presence of baryons reduces the number of subhaloes, especially at the low mass end, by different amounts depending on the model. The variations in the subhalo mass function are strongly dependent on those in the halo mass function, which is shifted by the effect of stellar and AGN feedback. We will investigate these effects on the halo mass function in Section 2.3.

2.3. Halo mass function

Different to the power spectrum and 2-PCF, HMF shows another interesting statistic of the large-scale structure. Located on the central structure which connects theory with observation, HMF provides the statistical view of the halo abundance. The two most common methods used for halo identification in simulations are the FoF algorithm (e.g. [76]) and the spherical overdensity (SO) algorithm (e.g. [77]). Interested readers refer to Ref. [78] for the comparison of different halo finding codes.

A series of three versions of cosmological simulations are used in Ref. [31] for their study. Starting from the same initial condition, these simulations share the same number of dark matter particles (1024^3) and gas particles (1024^3) within a simulation box size of 410 h^{-1} Mpc. A first hydro-dynamical simulation includes radiative cooling, star formation and kinetic SN feedback (CSF hereafter), while the second one also includes the effect of AGN feedback (AGN[1] hereafter). As for the DM simulation, it simply replaces the gas particle by collisionless particles, so as to have the same description of the initial density and velocity fields as in the hydro-dynamical simulations.

FoF HMFs are compared on the top panel of **Figure 5** between the three different versions of simulations. While the bottom panel shows the halo number ratio in a mass bin respected to the DM simulation. The baryonic effect from the CSF with respect to the DM case has clear redshift evolution as well as halo mass dependence. From higher redshift to lower redshift, the HMF ratios between the CSF and DM runs decrease from ~1.6 to ~1.1, with a weak increasing trend along halo mass changes. Quite remarkably, including AGN feedback in the baryonic model reduces the difference with respect to the DM-only case: the HMF ratio drops to about

[1]Note that this simulation with AGN feedback is also named AGN. It is different in simulation box, resolution and models from the OWLS AGN simulation shown before.

[2]https://github.com/ilaudy/PIAO.

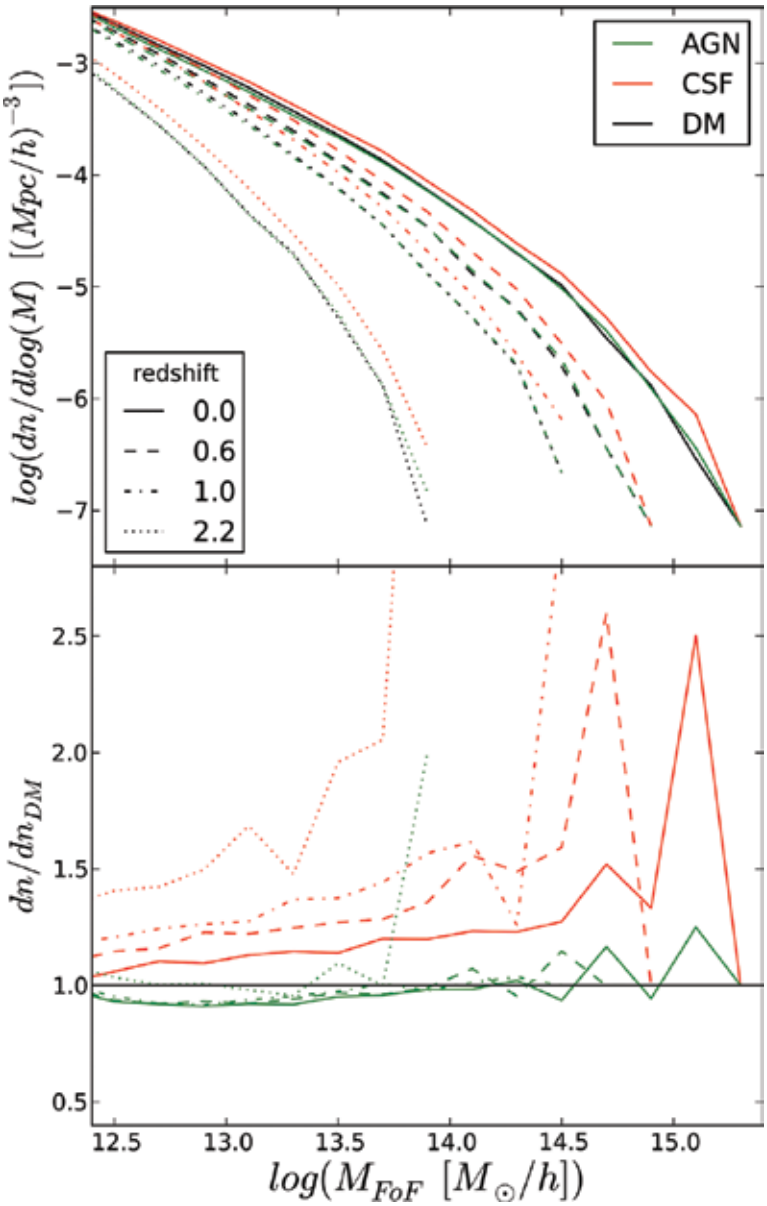

Figure 5. Upper panel: FoF HMFs from DM, CSF and AGN. The HMFs from CSF are always higher than the results from AGN and DM. Different redshifts are shown with different line styles (see the lower left legend for details). Lower panel: relative difference between the HMFs from the hydro-dynamic simulations and from the DM simulation from all four redshifts. This figure is from Ref. [31]. (Please refer to the online publication for a colorful figure).

unity for massive haloes with $M_{FoF} \approx 10^{14}\ h^{-1}\ M_\odot$, while at smaller halo mass it decreases to ~0.9 for $M_{FoF} \approx 10^{13}\ h^{-1}\ M_\odot$. Different to the CSF case, there is no clear redshift evolution in these ratios from z = 1 to 0. At the highest redshift, z = 2.2, this HMF ratio keeps fluctuating around 1. This could be a consequence of the limited statistics of haloes due to the finite box size.

http://dx.doi.org/10.5772/68116

Using the PIAO[2] code [79], the SO haloes are identified with three overdensities Δ_c = 2500, 500 and 200. These HMFs are shown in **Figure 6** from left to right top panels, respectively. While the HMF ratios from the CSF and AGN simulations with respect to the one from DM run are shown in lower panels. Baryons show a larger impact on the HMF at the higher overdensity. With Δ_c = 2500, the ratio between the CSF and DM HMFs shows a redshift evolution ranging from ~1.4 at z = 0 to ~2.5 at z = 2.2, but with no significant dependence on the halo mass. At lower overdensities, the redshift evolution becomes weaker and the differences with respect to the DM case are also reduced. When AGN feedback is included in the hydro-dynamical simulation, the corresponding HMF drops below the HMF from the DM simulation, by an amount that decreases for lower Δ_c values, with no evidence for redshift dependence on the HMF difference. Generally speaking, the baryonic effect on the HMF goes in the same direction, qualitatively independent of whether FoF or SO halo finders are used. However, as expected, quantitative differences between FoF and SO results are found, especially for the AGN case. This is rooted in intrinsic algorithm difference of these halo finder methods (we refer interested readers to Ref. [78] for details).

The three simulations share the same dark matter particles, which have the same progressive identification number (ID). Therefore, we can use the halo from the DM simulation as the reference. The halo in the CSF or AGN simulation is defined as the counterpart of the DM halo, if it includes the largest number of DM particles belonging to the latter. In their paper,

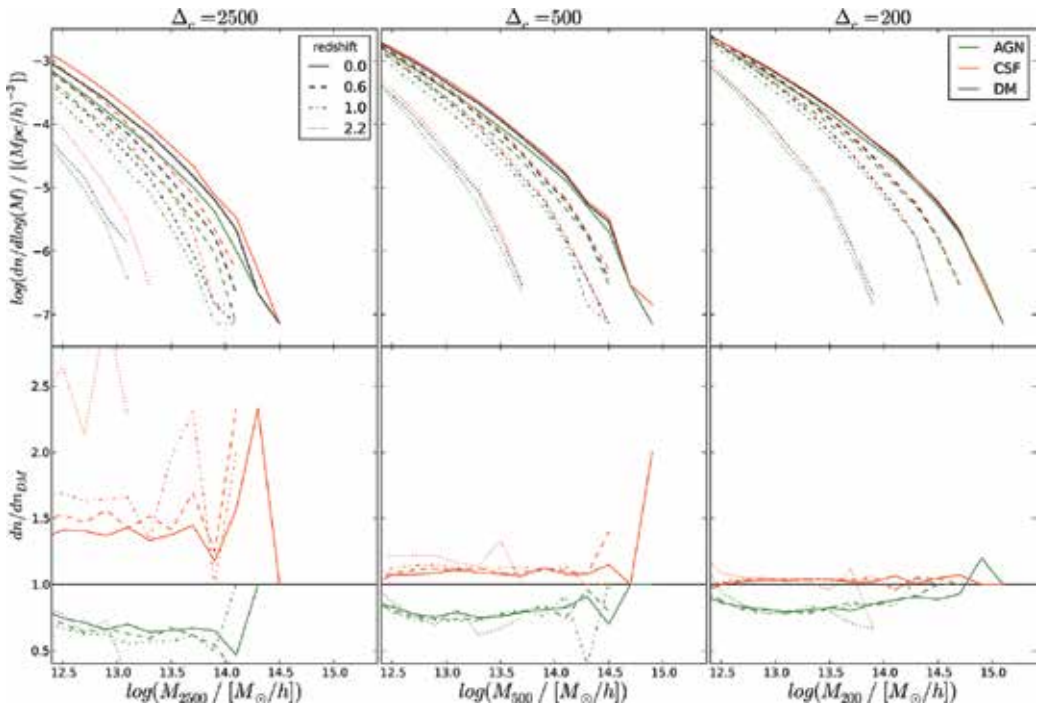

Figure 6. Similar to Figure 5 but for the HMFs of SO haloes. Three different overdensities Δ_c = 2500 (left-hand panel), 500 (middle panel) and 200 (right-hand panel) are used to identify SO haloes. Again, top panels show the SO HMFs, while bottom panels show the HMF difference. This figure is from Ref. [31].

a matching rate is defined as the ratio of matched to total number of dark matter particles in the DM halo. To avoid multiple-to-1 matching from CSF/AGN simulation to the DM one, only haloes with matching rate larger than 0.5 are selected.

Figure 7 shows the halo mass ratios between these matched haloes. Red points indicate the halo pairs, which are coming from CSF and DM simulations, while green points are for the pairs from AGN and DM simulations. The thick lines show the mean value of these data points computed within each mass bin (magenta for CSF and blue for AGN, respectively). For the CSF-DM halo pairs, the increased halo mass is almost independent of redshift. At each redshift, the ratio shows a weak decrease with halo mass, from ~ 1.1 at $M_{500} = 10^{12.5}$ h^{-1} $M_{\odot}$ to ~ 1.05 at $M_{500} > 10^{13.5}$ h^{-1} $M_{\odot}$, then becoming constant. However, for the AGN-DM pairs, the strong AGN feedback makes the ratio go in the opposite direction (decreased halo masses). Thereby, this will result in a decreased HMF, which has been shown in **Figure 6**. There also shows no evidence of redshift evolution for the halo mass ratio, at least below z = 1.0. However, this ratio

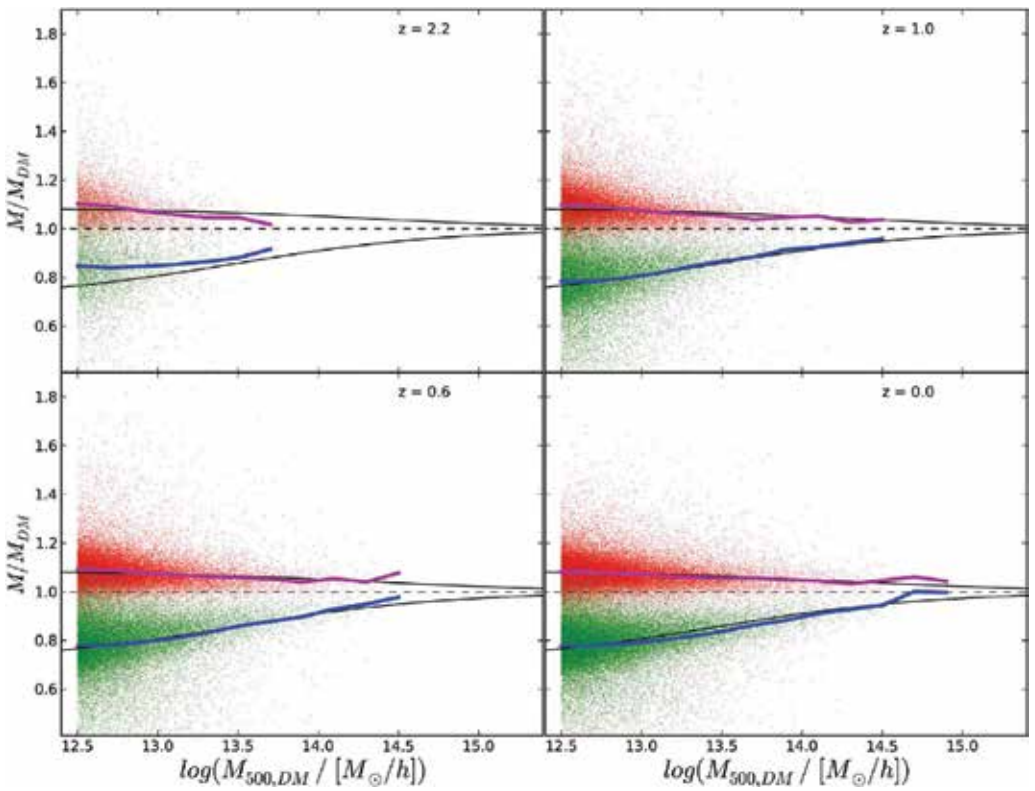

Figure 7. The ratio of masses of matched SO haloes as function of M_{DM} computed for $\Delta_c = 500$ at four different redshifts. Each data point indicates a halo mass ratio between the matched CSF or AGN halo to its corresponding DM one. These misty data points above the horizon dashed lines are normally from CSF run, while lower ones are coming from AGN run. The mean values of these ratios within each mass bin are shown by thick magenta (CSF) and blue lines (AGN), respectively. The solid black lines are the best-fitting results for the mass correction, which are used for the HMF correction in Ref. [31]. This figure is from Ref. [31]. (Please refer to the online publication for a colorful figure).

http://dx.doi.org/10.5772/68116

shows a strong dependence on the halo mass, which increases from ~ 0.8 at $M_{500} = 10^{12.5}\ h^{-1}\ M_{\odot}$ to ~ 1 for the most massive haloes found in their simulation box.

2.4. Summary

Stepping from dark-matter-only to hydro-dynamical simulations allows us to view the galaxy formation and evolution in the Universe in a self-consistent and realistic way. Hydro-dynamical simulations estimate tight connections between theoretical and observational researches, therefore providing a perfect test lab for examining theories. Through these comparisons between state-of-the-art hydro-dynamical simulations and dark-matter-only ones, we summarized the recent findings of baryonic effects on the large-scale structure of the Universe by showing the changes on power spectrum, two-point correlation function and halo mass functions:

1. Power spectrum. There is a decreased power (1%) at k ~ 0.8–5 h Mpc^{-1} (~8–1 h^{-1} Mpc). At smaller scales (<1 h^{-1} Mpc or k > 6 h Mpc^{-1}), the power rises quickly far above the dark-matter-only simulations because of the baryon processes. However, this increase is reduced by >10% when the AGN feedback is switched on. Power spectra for individual component reveal at which scales they are responsible for these changes: cold dark matter dominates the power spectrum on large scales; gas component contributes mildly over all scales; stellar component is the reason for the high power at small scales.
2. Two-point correlation function. The correlation functions for subhalo are typically ~10% higher in hydro-dynamical simulations than in dark-matter-only ones. While this change is significantly larger at smaller scale. With AGN feedback on, the differences are slightly higher at large scale and lower at small scale compared to the reference one without AGN feedback. Subhaloes are also strongly clustered with matter in the baryonic simulations than in the dark-matter-only ones.
3. Halo mass function. The halo mass functions are also higher from hydro-dynamical simulations than from dark-matter-only simulations. These differences depend on redshifts, halo mass ranges and halo finding methods. With AGN feedback, the halo mass functions are normally lower than their counterparts from the dark-matter-only simulations. These changes are vividly indicated by the variances of the halo masses, which are matched one to one between these simulations.

Besides these statistics methods investigated in upper paragraphs, baryonic processes can also leave an impact on cosmological structures, such as cosmic webs, sheets and voids. Using the EAGLE simulation, Paillas et al. [80] studied the effect of baryons on void statistics. They found that the dark-matter-only simulation produces 24% more voids than the hydro-dynamical one, but this difference comes mainly from voids with radii smaller than 5 Mpc. They claimed that there are no significant differences in the density profiles between voids in hydro-dynamical and its dark-matter-only counterpart.

However, as we already see, all these results strongly depend on the included baryonic models and simulation codes. There is no guarantee of a perfect model yet, especially that most of the

implanted baryonic models are based on observational relations. Starting from the same initial condition of a galaxy cluster, the recent nIFTy project [40–44] has made vast comparisons between different simulation codes as well as baryonic models included in them. There is a good agreement between these simulation codes for the dark-matter-only runs. A larger disagreement is shown between the classic SPH codes and mesh/modern SPH/moving mesh codes for the non-radiative hydro-dynamical runs. In the full physics runs, the largest difference is lying between the runs with AGN feedback and the ones without AGN feedback. However, even inside both families, there are a lot of variances between different simulation codes.

To simulate the observed Universe, more efforts are needed to understand the sub-grid baryonic models, such as their parameter choice, resolution and method dependence. To understand and pin down these sub-grid models, we need direct and detailed comparisons between the simulation results and observational ones. Thus, a one-to-one comparison is much helpful than the statistical relations. These constrained simulation projects aiming to represent the observed Universe, the ELUCID project [81–83], the CLUES project [84], [85] and the APOSTLE project [86], point to the direction of future simulation studies.

Acknowledgements

The authors are particularly grateful to Dr Marcel van Daalen for freely using the figures from his papers [46] and [50]. W.C. would like to thank his wife Ms Yufang Liu for her kind help. Y.Z. acknowledges the support from the 973 Program (No. 2015CB857002).

Author details

Weiguang Cui[1]* and Youcai Zhang[2]

*Address all correspondence to: cuiweiguang@gmail.com

1 Dover Court, Western Australia, Australia

2 ShangHai Astronomical Observatory, Shanghai, China

References

[1] D. N. Spergel *et al*., "First year Wilkinson microwave anisotropy probe (WMAP) observations: determination of cosmological parameters," *Astrophys. J. Suppl. Ser*., Vol. 148, pp. 175–194, 2003.

[2] Planck Collaboration, "Planck 2013 results. I. Overview of products and scientific results," *Astron. Astrophys*., Vol. 571, pp. 1–44, 2013.

[3] P. Collaboration, "Planck 2015 results. XIII. Cosmological parameters," *ArXiv e-prints*, Vol. 1502, pp. 1–67, 2015.

[4] Y. B. Zel'dovich, "Gravitational instability: an approximate theory for large density perturbations," *Astron. Astrophys*., Vol. 5, pp. 84–89, 1970.

[5] Y. P. Jing, H. J. Mo, and G. Boerner, "Spatial correlation function and pairwise velocity dispersion of galaxies: CDM models versus the Las Campanas survey," *Astrophys. J*., Vol. 494, Issue 1, pp. 1–12, 1997.

[6] Y. P. Jing, G. Boerner, and Y. Suto, "Spatial correlation functions and the pairwise peculiar velocity dispersion of galaxies in the PSCz survey: implications for the galaxy biasing in cold dark matter models," *Astrophys. J*., Vol. 564, Issue 1, pp. 15–22, 2001.

[7] X. Yang, H. J. Mo, and F. C. van den Bosch, "Constraining galaxy formation and cosmology with the conditional luminosity function of galaxies," *Mon. Not. R. Astron. Soc*., Vol. 339, Issue 4, pp. 1057–1080, 2002.

[8] F. C. van den Bosch *et al*., "Towards a concordant model of halo occupation statistics," *Mon. Not. R. Astron. Soc*., Vol. 376, Issue 2, pp. 841–860, 2006.

[9] A. Rodríguez-Puebla, V. Avila-Reese, X. Yang, S. Foucaud, N. Drory, and Y. P. Jing, "The stellar-to-halo mass relation of local galaxies segregates by color," *Astrophys. J*., Vol. 799, Issue 2, p. 130, 2015.

[10] Y. Zu and R. Mandelbaum, "Mapping stellar content to dark matter halos using galaxy clustering and galaxy-galaxy lensing in the SDSS DR7," *Mon. Not. R. Astron. Soc*., Vol. 454, Issue 2, pp. 1161–1191, 2015.

[11] S. D. M. White and C. S. Frenk, "Galaxy formation through hierarchical clustering," *Astrophys. J*., Vol. 379, p. 52, 1991.

[12] H. J. Mo and S. D. M. White, "An analytic model for the spatial clustering of dark matter haloes," *Mon. Not. R. Astron. Soc*., Vol. 282, Issue 2, pp. 347–361, 1995.

[13] G. De Lucia, G. Kauffmann, and S. D. M. White, "Chemical enrichment of the intracluster and intergalactic medium in a hierarchical galaxy formation model," *Mon. Not. R. Astron. Soc*., Vol. 349, Issue 3, pp. 1101–1116, 2003.

[14] D. J. Croton *et al*., "The many lives of active galactic nuclei: cooling flows, black holes and the luminosities and colours of galaxies," *Mon. Not. R. Astron. Soc*., Vol. 365, Issue 1, pp. 11–28, 2005.

[15] X. Kang, Y. P. Jing, H. J. Mo, and G. Boerner, "Semi-analytical model of galaxy formation with high-resolution N-body simulations," *Astrophys. J*., Vol. 631, Issue 1, pp. 21–40, 2004.

[16] C. M. Baugh and C. M., "A primer on hierarchical galaxy formation: the semi-analytical approach," *Reports Prog. Physics*, Vol. 69, Issue 12, pp. 3101–3156, 2006.

[17] Q. Guo *et al*., "From dwarf spheroidals to cDs: simulating the galaxy population in a LCDM cosmology," *Mon. Not. R. Astron. Soc*., Vol. 413, Issue 1, pp. 101–131, 2010.

[18] A. Knebe *et al*., "nIFTy Cosmology: comparison of galaxy formation models," *Mon. Not. R. Astron. Soc*., Vol. 451, Issue 4, pp. 4029–4059, 2015.

[19] V. Springel, N. Yoshida, and S. D. M. White, "GADGET: a code for collisionless and gasdynamical cosmological simulations," *New Astron.*, Vol. 6, Issue 2, pp. 79–117, 2000.

[20] V. Springel and Volker, "The cosmological simulation code GADGET-2," *Mon. Not. R. Astron. Soc.*, Vol. 364, Issue 4, pp. 1105–1134, 2005.

[21] J. Wadsley, J. Stadel, and T. Quinn, "Gasoline: an adaptable implementation of TreeSPH," *New Astron.*, Vol. 9, Issue 2, pp. 137–158, 2003.

[22] A. M. Beck *et al.*, "An improved SPH scheme for cosmological simulations," *Mon. Not. R. Astron. Soc.*, Vol. 455, Issue 2, pp. 2110–2130, 2015.

[23] A. V. Kravtsov, A. A. Klypin, and A. M. Khokhlov, "Adaptive refinement tree—a new high-resolution N-body code for cosmological simulations," *Astrophys. J. Suppl. Ser.*, Vol. 111, Issue 1, pp. 73–94, 1997.

[24] R. Teyssier, "Cosmological hydrodynamics with adaptive mesh refinement: a new high resolution code called RAMSES," *Astron. Astrophys.*, Vol. 385, pp. 337–364, 2001.

[25] G. L. The Enzo Collaboration *et al.*, "Enzo: an adaptive mesh refinement code for astrophysics," *Astrophys. J. Suppl.*, Vol. 211, Issue 2, Artic. id. 19, 52 pp. (2014), 2013.

[26] V. Springel and Volker, "E pur si muove: galiliean-invariant cosmological hydrodynamical simulations on a moving mesh," *Mon. Not. R. Astron. Soc.*, Vol. 401, Issue 2, pp. 791–851, 2009.

[27] G. F. Lewis, A. Babul, N. Katz, T. Quinn, L. Hernquist, and D. H. Weinberg, "The effects of gas dynamics, cooling, star formation, and numerical resolution in simulations of cluster formation," *Astrophys. J.*, Vol. 536, Issue 2, pp. 623–644, 1999.

[28] O. Y. Gnedin, A. V. Kravtsov, A. A. Klypin, and D. Nagai, "Response of dark matter halos to condensation of baryons: cosmological simulations and improved adiabatic contraction model," *Astrophys. J.*, Vol. 616, Issue 1, pp. 16–26, 2004.

[29] W. P. Lin, Y. P. Jing, S. Mao, L. Gao, and I. G. McCarthy, "The influence of baryons on the mass distribution of dark matter halos," *Astrophys. J.*, Vol. 651, Issue 2, pp. 636–642, 2006.

[30] W. Cui, S. Borgani, K. Dolag, G. Murante, and L. Tornatore, "The effects of baryons on the halo mass function," *Mon. Not. R. Astron. Soc.*, Vol. 423, Issue 3, pp. 2279–2287, 2011.

[31] W. Cui, S. Borgani, and G. Murante, "The effect of AGN feedback on the halo mass function," *Mon. Not. R. Astron. Soc.*, Vol. 441, Issue 2, pp. 1769–1782, 2014.

[32] J. Schaye *et al.*, "The physics driving the cosmic star formation history," *Mon. Not. R. Astron. Soc.*, Vol. 402, Issue 3, pp. 1536–1560, 2009.

[33] J. Schaye *et al.*, "The EAGLE project: simulating the evolution and assembly of galaxies and their environments," *Mon. Not. R. Astron. Soc.*, Vol. 446, Issue 1, 2015.

[34] M. Vogelsberger *et al.*, "Properties of galaxies reproduced by a hydrodynamic simulation," *Nature*, Vol. 509, Issue 7499, pp. 177–182, 2014.

[35] Y. Dubois *et al*., "The Horizon-AGN simulation: morphological diversity of galaxies promoted by AGN feedback," *Mon. Not. R. Astron. Soc*., Vol. 463, Issue 4, pp. 3948–3964, 2016.

[36] L. Wang *et al*., "NIHAO project I: reproducing the inefficiency of galaxy formation across cosmic time with a large sample of cosmological hydrodynamical simulations," *Mon. Not. R. Astron. Soc*., Vol. 454, Issue 1, pp. 83–94, 2015.

[37] P. F. Hopkins *et al*., "Galaxies on FIRE (feedback in realistic environments): stellar feedback explains cosmologically inefficient star formation," *Mon. Not. R. Astron. Soc*., Vol. 445, Issue 1, pp. 581–603, 2013.

[38] C. Scannapieco *et al*., "The aquila comparison project: the effects of feedback and numerical methods on simulations of galaxy formation," *Mon. Not. R. Astron. Soc*., Vol. 423, Issue 2, pp. 1726–1749, 2011.

[39] J. Kim *et al*., "The AGORA high-resolution galaxy simulations comparison project," *Astrophys. J. Suppl*., Vol. 210, Issue 1, Artic. id. 14, 20 pp. (2014), 2013.

[40] F. Sembolini *et al*., "nIFTy galaxy cluster simulations I: dark matter & non-radiative models," *Mon. Not. R. Astron. Soc*., Vol. 457, Issue 4, pp. 4063–4080, 2015.

[41] F. Sembolini *et al*., "nIFTy galaxy cluster simulations II: radiative models," *Mon. Not. R. Astron. Soc*., Vol. 459, Issue 3, pp. 2973–2991, 2015.

[42] P. J. Elahi *et al*., "nIFTY galaxy cluster simulations III: the similarity & diversity of galaxies & subhaloes," *Mon. Not. R. Astron. Soc*., Vol. 458, Issue 1, pp. 1096–1116, 2015.

[43] W. Cui *et al*., "nIFTy galaxy cluster simulations IV: quantifying the influence of baryons on halo properties," *Mon. Not. R. Astron. Soc*., Vol. 458, Issue 4, pp. 4052–4073, 2016.

[44] J. Arthur *et al*., "nIFTy galaxy cluster simulations V: investigation of the cluster infall region," *Mon. Not. R. Astron. Soc*., Vol. 464, Issue 2, pp. 2027–2038, 2016.

[45] D. H. Rudd, A. R. Zentner, and A. V. Kravtsov, "Effects of baryons and dissipation on the matter power spectrum," *Astrophys. J*., Vol. 672, Issue 1, Artic. id. 19–32, pp. (2008), 2007.

[46] M. P. van Daalen, J. Schaye, C. M. Booth, and C. D. Vecchia, "The effects of galaxy formation on the matter power spectrum: a challenge for precision cosmology," *Mon. Not. R. Astron. Soc*., Vol. 415, Issue 4, pp. 3649–3665, 2011.

[47] L. Casarini *et al*., "Tomographic weak lensing shear spectra from large N-body and hydrodynamical simulations," *Astron. Astrophys*., Vol. 542, id.A126, 13 pp., 2012.

[48] M. P. van Daalen and J. Schaye, "The contributions of matter inside and outside of haloes to the matter power spectrum," *Mon. Not. R. Astron. Soc*., Vol. 452, Issue 3, 2015.

[49] X. Zhu and J. Pan, "Influence of baryons on spatial distribution of matter: higher order correlation functions," *Res. Astron. Astrophys*., Vol. 12, Issue 12, pp. 1603–1612, 2012.

[50] M. P. van Daalen, J. Schaye, I. G. McCarthy, C. M. Booth, and C. D. Vecchia, "The impact of baryonic processes on the two-point correlation functions of galaxies, subhaloes and matter," *Mon. Not. R. Astron. Soc*., Vol. 440, Issue 4, pp. 2997–3010, 2014.

[51] A. R. Duffy, J. Schaye, S. T. Kay, C. D. Vecchia, R. A. Battye, and C. M. Booth, "Impact of baryon physics on dark matter structures: a detailed simulation study of halo density profiles," *Mon. Not. R. Astron. Soc.*, Vol. 405, Issue 4, pp. 2161–2178, 2010.

[52] M. Killedar, S. Borgani, M. Meneghetti, K. Dolag, D. Fabjan, and L. Tornatore, "How baryonic processes affect strong lensing properties of simulated galaxy clusters," *Mon. Not. R. Astron. Soc.*, Vol. 427, Issue 1, pp. 533–549, 2012.

[53] M. Schaller *et al.*, "Baryon effects on the internal structure of LCDM halos in the EAGLE simulations," *Mon. Not. R. Astron. Soc.*, Vol. 451, Issue 2, pp. 1247–1267, 2014.

[54] S. Bhattacharya, S. Habib, K. Heitmann, and A. Vikhlinin, "Dark matter halo profiles of massive clusters: theory vs. observations," *Astrophys. J.*, Vol. 766, Issue 1, Artic. id. 32, 16 pp. (2013), 2011.

[55] E. Rasia, S. Borgani, S. Ettori, P. Mazzotta, and M. Meneghetti, "On the discrepancy between theoretical and X-ray concentration-mass relations for galaxy clusters," *Astrophys. J.*, Vol. 776, Issue 1, Artic. id. 39, 14 pp. (2013), 2013.

[56] A. Knebe, N. I. Libeskind, S. R. Knollmann, G. Yepes, S. Gottloeber, and Y. Hoffman, "The impact of baryonic physics on the shape and radial alignment of substructures in cosmological dark matter haloes," *Mon. Not. R. Astron. Soc.*, Vol. 405, Issue 2, pp. 1119–1128, 2010.

[57] W. Cui *et al.*, "On the dynamical state of galaxy clusters: insights from cosmological simulations II," *Mon. Not. R. Astron. Soc.*, Vol. 464, Issue 2, pp. 2502–2510, 2016.

[58] R. Stanek, D. Rudd, and A. E. Evrard, "The effect of gas physics on the halo mass function," *Mon. Not. R. Astron. Soc. Lett.*, Vol. 394, Issue 1, pp. L11–L15, 2008.

[59] S. J. Cusworth, S. T. Kay, R. A. Battye, and P. A. Thomas, "Impact of baryons on the cluster mass function and cosmological parameter determination," *Mon. Not. R. Astron. Soc.*, Vol. 439, Issue 3, pp. 2485–2493, 2013.

[60] D. Martizzi, I. Mohammed, R. Teyssier, and B. Moore, "The biasing of baryons on the cluster mass function and cosmological parameter estimation," *Mon. Not. R. Astron. Soc.*, Vol. 440, Issue 3, pp. 2290–2299, 2013.

[61] T. Sawala *et al.*, "The abundance of (not just) dark matter haloes," *Mon. Not. R. Astron. Soc.*, Vol. 431, Issue 2, pp. 1366–1382, 2012.

[62] W. Cui, V. Springel, X. Yang, G. De Lucia, and S. Borgani, "Properties of fossil groups in cosmological simulations and galaxy formation models," *Mon. Not. R. Astron. Soc.*, Vol. 416, Issue 4, pp. 2997–3008, 2011.

[63] W. Cui *et al.*, "Characterizing diffused stellar light in simulated galaxy clusters," *Mon. Not. R. Astron. Soc.*, Vol. 437, Issue 1, pp. 816–830, 2013.

[64] W. Cui *et al.*, "How does our choice of observable influence our estimation of the centre of a galaxy cluster? Insights from cosmological simulations," *Mon. Not. R. Astron. Soc.*, Vol. 456, Issue 3, pp. 2566–2575, 2015.

[65] W. Cui, L. Liu, X. Yang, Y. Wang, L. Feng, and V. Springel, "An ideal mass assignment scheme for measuring the power spectrum with FFTs," *Astrophys. J.*, Vol. 687, Issue 2, Artic. id. 738–744, pp. (2008), 2008.

[66] S. Colombi, A. H. Jaffe, D. Novikov, and C. Pichon, "Accurate estimators of power spectra in N-body simulations," *Mon. Not. R. Astron. Soc.*, Vol. 393, Issue 2, pp. 511–526, 2008.

[67] Y. P. Jing, P. Zhang, W. P. Lin, L. Gao, and V. Springel, "The influence of baryons on the clustering of matter and weak lensing surveys," *Astrophys. J.*, Vol. 640, Issue 2, pp. L119–L122, 2005.

[68] T. Guillet, R. Teyssier, and S. Colombi, "The effect of baryons on the variance and the skewness of the mass distribution in the universe at small scales," *Mon. Not. R. Astron. Soc.*, Vol. 405, Issue 1, pp. 525–534, 2009.

[69] X. Yang, H. J. Mo, F. C. van den Bosch, and Y. P. Jing, "The two-point correlation of galaxy groups: probing the clustering of dark matter haloes," *Mon. Not. R. Astron. Soc.*, Vol. 357, Issue 2, pp. 608–618, 2004.

[70] X. Yang, H. J. Mo, F. C. van den Bosch, S. M. Weinmann, C. Li, and Y. P. Jing, "The cross-correlation between galaxies and groups: probing the galaxy distribution in and around dark matter haloes," *Mon. Not. R. Astron. Soc.*, Vol. 362, Issue 2, pp. 711–726, 2005.

[71] V. Springel, S. White, G. Tormen, and G. Kauffmann, "Populating a cluster of galaxies—I. Results at z = 0," *Mon. Not. R. Astron. Soc.*, Vol. 328, Issue 3, pp. 726–750, 2000.

[72] K. Dolag, S. Borgani, G. Murante, and V. Springel, "Substructures in hydrodynamical cluster simulations," *Mon. Not. R. Astron. Soc.*, Vol. 399, Issue 2, pp. 497–514, 2008.

[73] A. Knebe *et al.*, "Structure finding in cosmological simulations: the state of affairs," *Mon. Not. R. Astron. Soc.*, Vol. 435, Issue 2, pp. 1618–1658, 2013.

[74] M. Velliscig *et al.*, "The impact of galaxy formation on the total mass, mass profile and abundance of haloes," *Mon. Not. R. Astron. Soc.*, Vol. 442, Issue 3, pp. 2641–2658, 2014.

[75] G. Despali and S. Vegetti, "The impact of baryonic physics on the subhalo mass function and implications for gravitational lensing," *eprint arXiv:1608.06938*, p. 16, 2016.

[76] M. Davis, G. Efstathiou, C. S. Frenk, and S. D. M. White, "The evolution of large-scale structure in a universe dominated by cold dark matter," *Astrophys. J.*, Vol. 292, pp. 371, 1985.

[77] C. Lacey and S. Cole, "Merger rates in hierarchical models of galaxy formation. II: comparison with N-body simulations," *Mon. Not. R. Astron. Soc.*, Vol. 271, NO. 3/DEC1, P. 676, 1994.

[78] A. Knebe *et al.*, "Haloes gone MAD: the halo-finder comparison project," *Mon. Not. R. Astron. Soc.*, Vol. 415, Issue 3, pp. 2293–2318, 2011.

[79] W. Cui and Weiguang, "PIAO: python spherIcAl overdensity code," *Astrophys. Source Code Libr. Rec. ascl1412.007*, 2014.

[80] E. Paillas, C. D. P. Lagos, N. Padilla, P. Tissera, J. Helly, and M. Schaller, "Baryon effects on void statistics in the EAGLE simulation," *eprint arXiv:1609.00101*, Aug. 2016.

[81] H. Wang, H. J. Mo, X. Yang, and F. C. van den Bosch, "Reconstructing the initial density field of the local universe: method and test with mock catalogs," *Astrophys. J.*, Vol. 772, Issue 1, Artic. id. 63, 19 pp. (2013), 2013.

[82] H. Wang, H. J. Mo, X. Yang, Y. P. Jing, and W. P. Lin, "ELUCID—exploring the local universe with reconstructed initial density field I: Hamiltonian Markov chain Monte Carlo method with particle mesh dynamics," *Astrophys. J.*, Vol. 794, Issue 1, Artic. id. 94, 21 pp. (2014), 2014.

[83] H. Wang *et al.*, "ELUCID—exploring the local universe with reconstructed initial density field III: constrained simulation in the SDSS volume," *Astrophys. J.*, Vol. 831, Issue 2, Artic. id. 164, 18 pp. (2016), 2016.

[84] S. Gottloeber, Y. Hoffman, and G. Yepes, "Constrained local universe simulations (CLUES)," arXiv:1005.2687, May 2010.

[85] E. Carlesi *et al.*, "Constrained local universe simulations: a local group factory," *Mon. Not. R. Astron. Soc.*, Vol. 458, Issue 1, pp. 900–911, 2016.

[86] T. Sawala *et al.*, "The APOSTLE simulations: solutions to the local group's cosmic puzzles," *Mon. Not. R. Astron. Soc.*, Vol. 457, Issue 2, pp. 1931–1943, 2015.

Chapter 8

Cosmological Consequences of a Quantum Theory of Mass and Gravity

Brian Albert Robson

Additional information is available at the end of the chapter

http://dx.doi.org/10.5772/intechopen.68410

Abstract

The understanding of several cosmological problems that has been obtained from the development of the Generation Model (GM) of particle physics is presented. The GM is presented as a viable simpler alternative to the Standard Model (SM). The GM considers the elementary particles of the SM to be composite particles and this substructure leads to new paradigms for both mass and gravity, which in turn lead to an understanding of several cosmological problems: the matter-antimatter asymmetry of the universe, dark matter and dark energy. The GM provides a unified origin of mass and the composite nature of the leptons and quarks of the GM leads to a solution of the cosmological matter-antimatter asymmetry problem. The GM also provides a new universal quantum theory of gravity in terms of a residual interaction of a strong color-like interaction, analogous to quantum chromodynamics (QCD). This very weak residual interaction has two important properties: antiscreening and finite range, that provide an understanding of dark matter and dark energy, respectively, in the universe.

Keywords: generation model, gravity, dark matter, MOND theory, dark energy, antimatter, big bang

1. Introduction

The main purpose of this chapter is to present the contributions to an understanding of several cosmological problems that have been obtained from the development of an alternative to the Standard Model (SM) of particle physics [1]. This alternative model, named the Generation Model (GM) [2], not only describes all the transition probabilities for interactions involving all the elementary particles of the SM but also provides new paradigms, including the origin of both mass [3] and gravity [4].

The GM considers the elementary particles, the six leptons, six quarks and three weak bosons, of the SM to be composite particles. Their constituents are called rishons and antirishons. It will be demonstrated that this substructure leads to new paradigms for both mass and gravity, which in turn lead to an understanding of several cosmological problems: the matter-antimatter asymmetry of the universe, dark matter and dark energy.

It will be shown that the GM provides a unified origin of mass in which the mass of a particle is described in terms of the energy content of its constituents [5], while in the SM, the elementary leptons, quarks and weak bosons, are described in terms of the Higgs mechanism [6, 7]. It will be demonstrated that the composite nature of the leptons and quarks of the GM leads to a solution of the cosmological matter-antimatter asymmetry problem.

In particular, it will be shown that the GM provides a new universal theory of gravity in terms of a residual interaction of a strong color-like interaction [4], analogous to quantum chromodynamics (QCD) [8], the theory of strong interactions, in the SM. This very weak residual interaction has two important properties: asymptotic freedom (antiscreening) [9, 10] and finite range [11], that provide an understanding of dark matter [12] and dark energy [13], respectively, in the universe.

Section 2 discusses the *incompleteness* of the SM and examines some basic assumptions upon which the SM has been built. Section 3 introduces the GM which replaces several *dubious assumptions* within the SM by different and simpler assumptions, without destroying any agreement with experiment. These lead to the notion that the elementary particles, the six leptons, six quarks and three weak bosons of the SM are *composite particles*. Section 4 describes the development of a viable composite GM in which the elementary particles of the SM are composites of elementary spin-1/2 particles called rishons and antirishons. Section 5 discusses a *new paradigm* provided by the composite GM for *all* mass, and indicates a qualitative understanding of the mass hierarchy of leptons and quarks.

Section 6 presents a solution to the *cosmological matter-antimatter asymmetry problem* in terms of the composite GM. The composite GM also leads to a *new paradigm* for *gravity*. This is discussed in Section 7 in which a *quantum theory of gravity* is described. This new law of universal gravitation is shown to provide an understanding of both *dark matter* (Section 8) and *dark energy* (Section 9).

Section 10 discusses the possibility that the photon may be considered to be the singlet state of the corresponding QCD color octet binding together the constituents of the leptons and quarks. Finally, Section 11 gives a brief summary and conclusion.

2. Standard model of particle physics

The current formulation of the Standard Model (SM) of particle physics [1] was essentially finalized in the mid-1970s following the experimental confirmation of the existence of quarks [14, 15]. However, the model is regarded by most physicists as *incomplete* since it provides little understanding of several empirical observations. First, it does not explain the occurrence of three "generations" of the elementary particles of the SM [16]: the first generation comprising

http://dx.doi.org/10.5772/intechopen.68410

the up and down quarks, the electron and its neutrino, the second generation comprising the charmed and strange quarks, the muon and its neutrino and the third generation comprising the top and bottom quarks, the tau and its neutrino. Each generation behaves similarly except for mass. Second, it does not provide a unified description of the origin of mass nor describe the mass hierarchy of leptons and quarks. The SM also fails to describe the nature of gravity, dark matter, dark energy or the cosmological matter-antimatter asymmetry problem.

Because of the incompleteness of the SM, the basic assumptions upon which the SM has been erected have been examined [17]. There are three basic assumptions, which are considered to be *dubious* and also present major stumbling blocks preventing progress beyond the SM. These are (i) the assumption of a diverse complicated scheme of additive quantum numbers to classify its elementary particles; (ii) the assumption of weak isospin doublets in the quark sector to accommodate the universality of the charge-changing weak interactions and (iii) the assumption that the weak interactions are fundamental interactions described by a local gauge theory.

The elementary particles of the SM are six leptons: electron (e^-), electron neutrino (ν_e), muon (μ^-), muon neutrino (ν_μ), tau (τ^-), tau neutrino (ν_τ) and six quarks: up (u), down (d), charmed (c), strange (s), top (t) and bottom (b). These twelve particles all have spin-1/2 and are allotted several additive quantum numbers: charge Q, lepton number L, muon lepton number L_μ, tau lepton number L_τ, baryon number A, strangeness S, charm C, bottomness B and topness T (see **Table 1**). For each particle additive quantum number N, the corresponding antiparticle has the additive quantum number $-N$.

Table 1 demonstrates that this classification of the elementary particles in the SM is *nonunified*, since, except for charge, the leptons and quarks are allotted different kinds of additive quantum numbers. This diverse complicated scheme of additive quantum numbers for its elementary particles constitutes a basic problem for the SM, especially if the leptons and quarks are *not* elementary particles (see Section 4).

A second problem with the SM involves the method it uses to accommodate the universality of the charge-changing (CC) weak interactions, mediated by the W^+ and W^- bosons.

In the SM, the mass eigenstate leptons have weak isospin 1/2, whose third component is related to both charge and lepton number. Restricting the discussion in this chapter to only the first two generations for simplicity means that the two neutrinos interact with their corresponding charged leptons with the full strength of the CC weak interaction and do not interact at all with the other charged lepton. This is guaranteed by the conservation of lepton numbers.

On the other hand the universality of the CC weak interactions in the quark sector is treated differently. It is assumed that the u and c quarks form weak isospin doublets with so-called weak eigenstate quarks d' and s', respectively, where again for simplicity, the small mixing with the third generation quark b is neglected:

$$d' = d\cos\theta + s\sin\theta, \tag{1}$$

and

$$s' = -d\sin\theta + s\cos\theta, \tag{2}$$

Particle	Q	L	L_μ	L_τ	A	S	C	B	T
e^-	-1	1	0	0	0	0	0	0	0
ν_e	0	1	0	0	0	0	0	0	0
μ^-	-1	1	1	0	0	0	0	0	0
ν_μ	0	1	1	0	0	0	0	0	0
τ^-	-1	1	0	1	0	0	0	0	0
ν_τ	0	1	0	1	0	0	0	0	0
u	$+\frac{2}{3}$	0	0	0	$\frac{1}{3}$	0	0	0	0
d	$-\frac{1}{3}$	0	0	0	$\frac{1}{3}$	0	0	0	0
c	$+\frac{2}{3}$	0	0	0	$\frac{1}{3}$	0	1	0	0
s	$-\frac{1}{3}$	0	0	0	$\frac{1}{3}$	-1	0	0	0
t	$+\frac{2}{3}$	0	0	0	$\frac{1}{3}$	0	0	0	1
b	$-\frac{1}{3}$	0	0	0	$\frac{1}{3}$	0	0	-1	0

Table 1. SM additive quantum numbers for leptons and quarks.

and θ is a mixing angle introduced by Cabibbo [18] into the transition amplitudes prior to the development of the quark model in 1964. In the quark case the third component of weak isospin is related to both charge and baryon number.

The u and c quarks are assumed to interact with the weak eigenstate quarks d' and s', respectively, with the full strength of the CC weak interaction. In addition the u and c quarks are assumed to not interact at all with the weak eigenstate quarks s' and d', respectively. This assumption is dubious, since there are no conserved quantum numbers to support this assumption.

A third problem with the SM concerns the origin of mass. In the SM, the masses of hadrons arise mainly from the energy content of their constituent quarks and gluons, in agreement with Einstein's conclusion [5]. On the other hand the masses of the elementary particles, the leptons, the quarks and the W and Z bosons are interpreted differently, arising from the existence of the so-called Higgs field [6, 7]. The Higgs field was introduced mathematically to spontaneously break the $U(1) \times SU(2)$ local gauge symmetry of the electroweak interaction to generate the masses of the W and Z bosons. The Higgs field also cured the associated fermion mass problem: by coupling, with appropriate strength, originally massless fermions to the scalar Higgs field, it is possible to produce the observed fermion masses and to maintain local gauge invariance [19].

http://dx.doi.org/10.5772/intechopen.68410

There are several problems with the SM's interpretation of the origin of mass. First, there is no clear evidence for the existence of the hypothetical Higgs field. Second, the model provides no *unified* origin of mass. Third, the fermion-Higgs coupling strength is dependent upon the mass of the fermion so that a new parameter is introduced into the SM for each fermion mass. In fact fourteen new parameters are required, if one includes two more parameters to describe the masses of the W boson and the Higgs particle. Fourth, the Higgs mechanism does *not provide any physical explanation* for the origin of the masses of the elementary particles.

The assumption that the weak interactions are fundamental interactions arising from a local gauge theory, unlike both the electromagnetic and strong colour interactions, is at variance with the experimental facts: both the W and Z particles, mediating the weak interactions, are massive, and this conflicts with the requirement of a local gauge theory that the mediating particles should be massless in order to guarantee the gauge invariance. This assumption is very dubious, especially since it leads to more problems than it solves. It also leaves several questions unanswered: *How does the spontaneous symmetry breaking mechanism occur within the electroweak theory? What is the principle that determines the large range of fermion masses exhibited by the leptons and quarks?*

3. Generation model of particle physics

The GM of particle physics [2, 17] overcomes many of the problems inherent in the SM. In the GM the three dubious assumptions of the SM discussed previously are replaced by three different and simpler assumptions. These are (i) the assumption of a *simpler unified* classification of leptons and quarks; (ii) the assumption that the *mass eigenstate quarks* form weak isospin doublets and that hadrons are composed of *weak eigenstate quarks* and (iii) the assumption that the weak interactions are *not fundamental interactions*.

Table 2 shows the additive quantum numbers allotted to both leptons and quarks in the GM. This is a much simpler and unified classification scheme involving only three additive quantum numbers: charge Q, particle number p and generation quantum number g. All three quantum numbers are conserved in all interactions. In particular the generation quantum number g is strictly conserved in weak interactions unlike some of the quantum numbers, e.g. strangeness S, of the SM. As for **Table 1** the corresponding antiparticles have the opposite sign for each particle additive quantum number.

The conservation of the generation quantum number in weak interactions was only achieved by making two postulates, which means that the GM differs fundamentally from the SM in two more ways [20, 21]. First the GM postulates that it is the mass eigenstate quarks of the same generation, which form weak isospin doublets: (u, d) and (c, s). Thus the GM assumes, in the two generation approximation, that the u and c quarks interact with d and s, respectively, with the *full* strength of the CC weak interaction and that the u and c quarks do *not* interact at all with s and d, respectively. This result is a consequence of the conservation of the generation quantum number. Second, while the SM assumes that hadrons are composed of mass eigenstate quarks such as d and s, the GM postulates that hadrons are composed of the corresponding weak eigenstate quarks d' and s'. These two postulates overcome the second dubious assumption of the SM.

Particle	Q	p	g	Particle	Q	p	g
ν_e	0	−1	0	u	$+\frac{2}{3}$	$\frac{1}{3}$	0
e^-	−1	−1	0	d	$-\frac{1}{3}$	$\frac{1}{3}$	0
ν_μ	0	−1	±1	c	$+\frac{2}{3}$	$\frac{1}{3}$	±1
μ^-	−1	−1	±1	s	$-\frac{1}{3}$	$\frac{1}{3}$	±1
ν_τ	0	−1	0, ±2	t	$+\frac{2}{3}$	$\frac{1}{3}$	0, ±2
τ^-	−1	−1	0, ±2	b	$-\frac{1}{3}$	$\frac{1}{3}$	0, ±2

Table 2. GM additive quantum numbers for leptons and quarks.

The classification scheme given in **Table 2** provides a simpler and unified description of leptons and quarks. It also suggests that leptons and quarks are related and in particular allows the development of a composite model of leptons and quarks [4, 22].

The GM assumes that the leptons, quarks and the W and Z bosons are *composites*. Consequently, the weak interactions are *not* fundamental interactions arising from an $SU(2)$ local gauge theory. They are residual interactions of the strong color interaction binding the constituents of the leptons, quarks and the W and Z bosons together. This strong color interaction is completely analogous to that of QCD in the SM. The composite nature of leptons, quarks and the W bosons overcomes the dubious assumption of the SM that the weak interactions are fundamental. It should be noted that the treatment of the electromagnetic and weak interactions in the SM in terms of a $U(1) \times SU(2)$ local gauge theory is replaced in the GM by a $U(1) \times SU(2)$ global gauge theory [23].

The GM has only the charge Q additive quantum number in common with the SM (see **Tables 1** and **2**). The second additive quantum number of the GM, particle number p, replaces both baryon number A and lepton number L of the SM, while the third additive quantum number of the GM, generation quantum number g, effectively replaces the remaining additive quantum numbers, L_μ, L_τ, S, C, B and T of the SM.

4. Composite generation model

Although there is no direct experimental evidence that leptons and quarks have a substructure, there is considerable indirect evidence that leptons and quarks are actually *composites*.

First, the equal magnitude of the electric charges of the electron and proton, indicates that the charges of the up and down quarks are related to that of the electron.

Second, the leptons and quarks are considered [16] to form three families or generations, containing particles which have similar properties, except for mass. This feature is analogous to Mendeleev's periodic table of the elements, based essentially on elements having similar properties, except for mass. The existence of three repeating patterns suggests strongly that the members of each generation are composites, analogous to the elements of the periodic table.

The nonunified classification scheme of the SM provides a major stumbling block for the development of a composite model of leptons and quarks. On the other hand, the unified classification scheme of the GM (**Table 2**) makes feasible a composite version of the GM (CGM) [22]. Here we shall present the current version [4].

The composite GM is based on the unified classification scheme and also on 1979 composite models of Harari [24] and Shupe [25]. The current composite GM was proposed in 2011 and is described in detail in Chapter 1 [2] of the book *Particle Physics* published by InTech and in a review paper [17] published in *Advances in High Energy Physics*.

Both the models of Harari and Shupe are very similar and treat leptons and quarks as composites of two kinds of spin-1/2 particles, which Harari named "rishons" from the Hebrew word for primary. The CGM adopts this name for the constituents of both leptons and quarks and for consistency the same three additive quantum numbers are assigned to the constituents as were previously allotted in the GM to leptons and quarks (see **Table 2**).

In the Harari-Shupe Model (HSM), two kinds of rishons labeled T with charge $Q = +\frac{1}{3}$ and V with $Q = 0$ and their corresponding antiparticles labeled $\overline{T}$ with charge $Q = -\frac{1}{3}$ and $\overline{V}$ with $Q = 0$, are employed to construct the leptons, quarks and their antiparticles. In the HSM, each spin-1/2 lepton or quark is composed of three rishons or three antirishons.

Table 3 shows the proposed HSM structures of the first generation of leptons and quarks. Basically the HSM describes only the charge structure of the first generation of leptons and quarks and does not provide a satisfactory understanding of the second and third generations.

Particle	Structure	Q
e^+	TTT	$+1$
u	TTV	$+\frac{2}{3}$
$\bar{d}$	TVV	$+\frac{1}{3}$
ν_e	VVV	0
$\bar{\nu}_e$	$\overline{V}\overline{V}\overline{V}$	0
d	$\overline{T}\overline{V}\overline{V}$	$-\frac{1}{3}$
$\bar{u}$	$\overline{T}\overline{T}\overline{V}$	$-\frac{2}{3}$
e^-	$\overline{T}\overline{T}\overline{T}$	-1

Table 3. HSM of first generation of leptons and quarks.

To overcome some of the deficiencies of the simple HSM, the two-rishon model was extended [4, 22], within the framework of the CGM, by the introduction of a *third* kind of rishon labeled U and the allocation of all three additive quantum numbers, Q, p and g to each kind of rishon (see **Table 4**). It should be noted that each rishon additive quantum number N, the corresponding antirishon has the additive quantum number $-N$.

In the CGM, the substructure of the leptons and quarks is described in terms of massless rishons and/or antirishons. Each rishon carries a color charge, red, green or blue, while each antirishon carries an anticolor charge, antired, antigreen or antiblue. The constituents of leptons and quarks are bound together by a strong color-type interaction, corresponding to a local gauged $SU(3)$ symmetry (analogous to QCD in the SM) mediated by massless *hypergluons* (analogous to gluons in the SM).

Table 5 gives the structures of the first generation of leptons and quarks in the CGM. The u-quark has $p = +\frac{1}{3}$ since it contains two T-rishons and one $\overline{V}$-antirishon. It is essential that the u-quark should contain an $\overline{V}$-antirishon rather than a V-rishon as in the HSM, since its particle number is required to agree with its baryon number $A = +\frac{1}{3}$. It should be noted that leptons

Rishon	Q	p	g
T	$+\frac{1}{3}$	$+\frac{1}{3}$	0
V	0	$+\frac{1}{3}$	0
U	0	$+\frac{1}{3}$	-1

Table 4. CGM additive quantum numbers for rishons.

Particle	**Structure**	Q	p	g
e^+	TTT	$+1$	$+1$	0
u	$TT\overline{V}$	$+\frac{2}{3}$	$+\frac{1}{3}$	0
$\bar{d}$	$T\overline{V}\overline{V}$	$+\frac{1}{3}$	$-\frac{1}{3}$	0
ν_e	$\overline{V}\overline{V}\overline{V}$	0	-1	0
$\bar{\nu}_e$	VVV	0	$+1$	0
d	$\overline{T}VV$	$-\frac{1}{3}$	$+\frac{1}{3}$	0
$\bar{u}$	$\overline{T}\overline{T}V$	$-\frac{2}{3}$	$-\frac{1}{3}$	0
e^-	$\overline{T}\overline{T}\overline{T}$	-1	-1	0

Table 5. CGM of first generation of leptons and quarks.

http://dx.doi.org/10.5772/intechopen.68410

are composed of three rishons, while quarks are composed of one rishon and one rishon-antirishon pair.

Each lepton of the first generation is *colorless*, composed of three rishons carrying different colors. Each quark of the first generation is *colored*, composed of one rishon and one colorless rishon-antirishon pair. The first generation of particles are all built out of T and V rishons and their antiparticles so that each particle has $g = 0$. The second and third generations are identical to the first generation plus one and two *colorless* rishon-antirishon pair(s): $\bar{U}V$ or $\bar{V}U$ with $Q = p = 0$ but $g = \pm 1$ so that the second and third generations have $g = \pm 1$ and $g = 0, \pm 2$, respectively. This gives *three repeating patterns* [2].

It should be noted that if each of the three kinds of rishons is *conserved* then each of the three additive quantum numbers, Q, p and g is also conserved in all interactions [22].

5. Mass

Since the mass of a hadron arises mainly from the energy of its constituents [26–28], the CGM suggests [3] that the mass of a lepton, quark or weak boson arises from a characteristic energy E associated with its constituent rishons and hypergluons, according to $m = E/c^2$. Thus the CGM provides a *new paradigm* and a *unified* description for the origin of *all* mass: the mass of a body arises from the energy content E of its constituents. The mass is given by $m = E/c^2$ in agreement with Einstein's conclusion [5], so that there is no need for the existence of a Higgs field with its accompanying problems. A corollary of this idea is: *If a particle has mass, then it is composite*.

The CGM suggests that the mass hierarchy of the three generations arises from the substructures of the leptons and quarks. The mass of each composite particle is expected to be *greater* if the constituents are on average more widely spaced: this is a consequence of the nature of the strong color interactions, which are assumed to possess the property of "asymptotic freedom" [9, 10], whereby the color interactions become stronger for larger separations of the color charges. Particles with two or more like charged rishons will have larger structures due to electric repulsion.

Qualitatively, for the same generation, one expects that (i) a charged lepton will have a greater mass than the corresponding neutral lepton; (ii) a $Q = +\frac{2}{3}$ quark will have a greater mass than the corresponding $Q = -\frac{1}{3}$ quark. These are both generally true: (i) the electron has a larger mass than its corresponding neutrino, and (ii) the top quark mass (173 GeV) is > the bottom quark mass (4.2 GeV), the charmed quark mass (1.3 GeV) is > the strange quark mass (95 MeV), although the up quark mass (2 MeV) is < the down quark mass (5 MeV). The first generation quarks seem to present an anomaly since the proton consists of two up quarks and one down quark while the neutron consists of two down quarks and one up quark so that the proton is only stable if the down quark ($Q = -\frac{1}{3}$) is more massive than the up quark ($Q = +\frac{2}{3}$). In the CGM, this anomaly is accounted for by the constituents of hadrons being weak-eigenstate quarks rather than mass-eigenstate quarks. The proton is stable since the weak eigenstate quark d' has a larger mass than the up quark, containing about 5% of the strange quark mass, since $\sin^2\theta \approx 0.05$ [29].

6. Matter-antimatter asymmetry problem

According to the prevailing cosmological model [30] the universe was created in the so-called "Big Bang" from pure energy, and is currently composed of about 5% ordinary matter, 27% dark matter and 68% dark energy. It is generally assumed that the Big Bang and its aftermath produced *equal numbers* of particles and antiparticles, although the universe today appears to consist almost entirely of matter (particles) rather than antimatter (antiparticles). This constitutes the matter-antimatter asymmetry problem: *Where have all the antiparticles gone?* Currently there is no acceptable understanding of this asymmetry problem.

An understanding of the matter-antimatter asymmetry requires a precise definition of both matter and antimatter and knowledge of the physical nature of the Big Bang but unfortunately this knowledge is currently far from complete. The prevailing model of the Big Bang is based upon the theory of general relativity [31]: extrapolation of the expansion of the universe backwards in time yields an infinite density and temperature at a finite time in the past (approximately 13.8 billion years ago). Thus the "birth" of the universe seems to be associated with a "singularity", which not only signals a breakdown of general relativity but also all the laws of physics. This leads to serious impediments to understanding the physical nature of the Big Bang and consequently the development of the matter-antimatter asymmetry in the aftermath of the Big Bang.

Since the physical nature of the Big Bang is still not understood, it is not possible to discuss the matter-antimatter asymmetry problem from the initial singularity. Consequently, the matter-antimatter (i.e. particle-antiparticle) asymmetry problem will be discussed in terms of the observed nature of the universe, ignoring the singularity.

In the SM the universe is made essentially of matter comprising three kinds of elementary particles: electrons, up quarks and down quarks. The matter described by the SM refers to the 5% ordinary matter, which prior to the nucleosynthesis, i.e. the fusion into heavier elements, consisted of about 92% hydrogen atoms and 8% helium atoms [32], so that the ordinary matter of the universe was, and still is, essentially electrically neutral and colorless.

For many decades now the SM has been unable to provide an acceptable understanding of the matter-antimatter asymmetry problem. The main reason seems to be that the SM assumes that the leptons and quarks are elementary particles. Since this implies no relationship between leptons and quarks, as indicated by the different sets of additive quantum numbers employed by the SM to describe their interactions, this allows the matter/antimatter nature of leptons and quarks to be decided by pure convention. In the SM both leptons and quarks are assumed to be matter particles.

In the SM, neglecting the singularity, it is assumed that the Big Bang initially produces numerous elementary particle-antiparticle pairs such as electron-positron pairs and quark-antiquark pairs by converting energy into mass according to $m = E/c^2$. Thus the early universe consisted of a soup of particle-antiparticle pairs continually being created and annihilated. Later, as the universe cooled following an inflationary period, the quarks and antiquarks would form protons, neutrons, antiprotons, antineutrons, etc., and eventually atoms of hydrogen, antihydrogen,

helium and antihelium. These would later annihilate in pairs until only atoms of hydrogen and helium prevailed. In this scenario, it seems unlikely that either electrons or positrons would prevail so that neither hydrogen atoms nor antihydrogen atoms would prevail. This simply reflects that the creation and annihilation of electron-positron pairs constitute a unique process, since in the SM both electrons and positrons are elementary particles.

In the GM, neglecting the singularity, it is expected that the Big Bang would initially produce numerous elementary rishon-antirishon pairs. Then as the universe cooled following an inflationary period, the rishons and antirishons would form leptons, quarks and their antiparticles and eventually atoms of hydrogen, antihydrogen, helium and antihelium. These would later annihilate in pairs until only atoms of hydrogen and helium prevailed.

In order to understand this matter-antimatter asymmetry, it is necessary to define the matter/antimatter nature of composite particles. Historically, the term "particle" defines matter that is naturally occurring, i.e. electrons, protons, hydrogen atoms, etc. This is consistent within the SM in which the electron and the up and down quarks are elementary particles. However, it is not consistent within the GM in which the electron and the up and down quarks are composite particles consisting of elementary particles (rishons) and/or antiparticles (antirishons). In the GM, rishons are considered to be matter (particles) while antirishons are considered to be antimatter (antiparticles), since rishon-antirishon pairs are considered to be created/annihilated in the standard manner, e.g. in the Big Bang.

In the GM the elementary rishons and antirishons have particle number $p = +\frac{1}{3}$ and $p = -\frac{1}{3}$, respectively. Thus the particle number p allotted to a composite lepton or quark reflects its degree of matter or antimatter nature. In the GM the quarks are composed of both rishons and antirishons so that they have both a matter and an antimatter nature, although an electron is composed of three $\overline{T}$-rishons so that it has $p = -1$ and is pure antimatter.

The solution of the matter-antimatter asymmetry problem involves the particle number additive quantum number p of the GM: in particular the values of p corresponding to a weak eigenstate up quark ($p = +\frac{1}{3}$), a weak eigenstate down quark ($p = +\frac{1}{3}$) and an electron ($p = -1$). The values of $p = +\frac{1}{3}$ of the quarks, correspond to the values of their baryon number in the SM, while the value of $p = -1$ of the electron, corresponds to minus the value of the lepton number of the electron in the SM. In the GM, the electron consists entirely of antirishons, i.e. antiparticles, while in the SM it is assumed to be a particle, although as we have indicated earlier, there is no a priori reason for this assumption. It should be noted that the matter/antimatter nature of an electron in the GM is not merely a revised definition of the term "matter" but is a requirement for consistency of the nature of the constituents of the electron and the initial particle-antiparticle nature of the universe in the Big Bang: the elementary particles in the SM (leptons and quarks) and in the GM (rishons) are different.

In the GM the proton is assumed to consist of three weak eigenstate quarks, two up quarks and one down quark, so that the proton has particle number $p = +1$. Consequently, a hydrogen atom, consisting of one proton and one electron has particle number $p = 0$: the hydrogen atom in the GM consists basically of an equal number of rishons and antirishons, so that there is no asymmetry of matter and antimatter there.

In the GM the neutron consists of three weak eigenstate quarks, one up quark and two down quarks, so that the neutron also has particle number $p = +1$. Consequently, a helium atom, consisting of two protons, two neutrons and two electrons has particle number $p = +2$: the helium atom in the GM consists of six more rishons than antirishons, i.e. more matter than antimatter. In the GM it is assumed that during the formation of helium in the aftermath of the Big Bang that an equivalent surplus of antimatter was formed as neutrinos, which have $p = -1$, so that overall equal numbers of rishons and antirishons prevailed. This assumption is a consequence of the conservation of p in all interactions in the GM.

Thus the ordinary matter present in the universe, prior to the fusion process into heavier elements, has particle number $p = 0$. Since the additive quantum number p is conserved in all interactions, this implies that the overall particle number of the universe will remain as $p = 0$, i.e. symmetric in particle and antiparticle matter.

Indeed it should be noted that if the Big Bang produced equal numbers of particles and antiparticles so that the initial state of the universe had particle number $p = 0$, then the GM *predicts* that the present state of the universe should also have $p = 0$, since particle number p is conserved in all interactions.

To summarize: the ordinary matter present in the universe has an overall particle number of $p = 0$, so that it contains equal numbers of both rishons and antirishons. This implies that the original antimatter created in the Big Bang is now contained within the stable composite leptons, i.e. electrons and neutrinos, and the stable composite quarks, i.e. the weak eigenstate up and down quarks, which comprise the protons and neutrons. The hydrogen, helium and heavier atoms all consist of electrons, protons and neutrons. This explains where all the antiparticles have gone. Thus there is no matter-antimatter asymmetry in the present universe.

However, the above does not explain why the present universe consists primarily of hydrogen atoms and not antihydrogen atoms. In the SM this is considered to be the matter-antimatter asymmetry problem, since each of the elementary particles, the electron and both the up and down quarks are defined to be matter (particles). In the GM it has been demonstrated that this is not so: both hydrogen atoms and antihydrogen atoms have $p = 0$, consisting of six rishons and six antirishons. Indeed an antihydrogen atom consists of the same rishons and antirishons as does a hydrogen atom, although the rishons and antirishons are differently arranged in the two systems. A hydrogen atom consists of a proton (six rishons and three antirishons) and an electron (three antirishons), while an antihydrogen atom consists of an antiproton (three rishons and six antirishons) and a positron (three rishons).

This implies that both hydrogen atoms and antihydrogen atoms should be formed during the aftermath of the Big Bang with about the same probability. In fact, estimates from the cosmic microwave background data suggest [11] that for every billion hydrogen-antihydrogen pairs there was just one extra hydrogen atom. It is suggested that this extremely small difference, one extra hydrogen atom in 10^9 hydrogen-antihydrogen pairs, may arise from statistical fluctuations associated with the complex many-body processes involved in the formation of either a hydrogen atom or an antihydrogen atom. The uniformity of the universe [11], in particular

http://dx.doi.org/10.5772/intechopen.68410

the lack of antihydrogen throughout the universe, indicates that the above statistical fluctuations took place prior to the "inflationary period" [33, 34] associated with the Big Bang scenario.

7. Gravity

Let us now consider the nature of gravity within the framework of the GM. It is considered that the rishons of each colorless lepton, e.g. an electron, are very strongly localized since to date there is no direct experimental evidence for any substructure of these particles. It is expected that the product wave function describing the distribution of the constituent rishons is significant for only an extremely small volume of space so that the color fields almost cancel. It should be noted that the color fields would only cancel completely if each of the rishons occupied the same position, but quantum mechanics prevents this. This raises a question: *What is the residual interaction arising from the incomplete cancellation of the strong interactions?*

Between any two colorless leptons (e.g. electrons) there will be a very weak residual interaction, arising from the color interactions acting between the color charges of one lepton and the color charges of the other lepton. There will be a similar residual interaction between any two colorless hadrons such as neutrons and protons, each containing three differently colored quarks.

In two papers [3, 4] it was suggested that this residual interaction, arising from these "interfermion" color interactions, gives rise to the usual gravitational interaction.

The mass of a body of ordinary matter is essentially the total mass of its constituent colorless electrons, neutrons and protons. Each of these three composite particles is in a three-color antisymmetric state so that its behavior with respect to the color interactions is basically the same. This suggests [13] that the residual color interactions between electrons, neutrons and protons have several properties associated with the usual gravitational interaction: universality, very weak strength and attraction.

In the GM gravity essentially arises from the residual color forces between all electrons, neutrons and protons. This leads [13] to a *new law of gravity*: the residual color interactions between any two bodies of masses m_1 and m_2, separated by a distance r, leads to a universal law of gravitation, which closely resembles Newton's original law given by:

$$F = H(r)\, m_1\, m_2 / r^2, \tag{3}$$

where Newton's gravitational constant (G) is replaced by a function of r, $H(r)$.

The new gravitational interaction of the GM is based upon the residual color interactions acting between electrons, neutrons and protons. The GM assumes that the color interactions acting between rishons have the same characteristics as the color interactions acting between quarks in the SM. These color interactions have two important properties that differ from the Newtonian interaction: (i) asymptotic freedom [9, 10] and (ii) color confinement [11]. These determine the nature of the function $H(r)$.

In Sections 8 and 9, we shall indicate how these two additional properties of the interfermion color interactions provide an understanding of dark matter and dark energy, respectively.

8. Galaxy rotation problem and dark matter

For galaxies there is a major gravitational problem [12], which has been around for about 40 years. It was found that the rotation curves for galaxies disagreed with Newton's gravitational law for large r: the stars and gas were rotating much faster than expected from Newton's law and their orbital velocities were roughly constant. These observations implied that either Newton's law was incorrect at large distances or some considerable mass was missing.

The rotation curve for a galaxy is the dependence of the orbital velocity of the visible matter in the galaxy on its radial distance from the center of the galaxy. What the observations showed was that the rotation curves were essentially "flat" at the extremities of the visible matter, i.e. at large distances. This implies gross disagreement with Newton's universal law of gravitation, which predicts a fall-off as $1/\sqrt{r}$, as in the solar system.

Two solutions, which have been very successful, are first the *dark matter hypothesis*, which proposes that a galaxy is embedded within a giant halo of dark matter. This matter is considered to be nonatomic but otherwise its nature is unknown and so far has not been detected. The second solution is the *Modified Newtonian Dynamics* (MOND) hypothesis: Milgrom [35] proposed that gravity varies from Newton's law for low accelerations. This was an empirical hypothesis without physical understanding.

It was found that the *new law of universal gravitation* given by Eq. (3) is essentially equivalent to the MOND hypothesis so that the GM gravitational interaction provides a physical basis for the MOND hypothesis. The continuing success [36, 37] of the MOND hypothesis is a strong argument against the existence of undetected dark matter haloes, consisting of unknown matter embedding galaxies.

Asymptotic freedom is rather a misnomer. A better term is "antiscreening" as used by Wilczek in his 2004 Nobel lecture. The flat galactic rotation curves are described by the property of antiscreening provided by the self-interactions of the hypergluons mediating the residual color interactions. These antiscreening effects lead to an increase in the strength of the residual color interactions so that $H(r)$ becomes an increasing function of r. The flat rotation curves observed for galaxies indicate that:

$$H(r) = G(1 + kr), \tag{4}$$

where k is a factor representing the relative strengths of the modified and Newtonian gravitational fields.

In the GM $H(r) = G(1 + kr)$ arises from the self-interactions of the hypergluons mediating the gravitational interaction and explains the dark matter problem of the galaxy rotational curves: for small r, $H(r)$ is approximately G and gravity is approximately Newtonian; for large r, $H(r)$ is approximately Gkr and gravity is approximately $1/r$ rather than $1/r^2$, and the $1/r$ dependence gives the flat rotation curves observed.

http://dx.doi.org/10.5772/intechopen.68410

9. Dark energy

Color confinement is the phenomenon that color charged particles (e.g. quarks in the SM, rishons in the GM) cannot be isolated and consequently form colorless composite particles (e.g. mesons and baryons in the SM and also leptons in the GM). Color confinement leads to another phenomenon analogous to the "hadronization process" [11], i.e. the formation of hadrons out of quarks and gluons in the SM and implies $H(r) = 0$ for sufficiently large r in the GM [13].

In the GM, $H(r) = 0$ arises if the gravitational field energy is sufficient that it is energetically favorable to produce the mass of a particle-antiparticle colorless pair rather than the color field to extend further. This implies that gravity ceases to exist for sufficiently large cosmological distances.

The strong color interaction is known to have a finite range of approximately 10^{-15} m. Gravity is about 10^{-41} times weaker at 10^{-15} m [11] than the strong color interaction. This suggests that the "hadronization process" for gravity occurs at about 10^{26} m, i.e. roughly ten billion light years.

The new law of gravity implies that gravity ceases to exist for cosmological distances exceeding several billion light years, resulting in less slowing down of galaxies than expected from Newton's law. This result agrees well with observations [38, 39] of distant Type Ia supernovae, which indicate the onset of an accelerating expansion of the universe at about six billion light years. Thus the new law of gravity suggests that dark energy like dark matter may be understood as an effect arising from the nature of the gravitational interaction.

10. Photon

The nature of the photon within the framework of the GM is worthy of consideration. The photon has several properties that may be accommodated in the GM: (i) massless; (ii) neutral; (iii) colorless; (iv) spin-1; (v) $U(1)$ symmetry and (vi) interacts with matter gravitationally.

It is proposed that the photon may be the *singlet state* of the corresponding QCD color octet binding together the rishons and antirishons of the leptons and quarks. If the photon is the standard singlet state of QCD: $\left[(r\bar{r}) + (g\bar{g}) + (b\bar{b})\right]/\sqrt{3}$, containing all three color charges, red (r), green (g) and blue (b) and all three anticolor charges, antired ($\bar{r}$), antigreen ($\bar{g}$) and antiblue ($\bar{b}$), then it has each of the above six properties possessed by the photon.

In the GM the singlet state is a hypergluon, which is massless, electrically neutral, colorless and has spin-1 and $U(1)$ symmetry. Furthermore, in the GM it interacts with matter via the new gravitational interaction based upon the residual color interactions. In particular the GM predicts that it leads to *twice* the deflection of Newton's universal theory of gravity in agreement with Einstein's theory of general relativity but without any warping of spacetime. In this way the electromagnetic and strong color interactions are *unified* within a $U(3) = U(1) \times SU(3)$ symmetry.

11. Summary and conclusion

The GM considers that the elementary particles of the SM, the leptons, quarks and weak bosons are all composite particles. This substructure leads to new paradigms for both mass and gravity, which in turn lead to an understanding of several cosmological problems: the matter-antimatter asymmetry of the universe, dark matter and dark energy.

The GM provides a *unified* origin of mass and the composite nature of the leptons and quarks leads to a solution of the cosmological matter-antimatter asymmetry problem.

The GM also provides a new universal quantum theory of gravity. In the GM, gravity is a very weak residual interaction of a strong color-like interaction, which possesses two important properties: antiscreening and finite range that provide an understanding of dark matter and dark energy, respectively, in terms of gravitational effects.

Author details

Brian Albert Robson

Address all correspondence to: brian.robson@anu.edu.au

The Australian National University, Canberra, ACT, Australia

References

[1] Gottfried K, Weisskopf VF. Concepts of Particle Physics. Vol. 1. New York: Oxford University Press; 1984, 189p

[2] Robson BA. The generation model of particle physics. In: Kennedy E, editor. Particle Physics. Rijeka: InTech; 2012. pp. 1–28

[3] Robson BA. The generation model and the origin of mass. International Journal of Modern Physics E. 2009;**18**:1773–1780

[4] Robson BA. A quantum theory of gravity based on a composite model of leptons and quarks. International Journal of Modern Physics E. 2011;**20**:733–745

[5] Einstein A. Ist die Trägheit eines Körpers von seinem Energieinhalt abhängig. Annalen der Physik. 1905;**18**:639–641

[6] Englert F, Brout R. Broken symmetry and the mass of gauge vector bosons. Physical Review Letters. 1964;**13**:321–323

[7] Higgs PW. Broken symmetries and the masses of gauge bosons. Physical Review Letters. 1964;**13**:508–509

[8] Halzen F, Martin AD. Quarks and Leptons: An Introductory Course in Modern Particle Physics. New York: Wiley; 1984. 396p

[9] Gross DJ, Wilczek F. Ultraviolet behavior of non-abelian gauge theories. Physical Review Letters. 1973;**30**:1343–1346

[10] Politzer HD. Reliable perturbative results for strong interactions. Physical Review Letters. 1973;**30**:1346–1349

[11] Lincoln D. Understanding the Universe from Quarks to the Cosmos. Rev. Ed. Singapore: World Scientific; 2012. 567p

[12] Robson BA. The generation model of particle physics and galactic dark matter. International Journal of Modern Physics E. 2013;**22**. Article ID 1350067, 11pp.

[13] Robson BA. Dark matter, dark energy and gravity. International Journal of Modern Physics E. 2015;**24**. Article ID 1550012, 10pp.

[14] Bloom ED, et al. High-energy inelastic $e - p$ scattering at 6^0 and 10^0. Physical Review Letters. 1969;**23**:930–934

[15] Breidenbach M, et al. Observed behavior of highly inelastic electron-proton scattering. Physical Review Letters. 1969;**23**:935–939

[16] Veltman M. Facts and Mysteries in Elementary Particle Physics. Singapore: World Scientific; 2003. 340p

[17] Robson BA. Progressing beyond the standard model. Advances in High Energy Physics. 2013;**2013**. Article ID 341738, 12pp.

[18] Cabibbo N. Unitary symmetry and leptonic decays. Physical Review Letters. 1963;**10**: 531–533

[19] Aitchison IJR, Hey AJG. Gauge Theories in Particle Physics. Bristol: Hilger; 1982. 341p

[20] Robson BA. A generation model of the fundamental particles. International Journal of Modern Physics E. 2002;**11**:555–566

[21] Evans PW, Robson BA. Comparison of quark mixing in the standard and generation models. International Journal of Modern Physics E. 2006;**15**:617–625

[22] Robson BA. A generation model of composite leptons and quarks. International Journal of Modern Physics E. 2005;**14**:1151–1169

[23] Robson BA. The generation model and the electroweak connection. International Journal of Modern Physics E. 2008;**17**:1015–1030

[24] Harari H. A schematic model of quarks and leptons. Physics Letters B. 1979;**86**:83–86

[25] Shupe MA. A composite model of leptons and quarks. Physics Letters B. 1979;**86**:87–92

[26] Butler F, et al. Hadron mass predictions of the valence approximation to lattice QCD. Physical Review Letters. 1993;**70**:2849–2852

[27] Aoki S, et al. Quenched light hadron spectrum. Physical Review Letters. 2000;**84**:238–241

[28] Davies CTH, et al. High-precision lattice QCD confronts experiment. Physical Review Letters. 2004;**92**. Article ID 022001, 5pp.

[29] Amsler C, et al. Summary tables of particle properties. Physics Letters B. 2008;**667**:31–100

[30] Ade PAR, et al. (Planck Collaboration). Planck 2013 results. I. Overview of products and scientific results. Astronomy and Astrophysics. 2014;**571**. Article ID A1, 48pp.

[31] Einstein A. The basics of general relativity theory. Annalen der Physik. 1916;**49**:769–822

[32] Morris R. Cosmic Questions. New York: Wiley; 1993. 200p

[33] Guth AH. Inflationary universe—a possible solution to the horizon and flatness problems. Physical Review D. 1981;**23**:347–356

[34] Linde AD. A new inflationary universe scenario—a possible solution of the horizon, flatness, homogeneity, isotropy and primordial monopole problems. Physics Letters B. 1982;**108**:389–393

[35] Milgrom M. A modification of the newtonian dynamics as a possible alternative to the hidden mass hypothesis. Astrophysical Journal. 1983;**270**:365–370

[36] McGaugh SS, de Blok WJG. Testing the hypothesis of modified dynamics with low surface brightness galaxies and other evidence. Astrophysical Journal. 1998;**499**:66–81

[37] Famaey B, McGaugh SS. Modified newtonian dynamics (MOND): Observational phenomenology and relativistic extensions. Living Reviews in Relativity. 2012;**15**. Article ID 10, 159pp.

[38] Riess AG, et al. Observational evidence from supernovae for an accelerating universe and a cosmological constant. Astronomical Journal. 1998;**116**:1009–1038

[39] Perlmutter S, et al. Measurements of omega and lambda from 42 high-redshift supernovae. Astrophysical Journal. 1999;**517**:565–586

Chapter 9

Deformed Phase Space in Cosmology and Black Holes

E.A. Mena-Barboza, L.F. Escamilla-Herrera,

J.C. López-Domínguez and J. Torres-Arenas

Additional information is available at the end of the chapter

http://dx.doi.org/10.5772/intechopen.68282

Abstract

It is well known that one way to study canonical quantum cosmology is through the Wheeler DeWitt (WDW) equation where the quantization is performed on the minisuperspace variables. The original ideas of a deformed minisuperspace were done in connection with noncommutative cosmology, by introducing a deformation into the minisuperspace in order to incorporate an effective noncommutativity. Therefore, studying solutions to Cosmological models through the WDW equation with deformed phase space could be interpreted as studying quantum effects to Cosmology. In this chapter, we make an analysis of scalar field cosmology and conclude that under a phase space transformation and imposed restriction, the effective cosmological constant is positive. On the other hand, obtaining the wave equation for the noncommutativity Kantowski-Sachs model, we are able to derive a modified noncommutative version of the entropy. To that purpose, the Feynman-Hibbs procedure is considered in order to calculate the partition function of the system.

Keywords: noncommutativity, quantum cosmology, thermodynamics of black holes

1. Introduction

Since the initial use of the Hamiltonian formulation to cosmology, different issues have been studied. In particular, thermodynamic properties of black holes, classical and quantum cosmology, dynamics of cosmological scalar fields, and the problem of cosmological constant among others. In this chapter, we present some results in deforming the phase space variables, discussing recent advances on this special topic by presenting three models. In the first model (Section 2), we analyze the effects of the phase space deformations over different scenarios, we start with the noncommutative on Λ cosmological and comment on the possibility that the

origin of the cosmological constant in the (4 + 1) Kaluza-Klein universe is related to the deformation parameter associated to the four-dimensional scale factor and the compact extra dimensions. In Section 3, we study the effects of phase space deformations in late time cosmology. To introduce the deformation, we use the approach given in Refs. [1]. We conclude that for this model an effective cosmological constant Λ_{eff} appears.

In Section 4, the thermodynamic formalism for rotating black holes, characterized by noncommutative and quantum corrections, is constructed. From a fundamental thermodynamic relation, the equations of state are explicitly given, and the effect of noncommutativity and quantum correction is discussed; in this sense, the goal of this section is to explore how these considerations introduced in Bekenstein-Hawking (BH) entropy change the thermodynamic information contained in this new fundamental relation. Under these considerations, Section 4 examines the different thermodynamic equations of state and their behavior when considering the aforementioned modifications to entropy.

In this chapter, we mainly pretend to indulge in recollections of different studies on the noncommutative proposal that has been put forward in the literature by the authors of this chapter [2–4]; in this sense, our guideline has been to concentrate on resent results that still seem likely to be of general interest to those researchers that are interested in this noncommutative subject.

2. Model 1: Kaluza-Klein cosmology with Λ

Let us begin by introducing the model in a classical scenario which is an empty (4+1) theory of gravity with cosmological constant Λ as shown in Eq. (1). In this setup, the action takes the form:

$$I = \int \sqrt{-g}(R - \Lambda) dt d^3 r d\rho, \tag{1}$$

where $\{t, r^i\}$ are the coordinates of the 4-dimensional spacetime and ρ represents the coordinate of the fifth dimension. We are interested in Kaluza-Klein cosmology, so a Friedmann-Robertson-Walker (FRW)-type metric is assumed, which is of the form

$$ds^2 = -dt^2 + \frac{a^2(t) dr^i dr^i}{\left(1 + \frac{\kappa r^2}{4}\right)^2} + \phi^2(t) d\rho^2, \tag{2}$$

where $\kappa = 0, \pm 1$ and $a(t)$, $\phi(t)$ are the scale factors of the universe and the compact dimension, respectively. Substituting this metric into the action Eq. (1) and integrating over the spatial dimensions, we obtain an effective Lagrangian that only depends on (a, ϕ):

$$L = \frac{1}{2}\left(a\phi\dot{a}^2 + a^2\dot{a}\phi - \kappa a\phi + \frac{1}{3}\Lambda a^3\phi\right). \tag{3}$$

For the purposes of simplicity and calculations, we can rewrite this Lagrangian in a more convenient way:

$$L = \frac{1}{2}\left[\left(\dot{x}^2 - \omega^2 x^2\right) - \left(\dot{y}^2 - \omega^2 y^2\right)\right], \tag{4}$$

where the new variables were defined as

$$x = \frac{1}{\sqrt{8}}\left(a^2 + a\phi - \frac{3\kappa}{\Lambda}\right), y = \frac{1}{\sqrt{8}}\left(a^2 - a\phi - \frac{3\kappa}{\Lambda}\right), \tag{5}$$

and $\omega = -\frac{2\Lambda}{3}$. The Hamiltonian for the model is calculated as usual and reads

$$H = \left[\left(p_x^2 + \omega^2 x^2\right) - \left(p_y^2 + \omega^2 y^2\right)\right], \tag{6}$$

which describes an isotropic oscillator-ghost-oscillator system. A full analysis of the quantum behavior of this model is presented in Ref. [1].

2.1. Noncommutative model

As is well known, there are different approaches to introduce noncommutativity in gravity [5]. In particular, to study noncommutative cosmology [6, 7], there exist a well-explored path to introduce noncommutativity into a cosmological setting [6]. In this setup, the noncommutativity is realized in the minisuperspace variables. The deformation of the phase space structure is achieved through the Moyal brackets, which are based on the Moyal product. However, a more appropriate way to introduce the deformation is by means of the Poisson brackets rather than the Moyal ones.

The most conventional way to understand the noncommutativity between the phase space variables (minisuperspace variables) is by replacing the usual product of two arbitrary functions with the Moyal product (or star product) as

$$(f \star g)(x) = \exp\left[\frac{1}{2}\alpha^{ab}\partial_a^{(1)}\partial_b^{(2)}\right] f(x_1)g(x_2)|_{x_1=x_2=x}, \tag{7}$$

such that

$$\alpha_{ab} = \begin{pmatrix} \theta_{ij} & \delta_{ij} + \sigma_{ij} \\ -\delta_{ij} - \sigma_{ij} & \beta_{ij} \end{pmatrix}, \tag{8}$$

where the θ and β are 2×2 antisymmetric matrices and represent the noncommutativity in the coordinates and momenta, respectively, and $\sigma = \theta\beta/4$. With this product law, a straightforward calculation gives

$$\{x_i, x_j\} = \theta_{ij}, \quad \{x_i, p_j\} = \delta_{ij} + \sigma_{ij}, \quad \{p_i, p_j\} = \beta_{ij}. \tag{9}$$

The noncommutative deformation has been applied to the minisuperspace variables as well as to the corresponding canonical momenta; this type of noncommutativity can be motivated by

string theory correction to gravity [6, 8]. In the rest of this model, we use for the noncommutative parameters $\theta_{ij} = -\theta\varepsilon_{ij}$ and $\beta_{ij} = \beta\varepsilon_{ij}$.

If we consider the following change of variables in the classical phase space $\{x, y, p_x, p_y\}$

$$\begin{aligned} \hat{y} &= y - \frac{\theta}{2}p_x,\ \hat{x} = x - \frac{\theta}{2}p_y \\ \hat{p}_y &= p_y + \frac{\beta}{2}x,\ \hat{p}_x = p_x - \frac{\beta}{2}y, \end{aligned} \tag{10}$$

it can be verified that if $\{x,y,p_x,p_y\}$ obeys the usual Poisson algebra, then

$$\{\hat{y}, \hat{x}\} = \theta, \quad \{\hat{x}, \hat{p}_x\} = \left\{\hat{y}, \hat{p}_y\right\} = 1 + \sigma, \quad \left\{\hat{p}_y, \hat{p}_x\right\} = \beta. \tag{11}$$

Now that we have defined the deformed phase space, we can see the effects on the proposed cosmological model. From the action Eq. (4), we can obtain the Hamiltonian constraint Eq. (6); inserting relations Eq. (11), a Wheeler DeWitt (WDW) equation can be constructed as:

$$\begin{aligned} H\Psi(\hat{x}, \hat{y}) = \Bigg\{ &\left(\hat{p}_x - \frac{2(\beta - \theta\omega^2)}{4 - \omega^2\theta^2}\hat{y}\right)^2 - \left(\hat{p}_y + \frac{2(\beta - \theta\omega^2)}{4 - \omega^2\theta^2}\hat{x}\right)^2 \\ &+ \left(\frac{4(\beta - \theta\omega^2)^2}{(4 - \omega^2\theta^2)^2} + \frac{4(\omega^2 - \beta^2/4)}{4 - \omega^2\theta^2}\right)\hat{x}^2 - \left(\frac{4(\beta - \theta\omega^2)^2}{(4 - \omega^2\theta^2)^2} + \frac{4(\omega^2 - \beta^2/4)}{4 - \omega^2\theta^2}\right)\hat{y}^2 \Bigg\}\Psi(\hat{x}, \hat{y}) = 0, \end{aligned} \tag{12}$$

By a closer inspection of the equation, it is convenient to make the following definitions:

$$\begin{aligned} \omega'^2 &\equiv \frac{4(\beta - \theta\omega^2)^2}{(4 - \omega^2\theta^2)^2} + \frac{4(\omega^2 - \beta^2/4)}{4 - \omega^2\theta^2}, \\ A_{\hat{x}} &\equiv \frac{-2(\beta - \theta\omega^2)}{4 - \omega^2\theta^2}\hat{y}, \quad A_{\hat{y}} \equiv \frac{2(\beta - \theta\omega^2)}{4 - \omega^2\theta^2}\hat{x}, \end{aligned} \tag{13}$$

With these definitions, we can rewrite Eq. (12) in a much simpler and suggestive form:

$$H = \left\{ \left[\left(\hat{p}_x - A_{\hat{x}}\right)^2 + \omega'^2\hat{x}^2\right] - \left[\left(\hat{p}_y - A_{\hat{y}}\right)^2 + \omega'^2\hat{y}^2\right] \right\}, \tag{14}$$

which is a two-dimensional anisotropic ghost-oscillator [1]. From Eq. (14), we can see that the terms $(p_i - A_i)$ can be associated to a minimal coupling term as is done in electromagnetic theory. From this vector potential, we find that $B = \frac{4(\beta - \omega^2\theta)}{4 - \omega^2\theta^2}$ and the vector potential $\mathbf{A}$ can be rewritten as $A_{\hat{x}} = -\frac{B}{2}\hat{y}$ and $A_{\hat{y}} = \frac{B}{2}\hat{x}$. On the other hand, we already know from Eq. (11) that $\left\{\hat{p}_y, \hat{p}_x\right\} = \beta$ and if we set $\theta = 0$ in the above equation for B, we can conclude that the deformation of the momentum plays a role analogous to a magnetic field.

2.2. Discussion

We found that ω is defined in terms of the cosmological constant, then modifications to the oscillator frequency will imply modifications to the effective cosmological constant. Here, we have done a deformation of the phase space of the theory by introducing a modification to the momenta and to the minisuperspace coordinates, this gives two new fundamental constants θ and β. As expected, we obtain a different functional dependence for the frequency ω and the magnetic B field as functions of β and θ. With this in mind, we can construct a new frequency $\tilde{\omega}$ in terms of ω'^2 and the cyclotron term $B^2/4$:

$$\tilde{\omega}^2 = \omega'^2 - \frac{B^2}{4} = \frac{4(\omega^2 - \beta^2/4)}{4 - \omega^2\theta^2}. \tag{15}$$

This $\tilde{\omega}$ was obtained by a definition of the effective cosmological constant $\tilde{\Lambda}_{eff} = -\frac{3}{2}\tilde{\omega}^2$ as was done in Section 2, to finally get a redefinition of the effective cosmological constant due to noncommutative parameters:

$$\tilde{\Lambda}_{eff} = \frac{4(\Lambda_{eff} + \frac{3}{8}\beta^2)}{4 - \frac{2}{3}\theta^2|\Lambda_{eff}|}. \tag{16}$$

Now if we choose the case $\beta = 0$, this should be equivalent to the noncommutative minisuperspace model, hence we get an effective cosmological constant given by:

$$\tilde{\Lambda}_{eff} = \frac{4\Lambda_{eff}}{(4 - \frac{2}{3}\theta^2|\Lambda_{eff}|)} \tag{17}$$

We can see from Eq. (17) that the noncommutative parameter θ cannot take the place of the cosmological constant, but depending on the value of θ, the effective cosmological constant $\tilde{\Lambda}_{eff}$ is modified. Equation 17 is in agreement with the results given in Refs. [9, 10].

3. Model 2: Scalar field cosmology

Let us start with a homogeneous and isotropic universe with a flat Friedmann-Robertson-Walker (FRW) metric:

$$ds^2 = -N^2(t)dt^2 + a^2(t)\left[dr^2 + r^2 d\Omega\right] \tag{18}$$

As usual, $a(t)$ is the scale factor and $N(t)$ is the lapse function. We use the Einstein-Hilbert action and a scalar field ϕ as the matter content for the model. In units $8\pi G = 1$, the action takes the form:

$$S = \int dt \left\{ -\frac{3a\dot{a}^2}{N} + a^3\left(\frac{\dot{\phi}^2}{2N} - N\Lambda\right)\right\} \tag{19}$$

Now, we make the following change of variables:

$$x = m^{-1}a^{3/2}\sinh(m\phi), y = m^{-1}a^{3/2}\cosh(m\phi). \tag{20}$$

where $m^{-1} = 2\sqrt{2/3}$. Then the Hamiltonian is

$$H_c = N\left(\frac{1}{2}P_x^2 + \frac{\omega^2}{2}x^2\right) - N\left(\frac{1}{2}P_y^2 + \frac{\omega^2}{2}y^2\right), \tag{21}$$

with $\omega^2 = -\frac{3}{4}\Lambda$. To find the dynamics, we solve the equations of motion; for this model, it can easily be integrated [9].

To construct the deformed model, we usually follow the canonical quantum cosmology approach, where after canonical quantization [11], one formally obtains the WDW equation. In the deformed phase space approach, the deformation is introduced by the Moyal brackets to get a deformed Poisson algebra. To construct a deformed Poisson algebra, we use the approach given in Refs. [1, 9]. We start with the same transformation on the classical phase space variables $\{x,y,P_x,P_y\}$ that satisfy the usual Poisson algebra as shown in Section 2.1, Eqs. (10) and (11). With this deformed theory in mind, we first calculate the Hamiltonian which is formally analogous to Eq. (21) but constructed with the variables that obey the modified algebra Eq. (11)

$$H = \frac{1}{2}\left[\left(P_x^2 - P_y^2\right) - \omega_1^2\left(xP_y + yP_x\right) + \omega_2^2\left(x^2 - y^2\right)\right]. \tag{22}$$

where we have used the change of variables Eq. (10) and the following definitions:

$$\omega_1^2 = \frac{\beta - \omega^2\theta}{1 - \omega^2\theta^2/4}, \quad \omega_2^2 = \frac{\omega^2 - \beta^2/4}{1 - \omega^2\theta^2/4}. \tag{23}$$

Written in terms of the original variables, the Hamiltonian explicitly has the effects of the phase space deformation. These effects are encoded by the parameters θ and β. In Ref. [9], the late time behavior of this model was studied. From this formulation, two different physical theories arise, one that considers the variables x and y and a different theory based on $\hat{x}$ and $\hat{y}$. The first theory is interpreted as a "commutative" theory with a modified interaction, and this theory is referred as being realized in the commutative frame "*(C-frame)*" [12]. The second theory, which privileges the variables $\hat{x}$ and $\hat{y}$, is a theory with "noncommutative" variables but with the standard interaction and is referred to as realized in the noncommutative frame "*(NC-frame)*." In the "*C-frame*," our deformed model has a very nice interpretation that of a ghost-oscillator in the presence of constant magnetic field and allows us to write the effects of the noncommutative deformation as minimal coupling on the Hamiltonian and write the Hamiltonian in terms of the magnetic B-field [9].

To obtain the dynamics for the model, we derive the equations of motion from the Hamiltonian Eq. (22). The solutions for the variables $x(t)$ and $y(t)$ in the "*C-frame*" are:

$$\begin{aligned} x(t) &= \eta_0\, e^{\frac{-\omega_1^2}{2}t}\cosh(\omega' t+\delta_1) - \zeta_0\, e^{\frac{\omega_1^2}{2}t}\cosh(\omega' t+\delta_2),\\ y(t) &= \eta_0\, e^{\frac{-\omega_1^2}{2}t}\cosh(\omega' t+\delta_1) + \zeta_0\, e^{\frac{\omega_1^2}{2}t}\cosh(\omega' t+\delta_2), \end{aligned} \tag{24}$$

where $\omega' = \sqrt{\frac{\beta^2-4\omega^2}{4-\omega^2\theta^2}}$. For $\omega'^2 < 0$, the hyperbolic functions are replaced by harmonic functions. There is a different solution for $\beta = 2\omega$, the solutions in the "*C-frame*" are:

$$\begin{aligned} x(t) &= (a+bt)e^{\frac{-\omega_1^2}{2}t} + (c+dt)e^{\frac{\omega_1^2}{2}t},\\ y(t) &= (a+bt)e^{\frac{-\omega_1^2}{2}t} - (c+dt)e^{\frac{\omega_1^2}{2}t}. \end{aligned} \tag{25}$$

To compute the volume of the universe in the "*C-frame*," we use Eqs. (24) and (20).

$$a^3(t) = V_0\cosh^2(\omega' t), \tag{26}$$

where we have taken $\delta_1 = \delta_2 = 0$. For the case $\omega'^2 < 0$, the hyperbolic function is replaced by a harmonic function. For the case $\beta = 2\omega$, the volume is given by

$$a^3(t) = V_0 + At + Bt^2, \tag{27}$$

where V_0,A and B are constructed from the integration constants. To develop the dynamics in the "*NC-frame*," we start from the "*C-frame*" solutions and use Eq. (10), we get for the volume

$$\hat{a}^3(t) = \begin{cases} \hat{V}_0\left[\cosh^2(\omega' t) - \dfrac{\omega'^2\theta^2}{(2-\omega_1^2\theta)^2}\sinh^2(\omega' t)\right] & \text{for } \omega'^2 > 0;\\ \hat{V}_0 + Bt + Ct^2 & \text{for } \omega'^2 = 0;\\ \hat{V}_0\left[\cos^2(|\omega'|t) - \dfrac{|\omega'|^2\theta^2}{(2-\omega_1^2\theta)^2}\sin^2(|\omega'|t)\right] & \text{for } \omega'^2 < 0, \end{cases} \tag{28}$$

where $\hat{V}_0$ is the initial volume in the "*NC-frame*." We can see that for $\theta = 0$, the descriptions in the two frames are the same.

3.1. Discussion

As already discussed, phase space deformation gives two physical descriptions. If we say that both descriptions should be equal, then comparing the late time behavior for the two frames with the scale factor of de Sitter cosmology, an effective positive cosmological constant exists and is given by

$$\Lambda_{eff} = \frac{1}{3}\left(\frac{\beta^2+3\Lambda}{1+\frac{3}{16}\Lambda\theta^2}\right). \tag{29}$$

This result is the same as the one obtained from the WDW formalism of Kaluza-Klein cosmology. Therefore, one can start taking seriously the possibility that noncommutativity can shed light on the cosmological constant problem.

4. Model 3: Thermodynamics of noncommutative quantum Kerr black hole

Thermodynamics of black holes has a long history, focusing mainly on the problem of thermodynamic stability. It is known for a long time that this problem can be extended beyond the asymptotically flat spacetimes [13]. For example, in de Sitter spacetimes, thermodynamic information of black holes exhibit important differences with the previous case [14, 15]. Gibbons and Hawking found that, in analogy with the asymptotically flat space case, such black holes emit radiation with a perfect blackbody spectrum and its temperature is determined by their surface gravity. However, a feature of de Sitter space is that exists a cosmological event horizon, emitting particles with a temperature which is proportional to its surface gravity. The only way to achieve thermal equilibrium is when both surface gravities are equal, which corresponds to a degenerate case [16, 17].

Regarding AdS manifolds, it was shown that thermodynamic stability of black holes in this spacetime can be achieved [18]. In this manifold, gravitational potential produces a confinement for particles with nonzero mass, which acts as an effective cavity of finite volume, containing the black hole. An important feature of black holes in AdS manifolds is that their heat capacity is positive, opposite to the asymptotically flat case; additionally, this positiveness allows a canonical description of the system.

It is also known that thermodynamic stability of black holes is related with dynamical stability of those systems, which brings an additional motivation to study it. For example, in the asymptotically flat spacetime case, it is well known that Schwarzschild black holes are thermodynamically unstable, although they are dynamically stable [19]. For AdS spacetimes, however, it is known that both thermodynamic and dynamical stability are closely related [20, 21].

In this study, we study black holes in asymptotically flat spacetime, whereby it seems very legitimate to ask whether corrections like the above discussed noncommutativity or even semiclassical ones can modify thermodynamic properties of black holes in order to have thermodynamic stable systems.

In a number of studies [22–24], black hole entropy proposed by Bekenstein and Hawking is postulated to be the fundamental thermodynamic relation for black holes, which contains all thermodynamic information of the system. Under this assumption, corresponding classical thermodynamic formalism is constructed, finding that its thermodynamic structure resembles ordinary magnetic systems instead of fluids.

4.1. Schwarzschild and Kerr black holes

As previously discussed, it is well known that for an asymptotically flat spacetime, temperature of black holes is proportional to its surface gravity κ, as $T = \kappa\hbar/2\pi k_B c$, which is commonly

known as Hawking temperature [25]; this semiclassical result, along with Bekenstein bound for entropy, leads to the Bekenstein-Hawking entropy,

$$S_{BH} = \frac{c^3}{4G\hbar}A. \tag{30}$$

Where A stands for the area of the event horizon of the black hole. The Kerr metric, which describes a rotating black hole, can be written as:

$$ds^2 = -\left(1 - \frac{2Mr}{\Sigma}\right)dt^2 - \frac{4Mra\sin^2\theta}{\Sigma}dtd\theta + \frac{\Sigma}{\Delta}dr^2 + \Sigma d\theta^2 + \frac{B\sin^2\theta}{\Sigma}d\phi^2; \tag{31}$$

where, $\Sigma = r^2 + a^2\cos^2\theta$, $\Delta = r^2 - 2Mr + a^2$, $B = (r^2 + a^2)^2 - a^2\Delta\sin^2\theta$ and $a = J/Mc$. The area of the event horizon of a black hole is given by $A = \int_s \sqrt{\det|g_{\mu\nu}|}ds$. Applying for the elements of the metric tensor given in Eq. (31), the resulting area is:

$$A = 8\pi G^2M^2c^{-4}\left[1 + \sqrt{1 - \frac{c^2J^2}{G^2M^4}}\right]. \tag{32}$$

Assumed thermodynamic fundamental relation for Kerr black holes is found substituting the above result in Eq. (30); where $U = Mc^2$ is the internal energy of the system and J is its angular momentum. This relation can be written as [22]:

$$S_{BH}(U,J) = \frac{2\pi k_B}{\hbar c}\left(\frac{GU^2}{c^4} + \sqrt{\frac{G^2U^4}{c^8} - c^2J^2}\right); \tag{33}$$

where the following constants appear: G is the universal gravitational constant, c is the speed of light, $\hbar$ is the reduced Planck constant, and k_B is the Boltzmann constant. In recent years, in the search of suitable candidates of quantum gravity, that is, in the quest to understand microscopic states of black holes [26, 27], a number of quantum corrections to Bekenstein-Hawking (BH) entropy S_{BH} have arisen. We are interested not only in the possible thermodynamic implications of quantum corrections to this entropy but also in the consequences of introducing noncommutativity as proposed by Obregon et al. [28], considering that coordinates of minisuperspace are noncommutative. From a variety of approaches that have emerged in recent years to correct S_{BH}, logarithmic ones are a popular choice among those. These corrections arise from quantum corrections to the string theory partition function [29] and are related to infrared or low-energy properties of gravity. They are also independent of high-energy or ultraviolet properties of the theory [26, 29–31]. We will denote the selected expression for quantum and noncommutative corrected entropy as S^*, which is obtained by following the ideas presented in [28]. The starting point is the diffeomorphism between the Kantowski-Sachs cosmological model, describing a homogeneous but anisotropic universe [32], and the Schwarzschild interior solution, whose line element for $r < 2M$ is given by:

$$ds^2 = -\left(\frac{2M}{t} - 1\right)^{-1} dt^2 + \left(\frac{2M}{t} - 1\right) dr^2 + t^2(d\theta^2 + \sin^2\theta d\phi^2); \tag{34}$$

where the role of temporal t and the spatial r coordinates is swapped, that is, transformation $t \leftrightarrow r$ is performed, leading to a change on the causal structure of spacetime; considering the Misner parametrization of the Kantowski-Sachs metric it follows:

$$ds^2 = -N^2 dt^2 + e^{(2\sqrt{3}\gamma)} dr^2 + e^{(-2\sqrt{3}\gamma)} e^{(-2\sqrt{3}\lambda)} (d\theta^2 + \sin^2\theta d\phi^2). \tag{35}$$

Parameters λ and γ play the role of the *cartesian coordinates* in the Kantowski-Sachs minisuperspace. If Eqs. (34) and (35) are compared, it is straightforward to notice correspondence between components of the metric tensor, which allows us to identify the functions N, γ, and λ as:

$$N^2 = \left(\frac{2M}{t} - 1\right)^{-1}, \quad e^{(-2\sqrt{3}\gamma)} = \frac{2M}{t} - 1, \quad e^{(-2\sqrt{3}\gamma)} e^{(-2\sqrt{3}\lambda)} = t^2.$$

Next, the Wheeler DeWitt (WDW) equation for Kantowski-Sachs metric with the above parametrization of the Schwarzschild interior solution is found, along with the corresponding Hamiltonian of the system H through the Arnowitt-Deser-Misner (ADM) formalism. This Hamiltonian is introduced into the quantum wave equation $H\Psi = 0$, where $\Psi(\gamma,\lambda)$ is the wave function. This process leads to the WDW equation whose solution can be found by separation of variables.

However, we are not interested in the usual case, rather our point of interest is the solution that can be found when the symplectic structure of minisuperspace is modified by the inclusion of a noncommutativity parameter between the coordinates λ and γ, that is, the following commutation relation is obeyed: $[\lambda,\gamma] = i\theta$, where θ is the noncommutative parameter; this relation strongly resembles noncommutative quantum mechanics. It is also possible to introduce the aforementioned deformation in terms of a Moyal product [7], which modifies the original phase space, similarly to noncommutative quantum mechanics [33]:

These modifications allow us to redefine the coordinates of minisuperspace in order to obtain a noncommutative version of the WDW equation:

$$\left[\frac{\partial^2}{\partial\gamma^2} - \frac{\partial^2}{\partial\lambda^2} + 48e^{(-2\sqrt{3}\lambda + \sqrt{3}\theta P_\gamma)}\right]\Psi(\lambda,\gamma) = 0; \tag{36}$$

where P_γ is the momentum on coordinate γ. The above equation can be solved by separation of variables to obtain the corresponding wave function [6]:

$$\Psi(\lambda,\gamma) = e^{i\sqrt{3}\nu\gamma} K_{i\nu}[4e^{(-\sqrt{3}(\lambda + \sqrt{3}\nu\theta/2)}]; \tag{37}$$

where ν is the separation constant and $K_{i\nu}$ are the modified Bessel functions. We can see in Eq. (37) that the wave function has the form $\Psi(\lambda,\gamma) = e^{i\sqrt{3}\nu\gamma}\Phi(\lambda)$; therefore, dependence on the coordinate γ is the one of a plane wave. It is worth mentioning that this contribution vanishes when thermodynamic observables are calculated.

With the wave function presented in Eq. (37) for the noncommutative Kantowski-Sachs cosmological model, a modified noncommutative version of the entropy can be obtained. In order to calculate the partition function of the system, the Feynman-Hibbs procedure is considered [34]. Starting with the separated differential equation for λ:

$$\left[-\frac{d^2}{d\lambda^2}+48e^{-2\sqrt{3}\lambda+3\nu\theta}\right]\Phi(\lambda)=3\nu^2\Phi(\lambda); \tag{38}$$

In this equation, the exponential in the potential term $V(\lambda)=48\exp\left[-2\sqrt{3}\lambda+3\nu\theta\right]$ is expanded up to second order in λ and if a change of variables is considered, resulting differential equation can be compared with a one-dimensional quantum harmonic oscillator, which is a non-degenerate quantum system. In the Feynman-Hibbs procedure, the potential under study is modified by quantum effects, for the harmonic oscillator is given by:

$$U(x)=V(\overline{x})+\frac{\beta\hbar^2}{24m}V''(\overline{x});$$

where $\overline{x}$ is the mean value of x and $V''(\overline{x})$ stands for the second derivative of the potential. For the considered change of variables, the noncommutative quantum-corrected potential can be written as:

$$U(x)=\frac{3}{4\pi}\frac{E_p}{l_p^2}e^{3\nu\theta}\left[x^2+\frac{\beta l_p^2E_p}{12}\right]. \tag{39}$$

The above potential allows us to calculate the canonical partition function of the system:

$$Z(\beta)=C\int_{-\infty}^{\infty}e^{-\beta U(x)}dx; \tag{40}$$

where β^{-1} is proportional to the Bekenstein-Hawking temperature and $C=\left[2\pi l_p^2E_p\beta\right]^{-1/2}$ is a constant. Substituting $U(x)$ into Eq. (40) and performing the integral over x, the partition function is given by:

$$Z(\beta)=\sqrt{\frac{2\pi}{3}}\frac{e^{3\nu\theta/2}}{E_p\beta}\exp\left[-\frac{\beta^2E_p^2}{16\pi}e^{3\nu\theta}\right]; \tag{41}$$

This partition function allows us to calculate any desired thermodynamic observable by means of the thermodynamic connection of the Helmholtz free energy $A=-k_BT\ln Z(\beta)$, with the internal energy and the Legendre transformation:

$$\langle E\rangle=-\frac{\partial}{\partial\beta}\ln Z(\beta);\quad \frac{S}{k_B}=\ln Z(\beta)+\beta\langle E\rangle.$$

With this equation for $\langle E\rangle$, the value of β can be determined as a function of the Hawking temperature $\beta_H=8\pi Mc^2/E_p$, obtaining:

$$\beta = \beta_H e^{-3\nu\theta}\left[1 - \frac{1}{\beta_H e^{-3\nu\theta}}\frac{1}{Mc^2}\right]; \tag{42}$$

With the aid of this relation and the Legendre transformation for Helmholtz free energy presented above, an expression for the noncommutative quantum-corrected black hole entropy can be found:

$$S^\star = S_{BH}e^{-3\nu\theta} - \frac{1}{2}k_B \ln\left[\frac{S_{BH}}{k_B}e^{-3\nu\theta}\right] + \mathcal{O}(S_{BH}^{-1}e^{-3\nu\theta}). \tag{43}$$

Functional form of S^* is basically the same than quantum-corrected commutative case, besides the addition of multiplicative factor $e^{-3\nu\theta}$ to Bekenstein-Hawking entropy. From now on, we will denote the noncommutative term in this expression, for the sake of simplicity, as:

$$\Gamma = \exp\left[-3\nu\theta\right].$$

Likewise, natural units, $G = \hbar = k_B = c = 1$, will be considered through the rest of this chapter. In this section, the previous result found in Eq. (43) for the Schwarzschild noncommutative black hole is extended to the rotating case, that is, the Kerr black hole. This is not straightforward as an analog expression for the noncommutative entropy of the rotating black hole is required, implying the application of a similar procedure to the one presented above: A diffeomorphism between the Kerr metric and some appropriated cosmological model and the procedure is presented in Ref. [28]. To our knowledge, the implementation of this procedure has not been yet reported. However, we are interested to have an expression to study not only the static case but also the effect of angular momentum over the physical properties of the system. Our proposal to have an *approximated* relation for the extended Kerr black hole entropy starts with the assumption that for entropy found in Eq. (43), Bekenstein-Hawking entropy for Schwarzschild in this relation S_{BH} can be also substituted for its Kerr counterpart given in Eq. (33). As the noncommutative relation for quantum Schwarzschild black hole entropy is correct, it is clear that our proposal to the quantum noncommutative Kerr black hole entropy will be a good approximation for small values of J when compared to the values of U^2, whatever be the exact expression for the rotating case. For our proposal, in the vicinity of small values of angular momentum, λ and γ, the coordinates of the minisuperspace are the same than in the Schwarzschild case. Therefore, the corrected entropy that will be analyzed is:

$$S^\star = 2\pi\,\Gamma\left(U^2 + \sqrt{U^4 - J^2}\right) - \frac{1}{2}\ln\left[2\pi\,\Gamma\left(U^2 + \sqrt{U^4 - J^2}\right)\right]. \tag{44}$$

A clarification must be made that Eq. (44) is not a unique valid generalization for the quantum-corrected noncommutative entropy of a rotating black hole in the neighborhood of small J. However, we claim that this is the most natural extension from the Schwarzschild case to the Kerr one. Although, to our knowledge, there is no general argument to support that Eq. (43) remains valid for any other black hole besides the Schwarzschild one. However, there is some evidence that for the case of charged black holes, the functional form of Eq. (43) is maintained, at least partially [35].

Through the rest of this section, all thermodynamic expressions with superindex ⋆ will stand for noncommutative quantum-corrected quantities derived from Eq. (44), meanwhile, all thermodynamic functions without subindexes or superindexes will represent the corresponding noncommutative Bekenstein-Hawking counterparts. It is known that noncommutativity parameter θ in spacetime is small, from observational evidence [36, 37]; although in this study, noncommutativity on the coordinates of minisuperspace is considered instead, it is expected such parameter to be also small [38]; nonetheless, its actual bounds are not well known yet. We will consider that parameter Γ is bounded in the interval $0 < \Gamma \leq 1$. As previously mentioned for the non-corrected Kerr black hole, Eq. (44) is now assumed to be a fundamental thermodynamic relation for the rotating black hole, when noncommutative and quantum corrections are considered. It is well known from classical thermodynamics that fundamental equations contain all the thermodynamic information of the considered system [39], and, as a consequence, modifications introduced by corrections to entropy (which imply modifications to thermodynamic information) are carried through all thermodynamic quantities.

In **Figure 1**, plots for both Bekenstein-Hawking entropy and its quantum-corrected counterpart are presented for $\Gamma = 1$. **Figure 1a** shows plots for $S = S(U)$ and $S^{\star} = S^{\star}(U)$; Bekenstein-Hawking entropy is above the quantum-corrected one, in all its dominion, even in the region of low masses, where entropy is thermodynamically stable [22, 24]. **Figure 1b** presents the same curves as function of angular momentum instead, for $U = 1$; a similar behavior can be noticed in this case. If this analysis is performed over the noncommutative relation, it is found that for small values of θ, differences between both S_{BH} and S^{*} are negligible.

4.2. Equations of state

Working in entropic representation, fundamental Bekenstein-Hawking thermodynamic relation for a Kerr black hole has the form $S_{BH} = S_{BH}(U,J)$. For these systems, partial derivatives of S_{BH} $T \equiv (\partial_S U)_J$ and $\Omega \equiv (\partial_J U)_S$ play the role of thermodynamic equations of state; here, T

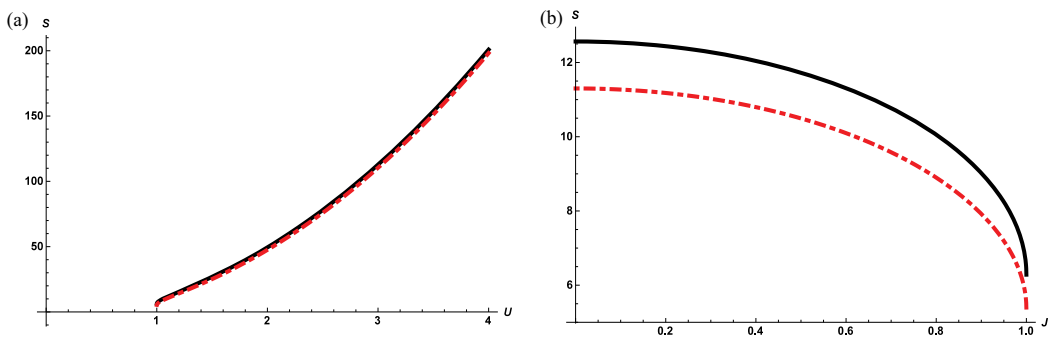

Figure 1. A comparison between Bekenstein-Hawking entropy (solid line) and its quantum-corrected counterpart (dash-dot line) is presented; both relations exhibit a region where entropy is a concave function, implying the existence of metastable states. (a) Entropy as a function of internal energy, $J = 1$. (b) Entropy as a function of angular momentum for $U = 1$, $S = S(1, J)$.

stands for Hawking temperature and Ω is the angular velocity. In entropic representation, equations of state are defined by:

$$\frac{1}{T} \equiv \left(\frac{\partial S_{BH}}{\partial U}\right)_J; \quad \frac{\Omega}{T} \equiv -\left(\frac{\partial S_{BH}}{\partial J}\right)_U. \tag{45}$$

For the entropy of the quantum-corrected entropy S^*, the above relations remain valid. In entropic representation, T and Ω for the noncommutative quantum-corrected entropy are given by:

$$\frac{1}{T^\star} = \frac{U\left(4\pi\,\Gamma\sqrt{U^4 - J^2} + 4\pi\,\Gamma U^2 - 1\right)}{\sqrt{U^4 - J^2}}, \tag{46a}$$

$$\frac{\Omega^\star}{T^\star} = \frac{1}{2}\frac{J\left(4\pi\,\Gamma\sqrt{U^4 - J^2} + 4\pi\,\Gamma U^2 - 1\right)}{\sqrt{U^4 - J^2}\left(U^2 + \sqrt{U^4 - J^2}\right)}. \tag{46b}$$

The same relations for noncommutative Bekenstein-Hawking entropy are calculated as:

$$\frac{1}{T} = \frac{4\pi\,\Gamma U(U^2 + \sqrt{U^4 - J^2})^2}{\sqrt{U^4 - J^2}}, \tag{47a}$$

$$\frac{\Omega}{T} = \frac{2\pi\,\Gamma J}{\sqrt{U^4 - J^2}}. \tag{47b}$$

When the overall effect over T and T^* of noncommutativity was analyzed, different values of parameter Γ were tested, including $\Gamma = 1$ (commutative case). The corresponding curves present a noticeable effect by the presence of Γ; nonetheless, functional behavior either of T or T^* is not modified. A comparison of the plots of both temperature is presented in **Figure 2** for Γ = 1, in order to illustrate how quantum corrections introduced in entropy affect thermodynamic properties of black holes. Resulting curves of T and T^* are very similar, although the latter one is slightly higher than $T(U,J)$, an opposite result to the one obtained when entropy was studied; it indicates that for a given change in its internal energy, variations of entropy are greater for quantum-corrected entropy when compared to the Bekenstein-Hawking one.

As previously mentioned, when values in the vicinity of Γ = 1 are considered, temperature is minimally affected by noncommutativity. We also tested smaller values of noncommutativity parameter, it was found that the maximum values that T and T^* are able to reach are noticeably increased. However, the shape of both curves is not modified by changing the value of Γ.

An interesting result is obtained for angular velocity Ω, this property seems to be independent of both quantum and noncommutative corrections to entropy, namely:

$$\Omega = \Omega^{\star} = \frac{J}{2U\left(U^2 + \sqrt{U^4 - J^2}\right)}. \tag{48}$$

In **Figure 3**, plots for angular velocity are presented. As this equation of state is not modified by any of the considered corrections, only one curve per graphic appears; first, in **Figure 3a**, Ω as a function of the black hole internal energy is presented, as can be noticed, angular velocity steadily decreases as black hole mass is increased, asymptotically going to zero. **Figure 3b** considers instead the case where the black hole mass is fixed at $U = 10$, for which Ω grows until it reaches a maximum value determined by the square root that appears in the denominator of Eq. (48), beyond this value angular velocity becomes complex.

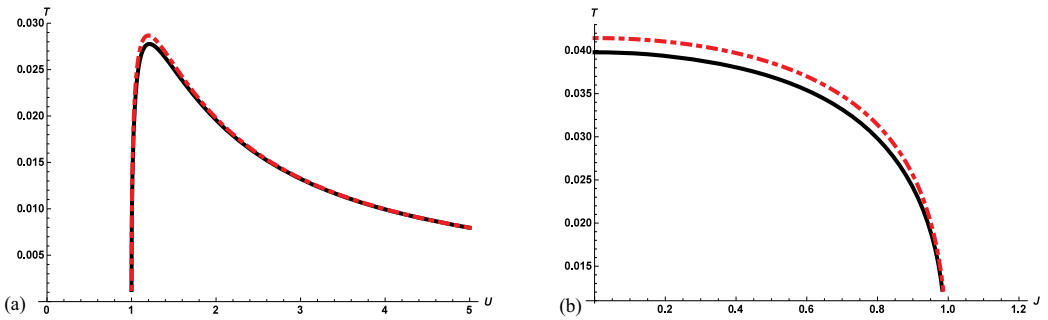

Figure 2. Temperature in the commutative case Γ = 1 for Bekenstein-Hawking usual entropy and its quantum-corrected counterpart. (a) Plots of $T(U,1)$ (solid line) versus $T^{\star}(U,1)$ (dash-dot line) as a function of internal energy for a fixed value of angular momentum $J = 1$. (b) The same curves, considering instead for variations in J at a fixed $U = 1$.

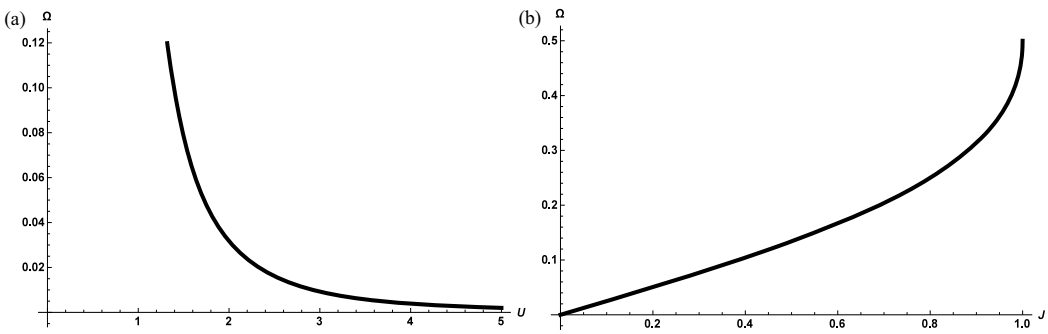

Figure 3. Angular velocity for Bekenstein-Hawking entropy and the quantum-corrected version are presented in Eq. (44). (a) Ω as a function of internal energy considering a fixed value of angular momentum ($J = 1$). (b) Angular velocity as a function of angular momentum considering $U = 10$.

5. Conclusions

In section 2, if we turn our attention to the case where there is no deformation on the coordinates. Taking the noncommutative parameter θ = 0, we have that the frequency and the effective cosmological constant are given by:

$$\tilde{\omega}^2 = \omega^2 - \frac{\beta^2}{4}, \qquad and \qquad \tilde{\Lambda}_{eff} = \Lambda_{eff} + \frac{3\beta^2}{8}. \tag{49}$$

From the last equation, we get the most interesting result of this section. We can see that noncommutative parameter β and Λ_{eff} compete to give the effective cosmological constant $\tilde{\Lambda}_{eff}$. If we consider the case of a flat universe with a vanishing Λ_{eff}, we see that $\tilde{\Lambda}_{eff} = \frac{3\beta^2}{8}$. This shows the relationship between the cosmological constant and the deformed parameter. Recently, some evidence on the possibility that the effects of the phase space deformation could be related to the late time acceleration of the universe as well as to the cosmological constant were presented [8]. Interestingly, in the particular case of $\beta = \omega^2\theta$, we find that frequency reduces to $\tilde{\omega}^2 = \omega^2$ and we have that $\tilde{\Lambda}_{eff} = \Lambda_{eff}$. In this case, even as we have done a deformation on the minisuperspace of the theory, the effects cancel out and the resulting theory behaves as in the commutative theory. The results are similar for model 2 (Section 3), where under a totally classical regime, we find the same functional relationship between the cosmological constant and the deformation parameter β. Therefore, we conclude that noncommutative phase space deformations can hold the answer to the cosmological constant problem.

Then, in Section 4, an analysis on the thermodynamic properties of noncommutative quantum-corrected Kerr black holes using an approximate relation was presented. Although the resulting expressions are mathematically more complicated, the thermodynamic properties still retain the same functional behavior with respect to those calculated through Bekenstein-Hawking entropy. It can be proved that Kerr black holes do not pass through a first-order phase transition [4]; since the local criteria to find the critical point are not fulfilled for any value in the domain, corresponding isotherms do not exhibit van der Waals loops, and the Maxwell construction cannot be obtained; all of which are characteristic of this kind of transition. Regarding the effective noncommutativity incorporated in the coordinates of minisuperspace, outside the vicinity where $\Gamma \approx 1$, changes introduced by this parameter over the thermodynamic information of the system are relevant. For a complete analysis using this phase deformations, for example, thermodynamic response functions, thermodynamic stability, and phase transitions for Kerr black holes, see Ref. [4].

Acknowledgements

Eri Atahualpa Mena Barboza thanks the financial support from C.U.CI., U. de G. project Desarrollo de la investigación y fortalecimiento del posgrado 235506.

Author details

E.A. Mena-Barboza[1]*, L.F. Escamilla-Herrera[2], J.C. López-Domínguez[3] and J. Torres-Arenas[4]

*Address all correspondence to: emena@cuci.udg.mx

1 Centro Universitario de la Ciénega, Universidad de Guadalajara Ave. Universidad, Ocotlán, Jalisco, México

2 Instituto de Ciencias Nucleares, Universidad Nacional Autónoma de México, Ciudad de, México

3 Unidad Académica de Física, Universidad Autónoma de Zacatecas, Calzada Solidaridad, Zacatecas, México

4 Departamento de Física de la Universidad de Guanajuato, León, Guanajuato, México

References

[1] Rezaei-Aghdam A, Darabi F, Rastkar AR. Physics Letters B. 2005;**615**:141-145. [gr-qc/0412089]

[2] Pérez-Payán S, Sabido M, Mena E. Available from: http://arxiv.org/abs/1111.6137v2

[3] Sinuhe Pérez-Payán, Sabido M, Mena E, Yee-Romero C. Analysis of scalar field cosmology with phase space deformations. Advances in High Energy Physics. 2014. Article ID 958137, 5 pages. DOI:10.1155/2014/958137

[4] Escamilla-Herrera LF, Mena-Barboza E, Torres-Arenas J. Entropy. 2016;**18**(11):406. DOI:10.3390/e18110406

[5] García-Compean H, Obregón O, Ramírez C, Sabido M. Physical Review D. 2003;**68:**044015; García-Compean H, Obregón O, Ramírez C, Sabido M. Physical Review D. 2003;**68:**045010; Aschieri P, Dimitrijevic M, Meyer F, Wess J. Classical and Quantum Gravity. 2006;**23**:1883; Calmet X, Kobakhidze A. Physical Review D. 2005;**72**:045010; Alvarez-Gaume L, Meyer F, Vazquez-Mozo MA. Nuclear Physics B. 2006;**753:**92; Estrada-Jimenez S, García-Compean H, Obregón O, Ramírez C. Physical Review D. 2008;**78**:124008

[6] García-Compeán H, Obregón O, Ramírez C. Noncommutative quantum cosmology. Physical Review Letters. 2002;**88**:161301

[7] Barbosa GD, Pinto-Neto N. Physical Review D. 2004;**70:**103512; Guzman W, Sabido M, Socorro J. Physical Review D. 2007;**76:**087302, International Journal of Modern Physics D. 2007;**16:**1625; Vakili B, Khosravi N, Sepangi HR. Classical and Quantum Gravity. 2007;**24:**931; Aguero, Aguilar JA, Ortiz SC, Sabido M, Socorro J. International Journal of

Theoretical Physics. 2007;**46:**2928; Ortiz C, Mena-Barboza E, Sabido M, Socorro J. International Journal of Theoretical Physics. 2008;**47:**1240; Guzman W, Ortiz C, Sabido M, Socorro J, Aguero MA. International Journal of Modern Physics D. 2007;**16:**1625; Obregon O, Quiros I. Physical Review. 2011;**D84**:044005; Guzman W, Sabido M, Socorro J, Physics Letters. 2011;**B697**:271-274.

[8] Vakili B, Pedram P, Jalalzadeh S. Physics Letters B. 2010;**687**:119-123

[9] Pérez-Payán S, Sabido M, Yee-Romero C. Physical Review D. 2013;**88**:027503

[10] Sabido M, Yee-Romero C. Physics Letters B. 2016;**757:**57

[11] Cordero R, Garcia-Compean H, Turrubiates FJ. Physical Review D. 2011;**83**:125030

[12] Barbosa GD. Physical Review D. 2005;**71**:063511

[13] Gibbons GW, Hawking SW. Cosmological event horizons, thermodynamics, and particle creation. Physical Review D. 1977;**15**:2738-2751

[14] Davies PCW. Thermodynamic phase transitions of Kerr-Newman black holes in de Sitter space. Classical and Quantum Gravity. 1989;**6**:1909

[15] Chamblin A, Emparan R, Johnson CV, Myers RC. Charged AdS black holes and catastrophic holography. Physical Review D. 1999;**60**:064018

[16] Nariai H. On some static solutions of Einstein's gravitational field equations in a spherically symmetric case. Science Reports of the Tohoku Imperial University. 1950;**34**:160-167

[17] Nariai H. On a new cosmological solution of Einstein's field equations of gravitation. Science Reports of the Tohoku Imperial University. 1950;**35**:62-67

[18] Hawking SW, Page DN. Thermodynamics of black holes in anti-de Sitter space. Communications in Mathematical Physics. 1983;**87**:577-588

[19] Price RH. Nonspherical perturbations of relativistic gravitational collapse. 1. Scalar and gravitational perturbations. Physical Review D. 1972;**5**:2419

[20] Gubser SS, Mitra I. The evolution of unstable black holes in anti-de Sitter space. Journal of High Energy Physics. 2001;**0108**:018

[21] Hollands S, Wald RM. Stability of black holes and black branes. Communications in Mathematical Physics. 2013;**321**:629-680

[22] Davies PCW. The thermodynamics of black holes. Proceedings of the Royal Society A. 1977;**353**:499

[23] Martinez EA. The postulates of gravitational thermodynamics. Physical Review D. 1996;**54**:6302

[24] Escamilla L, Torres-Arenas J. Thermodynamic response functions and Maxwell relations for a Kerr black hole. Revista Mexicana de Fisica. 2014;**60**:59-68

[25] Hawking SW. Gravitational radiation from colliding black holes. Physical Review Letters. 1971;**26**:1344

[26] Keeler C, Larsen F, Lisbão P. Logarithmic corrections to $\mathcal{N} \geq 2$ black hole entropy. Physical Review D. 2014;**90**:043011

[27] Sen A. Logarithmic corrections to Schwarzschild and other non-extremal black hole entropy in different dimensions. Journal of High Energy Physics. 2013;**04**:156

[28] López-Domínguez JC, Obregón O, Sabido M, Ramírez C. Towards noncommutative quantum black holes. Physical Review D. 2006;**74**:084024

[29] Sen A. Logarithmic corrections to $\mathcal{N} \geq 2$ black hole entropy: An infrared window into the microstates. General Relativity and Gravitation. 2012;**44**:1207-1266

[30] Banerjee S, Gupta RK, Mandal I, Sen A. Logarithmic corrections to and black hole entropy: A one loop test of quantum gravity. Journal of High Energy Physics. 2011;**03**:143

[31] Carlip S. Logarithmic corrections to black hole entropy, from the Cardy formula. Classical and Quantum Gravity. 2000;**17**:4175

[32] Kantowski R, Sachs RK. Some spatially homogeneous anisotropic relativistic cosmological models. Journal of Mathematical Physics. 1966;**7**:443

[33] Gamboa J, Loewe M, Rojas JC. Noncommutative quantum mechanics. Physical Review D. 2011;**64**:067901

[34] Feynman RP, Hibbs AR. Quantum Mechanics and Path Integrals. 1st ed. New York: McGraw-Hill; 1965

[35] Zacarias S, Escamilla-Herrera LF. To be published.

[36] Aoki H, Ishibashi N, Iso S, Kawai H, Kitazawa Y, Tada T. Noncommutative Yang-Mills in IIB matrix model. Nuclear Physics B. 2000;**565**:176

[37] Joby PK, Chingangbam P, Das S. Constraint on noncommutative spacetime from PLANCK data. Physical Review D. 2015;**91**:083503

[38] Guzmán W, Sabido M, Socorro J. On noncommutative minisuperspace and the Friedmann equations. Physics Letters B. 2011;**697**:271

[39] Callen HB. Thermodynamics and an Introduction to Thermo-statistics. 2nd ed. Singapore: John Willey & Sons; 1985. pp. 35, 183, 215

Chapter 10

Semi-Analytic Techniques for Solving Quasi-Normal Modes

Chun-Hung Chen, Hing-Tong Cho and
Alan S. Cornell

Additional information is available at the end of the chapter

http://dx.doi.org/10.5772/68114

Abstract

In this chapter, we discuss an approach to obtaining black hole quasi-normal modes known as the asymptotic iteration method, which was initially developed in mathematics as a new way to solve for eigenvalues in differential equations. Furthermore, we demonstrate that the asymptotic iteration method allows one to also solve for the radial quasi-normal modes on a variety of black hole spacetimes for a variety of perturbing fields. A specific example for Dirac fields in a general dimensional Schwarzschild black hole spacetime is given, as well as for spin-3/2 field quasi-normal modes.

Keywords: extra-dimensions, quasi-normal modes, quantum fields in curved space, supergravity, blackholes

1. Introduction

Quasi-normal modes (QNMs) are one of the most important theoretical results in modern cosmology, especially for studying the perturbations from various fields on black hole spacetimes. In this theory, the behaviour of a particle around a black hole is dominated by the radial equation, and the evolution of QNMs behaves like damped harmonic oscillators with specific frequencies. The frequencies are constructed by complex modes, where the real part is the actual frequency and the imaginary part represents the damping rate due to the gravitational emission. In lay terms, the QNMs are the characteristic sounds of the black hole.

With the recent ground breaking progress into the detection of gravitational wave data, where it is believed that the last part of the gravitational wave emission, called the ring down phase,

is dominated by the QNMs, it is exciting that perturbation theory in curved spacetimes can now be possibly tested in a real experimental system, and that a large number of scientists from all over the world are involved in the data analysis. Related issues of the QNMs within the range of research into cosmology include studying the stability of black holes and probing the dimensionality of spacetime. It is, however, the observable gravitational wave data from the collisions of binary black hole systems, which indicates how the background spacetime will finally become a Kerr black hole spacetime through gravitational wave emission. Perturbation theory on a Kerr black hole spacetime still includes some difficulties in the higher dimensional cases, which will be a challenge for the theoretical community for some time to come.

Methods that are used to obtain QNMs can be both semi-analytic and numerical methods and were introduced by Cho et al. [1], the most famous of these is the WKB approximation methods [2]. Note that, the WKB approximation has been extended to sixth order [3] and is powerful in many cases, but like all methods have several limitations. A new method has been developed in recent years called the asymptotic iteration method (AIM), which is more efficient in some cases. This method was used to solve eigenvalue problems for the second-order homogeneous linear differential equations [4, 5] and also successfully used in calculating QNMs [6]. Reviewing this AIM and providing the tools "in detail" for studying QNMs in the higher dimensional spacetimes are the key focus of this chapter.

As such, this chapter is organised as follows: In the next section, we shall review the recent progress on perturbation theory in curved spacetimes. More precisely, we shall present a comparison of the spin-3/2 field in general dimensional Schwarzschild spacetimes with other spin fields, including the spherical harmonics and the radial equations. In Section 3, we shall review the AIM and present an exercise detailing how the QNMs of Dirac fields are obtained in general dimensional Schwarzschild spacetimes. Furthermore, we can also compare to spin-3/2 QNMs results. We shall conclude with a brief summary.

2. Perturbation theory in a general dimensional Schwarzschild spacetime

2.1. Eigenvalue problem on spheres

For perturbation theory in curved spacetimes, separability can always simplify the equations of motion and plays an important role. For the maximally symmetric spacetime cases, the eigenmodes on spheres allow us to separate the angular part for various spin fields and simplify the equations of motion from the general form into a "radial-time" presentation. For the case of bosonic fields, an earlier study by Rubin and Ordóñez presented a systematic study [7, 8] as well as in a later work by Higuchi [9]. For the case of fermionic fields, Camporesi and Higuchi presented the eigenmodes for spinor fields on arbitrary dimensional spheres [10], and in a recent work by the authors [11], the spinor-vector eigenmodes on arbitrary dimensional spheres were derived using a similar approach to Camporesi and Higuchi's methods. In this section, we review the structure of these eigenmodes, especially for the case of spinor-vector fields, which shall be presented with the characteristics of both spinor and vector fields.

The metric of the N-sphere is given by

http://dx.doi.org/10.5772/68114

$$d\Omega_N^2 = d\theta_N^2 + sin^2\theta_N d\Omega_{N-1}^2, \tag{1}$$

where, in this metric, we restrict the sphere to radius $r = 1$. When we consider the eigenvalue problem in this spacetime, the bosonic field and fermionic field shall be studied with different operators. In the case of bosonic fields, the operator for the eigenvalue equation will be the Laplacian operator $\nabla^\mu\nabla_\mu$, whereas, in the case of fermionic fields, it will be the Dirac operator $\gamma^\mu\nabla_\mu$, where γ^μ is the Dirac gamma matrices. In **Table 1**, we present the structure of the eigenmodes with various spin fields on the sphere and also the conditions on the specific mode, such as the transverse, traceless and symmetric conditions.

Looking first at the longitudinal and non-transverse modes for bosonic fields, the longitudinal and non-transverse eigenfunctions for higher spins are the linear combination of the eigenfunctions for the lower spin one. For example, for the vector fields, the longitudinal eigenvector is the covariant derivative of a scalar eigenfunction. Furthermore, for the symmetric tensor fields, there are three types of non-transverse eigenfunctions. The first one is the metric element multiplied by a scalar eigenfunction, the second one is the longitudinal-longitudinal eigenfunction, which is the linear combination for longitudinal eigenvectors, and the last one is

Fields	**Eigenfunction**	**Eigenvalue**
Scalar	$T^{(l)}$	$-l(l+N-1), l = 0, 1, 2, ...$
Spinor	$\psi^{(j)}$	$\pm i(j+\frac{N-1}{2}), j = 1/2, 3/2, 5/2, ...$
Vector	Longitudinal eigenvector	
	$L_\mu^{(l)} = \nabla_\mu T^{(l)}$	$-l(l+N-1)+1, l = 1, 2, 3, ...$
	Transverse eigenvector	
	$T_\mu^{(l)}, \nabla^\mu T_\mu^{(l)} = 0$	$-l(l+N-1)+(N-1), l = 1, 2, ...$
Spin.-	Non-transverse-traceless eigenmode	
Vector	$\psi_\mu^{(j)} = \nabla_\mu\psi^{(j)} + a_{(\pm)}\gamma_\mu\psi^{(j)}$	$\pm i\sqrt{j^2+(N-1)j+\frac{1}{4}(N-5)(N-1)}$
	Transverse and traceless eigenmode	
	$\psi_\mu^{(j)} = (\psi_{\theta_N}, \psi_{\theta_i}), \nabla^\mu\psi_\mu = \gamma^\mu\psi_\mu = 0$	$\pm i(j+\frac{N-1}{2}), j = 1/2, 3/2..., N \geq 3$
Sym.-	$g_{\mu\nu}T^{(l)}$	$-l(l+N-1), l = 0, 1, 2, ...$
Tensor	Longitudinal-longitudinal (traceless) modes	
	$L_{L^{\mu\nu}}^{(l)} = 2\nabla_\mu\nabla_\nu T^{(l)} - (\frac{2}{N})g_{\mu\nu}\nabla^\alpha\nabla_\alpha T^{(l)}$	$-l(l+N-1)+2N, l = 2, 3, 4, ...$
	Longitudinal-transverse (traceless) modes	
	$L_{T^{\mu\nu}}^{(l)} = \nabla_\mu T_\nu^{(l)} + \nabla_\nu T_\mu^{(l)}$	$-l(l+N-1)+(N+2), l = 2, 3, 4, ...$
	Transverse-traceless modes	
	$T_{\mu\nu}^{(l)}, \nabla^\mu T_{\mu\nu}^{(l)} = g^{\mu\nu}T_{\mu\nu}^{(l)} = T_{[\mu\nu]}^{(l)} = 0$	$-l(l+N-1)+2, l = 2, 3, 4, ...$

Table 1. Structure of the eigenvalue problem for various fields on N-sphere.

the longitudinal-transverse eigenfunction, which is the linear combination of transverse eigenvectors. Analogous to the non-transverse-traceless modes for fermionic fields, the non-transverse-traceless eigenspinor-vector is the linear combination of the eigenspinor. We note that there are two non-transverse-traceless eigenspinor-vectors, due to the $a_{(+)}$ and $a_{(-)}$ being different factors where

$$a_{(\pm)} = -\frac{i}{2}\left(j+\frac{N-1}{2}\right) \pm i\sqrt{j^2+(N-1)j+\frac{1}{4}(N-5)(N-1)}. \tag{2}$$

This indicates a special signature for spinor-vector harmonics that do not have the transverse-traceless eigenmodes for S^2.

Next, we look at the transverse-traceless modes. For the bosonic fields, an unique way to construct this type of eigenfunction was suggested by Higuchi [9]. Analogous to the fermionic case, for the transverse-traceless eigenspinor-vector, $\psi_\mu = (\psi_{\theta_N}, \psi_{\theta_i})$, ψ_{θ_N} behaves like a spinor on $N-1$ spheres, and ψ_{θ_i} behaves like a spinor-vector on $N-1$ spheres. If we let ψ_{θ_i} be the linear combination of the non-transverse-traceless eigenspinor-vector on $N-1$ spheres, ψ_{θ_N} has to be non-zero to satisfy the transverse and traceless conditions. If we let ψ_{θ_i} be the linear combination of the transverse-traceless eigenspinor-vector on N – 1-spheres, ψ_{θ_N} has to be zero, because the ψ_{θ_i} already satisfies the transverse and traceless condition.

On the other hand, we can take a look at the eigenvalue. For the bosonic fields, all of the eigenvalues contain a similar first term, which is the eigenvalue of the scalar fields; however, the starting value of the angular momentum quantum number l has to be considered case by case, as well as the second term for higher spin cases. For the fermionic cases, the eigenvalue of the non-transverse-traceless eigenspinor-vector has a very different value from the spinor eigenvalue, though the eigenvalue of the transverse and traceless eigenspinor-vector is exactly the same as the eigenspinor for the spin-1/2 field.

As a remark on this section, the eigenfunctions and eigenvalues on N-spheres are independent for bosonic and fermionic fields, even though they have a very similar style of structure, which indicates that the spherical harmonics for a bosonic field cannot be constructed by the spherical harmonics of a fermionic field, and vice versa. In this section, we presented a review of the eigenvalue problem for scalar, spinor, vector, spinor-vector, and symmetric tensor fields on spheres, where further details can be found in the papers referred to in this section.

2.2. Effective potentials

In perturbation theory with various fields in the Schwarzschild black hole spacetime, a radial equation (Schrödinger-like equation) will be derived from the equations of motion, which shall be the master equation of this study. In a general way, the studies of perturbation theory in maximally symmetric spacetimes are well established and include the (A)dS and Reissner-Nordström spacetimes, but not for the spin-3/2 fields yet. With our recent progress in the study of spin-3/2 fields, we may now do a comparison of various massless fields in a general dimensional Schwarzschild black hole spacetime in this section.

http://dx.doi.org/10.5772/68114

The metric of a general dimensional Schwarzschild spacetime is given by

$$dS^2 = -f(r)dt^2 + f^{-1}(r)dr^2 + r^2 d\Omega_{D-2}^2, \tag{3}$$

where $f(r) = 1 - 2M/r^{D-3}$, D is the dimensional factor and M is the mass of the black hole. The master equation can be obtained from the equations of motion by a change of coordinates to give the Schrödinger-like equation

$$\frac{d^2}{dr_*^2}\Psi_s + (\omega^2 - V_s)\Psi_s = 0, \tag{4}$$

where the subscript s represents the "spin" and r^* represents the "tortoise" coordinate, which can be defined as follows $\frac{d}{dr_*} = f(r)\frac{d}{dr}$. The mathematical meaning of this coordinate is that a mapping of the location of the event horizon of the Schwarzschild black hole from r_0 (where $f(r_0) = 0$) is taken to minus infinity.

We shall first look at the four-dimensional cases, where, for the bosonic fields, the radial equation can be represented with the potential [12]

$$V_s = f\left[\frac{l(l+1)}{r^2} + (1 - s^2)\frac{2M}{r^3}\right], \tag{5}$$

where l is an integer, $s = 0$ represents the effective potential for scalar fields, $s = 1$ for the electromagnetic fields, and $s = 2$ represents the "vector-type" perturbation for gravitational fields (which is the Regge-Wheeler equation). The "scalar-type" perturbation for the gravitational field in the four-dimensional case is the Zerilli equation, with an effective potential

$$V_{Z,s=2} = \frac{2f}{r^3}\left[\frac{9M^3 + 3\lambda^2 Mr^2 + \lambda^2(1+\lambda)r^3 + 9M^2\lambda r}{(3M + \lambda r)^2}\right], \tag{6}$$

where $\lambda = (l-1)(l+2)/2$.

For the fermionic fields in the four-dimensional Schwarzschild case, the effective potential can be shown as follows [13, 14]:

$$V_s = \pm f\frac{dW_s}{dr} + W_s^2, \tag{7}$$

where

$$W_{s=\frac{1}{2}} = \frac{\sqrt{f}(j+\frac{1}{2})}{r}, j = \frac{1}{2}, \frac{3}{2}, ... \tag{8}$$

$$W_{s=\frac{3}{2}} = \frac{\sqrt{f}(j-\frac{1}{2})(j+\frac{1}{2})(j+\frac{3}{2})}{r\left[(j+\frac{1}{2})^2 - f\right]}, j = \frac{3}{2}, \frac{5}{2}, ... \tag{9}$$

Note that the "±" represents two isospectral potentials, which were known as the supersymmetric partner potentials.

For the higher dimensional cases, there are more types of effective potentials, which can be presented in the four-dimensional case, which indicates that some special cases will not exist in the four-dimensional cases but will exist in the higher dimensional one. In the following sections, we shall discuss the higher dimensional effective potentials as presented in **Table 2**.

Starting with bosonic fields, we have one effective potential for scalar fields in the higher dimensional Schwarzschild spacetime, and it is necessary to satisfy Eq. (5) when $D = 4$ and $s = 0$. For the case of electromagnetic fields, there are two types of effective potentials, which are the

Fields	V_s
Scalar [12]	
	$V_{s=0} = f\left[\frac{l(l+D-3)}{r^2} + \frac{D-2}{4}\left(\frac{D-4}{r^2}f + \frac{2f'}{r}\right)\right]$
	$l = 0, 1, 2, \ldots.$
Dirac [13]	
	$V_{s=1/2} = \pm f\frac{dW_{s=1/2}}{dr} + W^2_{s=1/2}$
	where
	$W_{s=1/2} = f(\frac{l+\frac{D-3}{2}}{r}), j = 1/2, 3/2, 5/2, \ldots.$
Electromagnetic [15]	
	Scalar-type perturbation
	$V_{S,s=1} = f\left[\frac{l(l+D-3)+\frac{(D-2)(D-4)}{4}}{r^2} - \frac{(3D-8)(D-4)M}{2r^{D-1}}\right].$
	$l = 1, 2, 3, \ldots.$
	Vector-type perturbation
	$V_{V,s=1} = f\left[\frac{l(l+D-3)+\frac{(D-2)(D-4)}{4}}{r^2} - \frac{D(D-4)M}{2r^{D-1}}\right].$
	$l = 1, 2, 3, \ldots.$
Rarita-Schwinger [11]	
	Related to the non-TT eigenmodes
	$V_{NTT,s=3/2} = \pm f\frac{dW_{NTT,s=3/2}}{dr} + W^2_{NTT,s=3/2}$
	where
	$W_{NTT,s=3/2} = \frac{\sqrt{f}(j+\frac{D-3}{2})}{r}\left[\frac{(\frac{2}{D-2})^2(j+\frac{D-3}{2})^2 - 1 - \frac{D-4}{D-2}(\frac{2M}{r^{D-3}})}{(\frac{2}{D-2})^2(j+\frac{D-3}{2})^2 - f}\right], j = 1/2, 3/2, 5/2\ldots.$
	Related to the TT eigenmodes
	$V_{TT,s=3/2} = \pm f\frac{dW_{TT,s=3/2}}{dr} + W^2_{TT,s=3/2}$
	where
	$W_{TT,s=3/2} = f(\frac{j+\frac{D-3}{2}}{r}), j = 1/2, 3/2, 5/2, \ldots.$

http://dx.doi.org/10.5772/68114

Fields	V_s
Gravitational [16, 17]	
	Scalar-type perturbation
	$V_{S,s=2} = \frac{fH}{16r^2\left[m+\frac{1}{2}N(N+1)(1-f)\right]^2}, N = D-2$
	$H = N^4(N+1)^2(1-f)^3$ $+ N(N+1)[4(2N^2-3N+4)m + N(N-2)(N-4)(N+1)](1-f)^2$ $- 12N[(N-4)m + N(N+1)(N-2)]m(1-f) + 16m^3 + 4N(N+2)m^2.$ $m = l(l+N-1) - N,\ l = 2,3,4....$
	Vector and tensor type perturbation
	$V_{V/T,s=2} = \frac{f}{r^2}\left[l(l+D-3) + \frac{(D-2)(D-4)}{4} - \frac{\mu_{V/T}}{2}\frac{(D-2)^2M}{r^{D-3}}\right].$
	$\mu_V = 3, l_V = 2,3,4\ldots$ for vector-type perturbation.
	$\mu_T = -1, l_T = 1,2,3,\ldots$ for tensor-type perturbation.

Table 2. The effective potential for various fields in the higher dimensional cases ($D \geq 5$).

"scalar-type perturbation potential" and the "vector-type perturbation potential". It is accidental that both of these effective potentials satisfy Eq. (5) when $D = 4$ and $s = 1$, but it has been shown they have different behaviours in the higher dimensional cases. It is believed that these two types of effective potentials are strongly linked to two types of eigenvectors on spheres, which are longitudinal and transverse ones. For the case of gravitational fields, the "scalar-type perturbation potential" becomes the potential for the Zerilli equation, and the "vector type perturbation potential" becomes the potential for the Regge-Wheeler equation when $D = 4$ and $s = 2$. The "tensor-type perturbation potential" will be present when $D \geq 5$ but absent in the four-dimensional case.

For the fermionic fields, the "$\pm$" still represents two isospectral supersymmetric partner potentials in the higher dimensional cases. We have one set of effective potentials for the Dirac field, which is strongly related to the eigenspinor on the sphere and reduces to Eq. (8) when $D = 4$. For the case of the Rarita-Schwinger field, the potentials related to the non-transverse-traceless eigenmodes are the leading equation both for the four-dimensional case and the higher dimensional one, which are strongly linked to the "non-transverse-traceless" eigenspinor-vector on spheres. Another effective potential for the Rarita-Schwinger fields is the one related to the transverse and traceless eigenmodes; however, this type of eigenspinor-vector was absent on the 2-sphere, which indicates that the potentials related to the transverse and traceless eigenmodes exist for the cases when $D \geq 5$. We must note that, in this case, the effective potentials are exactly the same as the Dirac case.

Lastly, note that, most of the effective potentials in **Table 2** are simple barrier like potentials. Nevertheless, some cases in the higher dimensions, or for the lowest energy state with $j = 1/2$, for the potentials related to the non-transverse-traceless eigenmodes exhibit special behaviours but not a simple barrier potential, which strongly suggests a link with the instabilities of the black hole [18] and warrants further study.

To summarise, we have in this section provided a brief review of the effective potentials, which play an important role in the perturbation theory of various spin fields in the general dimensional Schwarzschild black hole spacetimes.

3. QNM frequencies by AIM

3.1. AIM methods

The AIM is a well-established approach in solving the eigenvalue problem for the second-order differential equations, for example, Schrödinger-like equations. As mentioned in the previous section, the radial equations of the perturbation theory with various spin fields in general dimensional Schwarzschild spacetimes were presented as Schrödinger-like equations. The QNMs, which are the signature modes in the black hole perturbation theory, can be obtained naturally by using the AIM. In this subsection, we shall present a brief review of the AIMs, and in the next subsection, we shall present an example calculation, showing the methods used to obtain the quasi normal frequencies. We shall start with the second-order differential equation for the function $\chi(x)$

$$\chi^{''} = \lambda_0(x)\chi' + s_0(x)\chi, \tag{10}$$

where $\chi' = d\chi/dx$. The symmetric structure of the right-hand side of Eq. (10) leads to the method, where we differentiate on both sides of the equation we find that

$$\begin{aligned} \chi'' &= \lambda_0\chi^{''} + (\lambda'_0 + s_0)\chi' + s'_0\chi, \\ &= (\lambda'_0 + s_0 + \lambda_0^2)\chi' + (s'_0 + s_0\lambda_0)\chi, \\ &\equiv \lambda_1\chi' + s_1\chi. \end{aligned} \tag{11}$$

Taking the second derivative of Eq. (10) we have

$$\chi^{(4)} = \lambda_2\chi' + s_2\chi, \tag{12}$$

where

$$\lambda_2 = \lambda'_1 + s_1 + \lambda_0\lambda_1 \ ; \ s_2 = s'_1 + s_0\lambda_1. \tag{13}$$

Differentiating iteratively to the $(n+1)^{th}$ and the $(n+2)^{th}$ order, we have

$$\chi^{(n+1)} = \lambda_{n-1}\chi' + s_{n-1}\chi \ ; \ \chi^{(n+2)} = \lambda_n\chi' + s_n\chi, \tag{14}$$

where

$$\lambda_n = \lambda'_{n-1} + s_{n-1} + \lambda_0\lambda_{n-1} \ ; \ s_n = s'_{n-1} + s_0\lambda_{n-1}. \tag{15}$$

In the AIM, we suppose that for sufficiently large n, which represents the iterating number, the coefficients λ_n and s_n will have the relation

http://dx.doi.org/10.5772/68114

$$\frac{s_n}{\lambda_n} = \frac{s_{n+1}}{\lambda_{n+1}} = \beta(x), \tag{16}$$

where the general solution of Eq. (10) is

$$\chi(x) = exp\Big(-\int^x \beta(x')dx'\Big)[C_2 + C_1\int^x exp(\int^x (\lambda_0(x'') + 2\beta(x''))dx'')dx']. \tag{17}$$

C_1 and C_2 are constants determined by the normalisation, and the QNMs (or the energy eigenstates) can be obtained by the termination condition

$$s_n\lambda_{n+1} - s_{n+1}\lambda_n = 0. \tag{18}$$

This is the basic idea for the AIM, where to appreciate the effectiveness of this methods, we refer the reader to Ciftci et al. [4, 5], which presented some studies for the constant coefficient, harmonic oscillator, and the energy eigenvalue problem for several well-known potentials. For the study of perturbation theory in curved spacetimes by the AIM, Cho et al. [1] present a review of the QNMs for the bosonic fields in the four-dimensional maximally symmetric and the Kerr black hole spacetimes. In the next subsection, as an example, we shall present how to obtain the QNMs for Dirac fields in the higher dimensional Schwarzschild black hole spacetimes by the AIM and compare these with other numerical semi-analytic results.

3.2. Example: How to obtain the QNMs for Dirac fields in general dimensional Schwarzschild black hole spacetimes by the AIM

The QNMs for Dirac particles in the higher dimensional Schwarzschild black hole spacetimes had been done in the earlier work by some of the authors [13] using the third-order WKB approximation but not the AIM. With recent progress in spin-3/2 fields [11], we find that these results greatly overlap with some of the spin-3/2 particles, which are represented by the relations in the radial equations of the transverse and traceless eigenmodes. In this section, as an example, we are going to show how to reproduce the results by the AIM.

In **Table 2**, the effective potential of the radial equation, Eq. (4), for the Dirac particle is as follows:

$$V_{s=1/2} = f\frac{dW_{s=1/2}}{dr} + W^2_{s=1/2}\ ,\ \ W_{s=1/2} = f\left(\frac{j+\frac{D-3}{2}}{r}\right)\ ,\ \ j = \frac{1}{2}, \frac{3}{2}, \ldots. \tag{19}$$

As we are going to reproduce the results in Ref. [13], a similar choose of $f(r)$ will be

$$f(r) = 1 - \left(\frac{r_H}{r}\right)^{D-3}\ ,\ \ r_H^{D-3} = \frac{8\pi M\Gamma((D-1)/2)}{\pi^{(D-1)/2}(D-2)}\ ,\ \ M \equiv 1, \tag{20}$$

where r_H represents the location of the event horizon and M represents the mass of the black hole. By making a coordinate transformation

$$\xi^2(r) = 1 - \frac{r_H}{r}, \tag{21}$$

the radial equation becomes

$$\left[f\frac{d\xi}{dr}\frac{d}{d\xi}\left(f\frac{d\xi}{dr}\frac{d}{d\xi}\right) + \omega^2 - V_{s=1/2}\right]\Psi_{s=1/2} = 0. \tag{22}$$

Simplifying Eq. (22), we have

$$\left[\frac{d^2}{d\xi^2} + \left(\frac{f'}{f} + \frac{\xi''}{\xi'}\right)\frac{d}{d\xi} + \frac{\omega^2 - V_{s=1/2}}{f^2\xi'^2}\right]\Psi_{s=1/2} = 0, \tag{23}$$

where

$$f' = \frac{d}{d\xi}f(\xi)\ ,\ \ \xi' = \frac{d}{dr}\xi(r)|_{r=\frac{r_H}{1-\xi^2}}\ ,\ \ \xi'' = \frac{d}{d\xi}\xi'. \tag{24}$$

Next, by setting the boundary behaviour of $\Psi_{s=1/2} = \alpha(\xi)\chi(\xi)$ and together with Eq. (23), we have

$$\frac{d^2}{d\xi}\chi = -\left(\frac{f'}{f} + \frac{\xi''}{\xi} + \frac{2\alpha'}{\alpha}\right)\frac{d}{d\xi}\chi - \left[\frac{\omega^2 - V_{s=1/2}}{f'\xi'^2} + \frac{\alpha''}{\alpha} + \left(\frac{f'}{f} + \frac{\xi''}{\xi}\right)\frac{\alpha'}{\alpha}\right]\chi. \tag{25}$$

This is the second-order differential equation, which is the same as Eq. (10) with

$$\lambda_0 = -\left(\frac{f'}{f} + \frac{\xi''}{\xi} + \frac{2\alpha'}{\alpha}\right)\ ,\ \ s_0 = -\left[\frac{\omega^2 - V_{s=1/2}}{f'\xi'^2} + \frac{\alpha''}{\alpha} + \left(\frac{f'}{f} + \frac{\xi''}{\xi}\right)\frac{\alpha'}{\alpha}\right]. \tag{26}$$

Note that the last parameter we have to define is the asymptotic behaviour function $\alpha(\xi)$, and we approach this by starting with the asymptotic behaviour of $\Psi_{s=1/2}$, which can be represented as an outgoing plane wave

$$\begin{array}{ll} \Psi_{s=1/2} \sim e^{i\omega r_*} & \text{for} \quad r \to \infty, \\ \Psi_{s=1/2} \sim e^{-i\omega r_*} & \text{for} \quad r \to -\infty, \end{array} \tag{27}$$

with r^* being the tortoise coordinate, which has the relation with r

$$\frac{d}{dr_*} = f(r)\frac{d}{dr}. \tag{28}$$

Solving Eq. (28) in the four-dimensional case, we have

$$r_* = r + r_H \ln\left(\frac{r_H}{r} - 1\right), \tag{29}$$

together with Eqs. (21) and (27), we have

http://dx.doi.org/10.5772/68114

$$\begin{aligned}\Psi_{s=1/2} &\sim e^{\frac{i\omega r_H}{1-\xi^2}}(1-\xi^2)^{-i\omega r_H}\xi^{2i\omega r_H} \quad \text{for} \quad \xi \to 1,\\ \Psi_{s=1/2} &\sim e^{-\frac{i\omega r_H}{1-\xi^2}}(1-\xi^2)^{i\omega r_H}\xi^{-2i\omega r_H} \quad \text{for} \quad \xi \to 0.\end{aligned} \tag{30}$$

Collecting the leading terms, we can define $\alpha(\xi)$ in the four-dimensional case as follows:

$$\alpha(\xi) = e^{\frac{i\omega r_H}{1-\xi^2}}(1-\xi^2)^{-i\omega r_H}\xi^{-2i\omega r_H}. \tag{31}$$

If we now consider the higher dimensional cases, Eq. (29) will become more complicated with

$$r_* = r + \sum_{a=1}^{D-3}\frac{r_H\varepsilon}{D-3}\ln\left(\frac{r}{r_H\varepsilon}-1\right), \tag{32}$$

where $\varepsilon = e^{\frac{i\pi 2\pi}{D-3}}$. Eq. (27) in the higher dimensions can be presented in the general form

$$\begin{aligned}\Psi_{s=1/2} &\sim e^{\frac{i\omega r_H}{1-\xi^2}}\prod_{a=1}^{D-3}\left(\varepsilon(1-\xi^2)\right)^{-\frac{i\omega r_H\varepsilon}{D-3}}\left(1-\varepsilon(1-\xi^2)\right)^{\frac{i\omega r_H\varepsilon}{D-3}} \quad \text{for} \quad \xi \to 1,\\ \Psi_{s=1/2} &\sim e^{-\frac{i\omega r_H}{1-\xi^2}}\prod_{a=1}^{D-3}\left(\varepsilon(1-\xi^2)\right)^{\frac{i\omega r_H\varepsilon}{D-3}}\left(1-\varepsilon(1-\xi^2)\right)^{-\frac{i\omega r_H\varepsilon}{D-3}} \quad \text{for} \quad \xi \to 0.\end{aligned} \tag{33}$$

Next, we shall consider how to define the asymptotic behaviour function $\alpha(\xi)$ in the higher dimensional cases, where in our experience, finding the dominant terms in Eq. (33) is helpful to the AIM calculation. When $D = 5$, Eq. (33) becomes

$$\begin{aligned}\Psi_{s=1/2} &\sim e^{\frac{i\omega r_H}{1-\xi^2}}(\xi^2-2)^{-\frac{i\omega r_H}{2}}(\xi^2)^{\frac{i\omega r_H}{2}} \quad \text{for} \quad \xi \to 1,\\ \Psi_{s=1/2} &\sim e^{-\frac{i\omega r_H}{1-\xi^2}}(\xi^2-2)^{\frac{i\omega r_H}{2}}(\xi^2)^{-\frac{i\omega r_H}{2}} \quad \text{for} \quad \xi \to 0.\end{aligned} \tag{34}$$

By considering the dominant term for the boundary behaviour, a suitable choice of the asymptotic behaviour function is as follows:

$$\alpha_{(D=5)}(\xi) = e^{\frac{i\omega r_H}{1-\xi^2}}(\xi^2)^{-\frac{i\omega r_H}{2}}. \tag{35}$$

For $D = 6$, Eq. (33) becomes

$$\begin{aligned}\Psi_{s=1/2} \sim\ & e^{\frac{i\omega r_H}{1-\xi^2}}\left(e^{\frac{i2\pi}{3}}(1-\xi^2)\right)^{-\frac{i\omega r_H e^{\frac{i2\pi}{3}}}{3}}\left(1-e^{\frac{i2\pi}{3}}(1-\xi^2)\right)^{\frac{i\omega r_H e^{\frac{i2\pi}{3}}}{3}}\left(e^{\frac{i4\pi}{3}}(1-\xi^2)\right)^{-\frac{i\omega r_H e^{\frac{i4\pi}{3}}}{3}}\\ &\left(1-e^{\frac{i4\pi}{3}}(1-\xi^2)\right)^{\frac{i\omega r_H e^{\frac{i4\pi}{3}}}{3}}(1-\xi^2)^{-\frac{i\omega r_H}{3}}(1-\xi^2)^{-\frac{i\omega r_H}{3}} \ \text{for} \ \xi \to 1,\\ \Psi_{s=1/2} \sim\ & e^{-\frac{i\omega r_H}{1-\xi^2}}\left(e^{\frac{i2\pi}{3}}(1-\xi^2)\right)^{\frac{i\omega r_H e^{\frac{i2\pi}{3}}}{3}}\left(1-e^{\frac{i2\pi}{3}}(1-\xi^2)\right)^{-\frac{i\omega r_H e^{\frac{i2\pi}{3}}}{3}}\left(e^{\frac{i4\pi}{3}}(1-\xi^2)\right)^{\frac{i\omega r_H e^{\frac{i4\pi}{3}}}{3}}\\ &\left(1-e^{\frac{i4\pi}{3}}(1-\xi^2)\right)^{-\frac{i\omega r_H e^{\frac{i4\pi}{3}}}{3}}(1-\xi^2)^{-\frac{i\omega r_H}{3}}(1-\xi^2)^{-\frac{i\omega r_H}{3}} \ \text{for} \ \xi \to 0.\end{aligned} \tag{36}$$

The dominant term for the boundary behaviour can be chosen as follows:

$$\alpha_{(D=6)}(\xi) = e^{\frac{i\omega r_H}{1-\xi^2}}(\xi^2)^{-\frac{i\omega r_H}{3}}(1-\xi^2)^{-\frac{i\omega r_H}{3}}. \tag{37}$$

For a similar discussion on the higher dimensional cases, we find that $\alpha(\xi)$ can be defined separately for the odd dimensional and even dimensional cases, where

$$\begin{aligned} \alpha(\xi) &= e^{\frac{i\omega r_H}{1-\xi^2}}(\xi^2)^{-\frac{i\omega r_H}{D-3}}, \qquad D \in \text{odd}; \\ \alpha(\xi) &= e^{\frac{i\omega r_H}{1-\xi^2}}(\xi^2)^{-\frac{i\omega r_H}{D-3}}(1-\xi^2)^{-\frac{i\omega r_H}{D-3}}, \quad D \in \text{even}. \end{aligned} \tag{38}$$

Substituting Eqs. (19), (20), (21) and (38) into Eq. (26), we find λ_1 and s_1 by the relation in Eq. (15). Next, by defining a suitable initial value of ω_0, which represents the parameter ω in s_0, with the termination condition Eq. (18), we can solve the parameter ω_1, which represents the parameter ω in s_1. This loop iterates, as with ω_1 we can solve for ω_2 in the next iteration and so on. For a sufficiently large number of iterations, the $\omega_{n\text{-}1}$ and ω_n will become stable, and it will be the quasi normal frequency we are seeking.

The QNM results are obtained with the iteration number = 200 in **Table 3**, for the D = 5,6 dimensional Schwarzschild spacetimes, and in **Table 4**, for D = 7,8. The results using the third-order WKB methods are the same as presented in our previous work [13], where for completeness we also list the sixth-order WKB results.

		5 Dimensions		
l	n	Third-order WKB	Sixth-order WKB	AIM
0	0	0.7247–0.3960 i	0.7823–0.3635 i	0.7252–0.3960 i
1	0	1.3158–0.3839 i	1.3301–0.3852 i	1.3163–0.3839 i
1	1	1.1490–1.2192 i	1.1800–1.2021 i	1.1495–1.2192 i
2	0	1.8754–0.3838 i	1.8801–0.3844 i	1.8802–0.3840 i
2	1	1.7541–1.1818 i	1.7672–1.1791 i	1.7674–1.1779 i
2	2	1.5588–2.0318 i	1.5620–2.0517 i	1.5593–2.0318 i
3	0	2.4251–0.3839 i	2.4271–0.3840 i	2.4256–0.3839 i
3	1	2.3322–1.1686 i	2.3382–1.1674 i	2.3327–1.1686 i
3	2	2.1704–1.9891 i	2.1691–1.9980 i	2.1709–1.9891 i
3	3	1.9611–2.8411 i	1.9385–2.9063 i	1.9616–2.8411 i
4	0	2.9716–0.3839 i	2.9726–0.3839 i	2.9721–0.3839 i
4	1	2.8963–1.1624 i	2.8994–1.1618 i	2.8968–1.1624 i
4	2	2.7596–1.9668 i	2.7574–1.9711 i	2.7601–1.9668 i
4	3	2.5773–2.7984 i	2.5569–2.8330 i	2.5778–2.7984 i
4	4	2.3583–3.6512 i	2.3126–3.7665 i	2.3588–3.6512 i
5	0	3.5166–0.3838 i	3.5171–0.3838 i	3.5171–0.3838 i
5	1	3.4533–1.1591 i	3.4550–1.1588 i	3.4538–1.1591 i
5	2	3.3353–1.9536 i	3.3333–1.956 i	3.3358–1.9536 i

http://dx.doi.org/10.5772/68114

		5 Dimensions		
5	3	3.1741–2.7711 i	3.1580–2.7908 i	3.1746–2.7711 i
5	4	2.9785–3.6089 i	2.9383–3.6779 i	2.9790–3.6089 i
5	5	2.7525–4.4625 i	2.6857–4.6302 i	2.7530–4.4625 i
		6 Dimensions		
0	0	1.2806–0.6391 i	1.4364–0.5821 i	1.2811–0.6391 i
1	0	2.1006–0.6276 i	2.1350–0.6423 i	2.1011–0.6276 i
1	1	1.7071–2.0417 i	1.8139–1.9981 i	1.7076–2.0417 i
2	0	2.8671–0.6308 i	2.8797–0.6354 i	2.8676–0.6308 i
2	1	2.5777–1.962 i	2.6235–1.9629 i	2.5782–1.962 i
2	2	2.1056–3.4196 i	2.1297–3.4716 i	2.1061–3.4196 i
3	0	3.6132–0.6321 i	3.6194–0.6329 i	3.6196–0.6325 i
3	1	3.3917–1.9342 i	3.4143–1.9318 i	3.4180–1.9342 i
3	2	3.0002–3.3204 i	3.0081–3.3404 i	3.0007–3.3204 i
3	3	2.4883–4.7849 i	2.4206–4.9568 i	2.4888–4.7849 i
4	0	4.3518–0.6324 i	4.3550–0.6325 i	4.3523–0.6324 i
4	1	4.1724–1.9214 i	4.1845–1.9192 i	4.1729–1.9214 i
4	2	3.8423–3.2694 i	3.8437–3.2771 i	3.8428–3.2694 i
4	3	3.3973–4.6831 i	3.3411–4.7697 i	3.3978–4.6831 i
4	4	2.8578–6.1516 i	2.6999–6.4718 i	2.8583–6.1516 i
5	0	5.0872–0.6325 i	5.0890–0.6324 i	5.0877–0.6325 i
5	1	4.9359–1.9143 i	4.9428–1.9128 i	4.9364–1.9143 i
5	2	4.6513–3.2399 i	4.6503–3.2435 i	4.6518–3.2399 i
5	3	4.2586–4.6195 i	4.2147–4.6677 i	4.2591–4.6195 i
5	4	3.7773–6.0494 i	3.6482–6.2378 i	3.7778–6.0494 i
5	5	3.2168–7.5218 i	2.9732–8.0104 i	3.2173–7.5218 i

Table 3. Low-lying ($n \leq l$, with $l = j - 1/2$) spin-1/2 field QNM frequencies using the WKB methods and the AIM with D = 5,6.

		7 Dimensions		
l	n	Third-order WKB	Sixth-order WKB	AIM
0	0	1.7861–0.8090 i	2.0640–0.7502 i	1.7866–0.8090 i
1	0	2.7344–0.8066 i	2.7827–0.8558 i	2.7349–0.8066 i
1	1	2.0521–2.6832 i	2.2892–2.6106 i	2.0526–2.6832 i
2	0	3.6130–0.8166 i	3.6327–0.8322 i	3.6135–0.8166 i
2	1	3.1092–2.5590 i	3.2053–2.5943 i	3.1097–2.5590 i
2	2	2.2671–4.5340 i	2.3344–4.6355 i	2.2676–4.5340 i
3	0	4.4610–0.8206 i	4.4730–0.8233 i	4.4615–0.8206 i
3	1	4.0779–2.5187 i	4.1298–2.5218 i	4.0784–2.5187 i

		7 Dimensions		
3	2	3.3809–4.3622 i	3.4158–4.4006 i	3.3814–4.3622 i
3	3	2.4624–6.363 i	2.3163–6.6549 i	2.4629–6.363 i
4	0	5.2968–0.8218 i	5.3035–0.8220 i	5.3033–0.8220 i
4	1	4.9878–2.5009 i	5.0176–2.4966 i	4.9883–2.5009 i
4	2	4.4049–4.2771 i	4.4224–4.2810 i	4.4054–4.2772 i
4	3	3.6066–6.1782 i	3.4954–6.3058 i	3.6071–6.1782 i
4	4	2.6393–8.1950 i	2.2624–8.7432 i	2.6398–8.1950 i
5	0	6.1273–0.8221 i	6.1310–0.8219 i	6.1309–0.8221 i
5	1	5.8671–2.4910 i	5.8847–2.4870 i	5.8676–2.4910 i
5	2	5.3673–4.2295 i	5.3756–4.2263 i	5.3678–4.2295 i
5	3	4.6654–6.0660 i	4.5819–6.1252 i	4.6659–6.0660 i
5	4	3.8002–8.0044 i	3.5047–8.3081 i	3.8007–8.0044 i
5	5	2.7964–10.035 i	2.1874–10.910 i	2.7969–10.0348i
		8 Dimensions		
0	0	2.2437–0.9238 i	2.6486–0.8930 i	2.2442–0.9238 i
1	0	3.2663–0.9359 i	3.3105–1.0469 i	3.2668–0.9359 i
1	1	2.2397–3.1796 i	2.6722–3.0659 i	2.2402–3.1796 i
2	0	4.2077–0.9556 i	4.2279–0.9928 i	4.2082–0.9556 i
2	1	3.4491–3.0091 i	3.6051–3.1428 i	3.4496–3.0091 i
2	2	2.1453–5.4463 i	2.2891–5.5740 i	2.1458–5.4463 i
3	0	5.1097–0.9641 i	5.1285–0.9704 i	5.1102–0.9642 i
3	1	4.5378–2.9607 i	4.6284–2.9895 i	4.5383–2.9607 i
3	2	3.4576–5.1805 i	3.5481–5.2651 i	3.4581–5.1805 i
3	3	2.0383–7.6877 i	1.7944–8.0198 i	2.0388–7.6877 i
4	0	5.9947–0.9669 i	6.0062–0.9669 i	5.9952–0.9669 i
4	1	5.5365–2.9415 i	5.5943–2.9365 i	5.5370–2.9415 i
4	2	4.6421–5.0549 i	4.6967–5.0480 i	4.6426–5.0549 i
4	3	3.4017–7.3877 i	3.2284–7.5066 i	3.4022–7.3877 i
4	4	1.9199–9.9347 i	1.2118–10.564 i	1.9204–9.9347 i
5	0	6.8720–0.9677 i	6.8785–0.9669 i	6.8772–0.9659 i
5	1	6.4875–2.9309 i	6.5231–2.9224 i	6.4880–2.9309 i
5	2	5.7272–4.9883 i	5.7608–4.9630 i	5.7277–4.9883 i
5	3	4.6390–7.2092 i	4.5109–7.2241 i	4.6395–7.2092 i
5	4	3.3023–9.6186 i	2.7516–9.9294 i	3.3028–9.6186 i
5	5	1.7759–12.195 i	0.5680–13.282 i	1.7764–12.1949 i

Table 4. Low-lying ($n \leq l$, with $l = j - 1/2$) spin-1/2 field QNM frequencies using the WKB methods and the AIM with D = 7,8.

http://dx.doi.org/10.5772/68114

4. A remark on the spin-3/2 field QNMs

In this section, we are going to present a discussion of our recent work [11] on the spin-3/2 fields in general dimensional Schwarzschild spacetimes. Note that, this section will not go into as great a detail as the previous one but shall just list some improvements made in light of recent considerations. Starting with the radial equation related to the "non-TT eigenmodes", the radial equation can still be represented as the Schrödinger like one, Eq. (4), where

$$\begin{aligned} V_{NTT,s=3/2} &= \pm f\frac{dW_{NTT,s=3/2}}{dr} + W^2_{NTT,s=3/2}, \\ W_{NTT,s=3/2} &= \frac{\sqrt{f}(j+\frac{D-3}{2})}{r}\left[\frac{(\frac{2}{D-2})^2(j+\frac{D-3}{2})^2 - 1 - \frac{D-4}{D-2}(\frac{2M}{r})^{D-3}}{(\frac{2}{D-2})^2(j+\frac{D-3}{2})^2 - f}\right], \end{aligned} \tag{39}$$

and

$$f(r) = 1 - \left(\frac{2M}{r}\right)^{D-3}. \tag{40}$$

Because the general form of the radial equation is the same as the Dirac case, Eqs. (22)–(38) are still sufficient in this case, but the effective potential will be Eq. (39), not Eq. (19). What we need to consider here is that the asymptotic behaviour function is simpler than what we had used previously and successfully generates better results for the QNMs.

In **Table 5**, for some lower modes in the seven-dimensional spacetime, the new AIM results (with the current choice of boundary behaviour function, Eq. (38)) are better than the previous

		7 Dimensions			
l	n	Third-order WKB	Sixth-order WKB	AIM (earlier)	AIM (new)
0	0	0.7725–0.2978 i	0.7530–0.3037 i	0.7008–0.3036 i	0.7535–0.3036 i
1	0	1.1441–0.2893 i	1.1415–0.2831 i	1.1231–0.2976 i	1.142–0.2831 i
1	1	0.9465–0.9065 i	0.9267–0.8783 i	0.9266–0.8782 i	0.9271–0.8782 i
⋮	⋮	⋮	⋮	⋮	⋮
		8 Dimensions			
⋮	⋮	⋮	⋮	⋮	⋮
4	4	1.0674–3.5290 i	0.7606–3.5381 i	1.0674–3.5290 i	1.0679–3.5291 i
5	4	1.5711–3.4654 i	1.3755–3.4609 i	1.5711–3.4653 i	1.5716–3.4654 i
5	5	1.0321–4.3822 i	0.5837–4.5299 i	1.0321–4.3822 i	1.0326–4.3822 i
⋮	⋮	⋮	⋮	⋮	⋮

Table 5. Selected QNM frequencies of low-lying ($n \le l$, with $l = j - 3/2$) for spin-3/2 field related to the non-TT eigenmodes by using the WKB methods and the AIM.

results for the first few modes. This is why we believe Eq. (38) is a suitable choice of the boundary behaviour function for the AIM methods in the higher dimensional spacetimes.

5. Summary

In this chapter, we presented a brief review of recent progress on perturbation theory with various fields in curved spacetimes, especially for a systematic comparison to the fermionic and bosonic fields. Generally, the first step in this topic is the obtaining of the radial equations as discussed in Section 2. There are then various methods, but no unique approach for considering a specific field on a specific spacetime, where we strongly suggest the reader follow the references provided to develop a step-by-step approach. On the other hand, the process for obtaining the radial equations always relates to the separability of a spacetime, this being the main reason that we still have difficulties for perturbation theory in the higher dimensional Kerr spacetimes. As such we mentioned in the introduction section that for the gravitational wave experiments, the QNMs in the higher dimensional Kerr spacetimes are definitely an interesting next stage of study for this area, and it shall be interesting seeing further progress in this direction.

In Section 3, we presented the AIM, giving an in detail example to study the perturbation theory in the higher dimensional spacetimes and also presented a remark for our recent work on the spin-3/2 fields. Since there are several numerical methods for obtaining the QNMs, we believe that the AIM is a straightforward way to study the QNMs due to its simple mathematical structure.

Author details

Chun-Hung Chen[2], Hing-Tong Cho[3] and Alan S. Cornell[1]*

*Address all correspondence to: alan.cornell@wits.ac.za

1 National Institute for Theoretical Physics, School of Physics, University of the Witwatersrand, Wits, South Africa

2 Institute of Physics, Academia Sinica, Taipei, Taiwan

3 Department of Physics, Tamkang University, Tamsui, Taipei, Taiwan

References

[1] H. T. Cho, A. S. Cornell, J. Doukas, T. R. Huang and W. Naylor, Adv. Math. Phys. **2012**, 281705 (2012). doi:10.1155/2012/281705 [arXiv:1111.5024 [gr-qc]].

[2] S. Iyer and C. M. Will, Phys. Rev. D **35**, 3621 (1987). doi:10.1103/PhysRevD.35.3621

[3] R. A. Konoplya, Phys. Rev. D **68**, 024018 (2003). doi:10.1103/PhysRevD.68.024018 [gr-qc/0303052].

[4] H. Ciftci, R. L. Hall and N. Saad, J. Phys. A: Math. Gen. **36**, 11807–11816 (2003).

[5] H. Ciftci, R. L. Hall and N. Saad, Phys. Lett. A **340**, 388–396 (2005).

[6] H. T. Cho, A. S. Cornell, J. Doukas and W. Naylor, Class. Quant. Grav. **27**, 155004 (2010). doi:10.1088/0264-9381/27/15/155004 [arXiv:0912.2740 [gr-qc]].

[7] M. A. Rubin and C. R. Ordonez, Journal of Mathematical Physics 25, 2888 (1984); doi: 10.1063/1.526034

[8] M. A. Rubin and C. R. Ordonez, J. Math. Phys. **26**, 65 (1985). doi:10.1063/1.526749

[9] A. Higuchi, J. Math. Phys. **28**, 1553 (1987). Erratum: [J. Math. Phys. **43**, 6385 (2002)]. doi:10.1063/1.527513

[10] R. Camporesi and A. Higuchi, J. Geom. Phys. **20**, 1 (1996). doi:10.1016/0393-0440(95)00042-9 [gr-qc/9505009].

[11] C.-H. Chen, H. T. Cho, A. S. Cornell and G. Harmsen, Phys. Rev. D **94**, 044052 (2016). doi:10.1103/PhysRevD.94.044052 [arXiv:1605.05263 [gr-qc]].

[12] E. Berti, V. Cardoso and A. O. Starinets, Class. Quant. Grav. **26**, 163001 (2009). doi:10.1088/0264-9381/26/16/163001 [arXiv:0905.2975 [gr-qc]].

[13] H. T. Cho, A. S. Cornell, J. Doukas and W. Naylor, Phys. Rev. D **75**, 104005 (2007). doi:10.1103/PhysRevD.75.104005 [hep-th/0701193].

[14] C.-H. Chen, H. T. Cho, A. S. Cornell, G. Harmsen and W. Naylor, Chin. J. Phys. **53**, 110101 (2015). doi:10.6122/CJP.20150511 [arXiv:1504.02579 [gr-qc]].

[15] L. C. B. Crispino, A. Higuchi and G. E. A. Matsas, Phys. Rev. D **63**, 124008 (2001). Erratum: [Phys. Rev. D **80**, 029906 (2009)]. doi:10.1103/PhysRevD.63.124008, 10.1103/PhysRevD.80.029906 [gr-qc/0011070].

[16] H. Kodama and A. Ishibashi, Prog. Theor. Phys. **110**, 701 (2003). doi:10.1143/PTP.110.701 [hep-th/0305147].

[17] H. Kodama and A. Ishibashi, Prog. Theor. Phys. **111**, 29 (2004). doi:10.1143/PTP.111.29 [hep-th/0308128].

[18] A. Ishibashi and H. Kodama, Prog. Theor. Phys. **110**, 901 (2003). doi:10.1143/PTP.110.901 [hep-th/0305185].

Edited by Abraao Jesse Capistrano de Souza

The modern cosmology has been turned into an outstanding field of active research through the years. Today, we have more scientific data in modern cosmology than we could get rid of it, which makes the present days an exciting era for scientific knowledge. "Trends in Modern Cosmology" invites the reader to tackle the big questions of the universe from cultural aspects of cosmology and its influence on arts, philosophy, and politics to more specialized technical advances in the field as the physics of dark sector, black holes, galaxies, large structure formation, and particles. In fact, it reveals our endless searching for the better understanding of the universe as a legacy of knowledge for next generations.

ISBN 978-953-51-4810-4

Photo by rajeshbac / iStock

IntechOpen